MECHANISTIC STUDIES ON GOLD(I) AND GOLD(III) CATALYTIC TRANSFORMATIONS

Isabel Arranz De La Calle

UNIVERSITAT ROVIRA i VIRGILI

Mechanistic Studies on Gold(I) and Gold(III) Catalytic Transformations

Isabel Arranz de la Calle

DOCTORAL THESIS
2024

UNIVERSITAT ROVIRA I VIRGILI
MECHANISTIC STUDIES ON GOLD(I) AND GOLD(III) CATALYTIC TRANSFORMATIONS
Isabel Arranz De La Calle

UNIVERSITAT ROVIRA I VIRGILI
MECHANISTIC STUDIES ON GOLD(I) AND GOLD(III) CATALYTIC TRANSFORMATIONS
Isabel Arranz De La Calle

Isabel Arranz de la Calle

Mechanistic Studies on Gold(I) and Gold(III) Catalytic Transformations

DOCTORAL THESIS

Supervised by Prof. Antonio M. Echavarren and Prof. Feliu Maseras

Institut Català d'Investigació Química (ICIQ)

UNIVERSITAT ROVIRA i VIRGILI

Tarragona 2024

UNIVERSITAT ROVIRA I VIRGILI
MECHANISTIC STUDIES ON GOLD(I) AND GOLD(III) CATALYTIC TRANSFORMATIONS
Isabel Arranz De La Calle

WE STATE that the present study, entitled "***Mechanistic Studies on Gold(I) and Gold(III) Catalytic Transformations***", presented by Isabel Arranz de la Calle to award the degree of Doctor, has been carried out under our supervision at the Institut Català d´Investigació Química (ICIQ).

Tarragona, 2nd September 2024

Doctoral Thesis Supervisors

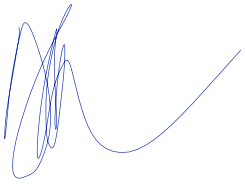

Prof. Antonio M. Echavarren

Prof. Feliu Maseras

UNIVERSITAT ROVIRA I VIRGILI
MECHANISTIC STUDIES ON GOLD(I) AND GOLD(III) CATALYTIC TRANSFORMATIONS
Isabel Arranz De La Calle

A mis padres y mi hermano

UNIVERSITAT ROVIRA I VIRGILI
MECHANISTIC STUDIES ON GOLD(I) AND GOLD(III) CATALYTIC TRANSFORMATIONS
Isabel Arranz De La Calle

"Nothing in life is to be feared; it is only to be understood."

Marie Skłodowska-Curie

UNIVERSITAT ROVIRA I VIRGILI
MECHANISTIC STUDIES ON GOLD(I) AND GOLD(III) CATALYTIC TRANSFORMATIONS
Isabel Arranz De La Calle

Acknowledgments

En primer lugar, me gustaría agradecer a mis directores de tesis, Prof. Antonio M. Echavarren y Prof. Feliu Maseras, por aceptarme allá por 2018 como Summer Fellow y más adelante como estudiante de doctorado. Muchas gracias por confiar en mí desde el principio, por guiarme durante estos años en el mundo de la química y enseñarme una ínfima parte de tanto que conocéis.

Por otro lado, dar las gracias a Sònia Gavaldà, Dr. Imma Escofet por ser partes indispensables del puzle para que todo funcione, por ayudarnos constantemente y estar pendientes. De la misma manera, agradecer a Martín Gumbau toda la ayuda informática, que no ha sido poca, siempre dispuesto a echar una mano.

I would like to express my gratitude to Dr. Per-Ola Norrby for giving me the unique opportunity to join their research group in AstraZeneca, Gothemburg. Thank you for making me feel like a member of the group, for the insightful chemistry discussions, the valuable guidance and the attention during these three months. I also want to thank the rest of the group members, from whom I have learnt so much.

I would also like to thank the research support units at ICIQ : NMR, X-Ray Diffraction, HRMS, HTE, CHROMTAE, CRTU and Informatics.

I want to sincerely thank everyone I have shared time with in the lab. I have learnt so much from each of you, and together we created a great atmosphere of work and respect. I feel really lucky to have crossed paths with all of you, because beyond being a group of chemists, we have shared memorable moments like hiking in the mountains, enjoying afternoons at the beach and playing volleyball, board games during the pandemic, as well as countless dinners, beers, and parties.

Gracias, Andrea, por ser como un hermano, por iluminar mis días y por siempre estar, superando cada etapa juntos. Por los ánimos y tan importantes risas. Eres una persona modelo para mí. Gracias Eduardo por hacernos reír a carcajadas con bromas malas y bailes en el lab, por no parar de sorprenderme, ayudarme tanto y enseñarme química e incluso armonía musical, vales mucho. Gracias a ambos por formar el equipo de los 2.2 explorers y por compartir tanta vida juntos. No tengo palabras suficientes para agradeceros todo vuestro apoyo cuando más lo necesité. Esas llamadas fueron pura energía en aquellos días negros. *"You light my morning sky"* – Elvis Presley

Gracias a Leo por enseñarme y guiarme en el lab al comienzo, siempre con una mirada positiva y relajada. Por todos los desayunos y comidas sin parar literalmente de reir, con tu risa contagiosa, que se echa de menos, y por ser tan bueno y generoso con todos. Gracias a Elena por hacer que mi vuelta al lab fuera motivante y mucho más divertida. He disfrutado mucho trabajando a tu lado. Gracias Anna S. por tu ayuda en química, en la pequeña parte del proyecto que compartimos, y en el resto de aspectos, por ser tan enérgica y paciente.

Gracias Eric por tener la capacidad de hacerme sonreír nada más verte, por ser compañero de pádel y por tus bromas (y por la única que te pude hacer: piel de toro). Gracias Pablo por ser tan auténtico, por las tardes de guitarra y las rutas en bici. Gracias Laura por ser la peque del lab que se ha hecho mayor y por enseñarme a ser más cariñosa con todos tus abrazos. Gracias Ali por todo el cariño, la amabilidad, las aventuras en Suecia y por ser la mejor vecina que puede existir. Gracias Lucía por tu energía, por estar siempre disponible para ayudar y por tu alegría constante. Gracias Tania por esa motivación en las comidas que tanta falta hace y por las anécdotas divertidas. Gracias Gala por estar pendiente y ayudar en cada situación. Gracias a las 'Golden Girls': Alba, Ana, Inma, Gala, Tania, Anna, Fede y Elena por crear ese ambiente acogedor y siempre dar

ánimos. Gracias Àlex por ser atento y proactivo e impulsarnos a hacer nuevas actividades divertidas. Gracias Alessio por compartir el ser medio compu medio experimentales y por entendernos bien. To the funniest german teacher, vielen dank Paul, I have really enjoyed your company and all the laughs we have shared in the lab. Gracias Nicolás por los consejos y por endulzar los días con tus tartas de profesional. Gracias Marina por tu positivismo y por informarnos de todo lo que acontece de manera tan graciosa. Gracias Arnau por las conversaciones sobre música y por dejarnos conocerte un poco más. Thank you Xiaoqing for your sweetness and perseverance. *"What a wonderful world..."* – Louis Armstrong

I want to thank all as well the former and present members of the Echavarren and Maseras groups for all the moments we shared, for supporting and helping me: Joan, Otilia, Mauro, Marc, Franco, Allegra, Margherita, Ulysse, Remi, Victor, Sara, Iogann, Anders, Anna. A, Edmond and Luyu. Special thanks to Dr. Giuseppe Zuccarello, who taught me with dedication everything I needed to know since literally the first day of PhD, all the simple but essential tricks in the lab that made my life easier, and for the valuable advice. Gracias a Helena por tu calma, dulzura y por tantas enseñanzas. I specially want to thank as well Dr. Raúl Pérez, Dr. Akhilesh Sharma and Dr. Bruna Sánchez for helping me and introducing me to the DFT world. *"Ain't no mountain high enough..."* – Marvin Gaye & Tammi Terrel.

Gracias a mis amigas de toda la vida, Alba, Sara, Noemí, Cristina, Laura, por estar siempre ahí, a mi lado, por compartir miles de historias en atletismo, en jotas, en los campamentos… por hacer que cada vez que vuelvo a nuestro querido pueblo sienta que no ha pasado el tiempo. *"Es la chica segoviana, la mujer que yo más quiero…"* – Nuevo Mester de Juglaría

Gracias a mis queridos atletas en activo y pasivo, Alba, Carlos y Edu, por ser compañeros durante muchos años de disciplina y sufrimiento; pero lo más importante, por la amistad, las risas y competiciones por toda España. No puede faltar dar las gracias a nuestro maestro y entrenador Don Mariano por todos los valores que nos inculcaste desde pequeños, por enseñarnos lo que es el trabajo duro, por toda la dedicación desinteresada y el tiempo que nos has regalado. *"I get by with a little help from my friends…"* – The Beatles

Gracias a Adrián, por ser la persona tan especial que eres, por ayudarme y estar a mi lado a cada paso, por enseñarme a reflexionar, a mirar con otra perspectiva, a parar para poder continuar, por cuidarme tanto y quererme tan bien. *"Gracias a la vida, que me ha dado tanto..."* – Violeta Parra

Durante estos cuatro años he perdido a mis dos abuelos y a mi padre, y aunque me encargué de hacerles saber la admiración y amor que les tenía, quería aprovechar a dejarlo plasmado también aquí. Sólo puedo dar las gracias a mi familia por apoyarme en todo momento aun sin saber de qué va esto de la química, por enseñarme todo lo que sé hasta ahora y por crear un hogar, que según crecemos, se ve que no es tarea fácil. Gracias a mis abuelos por ser unas personas ejemplares y por cuidarnos tanto desde pequeños. Gracias mamá por tu bondad y dedicación a tus hijos, marido, hermanos, padres y gente que te rodea. La fortaleza es una de tus mayores características. Gracias Juan por ser motivación y alegría, por tu forma de ser, por enseñarme tantas cosas. Te admiro muchísimo y ojalá poder parecerme más a ti. Gracias también a Almudena por su apoyo constante, más que una tía eres una segunda madre. Y, por último, gracias a ti papá, por ser la persona con la que nunca se podía estar triste o llorar, tu simple presencia me curaba. Esa energía y ganas de vivir que tenías, tu valentía, tu pasión en todo lo que hacías, tu risa y tus abrazos estarán siempre con nosotros. Sé toda la suerte que tengo y he tenido de teneros a mi lado. *"Comprendimos que si vimos sombras es que siempre hubo luz…"* – Shinova.

We thank Severo Ochoa predoctoral fellowship FPI-SO (PID2019-104815GB-I00), Severo Ochoa Excellence Accreditation 2020-2023 (CEX2019-000925-S), the Ministerio de Ciencia e Innovación (PID2022-136623NB-I00/MICIU/AEI/10.13039/501100011033/ FEDER, UE) and the Agència de Gestió d'Ajuts Universitaris i de Recerca (2021 SGR 001256) for financial support.

UNIVERSITAT ROVIRA I VIRGILI
MECHANISTIC STUDIES ON GOLD(I) AND GOLD(III) CATALYTIC TRANSFORMATIONS
Isabel Arranz De La Calle

At the time of writing this Doctoral Thesis, part of the worked detailed in this manuscript has been published in the following article:

Enantioselective Catalysis with Pyrrolidinyl Gold(I) Complexes: DFT and NEST Analysis of the Chiral Binding Pocket.

Zuccarello, G.; Nannini, L.; Arroyo-Bondía, A.; Fincias, N.; Arranz, I.; Pérez-Jimeno, A. H.; Peeters, M.; Martín-Torres, I.; Sadurní, A.; García-Vázquez, V.; Wang, Y.; Kirillova, M. S.; Montesinos-Magraner, M.; Caniparoli, U.; Núñez, G. D.; Maseras, F.; Besora, M.; Escofet, I.; Echavarren A. M. *JACS Au* **2023**, *3*, 1742–1754.

UNIVERSITAT ROVIRA I VIRGILI
MECHANISTIC STUDIES ON GOLD(I) AND GOLD(III) CATALYTIC TRANSFORMATIONS
Isabel Arranz De La Calle

Table of Contents

Prologue

This Doctoral Thesis manuscript has been divided into four core parts: a general introduction on gold(I) catalysis and three research chapters. The abstract and the general objectives of the work presented in this Thesis precede the main parts. The research chapters are followed by the general conclusions. Each research chapter is in turn structured into five parts: a more detailed introduction into the chapter topic, the specific objectives of the work, the results and discussion, the chapter conclusions, and finally the experimental section. The numbering of the mentioned compounds, computational geometries, tables, schemes, figures, and references is organized by chapter.

The **General Introduction** explores the development of homogeneous gold catalysis, with an emphasis on the activation of alkynes, 1,*n*-enyne cycloisomerisations and the computational understanding using DFT methods.

Chapter I collects the experimental work in the ligand design, synthesis and applications of new catalysts of the family of chiral pyrrolidinyl-biaryl phosphine complexes (gold, silver and copper complexes are described). Additionally, kinetic studies on the formal [4+2] cycloaddition of 1,6-enynes have been provided; guided by the initial work performed by Dr. Giuseppe Zuccarello, which is briefly discussed at the beginning of the section for consistence and context.

Chapter II collects our studies on the oxidative addition of allyl halides to simple alkylphosphines gold(I) complexes, encompassing both experimental and computational efforts to provide mechanistic insight as well as synthetic outcomes. Part of the experimental work was performed in collaboration with Dr. Anna Sadurní.

Chapter III describes the synthesis of diiodomethylgold(I) and iodomethylgold(I) carbenoids by transmetalation from zinc carbenoids. The stability of the new compounds has been assessed and studied as well as its discovered reactivity towards benzene, yielding benzyl iodide with the need of halogen abstractors in the reaction media. A brief computational analysis of the system was as well carried out. The experimental work was carried out in collaboration with Dr. Elena Borrego, and some of her results have been included and discussed for consistence.

Abbreviations and Acronyms

In this manuscript, the abbreviations and acronyms most commonly used in organic and organometallic chemistry have been used following the recommendations of "Guidelines of Authors" of the Journal of Organic Chemistry.

Additional abbreviations and acronyms used in this manuscript are listed below:

APCI	atmospheric pressure chemical ionization
BAr^F_4	tetrakis[3,5-bis(trifluoromethyl)phenylborate]
BINAP	2,2'-bis(diphenylphosphino)-1,1'-binaphthyl
BINOL	1,1'-binaphthol
CyJohnPhos	Chloro[2-(dicyclohexylphosphino)biphenyl]gold(I)
dr	diastereomeric ratio
er	enantiomeric ratio
DAD	diode array detector
DBU	1,3-diaza-bicyclo[5.4.0]undec-7-ene
ESI	electrospray ionization
FID	Flame ionization detector
JohnPhos	(2-biphenyl)di-*tert*-butylphosphine
HMBC	Heteronuclear Multiple Bond Correlation
HSQC	Heteronuclear Single Quantum Coherence
Int	intermediate
IPr	1,3-bis(2,6-diisopropylphenyl)imidazol-2-ylidene
L	ligand
MALDI	matrix assisted laser desorption ionization
MeDalPhos	di(1-adamantyl)-2-dimethylaminophenylphosphine
Mes	2,4,6-trimethylphenyl
MS	mass spectrometry/molecular sieves
MW	microwave irradiation
NHC	N-heterocyclic carbene
NTf_2^-	bis(trifluoromethyl)imidiate
OTf^-	triflate
ORTEP	oak ridge thermal ellipsoid plot
Pdt	product
S	substrate
SEGPHOS	4,4'-bi-1,3-benzodioxole-5,5'-diylbis(diphenylphosphane)
SFC	Supercritical Fluid Chromatograph
*t*BuXPhos	2-(di-*tert*-butylphosphino)-2′,4′,6′-triisopropyl-1,1′-biphenyl

TS	transition state
XPhos	2-Dicyclohexylphosphino-2’,4’,6’-triisopropylbiphenyl

Abstract

The potential of gold as a catalyst was largely dismissed until the late 20th century due to its assumed inertness. This situation has significantly shifted in both gold(I) and gold(I)/(III) catalysis. The ability of gold(I) to selectively activate alkynes has led to the construction of molecular complexity over the years, generally under mild conditions. Moreover, gold(I) linear complexes have been recently shown to promote oxidative addition, via rational ligand design, giving access to planar gold(III) complexes. In this Doctoral Thesis, both modes of gold catalysis have been explored in different systems.

Our group had devised a folding strategy through the development of a novel ligand design, achieving outstanding results in gold(I)-catalyzed enantioselective enyne cyclizations. This approach relies on the capability of a series of JohnPhos gold(I) complexes with C_2-symmetric 2,5-diarylpyrrolidines. The structure of the ligands was further modified in this work, as well as their performance in asymmetric cyclizations when complexed with gold, silver, and copper. Kinetic investigations have been carried out, contributing to a deeper understanding of the mode of action in the formal [4+2] cycloaddition of 1,6-enynes using this kind of chiral complexes.

We studied a new gold(I)/(III) catalytic system involving simple alkyl phosphines as ligands. The use of allyl bromides and organostannanes in the catalytic setting allows a cross-coupling reaction catalyzed by gold, as demonstrated by several control experiments. Furthermore, the stereochemistry of the oxidative addition was evaluated, revealing overall retention at the reaction center. A comprehensive computational mechanistic study indicated an unexpectedly complex behavior of this type of systems.

We developed an alternative synthesis of gold(I) carbenoids bearing phosphines as ligands via transmetalation with zinc carbenoids, avoiding the use of previously required diazo compounds. Additionally, their carbene-like reactivity was tested and confirmed in the formal C-H insertion of benzene. DFT calculations were pursued with the aim of understanding the observed selectivity.

General Objectives

The aims of this Doctoral Thesis are the following:

- Obtaining a comprehensive mechanistic picture of the mode of action of the chiral pyrrolidinyl-biaryl phosphine gold(I) complexes by synthesizing new ligands, guided through rational design, and applying them in asymmetric gold(I) catalysis.
- Deepen the understanding, through both experiment and calculation, of the oxidative addition of allyl halides to gold(I) complexes bearing simple alkylphosphines as ancillary ligands.
- Developing the synthesis of iodomethyl and diiodomethylgold(I) carbenoids via transmetalation with zinc carbenoids, analyzing their typical carbene reactivity and pursuing a computational analysis of the system.

A more thorough description of each of these objectives is presented in the corresponding section of each chapter in this manuscript.

UNIVERSITAT ROVIRA I VIRGILI
MECHANISTIC STUDIES ON GOLD(I) AND GOLD(III) CATALYTIC TRANSFORMATIONS
Isabel Arranz De La Calle

General Introduction

UNIVERSITAT ROVIRA I VIRGILI
MECHANISTIC STUDIES ON GOLD(I) AND GOLD(III) CATALYTIC TRANSFORMATIONS
Isabel Arranz De La Calle

Historical Evolution of Gold Catalysis

Gold is a precious metal with remarkable properties that has served various purposes along the history, from currency and jewelry to art and recognition. A prominent example of their symbolic use is in the Olympic Games. The tradition of awarding solid-gold medals to champions arose in the third modern Games, that took place in 1904 in St. Louis, USA; although it was an expensive and brief practice that ended after the 1912 edition in Stockholm, being followed by medals cast in silver and coated in 6 g of gold.[1] The low tendency of gold to oxidation in air makes it one of the only "shiny" metals found in nature, and as a result, gold has become a sign of immortality, wealth and power in many ancient cultures.

Figure 1. Solid-gold medals designed for Olympic Games of London 1908.[2]

In chemistry, due to its assumed inertness,[3] scientists initially overlooked gold's potential to catalyze reactions and only its stoichiometric coordination and organometallic chemistry was explored. It was not until the 1970s that its activity in heterogeneous catalysis was documented.[4] The first homogeneous gold-catalyzed reaction was not reported until 1998, when Teles et al. demonstrated that a well-defined gold(I) catalyst was active in the addition of alcohols to alkynes to form acetals under mild conditions (Scheme 1).[5] In the same line, in 2002 Tanaka's group used the same catalytic system for alkyne hydration, yielding Markovnikov-type products in both reactions.[6] These pioneering discoveries paved the way for the development of homogeneous gold(I) catalysis as a distinct field.

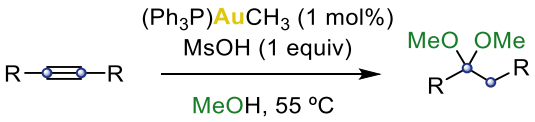

Scheme 1. Earliest homogeneous gold(I)-catalyzed reaction.

1 Guinness World Records. First Olympic Gold Medal. *Guinness World Records*. https://www.guinnessworldrecords.com/world-records/first-olympic-gold-medal (accessed 08/2024).
2 International Olympic Committee. Stockholm 1912 Medal Design. *Olympics*. https://olympics.com/en/olympic-games/stockholm-1912/medal-design (accessed 08/2024)
3 Stephen, A.; Hashmi, K. Homogeneous Catalysis by Gold, *Gold Bull.* **2004**, *37*, 51–65.
4 Bond, G. C.; Sermon, P. A.; Webb, G.; Buchanan, D. A.; Wells, P. B. Hydrogenation over Supported Gold Catalysts, *J. Chem. Soc. Chem. Commun.* **1973**, 444b–4445.
5 Teles, J. H.; Brode, S.; Chabanas, M. Cationic Gold(I) Complexes: Highly Efficient Catalysts for the Addition of Alcohols to Alkynes, *Angew. Chem. Int. Ed.* **1998**, *37*, 1415–1418.
6 Mizushima, E.; Sato, K.; Hayashi, T.; Tanaka, M. Highly Efficient Au^{I}-Catalyzed Hydration of Alkynes, *Angew. Chem.* **2002**, *114*, 4745–4747.

Nowadays, the situation has shifted significantly, and gold catalysis has evolved into a dynamic and thriving area of research.[7] The strong Lewis acidity of cationic gold(I), along with its ability to stabilize cationic reaction intermediates, gives these catalysts unique reactivity towards alkynes, alkenes and allenes under mild conditions. The distinct ability of gold complexes to selectively activate unsaturated bonds has been attributed to relativistic effects.[8] The theoretical foundation for relativistic effects arises from the combination of quantum mechanics and special relativity.[9] These effects increase proportionally with the atomic number and are linked to the acceleration of electrons close to a heavy nucleus. As the atomic number rises, the electrons closest to the nucleus accelerate, increasing their mass. This leads to energetic stabilization and contraction of the *s* and *p* orbitals, whose electrons experience stronger nuclear attraction. Conversely, the *d* and *f* orbitals expand and destabilize due to weaker nuclear attraction on their electrons. This contraction/expansion effect is particularly pronounced in heavy metals with filled 4*f* and 5*d* orbitals, reaching a peak in gold (Figure 2).

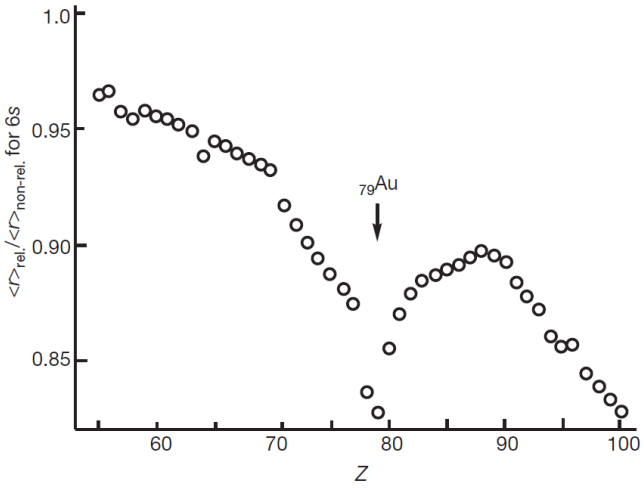

Figure 2. Computationally calculated relativistic contraction of the 6*s* orbital.

The contraction of the 6*s* orbital causes significant expansion of the 5*d* orbital, reducing electron–electron repulsion. This allows the interaction between the filled 5*d* orbital of gold and the filled π orbitals of unsaturated bonds, drawing electron density towards gold and activating these π-bonds for nucleophilic attack due to their increased electrophilicity. Thus, the Lewis acidic character, the highest electronegativity of gold (χ = 2.4) among the transition metals and the aurophilic interactions can be explained by the aforementioned phenomenon of the relativistic

7 a) Hashmi, A. S. K.; Hutchings, G. J. Gold Catalysis, *Angew. Chem. Int. Ed.* **2006**, *45*, 7896–7936. b) Dorel, R.; Echavarren, A. M. Gold(I)-Catalyzed Activation of Alkynes for the Construction of Molecular Complexity, *Chem. Rev.* **2015**, *115*, 9028–9072.

8 a) Gorin, D. J.; Toste, F. D. Relativistic Effects in Homogeneous Gold Catalysis, *Nature* **2007**, *446*, 395–403. b) Pyykkö, P. Theoretical Chemistry of Gold, *Angew. Chem. Int. Ed.* **2004**, *43*, 4412–4456.

9 a) Pitzer, K. S. Relativistic Effects on Chemical Properties, *Acc. Chem. Res.* **1979**, *12*, 271–276. b) McKelvey, D. R. Relativistic Effects on Chemical Properties, *J. Chem. Educ.* **1983**, *60*, 112.

contraction. The aurophilic interactions or aurophilicity stands for the tendency to form Au-Au interactions, in some cases exceeding the binding energies of strong hydrogen bonds.[10]

Apart from this, relativistic effects explain other experimental evidence including the yellow colour of Au. Moreover, the strong relativistic contraction of the 6*s* orbital in gold promotes efficient overlap with ligand orbitals, favouring *s/p* and *s/d* orbital hybridization, enhancing metal-ligand bonding and stabilizing low-coordinate gold complexes, which is exemplified by the preference of gold(I) complexes for the adoption of linear dicoordination geometry.[11]

As a result, gold(I) linear complexes are less likely than other analogous complexes to undergo β-hydride elimination or spontaneous oxidative addition,[12] a crucial step in redox catalytic cycles. This view in changing, as recent discoveries have shown that through rational ligand design, gold(I) complexes can promote oxidative addition.[13] In any case, to date, only square planar gold(III) complexes have been reported to promote β-hydride elimination.[14]

In the early stages of gold catalysis, both gold(I) and gold(III) were primarily used as chloride salts. As an example, in 1931 $AuCl_3$ was described to facilitate the chlorination of benzene in a stoichiometric reaction (Scheme 2).[15]

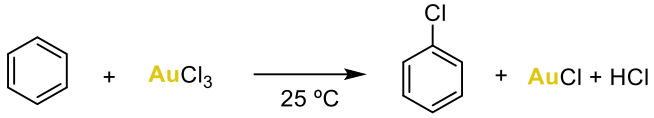

Scheme 2. Chlorination of benzene by treatment with $AuCl_3$.

10 Schmidbaur, H.; Schier, A. A Briefing on Aurophilicity, *Chem. Soc. Rev.* **2008**, *37*, 1931–1951.
11 Gimeno, M. C.; Laguna, A. Three- and Four-Coordinate Gold(I) Complexes, *Chem. Rev.* **1997**, *97*, 511–522.
12 Livendahl, M.; Goehry, C.; Maseras, F.; Echavarren, A. M. Rationale for the Sluggish Oxidative Addition of Aryl Halides to Au(I), *Chem Commun* **2014**, *50*, 1533–1536.
13 See some examples: a) Joost, M.; Zeineddine, A.; Estévez, L.; Mallet−Ladeira, S.; Miqueu, K.; Amgoune, A.; Bourissou, D. Facile Oxidative Addition of Aryl Iodides to Gold(I) by Ligand Design: Bending Turns on Reactivity, *J. Am. Chem. Soc.* **2014**, *136*, 14654–14657. b) Wu, C.-Y.; Horibe, T.; Jacobsen, C. B.; Toste, F. D. Stable Gold(III) Catalysts by Oxidative Addition of a Carbon-Carbon Bond, *Nature* **2015**, *517*, 449–454. c) Guenther, J.; Mallet-Ladeira, S.; Estevez, L.; Miqueu, K.; Amgoune, A.; Bourissou, D. Activation of Aryl Halides at Gold(I): Practical Synthesis of (P,C) Cyclometalated Gold(III) Complexes, *J. Am. Chem. Soc.* **2014**, *136*, 1778–1781. d) Zeineddine, A.; Estévez, L.; Mallet-Ladeira, S.; Miqueu, K.; Amgoune, A.; Bourissou, D. Rational Development of Catalytic Au(I)/Au(III) Arylation Involving Mild Oxidative Addition of Aryl Halides, *Nat. Commun.* **2017**, *8*, 565. e) Cadge, J. A.; Sparkes, H. A.; Bower, J. F.; Russell, C. A. Oxidative Addition of Alkenyl and Alkynyl Iodides to a AuI Complex, *Angew. Chem. Int. Ed.* **2020**, *59*, 6617–6621.
14 See some examples: a) Mankad, N. P.; Toste, F. D. C(Sp3)–F Reductive Elimination from Alkylgold(III) Fluoride Complexes, *Chem. Sci.* **2011**, *3*, 72–76. b) Klatt, G.; Xu, R.; Pernpointner, M.; Molinari, L.; Quang Hung, T.; Rominger, F.; Hashmi, A. S. K.; Köppel, H. Are β-H-Eliminations or Alkene Insertions Feasible Elementary Steps in Catalytic Cycles Involving Gold(I) Alkyl Species or Gold(I) Hydrides?, *Chem. – Eur. J.* **2013**, *19*, 3954–3961. c) Kumar, R.; Krieger, J.-P.; Gómez-Bengoa, E.; Fox, T.; Linden, A.; Nevado, C. The First Gold(III) Formate: Evidence for β-Hydride Elimination, *Angew. Chem. Int. Ed.* **2017**, *56*, 12862–12865.
15 Kharasch, M. S.; Isbell, H. S. The Chemistry of Organic Gold Compounds. III. Direct Introduction of Gold into the Aromatic Nucleus. *J. Am. Chem. Soc*. **1931**, *53*, 3053–3059.

However, it quickly became apparent that ligands play a crucial role in modulating the reactivity and selectivity of gold(I) catalyst due to the high degree of covalency in bonding. The nature of the complex can be significantly influenced by the ligand electronic effects to a higher extent than by the steric effects.[16] This understanding led to the design and synthesis of ligands to achieve the desired reactivity successfully.

As a rule, complexes with highly donating *N*-heterocyclic carbenes (NHC) as ancillary ligands are less electrophilic, while those with less donating phosphite ligands produce highly electrophilic catalysts (Figure 3). Additionally, gold(I) complexes with bulky phosphine ligands, such as dialkyl biarylphosphines, exhibit intermediate electrophilicity and have been demonstrated to be the most suitable in many catalytic reactions.[17]

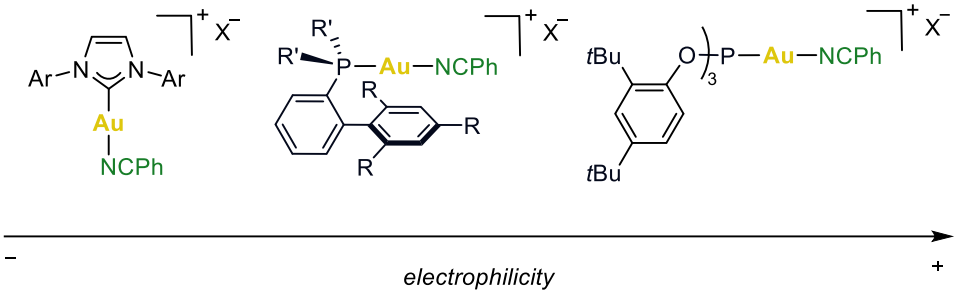

Figure 3. Ancillary ligand effect in the electrophilicity degree of gold(I) complexes.

The preparation of neutral gold(I) chloride complexes [LAuCl] proceeds via the treatment of the desired ligand with (dimethylsulfide)gold(I) chloride ($Me_2S{\cdot}AuCl$) (Scheme 3).

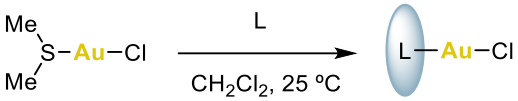

Scheme 3. Common synthesis of neutral LAuCl complexes.

Despite of the fact that neutral gold(I) complexes have been prominently used in the developed catalytic applications, the need to activate them by creating a formal vacancy of coordination is essential. This activation requires the abstraction of the chloride or halide present in the complex so that the given substrate coordinates to gold via an associative mechanism.[18] Active cationic

16 Chintawar, C. C.; Yadav, A. K.; Kumar, A.; Sancheti, S. P.; Patil, N. T. Divergent Gold Catalysis: Unlocking Molecular Diversity through Catalyst Control, *Chem. Rev.* **2021**, *121*, 8478–8558.

17 Zuccarello, G.; Zanini, M.; Echavarren, A. M. Buchwald-Type Ligands on Gold(I) Catalysis, *Isr. J. Chem.* **2020**, *60*, 360–372.

18 a) Amijs, C. H. M.; López-Carrillo, V.; Raducan, M.; Pérez-Galán, P.; Ferrer, C.; Echavarren, A. M. Gold(I)-Catalyzed Intermolecular Addition of Carbon Nucleophiles to 1,5- and 1,6-Enynes, *J. Org. Chem.* **2008**, *73*, 7721–7730. b) Schmidbaur, H.; Schier, A. Gold H2-Coordination to Unsaturated and Aromatic Hydrocarbons: The Key Step in Gold-Catalyzed Organic Transformations, *Organometallics* **2010**, *29*, 2–23. d) Nieto-Oberhuber, C.; López, S.; Muñoz, M. P.; Cárdenas, D. J.; Buñuel, E.; Nevado, C.; Echavarren, A. M. Divergent Mechanisms for the Skeletal Rearrangement and [2+2] Cycloaddition of Enynes Catalyzed by Gold, *Angew. Chem. Int. Ed Engl.* **2005**, *44*, 6146–6148.

gold(I) complexes are typically generated in situ employing a halide scavenger like silver[19] or, less commonly copper[20] salts (Scheme 4). Nonetheless, this procedure can lead to side reactions like to formation of much less reactive chloride-bridged dinuclear gold(I) species [LAuClAu]X (Scheme 4).[21] Thus, the use of weakly coordinating counteranions such as OTf^- or NTf_2^- or the synthesis of cationic complexes in which gold(I) is bound to a neutral ligand like acetonitrile or benzonitrile, being $X^- = SbF_6^-$, BF_4^-, PF_6^-.

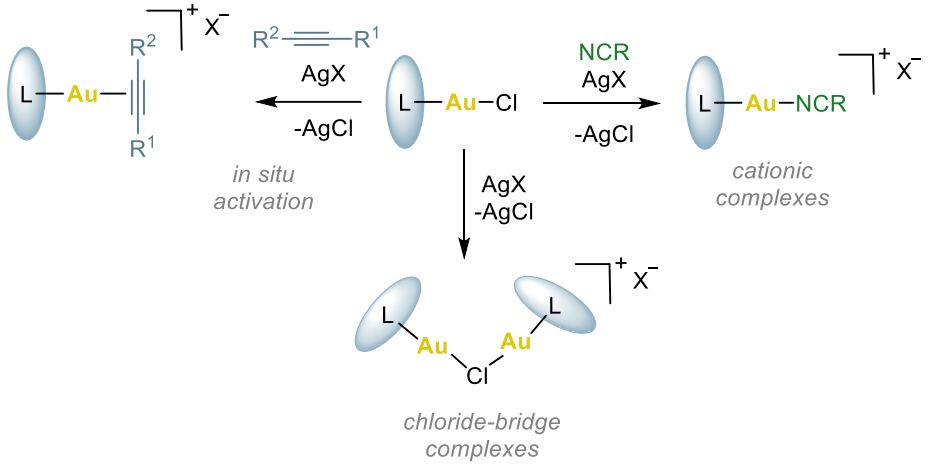

Scheme 4. Activation of neutral [LAuCl] complexes using different strategies.

Gold(I)-Catalyzed Cycloisomerization of Enynes

Gold(I) complexes selectively activate alkynes in the presence of alkenes or other functional groups, giving rise to (η^2-alkyne)gold(I) **1** intermediates, that are highly reactive towards nucleophilic attack (Scheme 5).

19 a) Partyka, D. V.; Robilotto, T. J.; Zeller, M.; Hunter, A. D.; Gray, T. G. Dialkylbiarylphosphine Complexes of Gold(I) Halides. Gold−Aryl π-Interactions in the Solid State, *Organometallics* **2008**, *27*, 28–32. b) Pérez-Galán, P.; Delpont, N.; Herrero-Gómez, E.; Maseras, F.; Echavarren, A. M. Metal–Arene Interactions in Dialkylbiarylphosphane Complexes of Copper, Silver, and Gold, *Chem. – Eur. J.* **2010**, *16*, 5324–5332. c) Fortman, G. C.; Nolan, S. P. Solution Calorimetric Study of Ligand Exchange Reactions in the [Au(L)Cl] System (L = Phosphine and Phosphite), *Organometallics* **2010**, *29*, 4579–4583.

20 Guérinot, A.; Fang, W.; Sircoglou, M.; Bour, C.; Bezzenine-Lafollée, S.; Gandon, V. Copper Salts as Additives in Gold(I)-Catalyzed Reactions, *Angew. Chem. Int. Ed.* **2013**, *52*, 5848–5852.

21 a) Zhu, Y.; Day, C. S.; Zhang, L.; Hauser, K. J.; Jones, A. C. A Unique Au–Ag–Au Triangular Motif in a Trimetallic Halonium Dication: Silver Incorporation in a Gold(I) Catalyst, *Chem. – Eur. J.* **2013**, *19*, 12264–12271. b) Homs, A.; Escofet, I.; Echavarren, A. M. On the Silver Effect and the Formation of Chloride-Bridged Digold Complexes, *Org. Lett.* **2013**, *15*, 5782–5785. c) Lu, Z.; Han, J.; Hammond, G. B.; Xu, B. Revisiting the Influence of Silver in Cationic Gold Catalysis: A Practical Guide, *Org. Lett.* **2015**, *17*, 4534–4537. d) Zhdanko, A.; Maier, M. E. Explanation of "Silver Effects" in Gold(I)-Catalyzed Hydroalkoxylation of Alkynes, *ACS Catal.* **2015**, *5*, 5994–6004.

Typically, the reaction of **1** with nucleophiles occurs in an *anti*-fashion manner, following Markovnikov regioselectivity and resulting in the *trans*-alkenyl gold(I) complex **2**.[22]

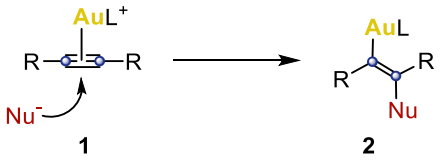

Scheme 5. Nucleophilic attack to (η^2-alkyne)gold(I) species.

The rise of gold catalysis was associated with the cyclizations of 1,*n*-enynes, where the access to increased molecular complexity structures is enabled by gold in a single step and under mild conditions.[23] For the majority of these processes catalyzed by gold, excellent atom economy is shown. Transformations involving 1,6-enynes have been thoroughly investigated (Scheme 6).

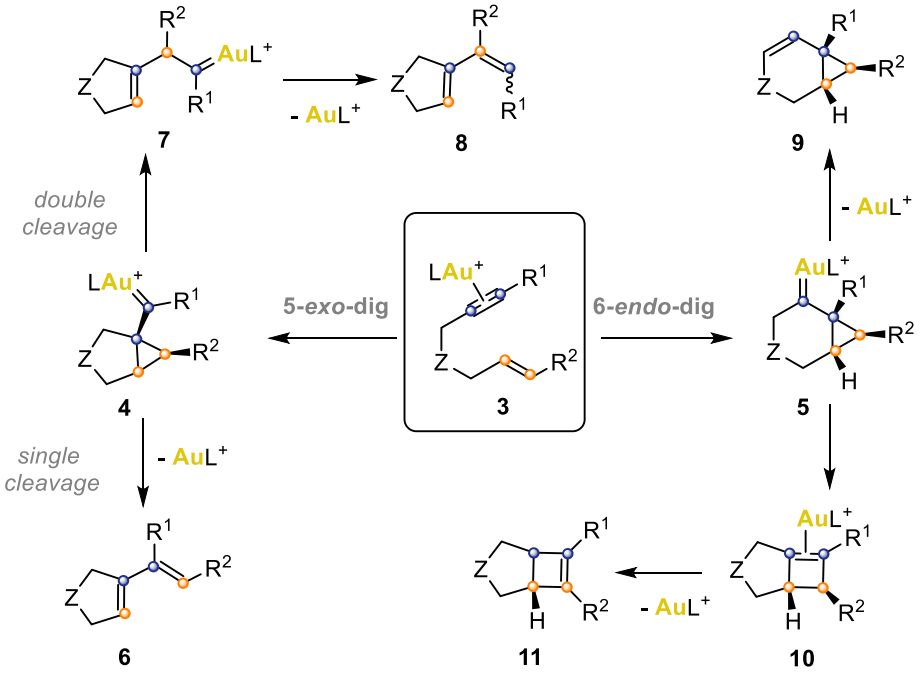

Scheme 6. Primary routes for gold(I)-catalyzed cycloisomerization of 1,6-enynes.

22 a) García-Mota, M.; Cabello, N.; Maseras, F.; Echavarren, A. M.; Pérez-Ramírez, J.; Lopez, N. Selective Homogeneous and Heterogeneous Gold Catalysis with Alkynes and Alkenes: Similar Behavior, Different Origin, *ChemPhysChem* **2008**, *9*, 1624–1629. b) Hashmi, A. S. K.; Weyrauch, J. P.; Frey, W.; Bats, J. W. Gold Catalysis: Mild Conditions for the Synthesis of Oxazoles from N-Propargylcarboxamides and Mechanistic Aspects, *Org. Lett.* **2004**, *6*, 4391–4394. c) Kennedy-Smith, J. J.; Staben, S. T.; Toste, F. D. Gold(I)-Catalyzed Conia-Ene Reaction of β-Ketoesters with Alkynes, *J. Am. Chem. Soc.* **2004**, *126*, 4526–4527.

23 a) Jiménez-Núñez, E.; Echavarren, A. M. Gold-Catalyzed Cycloisomerizations of Enynes: A Mechanistic Perspective, *Chem. Rev.* **2008**, *108*, 3326–3350. b) Fürstner, A. Gold and Platinum Catalysis—a Convenient Tool for Generating Molecular Complexity, *Chem. Soc. Rev.* **2009**, *38*, 3208–3221. c) Obradors, C.; M. Echavarren, A. Intriguing Mechanistic Labyrinths in Gold(I) Catalysis, *Chem. Commun.* **2014**, *50*, 16–28. d) Obradors, C.; Echavarren, A. M. Gold-Catalyzed Rearrangements and Beyond, *Acc. Chem. Res.* **2014**, *47*, 902–912. e) Fensterbank, L.; Malacria, M. Molecular Complexity from Polyunsaturated Substrates: The Gold Catalysis Approach, *Acc. Chem. Res.* **2014**, *47*, 953–965. f) Dorel, R.; Echavarren, A. M. Gold-Catalyzed Reactions via Cyclopropyl Gold Carbene-like Intermediates, *J. Org. Chem.* **2015**, *80*, 7321–7332.

First of all, (η^2-alkyne)gold(I) complex **3** can undergo 5-*exo*-dig or 6-*endo*-dig intramolecular nucleophilic attack by the alkene moiety, leading to **4** or **5** cyclopropyl gold(I) carbenes respectively. [16d,24] The substituents of the enyne, the ancillary ligand and the reaction conditions will mark the evolution of the cyclopropyl gold(I) carbenes towards the different pathways.[25] Skeletal rearrangements occur predominantly after the formation of intermediate **4**, via single or double cleavage. The single cleavage consists on the 1,3-migration of the alkene's terminal carbon to the alkyne's terminal carbon, forming 1,3-dienes **6**.[26] The double-cleavage rearrangement involves the formal insertion of the alkene's terminal carbon between the two carbons of the alkyne, producing gold(I) carbenes **7**, that after 1,2-*H* shift and protodeauration, yield substituted dienes **8**. Alternatively, following the 6-*endo*-dig route, the opening of the cyclopropane ring in intermediate **5** generates bicyclo[4.1.0]hept-2-ene derivative **9** after a 1,2-*H* shift and protodeauration. In contrast, the ring expansion of **5** leads to the formation of (η^2-cyclobutene)gold(I) complexes of type **10**, which can isomerize to form cyclobutenes **11** (Scheme 6).

The abovementioned processes take place in the absence of nucleophiles. With the addition of an external nucleophile, the range of possibilities becomes broader. Due to the ability to perform gold(I)-catalyzed reactions in air and to the broad functional group tolerance, a wide set of heteronucleophiles have been used in intra- and intermolecular gold(I)-catalyzed reactions.[22a,27]

---

24 a) Nieto-Oberhuber, C.; Muñoz, M. P.; Buñuel, E.; Nevado, C.; Cárdenas, D. J.; Echavarren, A. M. Cationic Gold(I) Complexes: Highly Alkynophilic Catalysts for the Exo- and Endo-Cyclization of Enynes, *Angew. Chem. Int. Ed Engl.* **2004**, *43*, 2402–2406. b) Ferrer, C.; Raducan, M.; Nevado, C.; Claverie, C. K.; Echavarren, A. M. Missing Cyclization Pathways and New Rearrangements Unveiled in the Gold(I) and Platinum(II)-Catalyzed Cyclization of 1,6-Enynes, *Tetrahedron* **2007**, *63*, 6306–6316. c) Soriano, E.; Marco-Contelles, J. Mechanistic Insights on the Cycloisomerization of Polyunsaturated Precursors Catalyzed by Platinum and Gold Complexes, *Acc. Chem. Res.* **2009**, *42*, 1026–1036. d) Escribano-Cuesta, A.; Pérez-Galán, P.; Herrero-Gómez, E.; Sekine, M.; Braga, A. A. C.; Maseras, F.; Echavarren, A. M. The Role of Cyclobutenes in Gold(i)-Catalysed Skeletal Rearrangement of 1,6-Enynes, *Org. Biomol. Chem.* **2012**, *10*, 6105.

25 Mattalia, J.-M.; Nava, P. Gold-Catalyzed Cycloisomerizations of 1,6-Enynes. A Computational Study, *J. Organomet. Chem.* **2014**, *749*, 335–342.

26 Cabello, N.; Jiménez-Núñez, E.; Buñuel, E.; Cárdenas, D. J.; Echavarren, A. M. On the Mechanism of the Puzzling "Endocyclic" Skeletal Rearrangement of 1,6-Enynes, *Eur. J. Org. Chem.* **2007**, *2007*, 4217–4223.

27 For some examples, see: a) Reetz, M. T.; Sommer, K. Gold-Catalyzed Hydroarylation of Alkynes, *Eur. J. Org. Chem.* **2003**, *2003*, 3485–3496Nevado, C.; Echavarren, A. M. Transition Metal-Catalyzed Hydroarylation of Alkynes, *Synthesis* **2005**, *2005*, 167–182. b) Hashmi, A. S. K.; Haufe, P.; Schmid, C.; Rivas Nass, A.; Frey, W. Asymmetric Rhodium-Catalyzed Hydrogenation Meets Gold-Catalyzed Cyclization: Enantioselective Synthesis of 8-Hydroxytetrahydroisoquinolines, *Chem. – Eur. J.* **2006**, *12*, 5376–5382. c) Nieto-Oberhuber, C.; Muñoz, M. P.; López, S.; JiménezNúñez, E.; Nevado, C.; Herrero-Gómez, E.; Raducan, M.; Echavarren, A. M. *Chem. Eur. J.* **2006**, *12*, 1677–1693; Corrigendum: *Chem. Eur. J.* **2008**, *14*, 5096. d) Ferrer, C.; Echavarren, A. M. Gold-Catalyzed Intramolecular Reaction of Indoles with Alkynes: Facile Formation of Eight-Membered Rings and an Unexpected Allenylation, *Angew. Chem.* **2006**, *118*, 1123–1127.

Computational Chemistry Applied to Gold Catalysis

Alongside the advancement of new synthetic methodologies utilizing gold catalysis, there remains a need to understand the often highly intriguing reaction mechanisms involved in these processes. In the 1980s, the use of computational techniques to analyze the reactivity of transition-metal complexes was still in its infancy. Over the past few decades, computational chemistry has become an invaluable tool for modelling, explaining, and predicting the properties of gold(I)-catalyzed reactions.[6b,28] Among the developed methodologies, quantum mechanical calculations have become the most precise techniques for representing the electronic structure of complex molecules in the fields of organometallic chemistry and catalysis.[29] Quantum Mechanics (QM) can describe small systems with high accuracy, while for larger systems, such as proteins, Molecular Mechanics (MM) or hybrid models combining QM/MM are the most effective approaches.

Unlike MM methods, QM methods enable the study of the electronic properties of the systems, as well as chemical processes that involve electronic changes, such as reactions where bonds are broken or formed. The trade-off is a significant increase in the computational cost of the calculations, which also results in limitations on the size of the systems that can be studied. There are different levels of approximation that allow the study of large chemical systems. The energy and molecular properties are determined using the principles of quantum mechanics, specifically the Schrödinger equation (Eq 1) after applying the Born−Oppenheimer approximation, which views the motion of the electrons as much faster than the nuclei, and therefore as negligible.[30]

(Eq 1)

$$H\Psi = E\Psi$$

H is the Hamiltonian, Ψ is the wavefunction that depends on the coordinates of the electrons and E is the potential energy.

The concept of Potential Energy Surface (PES) rests on the Born-Oppenheimer approximation. The capability to identify products and reactants on the PES, along with the transition state structures, is one of the most significant accomplishments in computational chemistry. The PES can in principle be obtained from solving Eq 1 to any degree of accuracy. The Schrödinger equation cannot be solved in an exact manner for multielectron systems, thus simplifications in

28 Pyykkö, P. Theoretical Chemistry of Gold. III, *Chem. Soc. Rev.* **2008**, *37*, 1967–1997.
29 a) Ziegler, T.; Autschbach, J. Theoretical Methods of Potential Use for Studies of Inorganic Reaction Mechanisms, *Chem. Rev.* **2005**, *105*, 2695–2722. b) Balcells, D.; Clot, E.; Macgregor, S. A.; Maseras, F.; Perrin, L. A Career in Catalysis: Odile Eisenstein, *ACS Catal.* **2019**, *9*, 10375–10388.
30 Levine, I. N. *Quantum Chemistry*, *Quantum Chemistry*, Seventh edition.; Pearson: Boston, 2014.

this regard are needed. These simplifications define the distinct QM methods. The most used ones are wavefunction (WFN) methods and density functional theory (DFT) methods

- Wavefunction methods: Wavefunction methods: They are based in the resolution of the Schrödinger equation. The Hartree-Fock (HF) method assumes that the wavefunction can be expressed as an antisymmetrized product of monolectronic functions, the molecular orbitals. Usually, it does not yield accurate results for transition metal complexes because it does not include correlation energy. One example of post-HF method is the coupled cluster (CC) approach. CCSD(T) (coupled-cluster with single and double excitations and perturbative triples correction) is a widely popular ab initio method, although its application is mostly limited to benchmark studies on very small systems due to its high computational cost.[31] To address this, significant efforts have been made to develop cost-effective methods that introduce approximations into ab initio techniques without sacrificing accuracy. Recently, Neese's group introduced the Domain-based Local Pair Natural Orbital Method (DLPNO), a correlation approach that leverages the locality of electron correlation through Pair Natural Orbitals (PNOs).[32] Utilizing PNOs in correlated calculations greatly reduces computational costs while maintaining minimal errors. The addition of perturbative treatment of triple excitations led to the DLPNO-CCSD(T) model, which provides highly accurate energies in a faster and more efficient manner. This method has been recently used for benchmarking the performance of density functionals,[33] like in this Thesis in Chapter II.

- Density Functional Theory (DFT): This method applies an alternative approach, focusing on the electronic density rather than on the wavefunction. It is based on a theorem by Kohn and Hohenberg, which states that the ground state energy is uniquely determined by the electron density.[34] However, the exact functional relationship between the energy and the electron density is not fully known, so the effectiveness of DFT relies on finding approximate yet accurate relationships between them based on physical principles. Kohn and Sham demonstrated that molecular orbitals can be also applied to the obtention of the DFT density.[35] Most density functionals differ in how they handle the exchange-correlation

31 Pitoňák, M.; Holka, F.; Neogrády, P.; Urban, M. Optimized Virtual Orbitals for Correlated Calculations: Towards Large Scale CCSD(*T*) Calculations of Molecular Dipole Moments and Polarizabilities, *J. Mol. Struct. THEOCHEM* **2006**, *768*, 79–89.

32 a) Riplinger, C.; Sandhoefer, B.; Hansen, A.; Neese, F. Natural Triple Excitations in Local Coupled Cluster Calculations with Pair Natural Orbitals, *J. Chem. Phys.* **2013**, *139*, 134101. b) Sparta, M.; Neese, F. Chemical Applications Carried out by Local Pair Natural Orbital Based Coupled-Cluster Methods, *Chem. Soc. Rev.* **2014**, *43*, 5032–5041.

33 Iron, M. A.; Janes, T. Evaluating Transition Metal Barrier Heights with the Latest Density Functional Theory Exchange-Correlation Functionals: The MOBH35 Benchmark Database, *J. Phys. Chem. A* **2019**, *123*, 3761–3781.

34 Hohenberg, P.; Kohn, W. Inhomogeneous Electron Gas, *Phys. Rev.* **1964**, *136*, B864–B871.

35 Kohn, W. Self-Consistent Equations Including Exchange and Correlation Effects, *Phys. Rev.* **1965**, *140*, A1133–A1138.

contributions. In order to evaluate the relative quality of functionals, erdew proposed some years ago a hierarchy of functionals that he labelled as a ladder.[36]

The lowest level of this series contains the local density approximation (LDA) functionals, in which the energy depends exclusively on the electron density. They are usually not suitable for the modelling of transition-metal catalyzed reactions.

The second rung on the ladder is constituted by the generalised gradient approximation functionals (GGA). This method considers the energy depends on the electron density and the gradient of this density. Common GGA methods include Becke´s functional BP86.[37] So far, the aforementioned functionals are considered as pure functionals, not containing any percentage of Hartree-Fock energy.

The GGA functionals can be further sophisticated by the introduction of terms involving the Hartree-Fock exchange energy. These are the hybrid functionals. One of the most popular and commonly used is B3LYP, which is based on Becke's exchange functional[36] and the Lee-Yang-Parr correlation functional.[38] B3LYP has been widely used for mechanistic studies in gold(I)-catalyzed reactions.[22,39]

Overall, in the field of transition metal catalysis, which is the focus of this manuscript, DFT methods have played a crucial role in providing mechanistic insights into various processes by balancing accuracy and computational cost.[40] Combining experimental and computational approaches can be highly effective in solving mechanistic problems.

36 Perdew, J. P.; Schmidt, K. Jacob's Ladder of Density Functional Approximations for the Exchange-Correlation Energy, *AIP Conf. Proc.* **2001**, *577*, 1–20.

37 Becke, A. D. Density-Functional Exchange-Energy Approximation with Correct Asymptotic Behavior, *Phys. Rev. A* **1988**, *38*, 3098–3100.

38 Lee, C.; Yang, W.; Parr, R. G. Development of the Colle-Salvetti Correlation-Energy Formula into a Functional of the Electron Density, *Phys. Rev. B* **1988**, *37*, 785–789.

39 For some examples, see: a) Nieto-Oberhuber, C.; López, S.; Muñoz, M. P.; Cárdenas, D. J.; Buñuel, E.; Nevado, C.; Echavarren, A. M. Divergent Mechanisms for the Skeletal Rearrangement and [2+2] Cycloaddition of Enynes Catalyzed by Gold, *Angew. Chem. Int. Ed Engl.* **2005**, *44*, 6146–6148. b) Nieto-Oberhuber, C.; Pérez-Galán, P.; Herrero-Gómez, E.; Lauterbach, T.; Rodríguez, C.; López, S.; Bour, C.; Rosellón, A.; Cárdenas, D. J.; Echavarren, A. M. Gold(I)-Catalyzed Intramolecular [4+2] Cycloadditions of Arylalkynes or 1,3-Enynes with Alkenes: Scope and Mechanism, *J. Am. Chem. Soc.* **2008**, *130*, 269–279. c) Nieto-Oberhuber, C.; Muñoz, M. P.; López, S.; Jiménez-Núñez, E.; Nevado, C.; Herrero-Gómez, E.; Raducan, M.; Echavarren, A. M. Gold(I)-Catalyzed Cyclizations of 1,6-Enynes: Alkoxycyclizations and Exo/Endo Skeletal Rearrangements, *Chem. – Eur. J.* **2006**, *12*, 1677–1693. d) Lee, Y. T.; Kang, Y. K.; Chung, Y. K. Au(I)-Catalyzed Cycloisomerization Reaction of Amide- or Ester-Tethered 1,6-Enynes to Bicyclo[3.2.0]Hept-6-En-2-Ones, *J. Org. Chem.* **2009**, *74*, 7922–7934. e) García-Morales, C.; Pei, X.-L.; Sarria Toro, J. M.; Echavarren, A. M. Direct Observation of Aryl Gold(I) Carbenes That Undergo Cyclopropanation, C−H Insertion, and Dimerization Reactions, *Angew. Chem. Int. Ed.* **2019**, *58*, 3957–3961.

40 Harvey, J. N.; Himo, F.; Maseras, F.; Perrin, L. Scope and Challenge of Computational Methods for Studying Mechanism and Reactivity in Homogeneous Catalysis, *ACS Catal.* **2019**, *9*, 6803–6813.

With the aim of obtaining an accurate description of the systems, there are two missing factors that need to be considered for the model: dispersion and solvation.

It is well-known that DFT methods do not accurately describe dispersion interactions, particularly for weak non-covalent interactions like van der Waals interactions. This limitation can be problematic when dispersion interactions play a significant role in the chemical system being studied. To address this issue, Grimme and colleagues developed an approach that incorporates dispersion interactions into DFT.[41]

Additionally, the reaction medium (solvent) can significantly influence chemical reactivity, making the inclusion of solvent a crucial factor in the optimization process. From a computational standpoint, the stabilization of intermediates and transition states can dramatically alter mechanistic pathways; having an increased effect when charged-separated species or anionic/cationic species are involved in the gold(I)-catalyzed reactions. The stabilization of the species in solution differs significantly to that in vacuum. Fortunately, tools have been developed to incorporate solvation effects into DFT calculations through two main approaches:

- Explicit Models: These models consist in explicitly modelling a certain number of solvent molecules to simulate the actual concentration of the solute in the solvent. While this approach allows for the detailed description of solute-solvent interactions, it is not feasible for our systems of interest due to the need to introduce large numbers of molecules, and consider their conformational arrangements, which leads to a high computational cost.

- Implicit Models: These models treat the solvent as a continuous medium, with the solute placed inside a cavity defined by a fixed dielectric constant. Several continuum solvation models are available for calculating energies in solution. One of the most used implicit solvation models is the Polarizable Continuum Model (PCM),[42] in which the solvent is represented as a polarizable continuum. Furthermore, the Solvation Model based on Density (SMD),[43] developed by Truhlar and coworkers in 2009, incorporates several additional parameters compared to PCM. These include two parameters related to hydrogen bond donor and acceptor abilities, one related to atomic surface tension, and two others concerning

41 a) Grimme, S.; Antony, J.; Ehrlich, S.; Krieg, H. A Consistent and Accurate Ab Initio Parametrization of Density Functional Dispersion Correction (DFT-D) for the 94 Elements H-Pu, *J. Chem. Phys.* **2010**, *132*, 154104. b) Grimme, S. Density Functional Theory with London Dispersion Corrections, *WIREs Comput. Mol. Sci.* **2011**, *1*, 211–228.

42 Cossi, M.; Barone, V.; Cammi, R.; Tomasi, J. Ab Initio Study of Solvated Molecules: A New Implementation of the Polarizable Continuum Model, *Chem. Phys. Lett.* **1996**, *255*, 327–335.

43 Marenich, A. V.; Cramer, C. J.; Truhlar, D. G. Universal Solvation Model Based on Solute Electron Density and on a Continuum Model of the Solvent Defined by the Bulk Dielectric Constant and Atomic Surface Tensions, *J. Phys. Chem. B* **2009**, *113*, 6378–6396.

aromatic and halogen components. This model, which is also widely used, is considered more suitable for solvents with more directional or localized interactions.

UNIVERSITAT ROVIRA I VIRGILI
MECHANISTIC STUDIES ON GOLD(I) AND GOLD(III) CATALYTIC TRANSFORMATIONS
Isabel Arranz De La Calle

UNIVERSITAT ROVIRA I VIRGILI
MECHANISTIC STUDIES ON GOLD(I) AND GOLD(III) CATALYTIC TRANSFORMATIONS
Isabel Arranz De La Calle

Chapter I

Design, Synthesis and Kinetic Studies of Chiral Pyrrolidine-Based Ligands

UNIVERSITAT ROVIRA I VIRGILI
MECHANISTIC STUDIES ON GOLD(I) AND GOLD(III) CATALYTIC TRANSFORMATIONS
Isabel Arranz De La Calle

1.1 Introduction

1.1.1 Asymmetric gold(I) catalysis

In contrast to the extensive range of gold(I)-catalyzed transformations reported over the past twenty years, the development of their enantioselective counterparts has been much slower.[1] The primary challenges to face are the preferred linear dicoordination adopted by gold(I), which positions the ancillary chiral ligand and the substrate opposite to each other, resulting in poor enantioinduction. Additionally, gold(I)-catalyzed addition reactions to unsaturated functional groups such as alkynes occur through outer-sphere mechanisms, making it more difficult to develop enantioselective processes.

Ligand design has been essential for the swift advancement of gold catalysis. Among the conceptual designs that have been proven successful in enantioselective gold(I) catalysis,[2] there is one of the most studied systems, that relies on the use of axially chiral binuclear gold(I) complexes, with ligands such as bisphosphines (Figure 1.1a).[3] Additionally, monodentate phosphoramidite ligands (Figure 1.1b)[4] have been used as highly modular and readily available structures, in which the substituents on the backbone and amine moieties are the ones providing the required chiral environment. Finally, the synergistic use of chiral counteranions, along with chiral or nonchiral gold(I) complexes (Figure 1.1c),[5] allows the formation of tight ion pairs placing in this way the source of chirality close to the reactive center.

---

1 a) Widenhoefer, R. A. Recent Developments in Enantioselective Gold(I) Catalysis, *Chem. – Eur. J.* **2008**, *14*, 5382–5391. b) Sengupta, S.; Shi, X. Recent Advances in Asymmetric Gold Catalysis, *ChemCatChem* **2010**, *2*, 609–619. c) Wang, Y.-M.; Lackner, A. D.; Toste, F. D. Development of Catalysts and Ligands for Enantioselective Gold Catalysis, *Acc. Chem. Res.* **2014**, *47*, 889–901. d) Escofet, I.; Zuccarello, G.; Echavarren, A. M. Chapter One - Gold-Catalyzed Enantioselective Cyclizations and Cycloadditions, Chapter One - Gold-Catalyzed Enantioselective Cyclizations and Cycloadditions. *Adv. Organomet. Chem*. **2022**, *77*, 1–42.

2 Zuccarello, G.; Escofet, I.; Caniparoli, U.; Echavarren, A. M. New-Generation Ligand Design for the Gold-Catalyzed Asymmetric Activation of Alkynes, *ChemPlusChem* **2021**, *86*, 1283–1296.

3 a) Ito, Yoshihiko.; Sawamura, Masaya.; Hayashi, Tamio. Catalytic Asymmetric Aldol Reaction: Reaction of Aldehydes with Isocyanoacetate Catalyzed by a Chiral Ferrocenylphosphine-Gold(I) Complex, *J. Am. Chem. Soc.* **1986**, *108*, 6405–6406. b) Luzung, M. R.; Mauleón, P.; Toste, F. D. Gold(I)-Catalyzed [2 + 2]-Cycloaddition of Allenenes, *J. Am. Chem. Soc.* **2007**, *129*, 12402–12403.

4 a) Teller, H.; Corbet, M.; Mantilli, L.; Gopakumar, G.; Goddard, R.; Thiel, W.; Fürstner, A. One-Point Binding Ligands for Asymmetric Gold Catalysis: Phosphoramidites with a TADDOL-Related but Acyclic Backbone, *J. Am. Chem. Soc.* **2012**, *134*, 15331–15342. b) Alonso, I.; Trillo, B.; López, F.; Montserrat, S.; Ujaque, G.; Castedo, L.; Lledós, A.; Mascareñas, J. L. Gold-Catalyzed [4C+2C] Cycloadditions of Allenedienes, Including an Enantioselective Version with New Phosphoramidite-Based Catalysts: Mechanistic Aspects of the Divergence between [4C+3C] and [4C+2C] Pathways, *J. Am. Chem. Soc.* **2009**, *131*, 13020–13030.

5 a) Hamilton, G. L.; Kang, E. J.; Mba, M.; Toste, F. D. A Powerful Chiral Counterion Strategy for Asymmetric Transition Metal Catalysis, *Science* **2007**, *317*, 496–499. b) LaLonde, R. L.; Wang, Z. J.; Mba, M.; Lackner, A. D.; Toste, F. D. Gold(I)-Catalyzed Enantioselective Synthesis of Pyrazolidines, Isoxazolidines, and Tetrahydrooxazines, *Angew. Chem. Int. Ed Engl.* **2010**, *49*, 598–601.

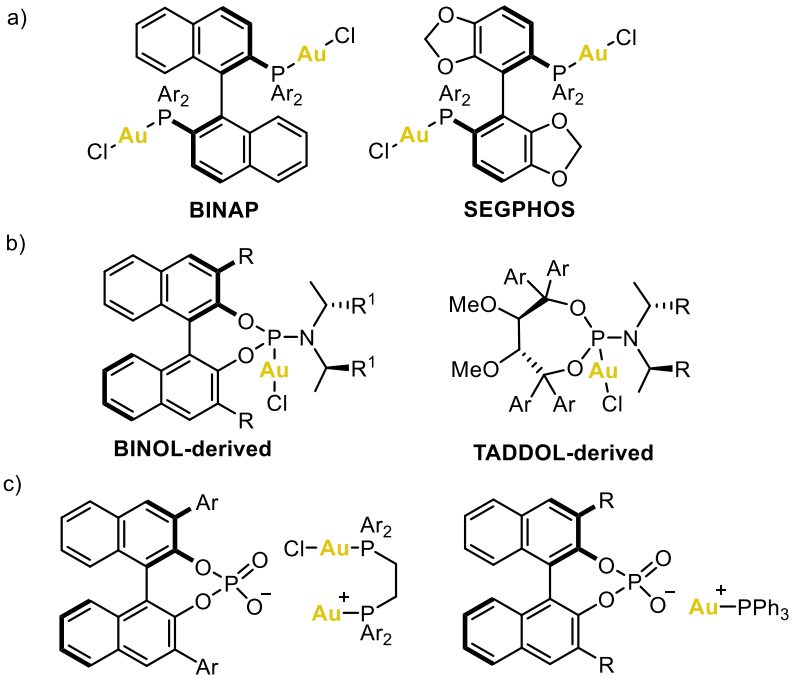

Figure 1.1. Various ligand design strategies in asymmetric gold(I) catalysis. a) Bisphosphines as binuclear complexes. b) Monodentate phosphoramidites. c) Non-chiral gold(I) complexes with phosphate chiral counteranions.

Recent advancements have focused on new concepts for enantioinduction through substrate fixation or preorientation via non-covalent interactions. For instance, helically chiral phosphine ligands attached to gold(I) (Figure 1.2a),[6] or systems with chiral sulfinamides in phosphine ligands which utilize non-covalent hydrogen bonding with substrates (Figure 1.2b).[7]

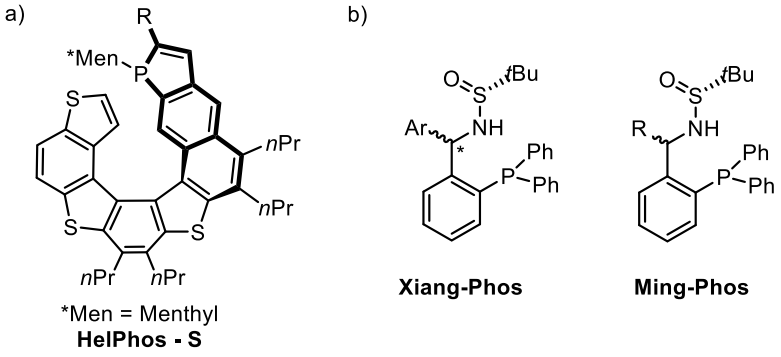

6 Yavari, K.; Aillard, P.; Zhang, Y.; Nuter, F.; Retailleau, P.; Voituriez, A.; Marinetti, A. Helicenes with Embedded Phosphole Units in Enantioselective Gold Catalysis, *Angew. Chem. Int. Ed.* **2014**, *53*, 861–865.

7 Zhang, Z.-M.; Chen, P.; Li, W.; Niu, Y.; Zhao, X.-L.; Zhang, J. A New Type of Chiral Sulfinamide Monophosphine Ligands: Stereodivergent Synthesis and Application in Enantioselective Gold(I)-Catalyzed Cycloaddition Reactions, *Angew. Chem. Int. Ed.* **2014**, *53*, 4350–4354. b) Wang, Y.; Zhang, Z.-M.; Liu, F.; He, Y.; Zhang, J. Ming-Phos/Gold(I)-Catalyzed Diastereo- and Enantioselective Synthesis of Indolyl-Substituted Cyclopenta[c]Furans, *Org. Lett.* **2018**, *20*, 6403–6406. c) Zhang, P.-C.; Wang, Y.; Zhang, Z.-M.; Zhang, J. Gold(I)/Xiang-Phos-Catalyzed Asymmetric Intramolecular Cyclopropanation of Indenes and Trisubstituted Alkenes, *Org. Lett.* **2018**, *20*, 7049–7052.

Figure 12.2. Chiral monophosphines used in asymmetric gold(I) catalysis.

Additional methods involve using chiral NHC-ligands bound to gold(I)[8] or employing supramolecular structures like gold(I) cavitands, which effectively encapsulate the substrates.[9]

1.1.2 Chiral pyrrolidinyl-biphenyl phosphine gold(I) complexes

Recently in 2019, our group developed a new family of chiral gold(I) complexes, based on a modified JohnPhos-type ligand (bulky biarylphosphine ligands developed by Buchwald for Pd-catalyzed couplings)[10] bearing a distal C_2-symmetric *trans*-2,5-diaryl pyrrolidines (Figure 1.3).[11] Through this innovative design, the chiral environment was placed next to the reactive center in the well-known outer-sphere mechanisms taking place in gold(I)-catalyzed transformations. The bulkiness of the disubstituted phosphine restricts the rotation around the C_{aryl}–P bond, positioning the P–Au–Cl axis towards the biphenyl scaffold that carries the chiral pyrrolidine; and therefore ensures that the substrate remains close to the ligand, enabling the desired facial discrimination during the reaction.

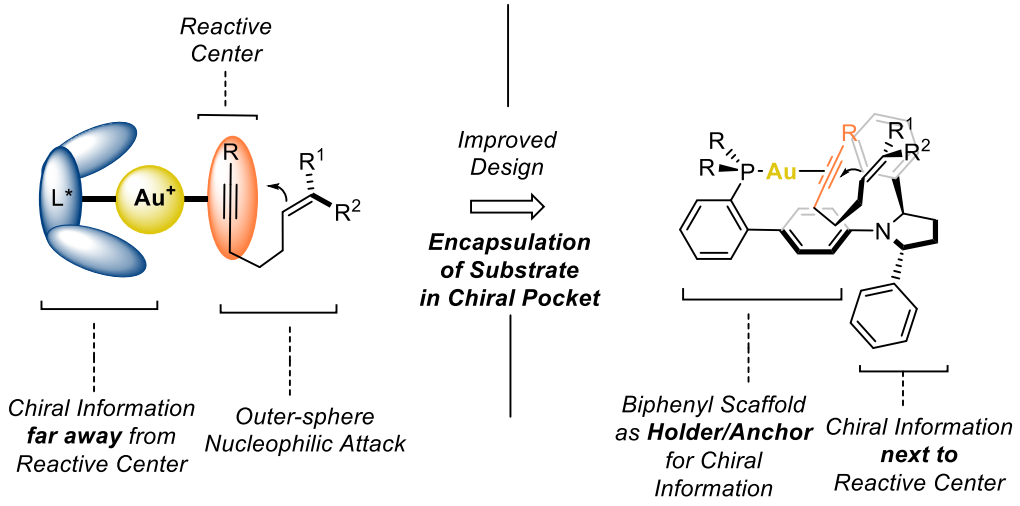

Figure 1.3. New catalyst design developed in the group to overcome the limitations associated with asymmetric gold(I) catalysis.

8 Zhang, P.; Tugny, C.; Meijide Suárez, J.; Guitet, M.; Derat, E.; Vanthuyne, N.; Zhang, Y.; Bistri, O.; Mouriès-Mansuy, V.; Ménand, M.; Roland, S.; Fensterbank, L.; Sollogoub, M. Artificial Chiral Metallo-Pockets Including a Single Metal Serving as Structural Probe and Catalytic Center, *Chem* **2017**, *3*, 174–191.

9 Martín-Torres, I.; Ogalla, G.; Yang, J.-M.; Rinaldi, A.; Echavarren, A. M. Enantioselective Alkoxycyclization of 1,6-Enynes with Gold(I)-Cavitands: Total Synthesis of Mafaicheenamine C, *Angew. Chem. Int. Ed.* **2021**, *60*, 9339–9344.

10 Old, D. W.; Wolfe, J. P.; Buchwald, S. L. A Highly Active Catalyst for Palladium-Catalyzed Cross-Coupling Reactions: Room-Temperature Suzuki Couplings and Amination of Unactivated Aryl Chlorides, *J. Am. Chem. Soc.* **1998**, *120*, 9722–9723.

11 Zuccarello, G.; Mayans, J. G.; Escofet, I.; Scharnagel, D.; Kirillova, M. S.; Pérez-Jimeno, A. H.; Calleja, P.; Boothe, J. R.; Echavarren, A. M. Enantioselective Folding of Enynes by Gold(I) Catalysts with a Remote C_2-Chiral Element, *J. Am. Chem. Soc.* **2019**, *141*, 11858–11863.

The gold(I) complexes resulted in good yields and enantioinductions in the intramolecular [4+2] cycloaddition of different 1,6-enynes (Scheme 1.1a), as well as in the synthesis of 1,2-dihydronaphtalenes via 6-*endo*-dig hydroxycyclization (Scheme 10b), among other applications.

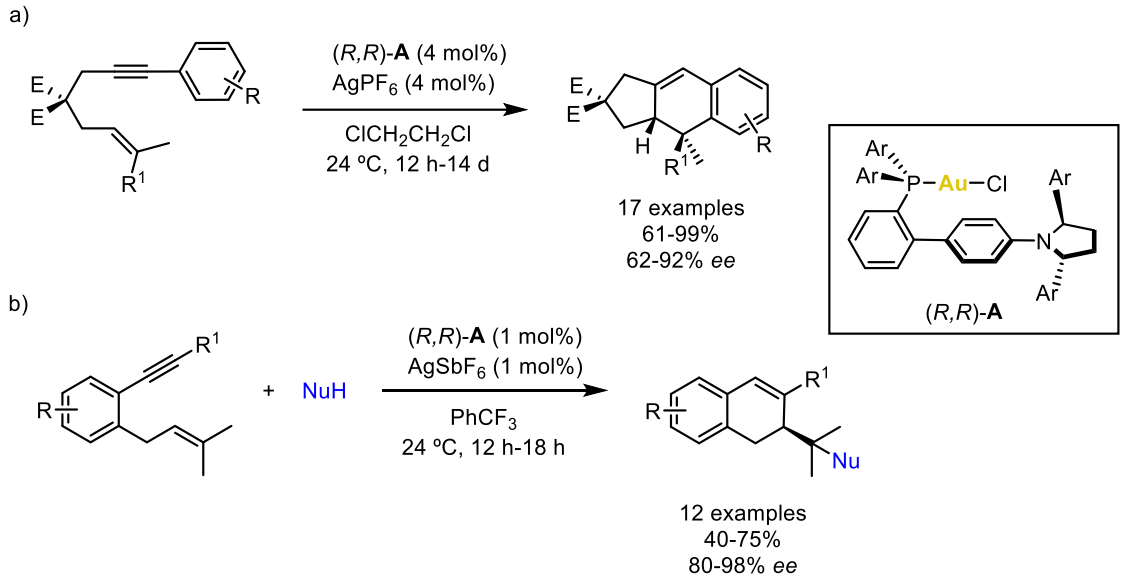

Scheme 1.1. Applications of complex (*R,R*)-**A**

Several modifications were done in the initial structure of the family ligands (Figure 1.4).[11] In this way they were able to modify the substituents in the top ring, in the pyrrolidine and in the phosphine, being able to get a hint on the working mode of the complexes.

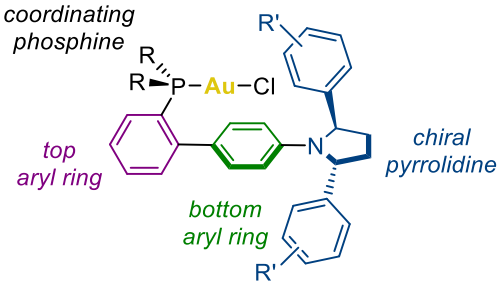

Figure 1.4. Dissection of the designed ligand

The modular synthetic route (Scheme 1.2) starts with the parallel synthesis of the biphenyl scaffold and the enantiopure benzylic diol, followed by cyclization of the amine and the 1,4-diarylbutane-1,4-diol to obtain the biaryl pyrrolidine. At this stage, two more steps remain to reach the final desired complexes, which are phosphine coupling and gold(I) complexation. The cyclisation step consists of first forming the bis-mesylate derivative of the chiral diol in situ and then S_N2 reaction with the biphenyl amine.

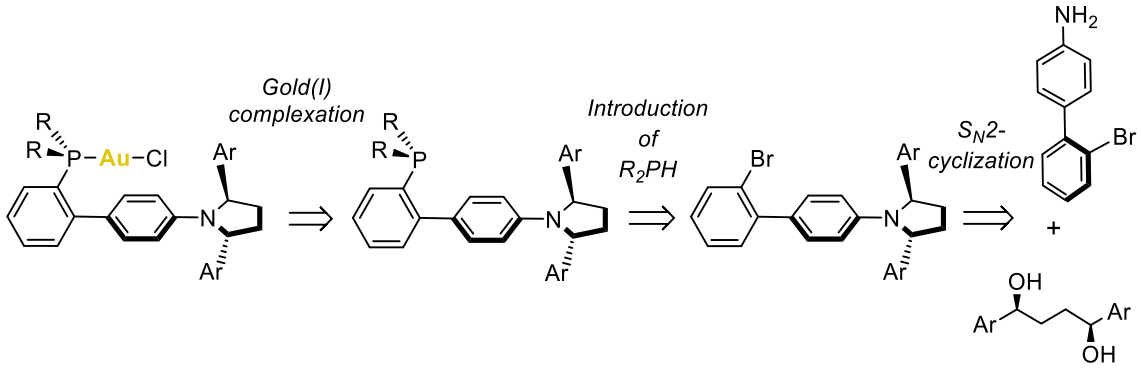

Scheme 1.2. Main retrosynthetic analysis of the developed ligand design

1.1.3 Kinetic analysis of catalytic reactions

Mechanistic understanding of chemical reactions is essential for research. Kinetic profiling is a powerful tool to understand complex catalytic networks, offering both qualitative and quantitative details of reaction progress. It consists of monitoring changes in the concentration of reactants for the study of the reaction rate. Experimental techniques can distinguish between potential mechanisms. This might involve disproving one possible mechanism or gathering evidence that supports another. Ideally, a specific reaction mechanism that aligns with all the collected evidence will be identified as the most probable chemical pathway. There are several methods and tools for deducing reaction mechanisms and kinetic profiling of catalytic reactions.

Classical kinetic analysis is carried out under *pseudo-first-order conditions*, by submitting the reaction to a >10-fold excess of a nonlimiting reagent, remaining its concentration as effectively constant during the reaction; and therefore simplifying the rate law (Eq 1.1, for a bimolecular reaction). Nevertheless, this simplification does not account for real reaction conditions.

(**Eq 1.1.**)

$$\mathrm{A} + \mathrm{B} \xrightarrow{k_1} \mathrm{P}$$

$$\text{rate} = \frac{d[\mathrm{P}]}{d\mathrm{t}} = k_1[\mathrm{A}]^x[\mathrm{B}]^y$$

$$\text{If } [\mathrm{B}] > 10[\mathrm{A}], \qquad \text{rate} = k_{obs}[\mathrm{A}]^x$$

- Reaction rate is expressed in concentration/time (usually M/s)
- k_1 is the specific rate constant
- A and B are molar concentrations of reactants, expressed in M
- x and y are partial kinetic orders of A and B in the reaction.

The order of a reaction in some species seems an obvious, trivial concept. However, in complex situations such as catalytic systems, the order of a reaction is not always a whole number. It can

be fractional, negative or function of other parameters. In general, analyzing experimental data in multistep catalytic reactions is complex, leading researchers to often seek simplified methods for representing kinetic data.

Catalytic reactions have been often studied using the initial rates method,[12] which considers the first moments of the reaction where the conversion has not surpassed a 10-15%. Additionally, it assumes the concentration of product as negligible; assumes irreversible reactions and discards an important part of the acquired data. Alternative analyses of non-equilibrium systems comprise the widely known reaction progress kinetic analysis (RPKA) developed by Blackmond in 2005,[13] and the variable time normalization analysis (VTNA) described by Burés in 2016.[14] Both are based on visual kinetic analysis (VKA), which involves monitoring of the full reaction evolution and later plotting the data to visually evaluate the reaction kinetics. The main advantage of these methods is that for example in kinetic order determination of a given species, just two experiments are needed, while in initial rates the more separate experiments you perform the better. However, when interpreting data using VKA techniques, it's important to remember that this approach typically has lower precision and is often qualitative in nature.

In RPKA, the reaction is analysed by measuring a parameter such as concentration or rate over time. This primary data is processed into variables suitable for visual analysis. For example, in NMR spectroscopy, signal intensities correlate with species concentrations. With sufficient data points these can be differentiated over time, often using a high-order polynomial fit to derive reaction rates, which are then plotted against substrate or product concentrations. RPKA involves three main types of experiments: same excess, different catalyst loading, and different excess. These experiments involve comparing reaction rates and concentrations to determine reaction orders and identify phenomena such as product inhibition or catalyst decomposition. It has been applied to several catalytic systems over the years.[15]

12 Yang, J.; White, P. S.; Brookhart, M. Scope and Mechanism of the Iridium-Catalyzed Cleavage of Alkyl Ethers with Triethylsilane, *J. Am. Chem. Soc.* **2008**, *130*, 17509–17518.

13 Blackmond, D. G. Reaction Progress Kinetic Analysis: A Powerful Methodology for Mechanistic Studies of Complex Catalytic Reactions, *Angew. Chem. Int. Ed.* **2005**, *44*, 4302–4320. Correction: Blackmond, D. G. *Angew. Chem., Int. Ed*. **2006**, *45*, 2162−2162.

14 a) Burés, J. Variable Time Normalization Analysis: General Graphical Elucidation of Reaction Orders from Concentration Profiles, *Angew. Chem. Int. Ed.* **2016**, *55*, 16084–16087. b) A Simple Graphical Method to Determine the Order in Catalyst, *Angew. Chem. Int. Ed.* **2016**, *55*, 2028–2031. c) Burés, J. What is the Order of a Reaction? *Top Catal*. **2017**, *60*, 631–633. d) Nielsen, C. D.-T.; Burés, J. Visual Kinetic Analysis, *Chem. Sci.* **2019**, *10*, 348–353.

15 a) Blackmond, D. G. Kinetic Profiling of Catalytic Organic Reactions as a Mechanistic Tool, *J. Am. Chem. Soc.* **2015**, *137*, 10852–10866. b) Baxter, R. D.; Sale, D.; Engle, K. M.; Yu, J.-Q.; Blackmond, D. G. Mechanistic Rationalization of Unusual Kinetics in Pd-Catalyzed C–H Olefination, *J. Am. Chem. Soc.* **2012**, *134*, 4600–4606. c) Göricke, F.; Haseloff, S.; Laue, M.; Schneider, M.; Brumme, T.; Schneider, C. Phosphoric Acid Catalyzed Formation of Hydrogen-Bonded *o* -Quinone Methides. Enantioselective Cycloaddition with β-Dicarbonyl Compounds toward Benzannulated Oxygen Heterocycles, *J. Org. Chem.* **2020**, *85*, 11699–11720.

VTNA method consists on determining the order in any component of a given reaction by direct visual comparison of reaction concentration profiles. In VTNA method, the profiles of experiments differing in concentration of one reactant, A, will only overlay when the time axis (x axis) is replaced by the time integral of the concentration of A raised to the correct power of α (kinetic partial order), as shown in the equation 1.2.

(Eq 1.2.)

$$\int_{t=0}^{t=n} [\mathrm{A}]^{\propto} dt = \sum_{i=1}^{n} \left(\frac{[\mathrm{A}]_i + [\mathrm{A}]_{i-1}}{2} \right)^{\propto} (t_i - t_{i-1})$$

The aim of this method is to generally elucidate reaction orders from concentration profiles by normalizing the time between each pair of data points using the average concentration of those points. This time scale normalization can be applied to any number of reaction components, regardless of whether their concentrations remain constant or vary throughout the reaction. For instance, in the following simulation of a two substrates catalyzed reaction (Figure 1.5), the partial kinetic order in substrates **A** and **B** is determined to be 1 (Figure 1.5a), as well as for the catalyst (Figure 1.5b). Apart from the partial kinetic orders in each component of the reaction, k_{obs} can as well be determined by plotting the normalized data for all kinetically significant components, resulting in a straight line with a slope equal to k_{obs} or $-k_{obs}$; depending whether the concentration of a product is plotted or the concentration of a reactant (Figure 1.5c).

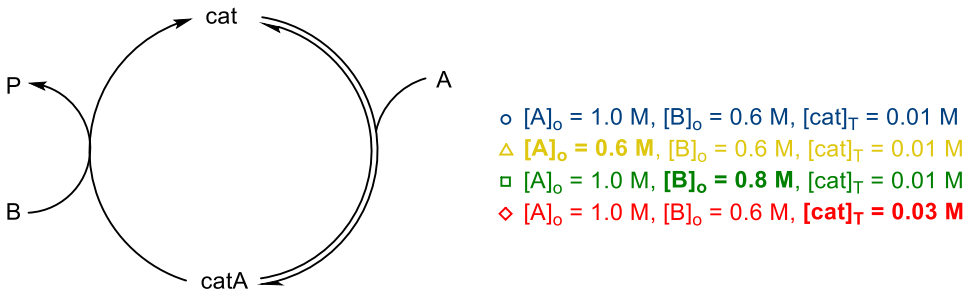

a)

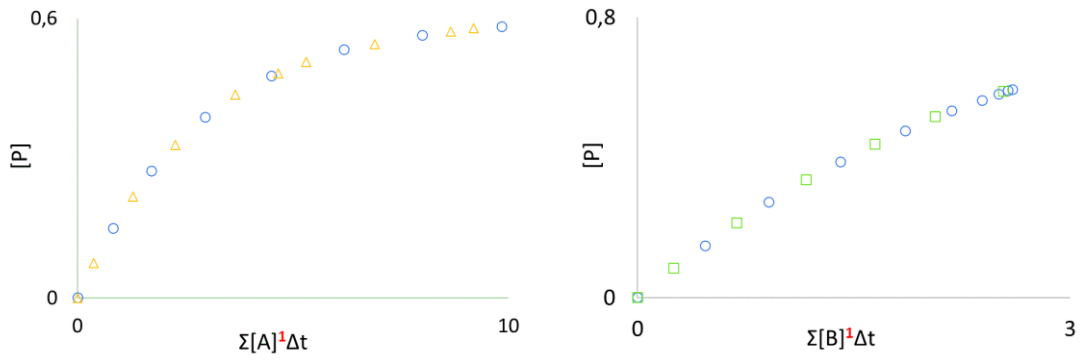

b)

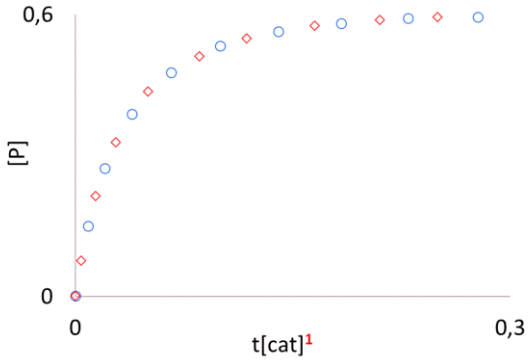

c)

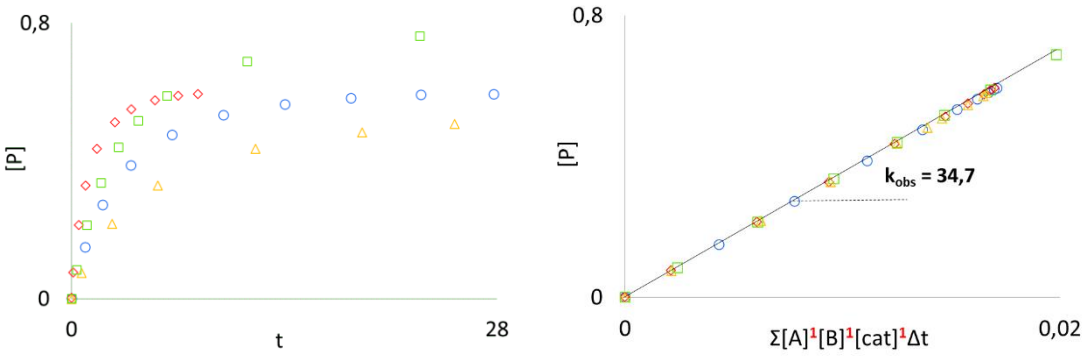

Figure 1.5. VTNA helps the determination of the order in substrate **A**, substrate **B** (a) and catalyst (b). Sequentially normalizing the time scale for **A**, **B**, and catalyst results in the overlap of all reaction profiles into a straight line with a slope corresponding to k_{obs} (c).

1.2 Objectives

Given the successful performance of the chiral pyrrolidinyl-biaryl phosphine gold(I) complexes discussed in the introduction of the chapter,[11] we envisioned to further modify the molecular structure of these complexes. These modifications would provide deeper insights into their mechanism of action and potentially expand their applicability in other asymmetric transformations.

Secondly, we aimed to investigate in detail the kinetics operating under the working mode of our pyrrolidinyl-biphenyl phosphine complexes, which gave enantioenriched products of formal [4+2] cycloaddition starting from 1,6-enynes; and compare the results with regard to JohnPhosAu(MeCN)SbF_6 catalyzed kinetic studies previously performed in the group.[16]

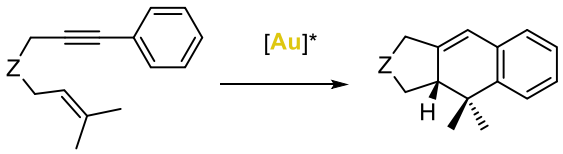

Z = $C(CO_2Me)_2$,
$C(CH_2OMe)_2$

16 Nieto-Oberhuber, C.; Pérez-Galán, P.; Herrero-Gómez, E.; Lauterbach, T.; Rodríguez, C.; López, S.; Bour, C.; Rosellón, A.; Cárdenas, D. J.; Echavarren, A. M. Gold(I)-Catalyzed Intramolecular [4+2] Cycloadditions of Arylalkynes or 1,3-Enynes with Alkenes: Scope and Mechanism, *J. Am. Chem. Soc.* **2008**, *130*, 269–279.

1.3 Results and discussion

1.3.1 Design and synthesis of chiral pyrrolidine-based ligands

To get a better understanding of the mode of action of the complexes, we decided to introduce electron-withdrawing substituents at the bottom aryl ring (Figure 1.6), based on previous calculations performed in the group,[17] in which one of the highest enantiomeric ratios on the formal [4+2] cycloaddition of a 1,6-enyne were obtained for a tetrafluoraryl bottom ring and 3,5-$(CF_3)_2C_6H_3$ as the aryl substituent.

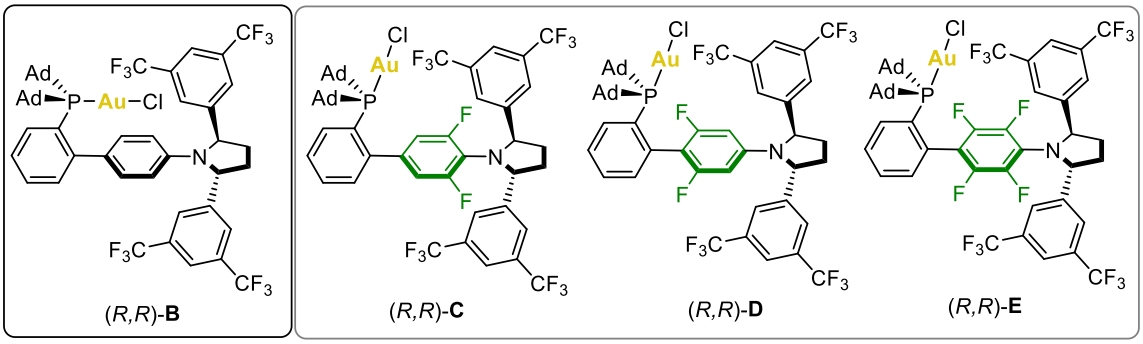

Figure 1.6. Former and targeted chiral pyrrolidinyl-biphenyl phosphine gold(I) complexes

Attempts of obtaining complexes (*R,R*)-**D** and (*R,R*)-**E** were unsuccessful and will be discussed later on in the section. However, complex (*R,R*)-**C** was synthesized and its synthetic route is described hereafter.

Synthesis of Complex (*R,R*)-**C**

The synthetic route for complex (*R,R*)-**C** was inspired by the modular approach developed for the first generation of catalysts as mentioned in the introduction (Figure 1.7).[11] In this case, an additional step had to be introduced for the cyclization to succeed. A cyclic sulfate derived from the enantiopure diol was used instead of the in situ formation of a bismesylate in the double S_N2 cyclization with the aniline. Furthermore, the introduction of the adamantly phosphine precedes the cyclization of the amine and the cyclic sulfate.

17 For more information see PhD Thesis of Dr. Imma Escofet entitled ´Computational Mechanistic Studies in Gold(I) Catalysis and Design of New Chiral Ligands', 2020, URV-ICIQ.

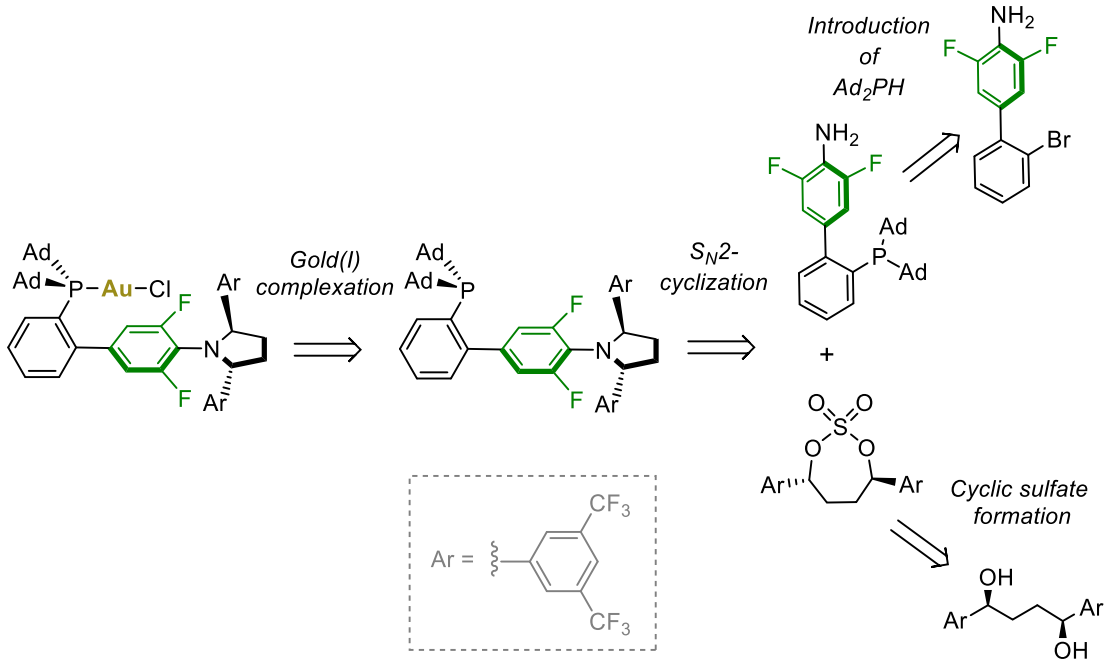

Figure 1.7. Retrosynthetic analysis for the synthesis of (*R*,*R*)-**C**.

The synthesis of (1*S*,4*S*)-1,4-bis(3,5-bis(trifluoromethyl)phenyl)butane-1,4-diol (**1.1**) was done following the already reported procedure developed in our group,[11] developed with the aim of having an uniform synthetic route that covers the obtention of the different diols in the pyrrolidine complexes family. From diol **1.2**, the more reactive intermediate cyclic sulfate **1.2** was achieved by following a procedure for a similar substrate (Figure 1.8).[18] Diol **1.1** was first converted to the cyclic sulfite by reaction with thionyl chloride and subsequently oxidized to the sulfate **1.2** in an overall 86% yield.

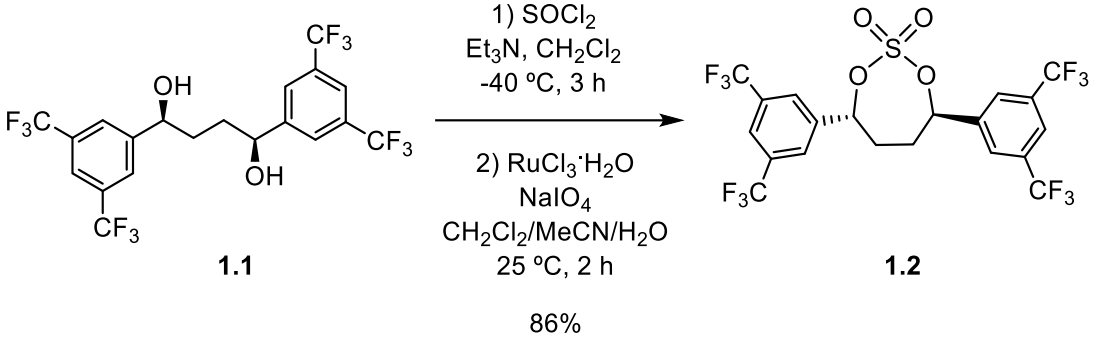

Figure 1.8. Synthesis of (4*R*,7*R*)-4,7-Bis(3,5-bis(trifluoromethyl)phenyl)-1,3,2-dioxathiepane 2,2-dioxide **1.2**.

Parallelly, the synthesis of aniline **1.5** was performed in two steps (Scheme **1.2**). Starting from 2,6-difluoro-4-iodoaniline (**1.3**), Suzuki-Miyaura cross-coupling with (2-bromophenyl)boronic acid led to compound **1.4** in 89% yield, which was submitted to Pd-catalyzed phosphine coupling

18 Burk, M. J.; Harper, T. G. P.; Kalberg, C. S. Highly Enantioselective Hydrogenation of β-Keto Esters under Mild Conditions *J. Am. Chem. Soc*. **1995**, *117*, 4423-4424.

conditions giving **1.5** in 80% yield. In the next step both **1.2** and **1.5** synthesis converge in a cyclization step using through a double S_N2 reaction using LiHMDS in THF to afford the chiral pyrrolidine ligand **1.6** in moderate yield. Lastly, the complexation with dimethyl sulfide gold(I) chloride lead to the desired complex (*R,R*)-**C** in excellent yield (Scheme **1.2**). The structure of gold(I) complex (*R,R*)-**C** was confirmed by X-ray diffraction (Figure **1.9**).

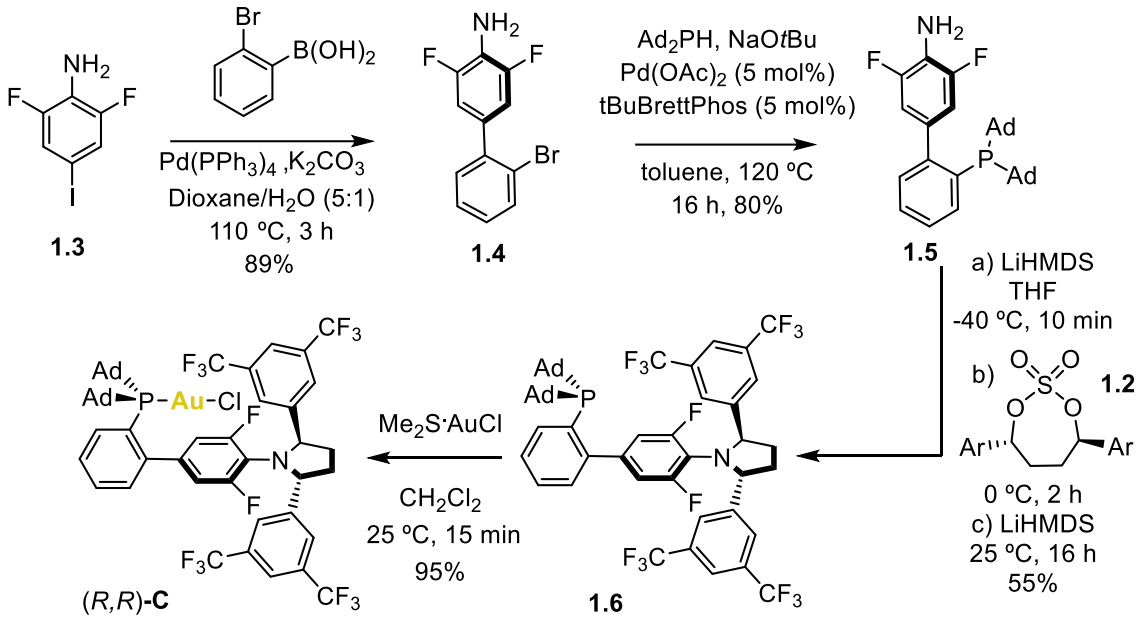

Scheme 1.2. Synthetic route for the obtention of (*R,R*)-**C.**

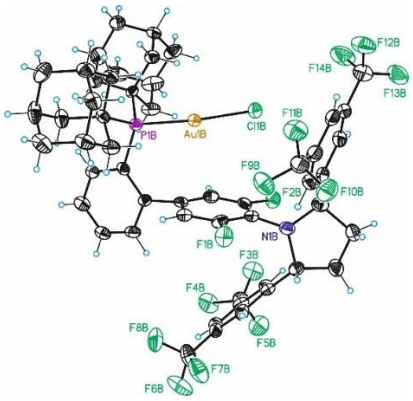

Figure 1.9. X-ray structure of gold(I) complex (*R,R*)-**C.**

Unsuccessful Attempts Towards Complex (*R,R*)-**D**

An apparently subtle change on the position of the two fluorine atoms in the bottom aryl ring from ortho to meta position, with respect to the pyrrolidine, made the approach to develop the synthetic route way more difficult following very similar steps (Scheme 1.3). Initially, operating according to a reported procedure for a similar substrate,[19] iodination in para position to the aniline in 3,5-

19 Davis, M. C. Chlorination of Aniline and Methyl Carbanilate by N-Chlorosuccinimide and Synthesis of 1,3,5-Trichlorobenzene, *Synth. Commun.* **2009**, *39*, 1100–1108.

difluoroaniline **1.7** gave 3,5-difluoro-4-iodoaniline **1.8** in 89% yield. Suzuki-Miyaura Pd-catalyzed cross-coupling to construct the biphenyl scaffold and cyclisation using cyclic sulfate **1.2** rendered compound **1.10** in moderate yields.

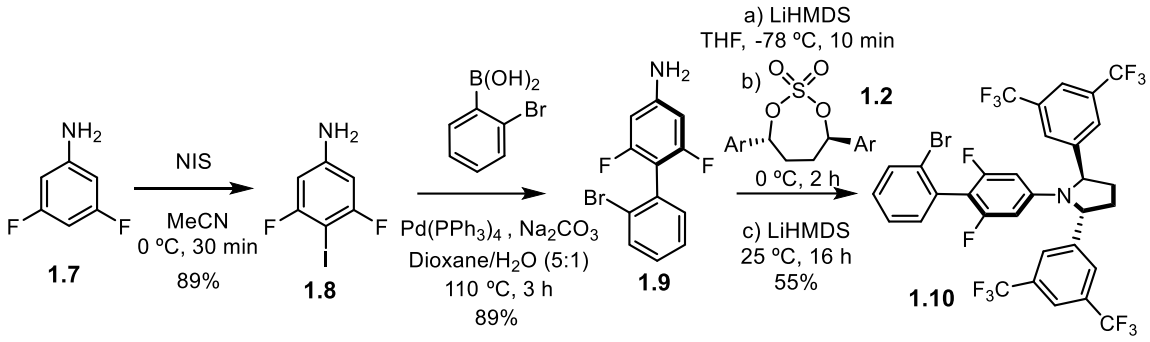

Scheme 1.3. First steps towards the synthesis of complex (*R,R*)-**D**

The challenging part appeared when the phosphine coupling was tried. Endless attempts testing different conditions ended in obtaining just unreacted starting material. Some of the conditions tried before performing HTE are shown in Table 1.1. More sophisticated palladacycle precatalysts (Table 1.1, entries 3 and 4) that are known for enabling high reactivity and selectivity in C–C and C–Heteroatom bonds,[20] or even nickel catalysis[21] (Table 1.1, entry 5) did not result helpful.

Table 1.1. Previous attempts to HTE in the phosphine coupling

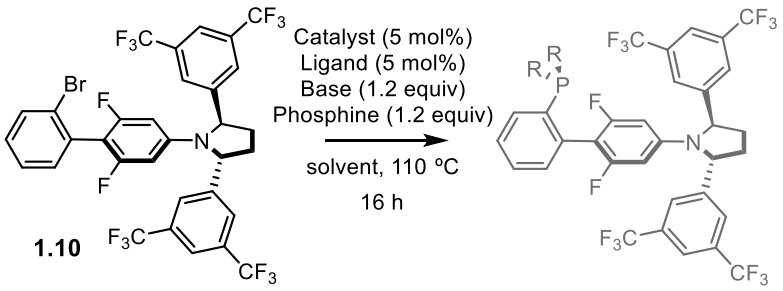

Entry	Catalyst/Ligand	Phosphine	Solvent	Base	Yield
1	$Pd(OAc)_2$, dppf	$HPAd_2$	Toluene	NaO*t*Bu	-[a]
2	$Pd(OAc)_2$, *t*BuBrettPhos	$HPAd_2$	Toluene	NaO*t*Bu	-[a]
3	XPhos Pd G3	$HPAd_2$	Toluene	NaO*t*Bu	-[a]
4	CPhos Pd G3	$HPAd_2$	Toluene	NaO*t*Bu	-[a]
5	$NiCl_2$(dppp)	$HPPh_2$	Dioxane	K_3PO_4	-[a]

[a] Mostly unreacted starting material.

20 Bruneau, A.; Roche, M.; Alami, M.; Messaoudi, S. 2-Aminobiphenyl Palladacycles: The "Most Powerful" Precatalysts in C–C and C–Heteroatom Cross-Couplings, *ACS Catal.* **2015**, *5*, 1386–1396.

21 Zhao, Y.-L.; Wu, G.-J.; Li, Y.; Gao, L.-X.; Han, F.-S. [$NiCl_2$(dppp)]-Catalyzed Cross-Coupling of Aryl Halides with Dialkyl Phosphite, Diphenylphosphine Oxide, and Diphenylphosphine, *Chem. – Eur. J.* **2012**, *18*, 9622–9627.

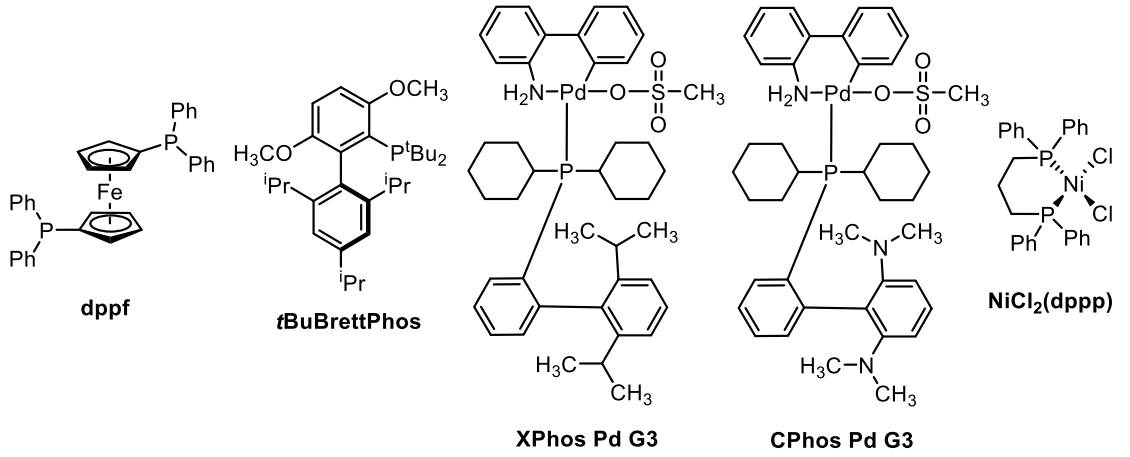

Therefore, we decided to carry out HTE on the phosphine coupling reaction. 192 conditions were tested using $Ni(acac)_2$ and $Pd(OAc)_2$ as Ni and Pd sources, 12 commercially available ligands (4 monodentate phosphines, 6 bidentate phosphines and 2 NHCs, see Figure 1.10), 4 bases (K_3PO_4, KO*t*Bu, Cs_2CO_3 and NEt_3) and 2 solvents (toluene and dioxane). As the needed amount of starting material was quite high, the system was simplified to use as starting material the free aniline **1.9** (Figure 1.10).

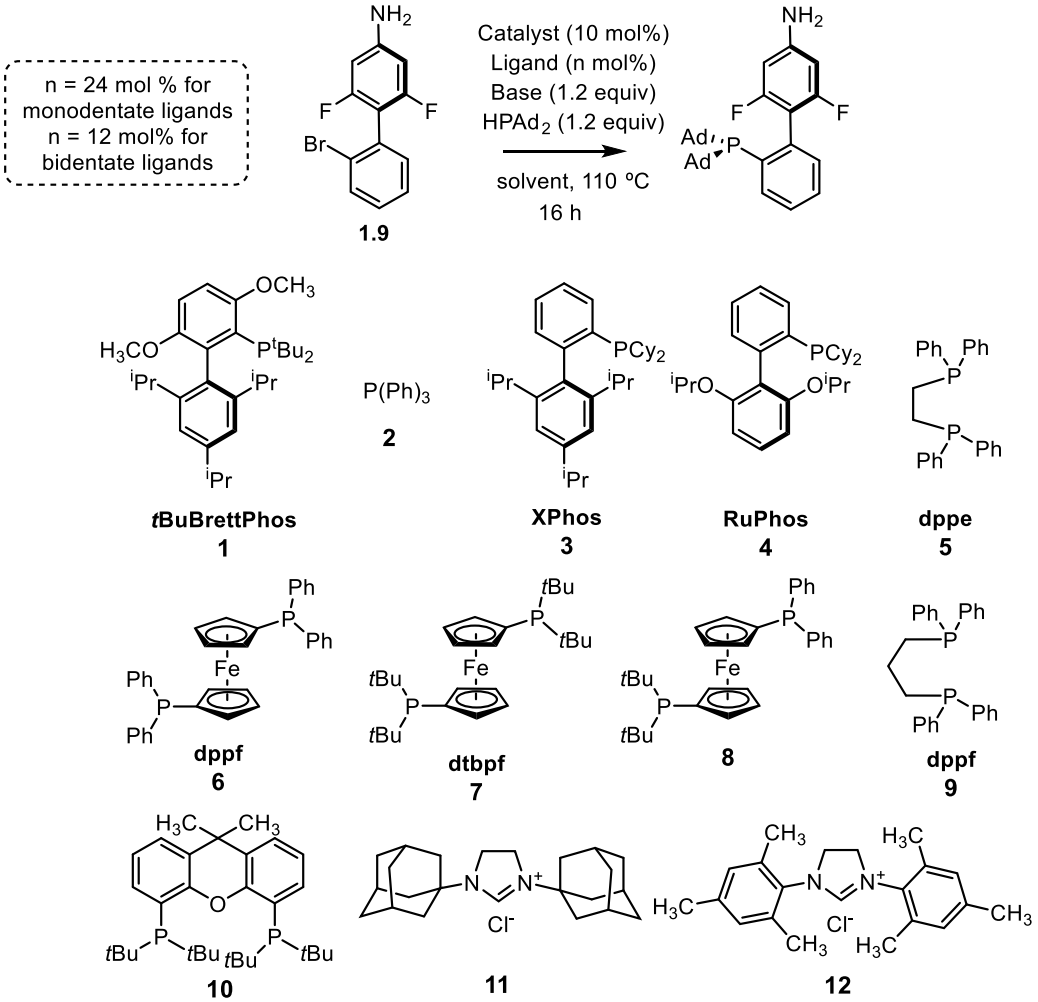

Figure 1.10. Series of different ligands used for HTE.

The 192 reactions were carried out in a 5 μmol scale and organized in plates (1 and 2). Plates 1 and 2 had the same organization but in plate 1 the catalyst was Pd and in plate 2 was Ni. Horizontally, there were 8 rows, from A to D there was a different base on each in the same order than from E to H, but from A to D reactions were set in toluene and from E to H in dioxane. Vertically, from 1 to 12, each column was a different ligand (Figure 1.11).

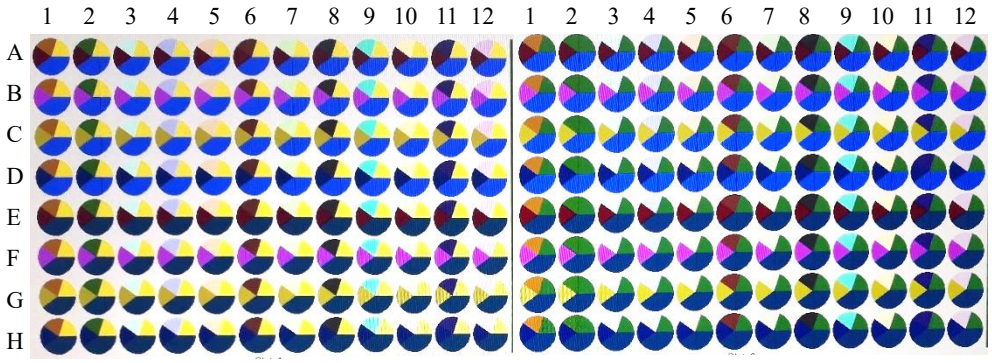

Figure 1.11. Organization of plates 1 and 2 during HTE

Internal standard used was biphenyl for the integration in LC-MS analysis. Two promising signals were observed in the chromatograms, hence the best reactions for their formation were scaled up. In one of the cases, we were surprised to see after isolation that traces of the product from aromatic nucleophilic substitution (S_NAr) **1.11** have been formed (Figure 1.12), among traces of other by-products like homocoupling product **1.12** or Buchwald-Hartwig amination product **1.13**. Mainly unreacted starting material was recovered from the crude reaction.

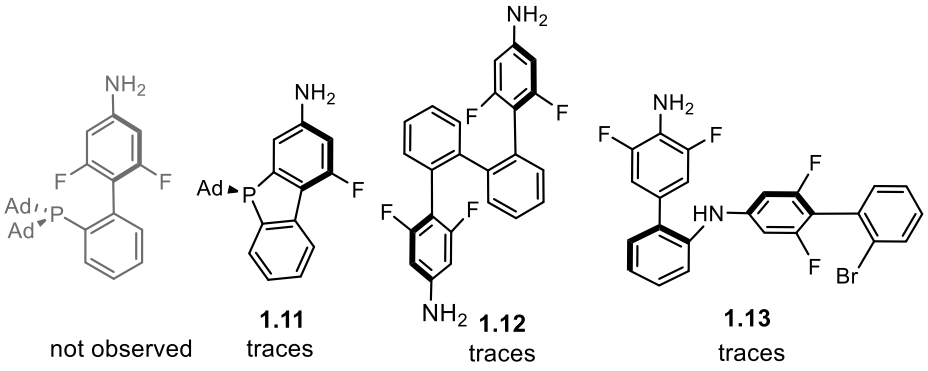

Figure 1.12. Desired product (not observed) and traces of by-products observed by LC-MS after the scale up of best conditions in HTE.

Consequently, to prevent unwanted intermolecular reactions of the phosphorus lone pair and oxygen oxidation (also observed in the $^{31}P\{^1H\}$ NMR crude), the phosphine coupling was

performed with a borane-protected phosphine.[22] However, the desired product was not observed either. Finally, the last approach was to use a Turbo-Grignard reagent,[23] invoking a halogen-magnesium exchange and activating the C–Br bond,[24] followed by the literature reported treatment with CuCl and PAd_2Cl (Scheme 1.4).[25] On this occasion, the starting material was modified to a non-chiral pyrrolidine **1.14** in order to mimic as much as possible the previously used starting material **1.10** (time-expensive synthesis). Nonetheless, the reaction did not take place under these conditions because the Br-Mg exchange did not even occur (as tested by HPLC analysis).

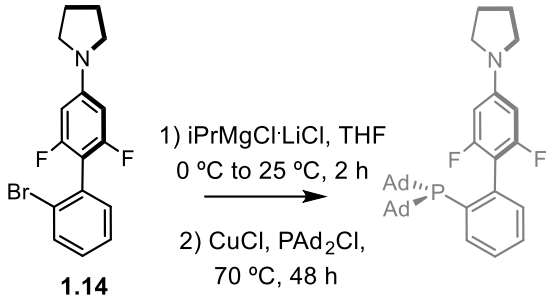

Scheme 1.4. Unsuccessful reaction using an achiral pyrrolidine as starting material.

After all the efforts of synthesizing complex (*R,R*)-**D**, we can understand that the electronic effect of the fluorine atoms is crucial and varies detrimentally depending on where the fluorine atoms are in the structure, in ortho ((*R,R*)-**C**) or meta ((*R,R*)-**D**) position with respect to the pyrrolidine.

Unsuccessful Attempts Towards Complex **(*R,R*)-E**

Aiming to follow a similar route to the rest of the ligand family, 4-bromo-2,3,5,6-tetrafluoroaniline **1.15** (Scheme 1.5) was taken as starting material and submitted to the Suzuki-Miyaura coupling with (2-bromophenyl)boronic acid, leading to partial conversions, some desired product and high quantities of homocoupling product. This could be due to the fact that the oxidative addition of the C–Br bond in **1.15** to the Pd(0) complex is disfavored given the presence of four fluorine atoms in the aromatic ring, making it electron-deficient. Thus, we opted for using (3-methoxyphenyl)boronic acid as the coupling partner, being able to obtain **1.16** in a moderate yield. From **1.16**, efforts towards the regioselective bromination or iodination using NBS or NIS

22 Low, C. H.; Nobbs, J. D.; van Meurs, M.; Stubbs, L. P.; Drent, E.; Aitipamula, S.; Pung, M. H. L. Palladium Complexes with Bulky Diphosphine Ligands as Highly Selective Catalysts for the Synthesis of (Bio-) Adipic Acid from Pentenoic Acid Mixtures., *Organometallics* **2015**, *34*, 4281–4292.

23 Ziegler, D. S.; Wei, B.; Knochel, P. Improving the Halogen–Magnesium Exchange by Using New Turbo-Grignard Reagents, *Chem. – Eur. J.* **2019**, *25*, 2695–2703.

24 McLaughlin, M.; Belyk, K. M.; Qian, G.; Reamer, R. A.; Chen, C. Synthesis of α-Hydroxyacetophenones, *J. Org. Chem.* **2012**, *77*, 5144–5148.

25 Sather, A. C.; Lee, H. G.; De La Rosa, V. Y.; Yang, Y.; Müller, P.; Buchwald, S. L. A Fluorinated Ligand Enables Room-Temperature and Regioselective Pd-Catalyzed Fluorination of Aryl Triflates and Bromides, *J. Am. Chem. Soc.* **2015**, *137*, 13433–13438.

respectively failed. A mixture of regioisomers were observed in ^{1}H and $^{19}F\{^{1}H\}$ NMR after several temperatures and equivalents of NBS/NIS tested.

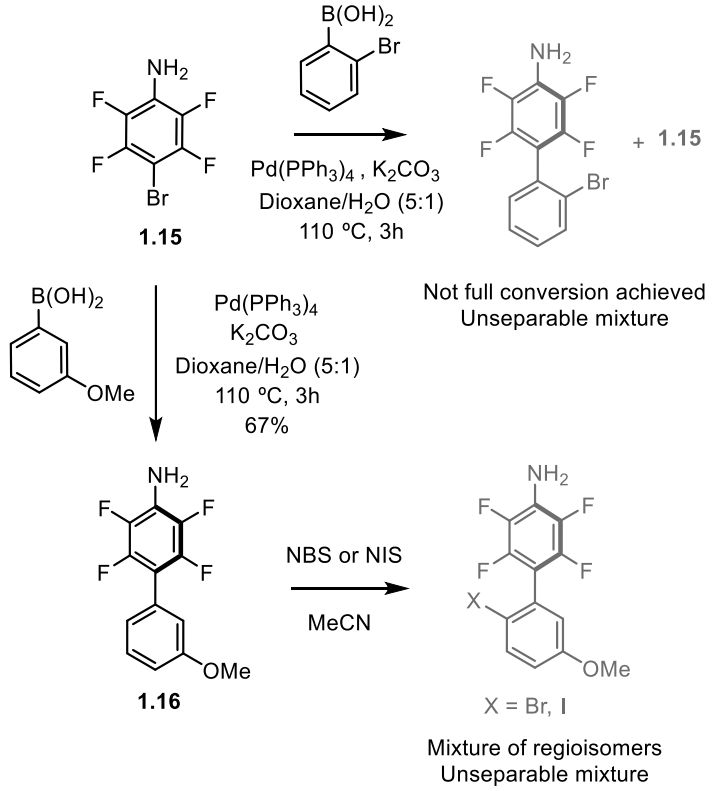

Scheme 1.5. Formation of biaryl scaffold in compound **1.16** via Suzuki-Miyaura coupling and failed attempts in grey color.

At this point, we continued with the usual procedure by performing the cyclization seeking the pyrrolidine intermediate **1.18**. As observed during other similar ligand synthesis, the bis-mesylate **1.17** of the diol **1.1** was prepared separately instead of formed in situ before the cyclization, and isolated for its subsequent use.

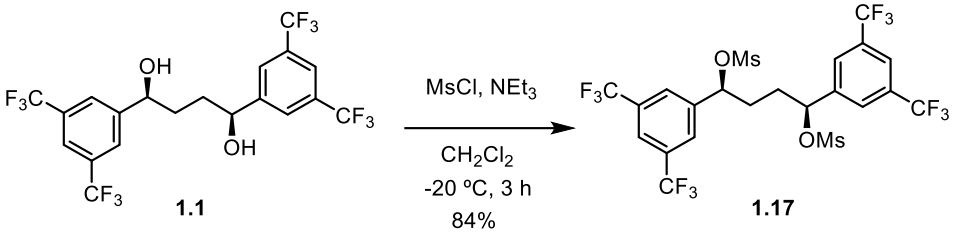

Scheme 1.6. Bis-mesylation reaction for the obtention of **1.17**.

Reaction of **1.16** with bis-mesylate **1.17** did not render any product, therefore cyclic sulfate **1.2** was introduced in the and optimization of the conditions was carried out (Table 1.2). After the temperature, base and equivalents of base were optimized, we concluded by increasing slightly the equivalents of **1.16**, being able to render **1.18** in a 66% isolated yield (Table 1.2, entry 7). It is

interesting to note that when no fluorine atoms are present in the bottom aryl ring, a weaker base (NEt_3) is enough for the cyclization to proceed. This indicates the electron-deficient character of the aniline in our system.

Table 1.2. Optimization of the pyrrolidine construction by treatment with cyclic sulfate **1.2**.

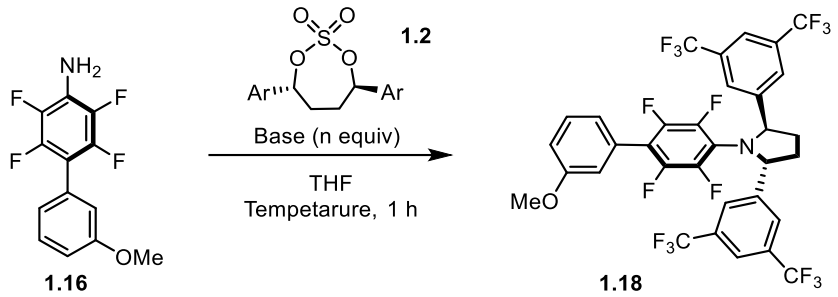

Entry	Base	Base (equiv)	1.16 (equiv)	Temperature (ºC)	Yield[a] (%)
1	NaH	4	1	0	23
2	NaH	20	1	0	40
3	NaH	20	1	0	35[b]
4	NaH	2	1	-40	51
5	NaHMDS	20	1	-40	51
6	LiHMDS	2	1	-70	13
7	**NaH**	**20**	**1.2**	**-40**	**66[b]**

[a] NMR yield calculated with respect to trichloroethylene as internal standard. [b] Isolated yield.

Having pyrrolidine **1.18** in hand, its regioselective bromination was attempted by treatment with NBS (Scheme **1.7**). Among the two most likely regioisomers that could result from the reaction, taking into account the ortho/para-directing methoxy group and steric hindrance, there was mainly conversion to **1.19**, isolated in a 34% yield, and only traces of **1.20**.

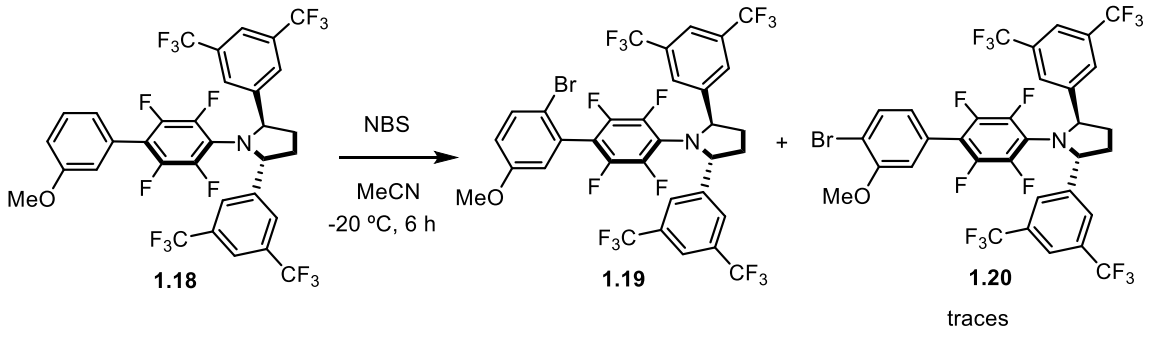

Scheme 1.7. Regioselective bromination of **1.18** using NBS.

The structure elucidation of product **1.19** was performed by mono and bidimensional NMR analysis. Although the ^{1}H NMR pattern of both regioisomers should be the same (two doublets and one double doublet), the first hint towards having **1.19** instead of **1.20** was the shielding of the signals with lower *J* coupling (J = 3.0 Hz) that appeared at 6.79 ppm and 6.65 ppm with

respect to the third signal of the top aromatic ring at 7.46 ppm (Figure 1.13). These two protons that are more upfield seem to be the protons in ortho-position to the methoxy group.

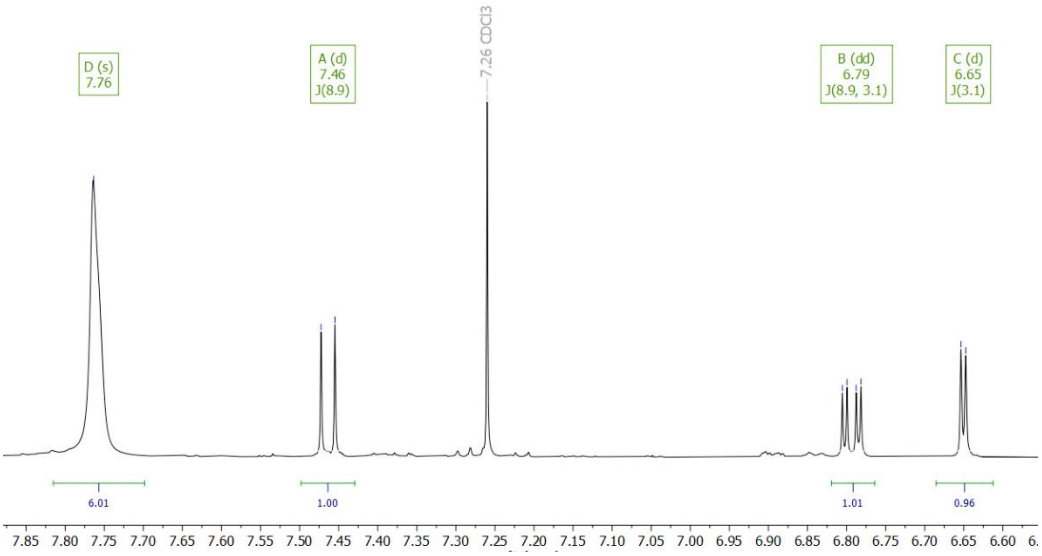

Figure 1.13. ^{1}H NMR spectra section of compound obtained by bromination.

The definitive proof was extracted from a ^{19}F-^{1}H HOESY experiment, where only one correlation signal can be seen, between the 6.6 ppm doublet and the fluorine signal at -141.4 ppm, corresponding to the fluorines in meta-position to the chiral pyrrolidine (Figure 1.14). This corroborates the previous hypothesis of having desired product **1.19**.

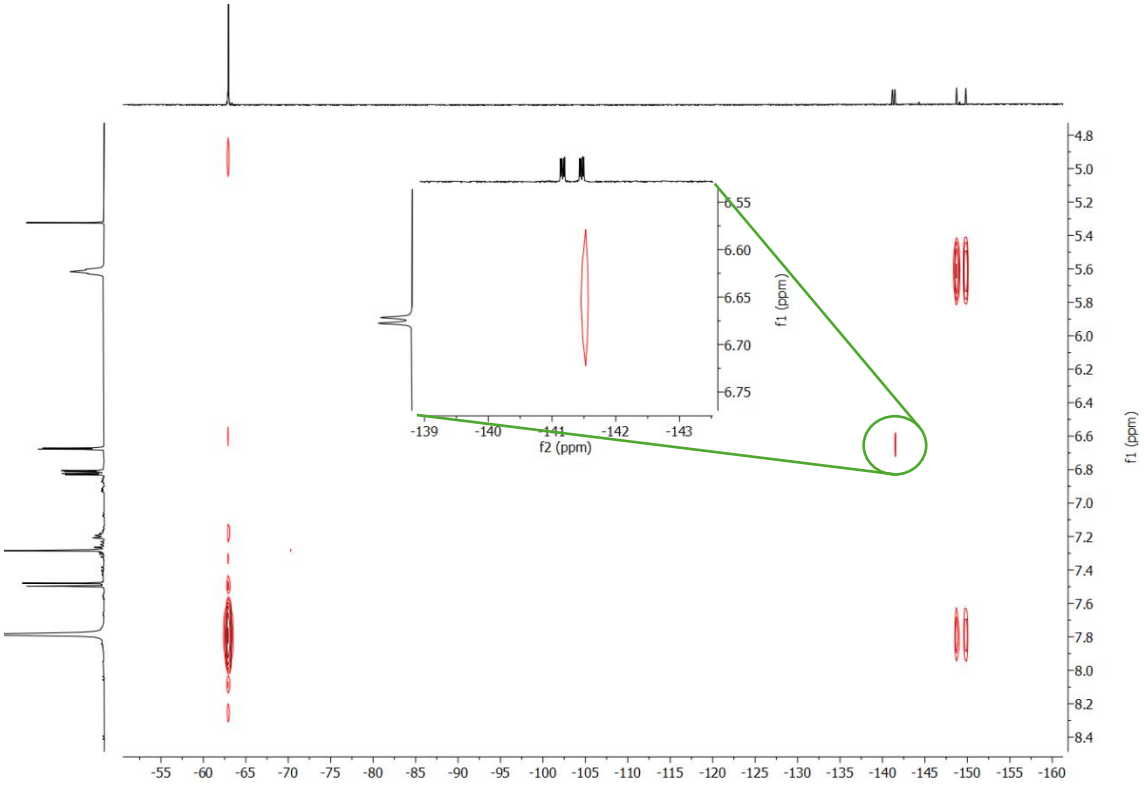

Figure 1.14. Section of ^{19}F-^{1}H HOESY experiment carried out to distinguish between the possible formation of **1.19** or **1.20**.

The last step before introducing gold was tried under the usual phosphine coupling conditions required for the synthesis of other ligands (Scheme 1.8). However, in this case only starting material was recovered from the crude of the reaction, as happened with complex (*R,R*)-**D**.

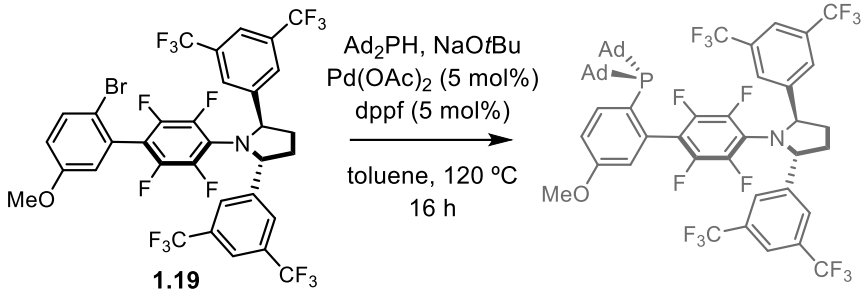

Scheme 1.8. Failed reaction in the Pd-catalyzed phosphine coupling of **1.19**.

Application of Complex (*R,R*)-**C** in Catalysis

The newly synthesized gold(I) complex (*R,R*)-**C** was tested in the formal [4+2] cycloaddition of 1,6-enyne **1.21** (Scheme 1.9, left) and in the atroposelective cyclization of naphthyl derivative **1.23** to form indole **1.24** (Scheme 1.9, right). The atroposelective reaction was previously studied and optimized in the group and tested with multiple gold(I) complexes developed within the family of chiral pyrrolidinyl-biaryl phosphine complexes.[26] The 1,6-enyne cycloaddition ended after 6 hours or reaction, implying good reactivity, and a quantitative formation of cyclized product **1.22** was observed. Despite this, and to our disappointment, the enantioselectivity obtained was almost non-existent, with almost racemic product being formed. In the case of the atroposelective reaction, complex (*R,R*)-**C** behaved better than the cycloaddition reaction in terms of enantioinduction, reaching a moderate 73:23 *er*, as well as quantitative formation of the enantioenriched product **1.24**.

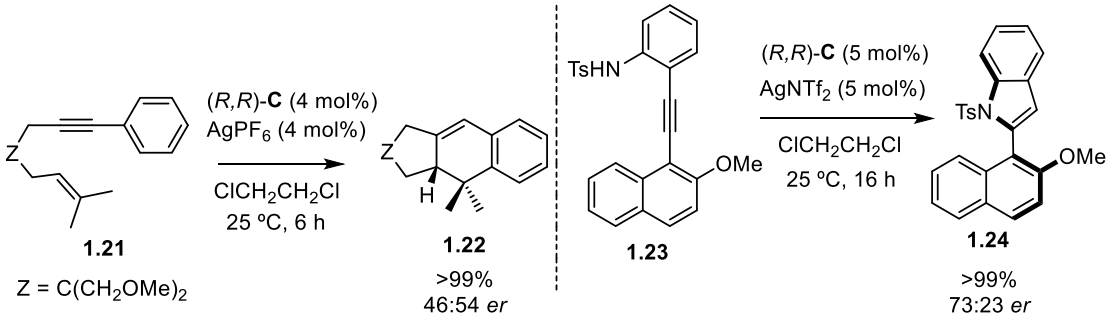

Scheme 1.9. Yield was determined by ^{1}H NMR against internal standard. Enantiomeric ratios were measured by supercritical fluid chromatography (SFC).

26 Zuccarello, G. Doctoral Thesis, Chiral Pyrrolidinyl–Biphenyl Phosphine Ligands in Gold(I) Catalysis, 2020, URV-ICIQ.

Application of Complex (*R,R*)-**C** to NEST[27]

To better describe the elongated gold(I) catalysts, the NEST tool has been developed.[28] The open-source web application NEST is designed to evaluate the steric effects of metal catalysts that have bulky ligands forming a non-spherical nest; inspired by SambVca[29] and MolQuo[30] tools.

In NEST, the volume is modeled as a capsule rather than a sphere (Figure 1.15), and its length (a) can be adjusted based on the system of interest. The capsule space is divided into quadrants surrounding the central atom. NEST calculates the percentage of occupied volume for each quadrant, designated as $Q1_{occ}$, $Q2_{occ}$, $Q3_{occ}$, and $Q4_{occ}$.

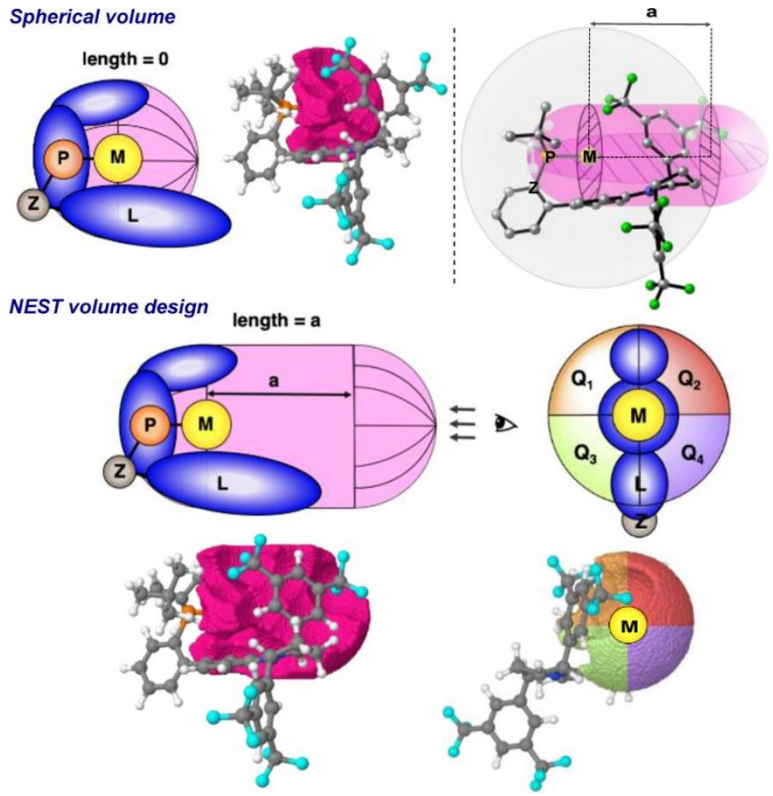

Figure 1.15. Spherical volume vs NEST volume for a pyrrolidine-based ligand developed in the group similar to (*R,R*)-**C**.

27 Zuccarello, G.; Nannini, L. J.; Arroyo-Bondía, A.; Fincias, N.; Arranz, I.; Pérez-Jimeno, A. H.; Peeters, M.; Martín-Torres, I.; Sadurní, A.; García-Vázquez, V.; Wang, Y.; Kirillova, M. S.; Montesinos-Magraner, M.; Caniparoli, U.; Núñez, G. D.; Maseras, F.; Besora, M.; Escofet, I.; Echavarren, A. M. Enantioselective Catalysis with Pyrrolidinyl Gold(I) Complexes: DFT and NEST Analysis of the Chiral Binding Pocket, *JACS Au* **2023**, *3*, 1742–1754.

28 Program NEST was developed by Dr. María Besora, Gonzalo D. Núñez, and Dr. Imma Escofet. More details directly on NEST App, or https://github.com/BesoraMaria/NEST.

29 Falivene, L.; Cao, Z.; Petta, A.; Serra, L.; Poater, A.; Oliva, R.; Scarano, V.; Cavallo, L. Towards the Online Computer-Aided Design of Catalytic Pockets, *Nat. Chem.* **2019**, *11*, 872–879.

30 a) Aguado-Ullate, S.; Urbano-Cuadrado, M.; Villalba, I.; Pires, E.; García, J. I.; Bo, C.; Carbó, J. J. Predicting the Enantioselectivity of the Copper-Catalysed Cyclopropanation of Alkenes by Using Quantitative Quadrant-Diagram Representations of the Catalysts, *Chem. – Eur. J.* **2012**, *18*, 14026–14036. b) Aguado-Ullate, S.; Saureu, S.; Guasch, L.; Carbó, J. J. Theoretical Studies of Asymmetric Hydroformylation Using the Rh (R,S)-BINAPHOS Catalyst—Origin of Coordination Preferences and Stereoinduction, *Chem. – Eur. J.* **2012**, *18*, 995–1005.

The equations derived for each substrate, along with the descriptors obtained from the NEST app, were used to predict the enantiomeric excesses. In most cases, these predictions reasonably agreed with the experimental results.[31]

1.3.2 Synthesis and comparison of Au, Ag and Cu chiral pyrrolidine-based ligands

To get a full picture on how group 11 transition metals affect the properties of these chiral pyrrolidine-based catalysts, we decided to introduce apart from gold, silver and copper in the system (Figure 1.16), and study the distinctions by comparing its structure and catalytic activities.

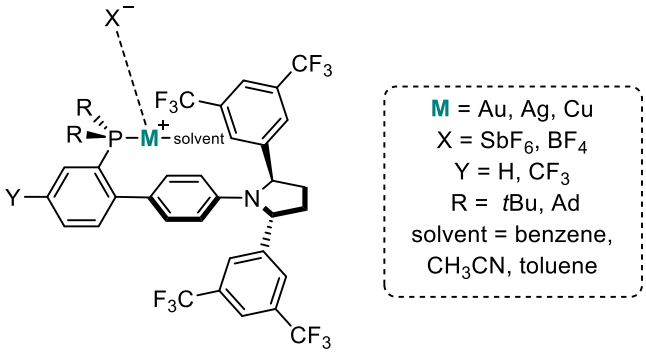

Figure 1.16. Group 11 transition metal complexes obtained

The synthetic process followed to achieve the desired gold(I) complex (*R,R*)-**F** was based on precedent reported literature by the group.[11] Chloride abstraction in (*R,R*)- **F** by treatment with $AgSbF_6$ afforded activated complex (*R,R*)- **F'** in 90% yield.[32] Crystallization in a pentane/benzene gave clear crystals that were analyzed by X-ray diffraction (Scheme 1.10). To our surprise, during the process of crystallization, benzene replaced acetonitrile as η^2 coordination ligand to gold(I) (Figure 1.16).

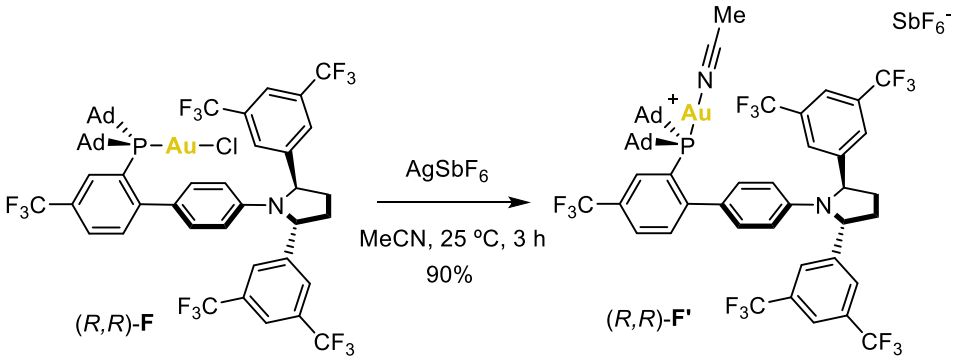

Scheme 1.10. Halogen abstraction of gold(I) complex (*R,R*)-**F** to obtain preactivated complex (*R,R*)-**F'**

31 See Supporting Information of reference 27 for more details.

32 Nieto-Oberhuber, C.; Muñoz, M. P.; López, S.; Jiménez-Núñez, E.; Nevado, C.; Herrero-Gómez, E.; Raducan, M.; Echavarren, A. M. Gold(I)-Catalyzed Cyclizations of 1,6-Enynes: Alkoxycyclizations and Exo/Endo Skeletal Rearrangements, *Chem. – Eur. J.* **2006**, *12*, 1677–1693.

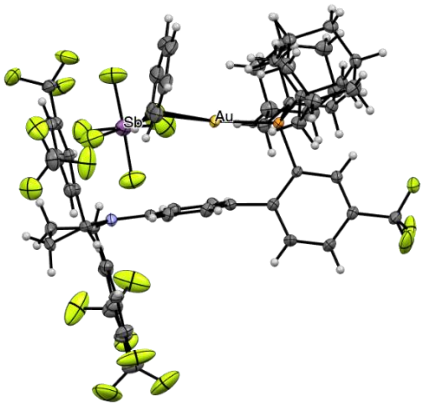

Figure 1.16. X-ray structure of cationic complex (*R,R*)-**F'**

For the Ag and Cu complexes (*R,R*)-**G** and (*R,R*)-**H**, reported procedures[33] were adapted to our systems ending in excellent yields (Scheme 1.11). The structure of complexes (*R,R*)-**G** and (*R,R*)-**H** were confirmed by single-crystal X-ray diffraction (Figure 1.17). Cationic silver complex crystallized in a mixture of pentane/toluene adding toluene in its structure by η^3 coordination whereas cationic copper complex crystallization took place in a mixture of CH_2Cl_2/pentane having in its coordination sphere two molecules of acetonitrile.

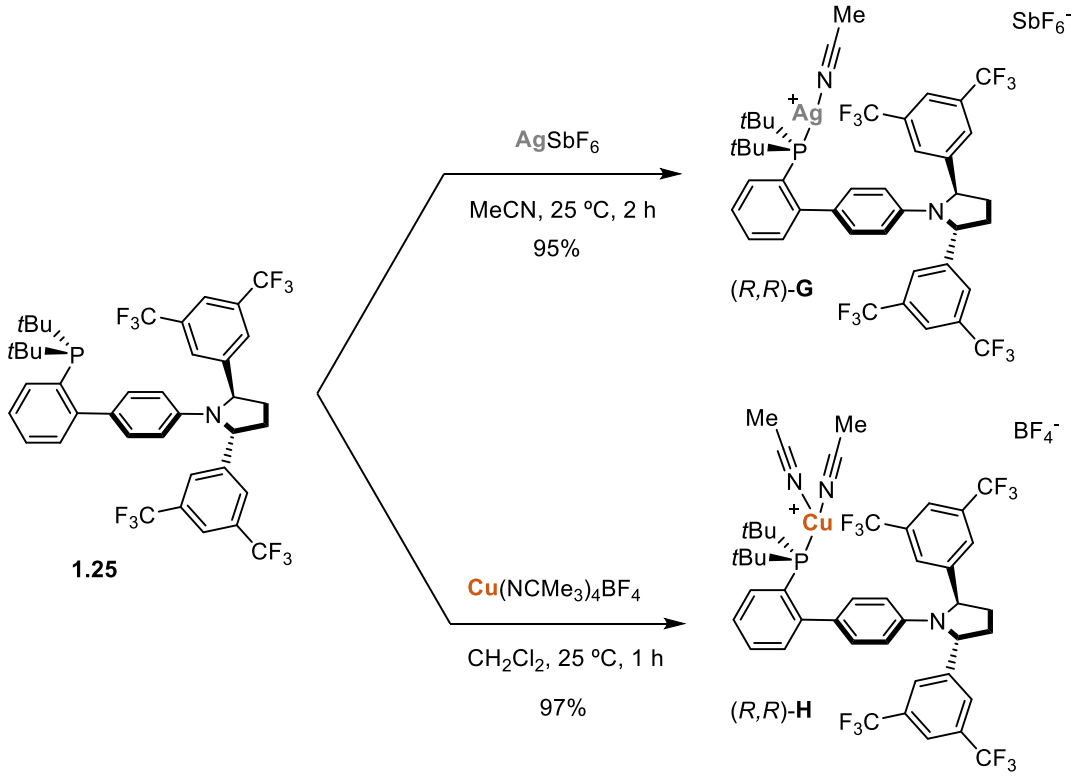

Scheme 1.11. Synthetic pathways for the isolation of silver(I) complex **(*R,R*)**-G and copper(I) complex **(*R,R*)**-H

33 Pérez-Galán, P.; Delpont, N.; Herrero-Gómez, E.; Maseras, F.; Echavarren, A. M. Metal–Arene Interactions in Dialkylbiarylphosphane Complexes of Copper, Silver, and Gold, *Chem. – Eur. J.* **2010**, *16*, 5324–5332.

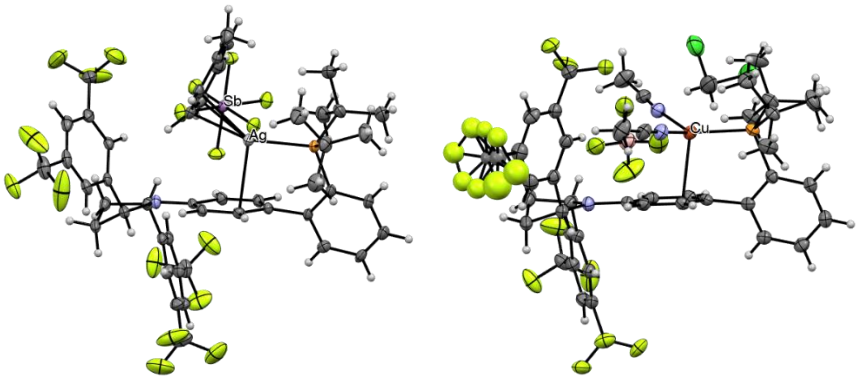

Figure 1.17. X-ray structures of (*R,R*)-**G** (on the right) and (*R,R*)-**H** (left)

With the crystal structure of the three group 11 transition metal complexes in hand, we proceeded to analyze the bonds and distances that could be relevant for their behavior in catalysis (Table 1.3).

Table 1.3. Selected experimental (X-ray diffraction) distances and angles.

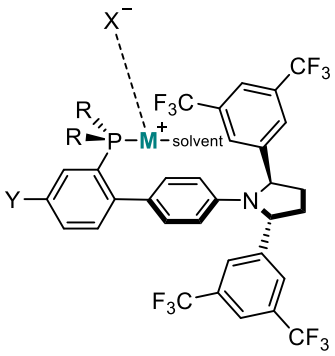

(*R,R*)-**F'**, M = Au, X = SbF_6, Y = CF_3, R = Ad, solvent = benzene
(*R,R*)-**G**, M = Ag, X = SbF_6,Y = H, R = *t*Bu, solvent = toluene
(*R,R*)-**H**, M = Cu, X = BF_4, Y = H, R = *t*Bu, solvent = $(NCCH_3)_2$

Complex	M-P	M-C_{ipso}	M-arene[a]	Angle P-M-solvent[c]	Dihedral Angle[b]
(*R,R*)-**F'**	2,26	2.99	2.99	168,75	83.53
(*R,R*)-**G**	2,38	2,93	2,71	160,37	111.17
(*R,R*)-**H**	2,22	2,74	2,53	124,49 121,18	114.80

X-ray values from .res file. Distances [Å] and angles [°]. [a] Distance to closest C from arene. [b] Dihedral angle between aryl groups. [c] Angle P-metal-closest atom/atoms to the metal center.

The most remarkable difference in this family of complexes is the distance between the metal and the bottom arene ring, which is closer for Cu (2.53 Å) and farther for Au (3.33 Å). Another factor that was perceptible consists of the deviation in the direction of solvent-M-P bond from the straight line that connects the pyrrolidine N with the two bonding C between the aryl rings; which is less for Au, then Ag and Cu; meaning that the replacement of solvent by a molecule of substrate will be further away from the encapsulating ligand in the case of Cu. The metal–ligand distances follow the trend observed in other examples (Cu<Au<Ag)[34,33]. This trend is also reproduced in the DFT calculations performed taking as input the X-ray coordinates (Table 1.4). The optimizations were performed without including counteranions using B3LYP-D3 functional,[35,36] basis set def2-TZVP,[37] and solvation using PCM[38] (CH_2Cl_2).

Table 1.4. Selected calculated (DFT) distances and angles

Complex	M-P	M-C_{ipso}	M-arene[a]	Angle P-M-solvent[c]	Dihedral Angle[b]
(*R,R*)-**F'**	2,32	3,07	3,08	176,41	-107,30
(*R,R*)-**G**	2,41	2,96	2,96	160,70	-103,23
(*R,R*)-**H**	2,26	2,95	2,62	121,35 120,10	-69,49

Values extracted from DFT calculations (B3LYP-D3/def2-TZVP/PCM(CH_2Cl_2)) taking as input the coordinates of the X-ray structures. Distances [Å] and angles [°]. [a] Distance to closest C from arene. [b] Dihedral angle between aryl groups

34 a) Ahrland, S.; Nilsson, K.; Persson, I.; Yuchi, A.; Penner-Hahn, J. E. Formation of Gold(I) Halide and Thiocyanate Complexes in Pyridine and Acetonitrile and the Structures of Gold(I) Solvates in These Solvents. A Thermodynamic and EXAFS Spectroscopic Study. *Inorg. Chem.* **1989**, *28*, 1833–1838. b) A. Bayler, A. Schier, G. A. Bowmaker, H. Schmidbaur, Gold Is Smaller than Silver. Crystal Structures of [Bis(trimesitylphosphine)gold(I)] and [Bis(trimesitylphosphine)silver(I)] Tetrafluoroborate, *J. Am. Chem. Soc*. **1996**, *118*, 7006 –7007.

35 a) Becke, A. D. Density-Functional Exchange-Energy Approximation with Correct Asymptotic Behavior, *Phys. Rev. A* **1988**, *38*, 3098–3100. b) Density-functional Thermochemistry. III. The Role of Exact Exchange, *J. Chem. Phys.* **1993**, *98*, 5648–5652.

36 Grimme, S. Density Functional Theory with London Dispersion Corrections, *WIREs Comput. Mol. Sci.* **2011**, *1*, 211–228.

37 Weigend, F.; Ahlrichs, R. Balanced Basis Sets of Split Valence, Triple Zeta Valence and Quadruple Zeta Valence Quality for H to Rn: Design and Assessment of Accuracy, *Phys. Chem. Chem. Phys.* **2005**, *7*, 3297.

38 Klein, R. A.; Mennucci, B.; Tomasi, J. Ab Initio Calculations of ^{17}O NMR-Chemical Shifts for Water. The Limits of PCM Theory and the Role of Hydrogen-Bond Geometry and Cooperativity, *J. Phys. Chem. A*. **2004**, *108*, 5851–5863.

1.3.3 Evaluation of complexes (*R,R*)-F', (*R,R*)-G and (*R,R*)-H in catalysis

The performance of complexes *R,R*)-**F'**, (*R,R*)-**G** and (*R,R*)-**H** was tested in the cyclopropanation of styrene **1.27** with phenyldiazoacetate **1.26** (Table 1.5)[39]. The best enantiomeric ratio towards the *trans*-isomer **1.28** was achieved when using cationic gold complex (*R,R*)-**F'**. Comparatively, the silver (*R,R*)-**G** and copper (*R,R*)-**H** analogs gave slightly lower enantioselectivities.

Table 1.5. Test of gold, silver and copper complexes in the cyclopropanation of styrene.

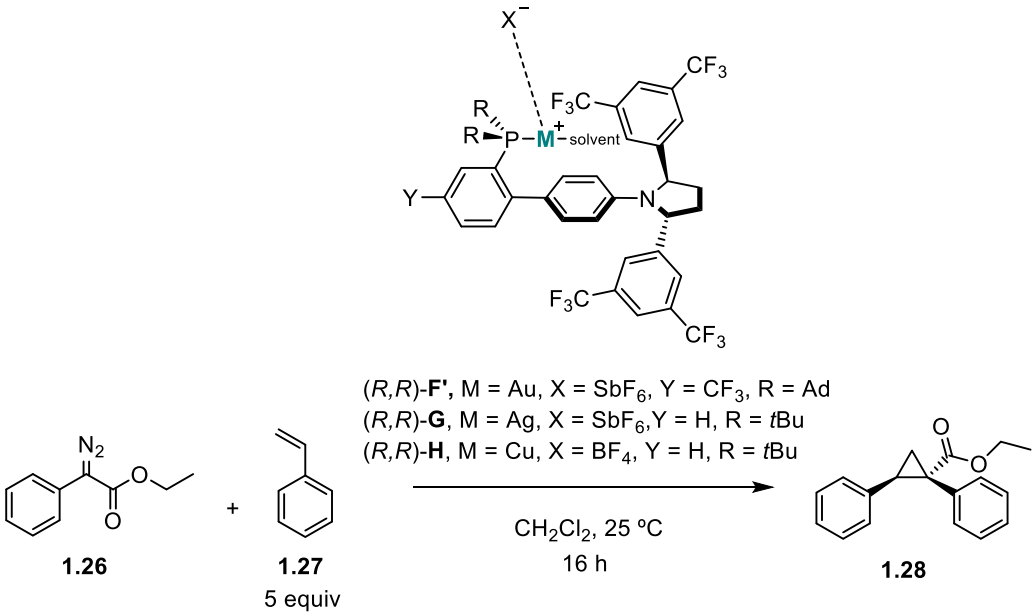

Catalyst (1.5 mol%)	Yield (%)[a]	er (%)[b]
(*R,R*)-**F'**	60	76:24
(*R,R*)-**G**	50	66:34
(*R,R*)-**H**	54	61:39

[a] Isolated yield. [b] Enantiomeric ratios determined by SFC.

The trend predicted in the previous section was manifested in the enantiomeric ratios obtained on the catalytic cyclopropanation of olefin **1.27**.

39 Prieto, A.; Fructos, M. R.; Mar Díaz-Requejo, M.; Pérez, P. J.; Pérez-Galán, P.; Delpont, N.; Echavarren, A. M. Gold-Catalyzed Olefin Cyclopropanation, *Tetrahedron.* **2009**, *65*, 1790–1793.

1.3.4 Mechanistic insights on the formal [4+2] cycloaddition of 1,6-enyne.

In 2008, our group published a mechanistic study on the gold(I)-catalyzed intramolecular formal [4+2] cycloaddition of enyne **1.29**[40], incorporating both experimental and computational analyses (Scheme 1.12). The reaction proceeds stepwise by the initial formation of a cyclopropyl gold(I)-carbene, followed by its opening to form a carbocation stabilized by a π interaction with the aryl ring and a Friedel-Crafts-type reaction. The highest computed energy barrier was associated with the formation of cyclopropyl gold(I) carbene **1.31**, whereas the Friedel-Crafts-type reaction leading to the Wheland intermediate **1.32** is exothermic.

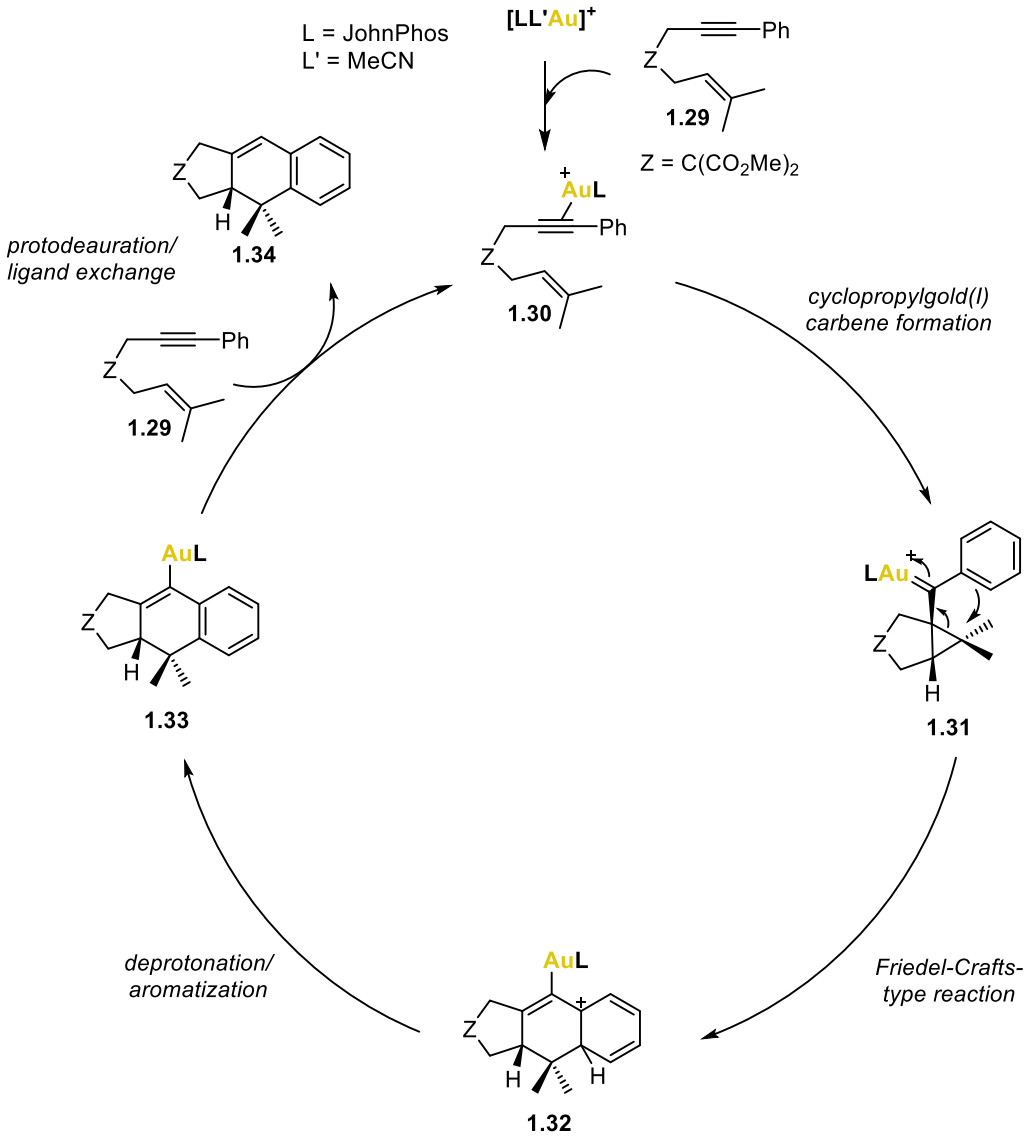

Scheme 1.12. Catalytic cycle in the formation of **1.29**, bearing gold as ligand JohnPhos or acetonitrile.

40 Nieto-Oberhuber, C.; Pérez-Galán, P.; Herrero-Gómez, E.; Lauterbach, T.; Rodríguez, C.; López, S.; Bour, C.; Rosellón, A.; Cárdenas, D. J.; Echavarren, A. M. Gold(I)-Catalyzed Intramolecular [4+2] Cycloadditions of Arylalkynes or 1,3-Enynes with Alkenes: Scope and Mechanism, *J. Am. Chem. Soc.* **2008**, *130*, 269–279.

The thermodynamic activation parameters were determined by Eyring analysis to be $\Delta G^{\ddagger}_{298}$ = 22.4 ± 0.5 kcal·mol^{-1}, $\Delta H^{\ddagger}$ = 12.6 ± 0.1 kcal·mol^{-1}, and $\Delta S^{\ddagger}$ = –33.1 ± 0.5 cal·mol^{-1}·K^{-1}, revealing a negative entropy of activation.

The formal [4+2] cycloaddition reaction of enyne **1.29** catalyzed by **A** required only 1 h,[41] meanwhile our pyrrolidine-containing biphenyl phosphine gold(I) catalysts exhibited lower reactivities, reaching complete conversion to the desired product **1.34** after 24 h (Table 1.6, entry 1).[42]

Table 1.6. Reaction times comparison on the [4+2] cycloaddition reaction of enyne **1.29**.

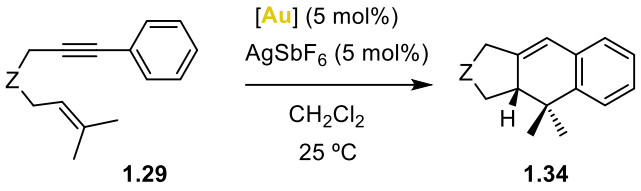

Entry	[Au]	Time (*h*)	Yield (*%*)[a]
1	**A**	1	86
2	(*R,R*)-**B**	24	88
3	(*R,R*)-**I**	6	70[c]

[a] Yield determined by ^{1}H NMR using 1,3,5-tribromobenzene as internal standard. [b] No addition of $AgSbF_6$. [c] Isolated yield.

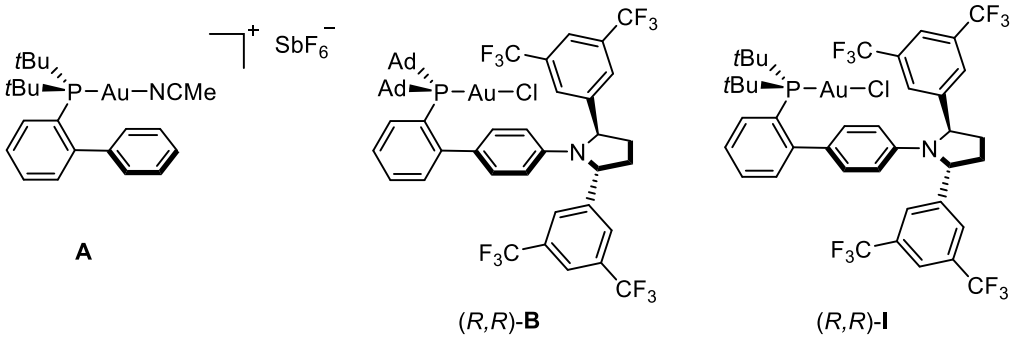

These results suggested that when the remote chiral pyrrolidine is present in the catalyst, influences the catalytic process by slowing down the reaction with respect to catalyst **A** (Table 1.6). The lower reactivity of (*R,R*)-**B** and (*R,R*)-**I** could be attributed to a reduced electrophilicity

41 Nieto-Oberhuber, C.; López, S.; Echavarren, A. M. Intramolecular [4+2] Cycloadditions of 1,3-Enynes or Arylalkynes with Alkenes with Highly Reactive Cationic Phosphine Au(I) Complexes. *J. Am. Chem. Soc*. **2005**, *127*, 6178-179.

42 Experiments performed by Dr. Giuseppe Zuccarello, described in his PhD Thesis (ref. 26)

of the catalyst, given the presence of the more electron-donating and bulkier bis-adamantyl or *tert*-butyl phosphines. Mechanistic investigations were carried out in the system using conditions in entry 3, Table 1.6. The chloride abstraction was considered to occur instantaneously[43] (using 1 equivalent of $AgSbF_6$). The partial kinetic orders of reaction of both catalyst (*R,R*)-**I** and starting enyne **1.29** were determined using initial rates method and resulted in first order and zeroth order respectively. Kinetic isotope effect (KIE) studies showed values close to 1, therefore discarding the deprotonation/aromatization step as rate-determining. Finally, it was considered that the longer reaction times could be attributed to a more sterically hindered ligand exchange process in which the molecule of product is released from the catalyst and replaced by a new molecule of substrate. The hypothesis was proven by carrying out the cycloaddition of enyne **1.29** in the presence of product **1.34** (2.5:1 ratio) and observing a drop in the rate constant, extracted by initial rates method. Therefore, a new catalytic cycle was proposed (Scheme 1.13) where the ligand exchange event and protodeauration from σ-gold intermediate **1.33** to give intermediate **1.35** were considered separately.[42]

43 Wang, D.; Cai, R.; Sharma, S.; Jirak, J.; Thummanapelli, S. K.; Akhmedov, N. G.; Zhang, H.; Liu, X.; Petersen, J. L.; Shi, X. "Silver Effect" in Gold(I) Catalysis: An Overlooked Important Factor, *J. Am. Chem. Soc.* **2012**, *134*, 9012–9019.

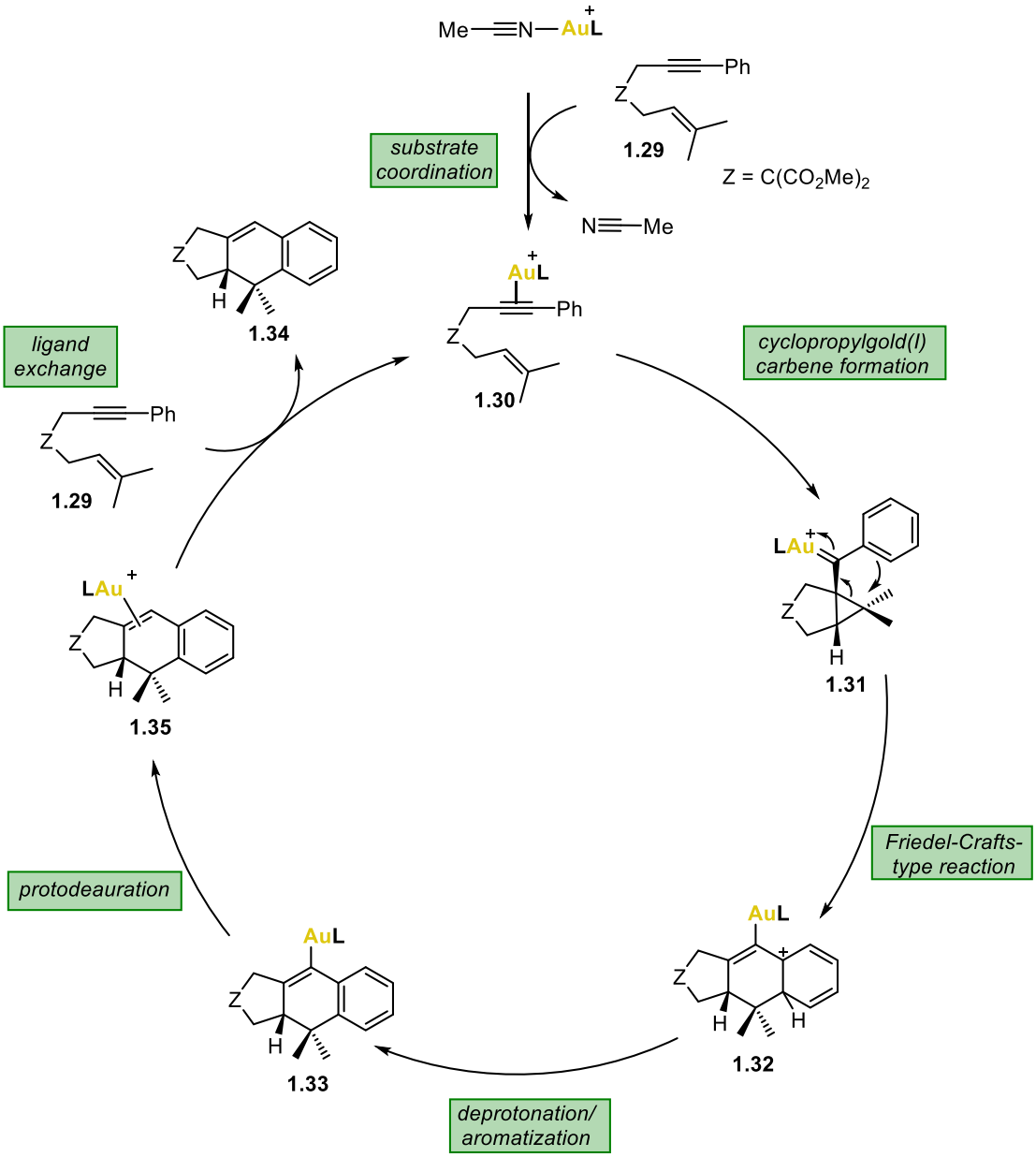

Scheme 1.13. Proposed catalytic cycle as a basis for the mechanistic investigations.

To compare and complement the previously mentioned mechanistic results obtained by Giuseppe Zuccarello during his PhD studies,[26] the first kinetic experiments were performed (Scheme 1.14) in the same system using 1,6-enyne **1.29** and 1,3,5-tribromobenzene as internal standard.

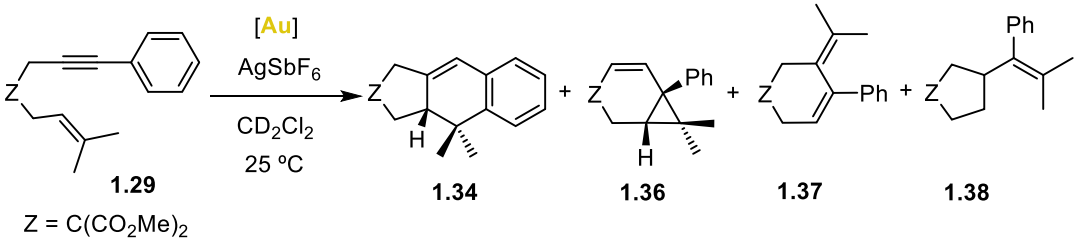

Scheme 1.14. Reaction whose kinetics was firstly studied.

Firstly, it was considered a variation on the gathering of the kinetic data, from monitoring the reaction by ^{1}H NMR to in situ FTIR spectroscopy.[44] Both kinetic methods rely on a relationship between the measurable parameter and concentration of species and are therefore called integral measurements because concentration is proportional to the integral of the reaction rate. Even though the first requirements needed for the technique to be suitable seemed fulfilled, in the end the method was not suitable for our system due to overlapping of IR bands in substrate and product. Then, the monitoring of the reaction was done by ^{1}H NMR at 25ºC.

It was found that with the malonate enyne **1.29** there are important side reactions occurring at the same time as the desired cycloaddition, reaching maximum a 70% conversion to product **1.34**. The main byproduct formed seemed to be coming from the 6-*endo*-dig pathway (Scheme 1.14), after 1,2-H shift giving product **1.36**. Also visible in the ^{1}H NMR spectra but in less extent were products **1.37** and **1.38**, both single-cleavage products after 6-*endo*-dig and 5-*exo*-dig cycloisomerizations respectively.[45] Therefore, we decided to continue with the experiments using the reduced malonate enyne **1.21** instead, which selectivity towards the [4+2] cycloaddition is very high (Scheme 1.15).[11]

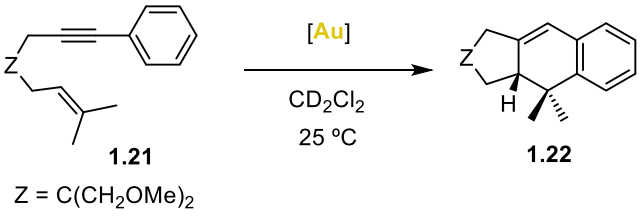

Scheme 1.15. [4+2] cycloaddition reaction submitted to kinetic investigations using as substrate reduced malonate **1.21**.

To understand the nature of the rate-determining step taking place in this unimolecular catalytic transformation, the use of silver salts to activate the gold complex has been avoided by preparing an isolated cationic gold(I) catalyst (*R,R*)-**F'** (Scheme 1.10). The usage of silver salts in the reaction mixture or other halide scavengers could lead to interferences in the accuracy of the kinetic studies (heterogeneous reaction taking place, silver effect, errors on the activation of the precatalyst due to challenging weighting and addition as it is an extra reagent in low quantity). The synthesis was achieved following a similar synthetic route reported previously in our group.[11]

In this case, VTNA method was applied[14], instead of initial rates method, for the determination of partial kinetic orders in gold(I) catalyst (*R,R*)-**F'**, substrate **1.21** and product **1.22**. The six

44 Pintar, A.; Batista, J.; Levec, J. In Situ Fourier Transform Infrared Spectroscopy as an Efficient Tool for Determination of Reaction Kinetics, *The Analyst* **2002**, *127*, 1535–1540.

45 Nieto-Oberhuber, C.; Muñoz, M. P.; Buñuel, E.; Nevado, C.; Cárdenas, D. J.; Echavarren, A. M. Cationic Gold(I) Complexes: Highly Alkynophilic Catalysts for the Exo- and Endo-Cyclization of Enynes, *Angew. Chem. Int. Ed Engl.* **2004**, *43*, 2402–2406.

individual experiments performed are summarized in Table 1.7, varying substrate, catalyst and product concentration.

Table 1.7. Conditions in the experiments performed for VTNA.

Experiment	[Substrate] / mM	[catalyst] / mM	[Product] / mM
A	100	7.5	0
B	50	7.5	0
C	200	7.5	0
D	100	10	0
E	100	5	0
F	100	7.5	50

From experiments A-C it was extracted the order in substrate; from A, D and E the order in catalyst; and finally from A and F the order in product. As observed in the plots represented in Figure 1.17, the reaction was found to be 0.6 order in substrate; approximately first order (0.9 order) in catalyst, discarding the possible formation of inactive dimeric species, and -0.2 order in product, implying product inhibition to some extent.

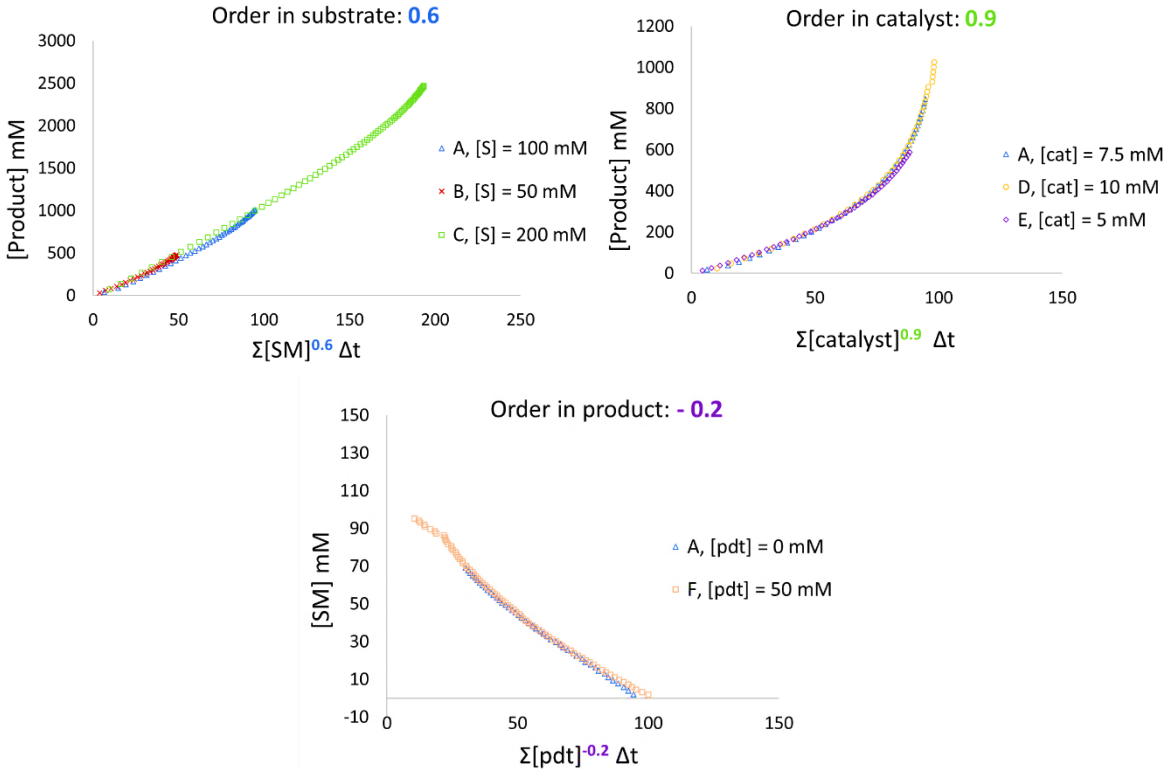

Figure 1.17. Best visual fits in the variable-time normalization analysis (VTNA) plots applied in the system for the determination of partial kinetic orders in substrate, catalyst, and product of the [4+2] cycloaddition.

At this point, the VTNA was applied to all components that influence the reaction kinetics, resulting in a plot with a straight line where the slope corresponds to k_{obs} (Figure 1.18), with value 0.016 $mM^{-0.5}min^{-1}$. Besides, the equation rate can be expressed (Eq 1.3).

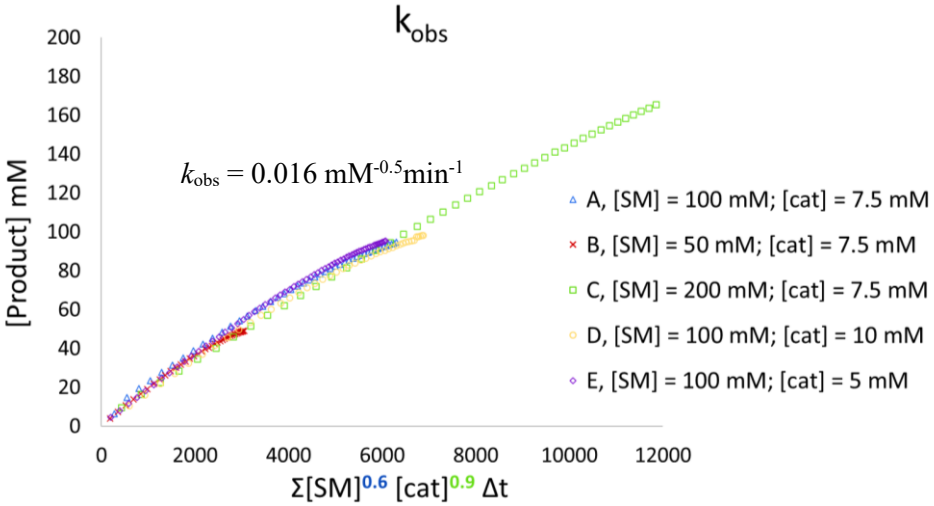

Figure 1.18. VTNA plot for the determination of k_{obs}.

(**Eq 1.3**) $$\text{rate} = k_{obs}\,[SM]^{0,6}\,[cat]^{0.9}\,[P]^{-0.2}$$

A fractional order in substrate could be explained in reactions that follow Briggs-Haldane kinetics (a refinement of the Michaelis-Menten model for enzyme kinetics),[46] as demonstrated previously in our group.[47] To test if the system falls within this scenario, RPKA[13] was applied by using kinetic data corresponding to a substrate/catalyst ratio (S/C) of 40, resulting in a non-optimal fit. The reason that could explain the fact that the studied system does not follow Michaelis-Menten kinetics is that the product dissociation from the catalyst is neither fast nor irreversible (the kinetic partial order in product is -0.2). Therefore, the other plausible explanation for the fractional order obtained in substrate might be due to the influence of more than one step in the turnover-limiting step. Based on previous experiments performed in the group mentioned above, the two candidate rate-determining steps are the gold carbene formation and ligand exchange (dissociative), making general order in substrate close to 0.5 (average from 1 order and 0 order respectively).

Eyring analysis[48]

An Eyring analysis was performed by monitoring five same concentration experiments at different temperatures ranging between 295-303 K. Based on initial rates, the first minutes of each reaction up to 15-20% conversion were plotted in Figure 1.19; assuming a pseudo-zeroth partial

46 Briggs, G. E.; Haldane, J. B. S. A Note on the Kinetics of Enzyme Action, *Biochem. J.* **1925**, *19*, 338–339.
47 Franchino, A.; Martí, À.; Echavarren, A. M. H-Bonded Counterion-Directed Enantioselective Au(I) Catalysis, *J. Am. Chem. Soc.* **2022**, *144*, 3497–3509.
48 The first attempts of the Eyring analysis were performed by Dr. Giuseppe Zuccarello.

order in substrate. Each of the slopes of every reaction corresponds to *k*. The Eyring equation was used (Eq 1.4), wherein:

(Eq 1.4)

$$\ln\frac{k}{T} = \frac{-\Delta H^{\neq}}{R} \cdot \frac{1}{T} + \ln\frac{\kappa k_B}{h} + \frac{\Delta S^{\neq}}{R}$$

Consequently, the Eyring plot consists on plotting 1/T against ln(*k*/T) (Figure 1.20) for the determination of the thermodynamic parameters of activation (Table 1.8). Accordingly to the fractional order in substrate obtained, the clearly observed inversion point (T_{inv} = 26 ºC) in the Eyring plot supported the presence of two competing rate-determining steps.[49]

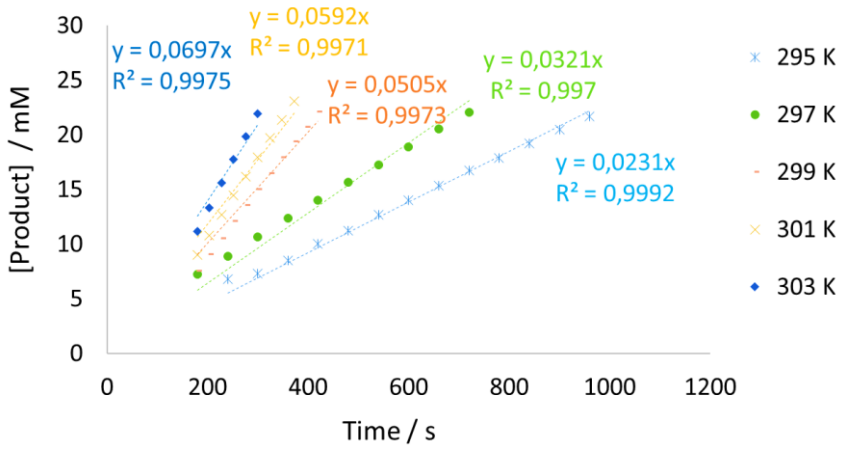

Figure 1.19. Plot of the five experiments run at different temperatures, assuming pseudo-zeroth order in substrate.

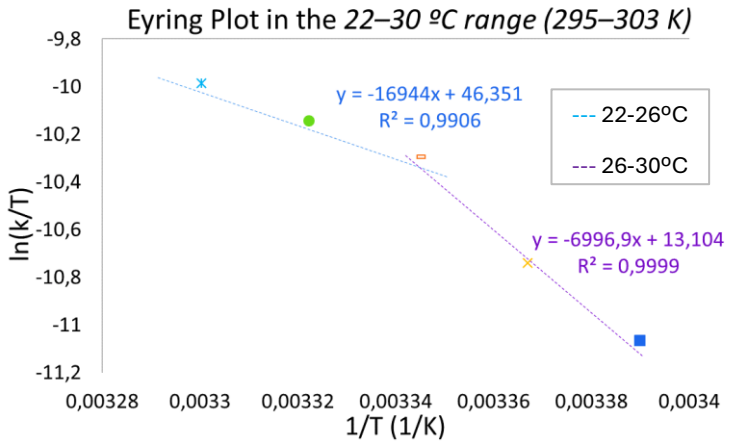

Figure 1.20. Eyring analysis at both ranges of temperatures.

49 Franchino, A.; Martí, À.; Nejrotti, S.; Echavarren, A. M. Silver-Free Au(I) Catalysis Enabled by Bifunctional Urea- and Squaramide-Phosphine Ligands via H-Bonding, *Chem. – Eur. J.* **2021**, *27*, 11989–11996.

The calculated $\Delta G^{\ddagger}$ at 298 K (20.3 kcal mol^{-1}) is in good agreement with a reaction occurring at room temperature in 2-3 h. It is important to note that the Gibbs free energies of activation remained similar when the temperature ranges were examined separately (Table 1.8). However, the entropies and enthalpies of activation examined in separate temperature ranges are variable. At higher temperatures (26-30 ºC) ($\Delta H^{\ddagger}$ = 13.9 kcal·mol-1, $\Delta S^{\ddagger}$ = –21.2 cal mol^{-1} K^{-1}) a negative entropy of activation supports that the formation of cyclopropyl gold(I) carbene **1.31**, in which two C–C bonds are formed ($\Delta S^{\ddagger} < 0$), predominates as the rate-determining step. Meanwhile, at lower temperatures (22–26 ºC), the entropy of activation is high and positive ($\Delta S^{\ddagger}$ = +44.9 cal mol^{-1} K^{-1}) compared to the entropy of activation determined for the entire temperature range ($\Delta S^{\ddagger}$ = +13.9 cal mol^{-1} K^{-1}); which suggests a scenario in which the energetic span of the catalytic cycle is composed of the ligand exchange, proceeding *via* pseudo-dissociative ligand exchange (associative with respect to gold(I) and dissociative with respect to the substrate, $\Delta S^{\ddagger} > 0$). The general positive entropy of activation ($\Delta S^{\ddagger}$ = +13.9 ± 6.0 cal mol^{-1} K^{-1}) found is in contrast to that obtained with JohnPhos gold(I) complex **A**[16,41] and to those observed for similar intramolecular cycloaddition reactions.[50] Importantly, among the gold(I)-catalyzed systems studied in our group this is the first example displaying a positive entropy of activation.[51,52]

Table 1.8. Thermodynamic parameters of activation calculated at high and low temperatures as well as in the whole range.

T (ºC)	$\Delta G^{\#}_{298}$ (kcal/mol)	$\Delta H^{\#}_{298}$ (kcal/mol)	$\Delta S^{\#}_{298}$ (kcal/mol)
22-30	20.3 ± 6.0	24.3 ± 3.0	13.5 ± 10.1
22-26	20.9 ± 6.5	33.6 ± 3.3	44.9 ± 11.0
26-30	20.2 ± 0.4	13.9 ± 0.2	-21.2 ± 0.6

50 Diedrich, M. K.; Klärner, F.-G.; Beno, B. R.; Houk, K. N.; Senderowitz, H.; Still, W. C. Experimental Determination of the Activation Parameters and Stereoselectivities of the Intramolecular Diels−Alder Reactions of 1,3,8-Nonatriene, 1,3,9-Decatriene, and 1,3,10-Undecatriene and Transition State Modeling with the Monte Carlo-Jumping Between Wells/Molecular Dynamics Method, *J. Am. Chem. Soc.* **1997**, *119*, 10255–10259.

51 Nieto-Oberhuber, C.; López, S.; Muñoz, M. P.; Cárdenas, D. J.; Buñuel, E.; Nevado, C.; Echavarren, A. M. Divergent Mechanisms for the Skeletal Rearrangement and [2+2] Cycloaddition of Enynes Catalyzed by Gold, *Angew. Chem. Int. Ed Engl.* **2005**, *44*, 6146–6148.

52 Escribano-Cuesta, A.; Pérez-Galán, P.; Herrero-Gómez, E.; Sekine, M.; Braga, A. A. C.; Maseras, F.; Echavarren, A. M. The Role of Cyclobutenes in Gold(i)-Catalysed Skeletal Rearrangement of 1,6-Enynes, *Org. Biomol. Chem.* **2012**, *10*, 6105.

The proposed ligand exchange process occurring through a pseudo-dissociative mechanism might happen by the rotation of the C_{aryl}–N bond, inducing the formation of a gold(I) species that is stabilized via Au-π interactions with the aromatic substituent of the pyrrolidine (Scheme 1.16).[53]

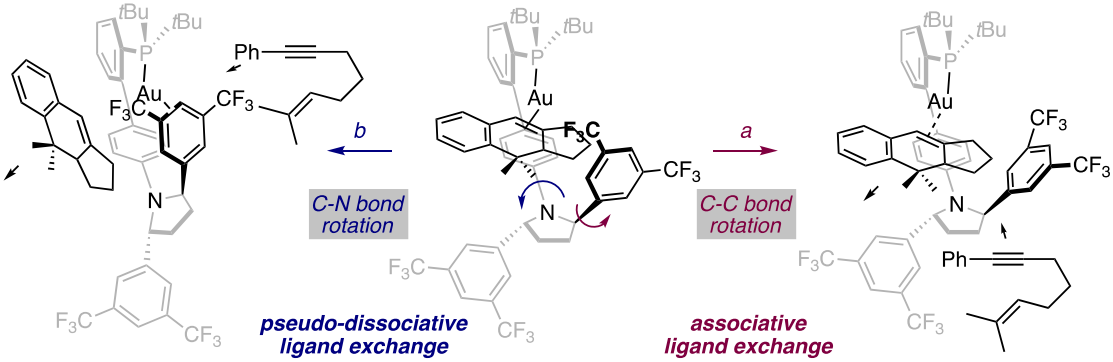

Scheme 1.16. Ligand exchange proposed mechanisms.

Influence of substituents Z in substrate

The effect of the nature of Z in the substrate chosen for the reaction was noticed. We decided to study to what extent this affected the reaction by preparing two experiments run under the exact same conditions, just varying the 1,6-enyne (**1.29** or **1.21**). As observed in Figure 1.21, the reaction is faster when the reduced malonate enyne **1.21** (Z = $C(CH_2OMe)_2$ was used instead of the ester malonate enyne **1.29** (Z = $C(CO_2Me)_2$).

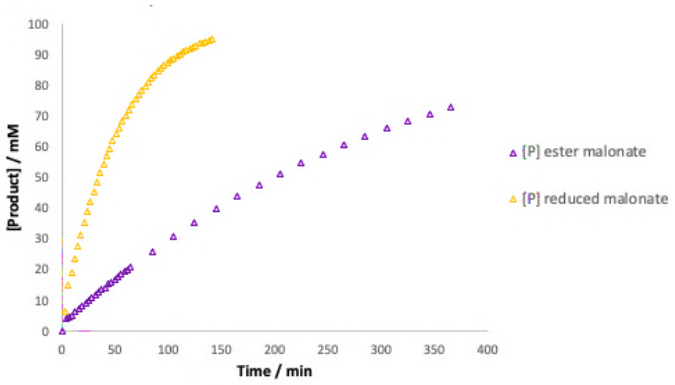

Figure 1.21. Product concentration plot for two experiments run under the same conditions.

As a change in mechanism is not plausible, the reason might be that the ester could be coordinating to Au (**1.39**) and therefore slowing down the reaction (Scheme 1.17). Another factor playing a

53 a) Mascal, M.; Kerdelhué, J.-L.; Blake, A.; Cooke, P. A.; Mortimer, R.; Teat, S. On the Nature of Arene H6 Interactions in the Solid State and the Use of Cylindrophanes as Ligands for Sandwich Complexation of Metals with Longer-Range Interactions with the Benzene Ring, *Eur. J. Inorg. Chem.* **2000**, *2000,* 485-490. *b)* Mecozzi, S.; West, A. P.; Dougherty, D. A. Cation−π Interactions in Simple Aromatics: Electrostatics Provide a Predictive Tool, *J. Am. Chem. Soc.* **1996**, *118*, 2307–2308.

role could be the diminished reactivity of the alkene due to the inductive effect present in esters, higher than in ethers.

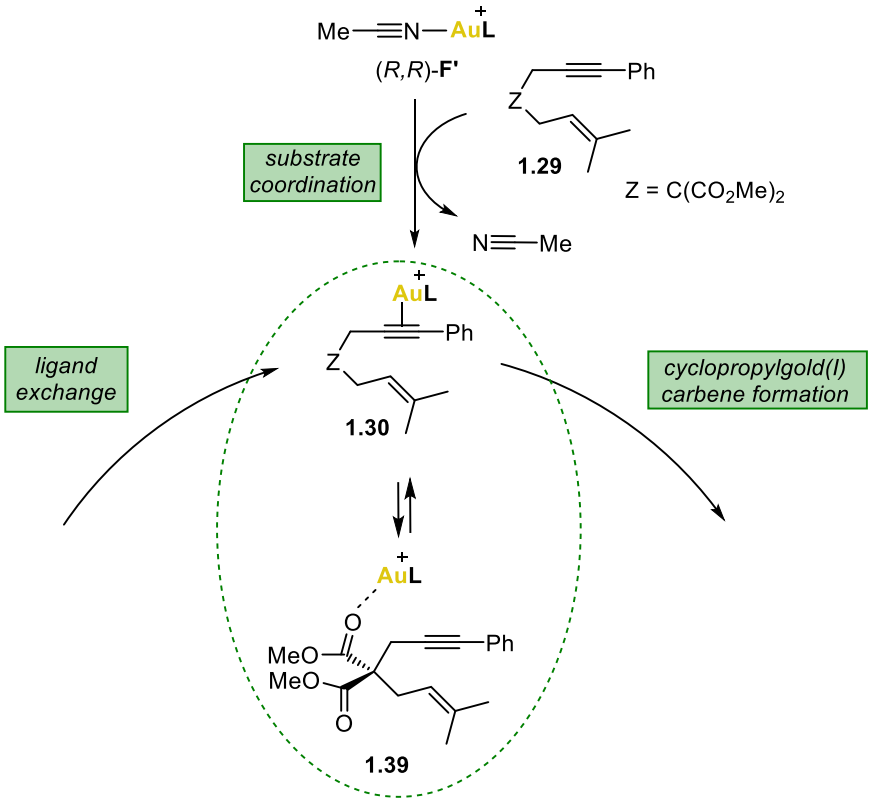

Scheme 1.17. Proposed equilibrium that might be affecting the kinetics of the reaction depending on the nature of Z.

1.4 Conclusions

The family of chiral biaryl-pyrrolidinyl phosphine gold(I) complexes has been expanded by including electron withdrawing substituents in the bottom aryl ring, not leading to the expected and desired enantioinductions in two types of gold(I) catalyzed reactions. Additionally, the metallic center has been replaced with other metals in group 11 of the periodic table: Ag and Cu; being able to observe a trend in enantioinduction and reactivities in asymmetric catalysis Au > Ag > Cu, that has been correlated with some studied structural properties of the complexes.

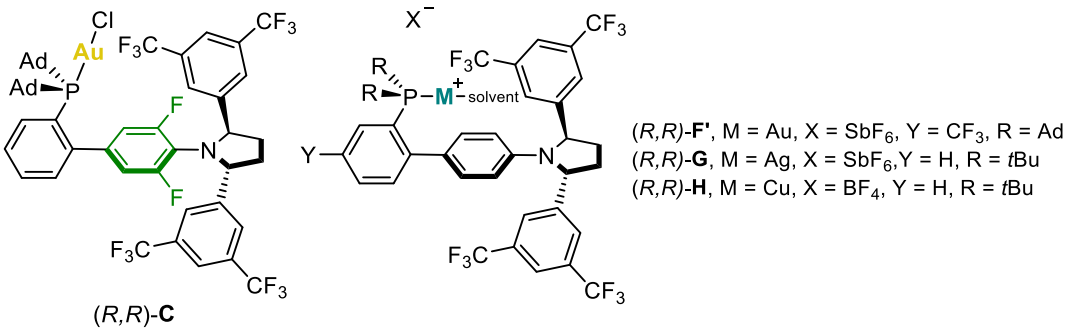

Figure 1.21. New complexes **s**ynthesized following the classical modular approach.

Parallelly, kinetic studies have been pursued in the formal [4+2] cycloaddition reaction of 1,6-enyne catalyzed by complex (*R,R*)-**F'**. The use of silver salts to activate the gold complex has been avoided by using isolated cationic gold(I) catalysts. A set of experiments has been designed to study the single steps involved in the catalytic cycle; among which are the determination of the reaction rate equation by VTNA and the determination of thermodynamic parameters of activation by Eyring analysis. Based on previous work performed in the group, we support the hypothesis of having two competing rate-determining steps (RDS) in the reaction: the formation of the cyclopropyl gold(I) carbene **1.31** and the ligand exchange step that closes the catalytic cycle, (Scheme 1.18).

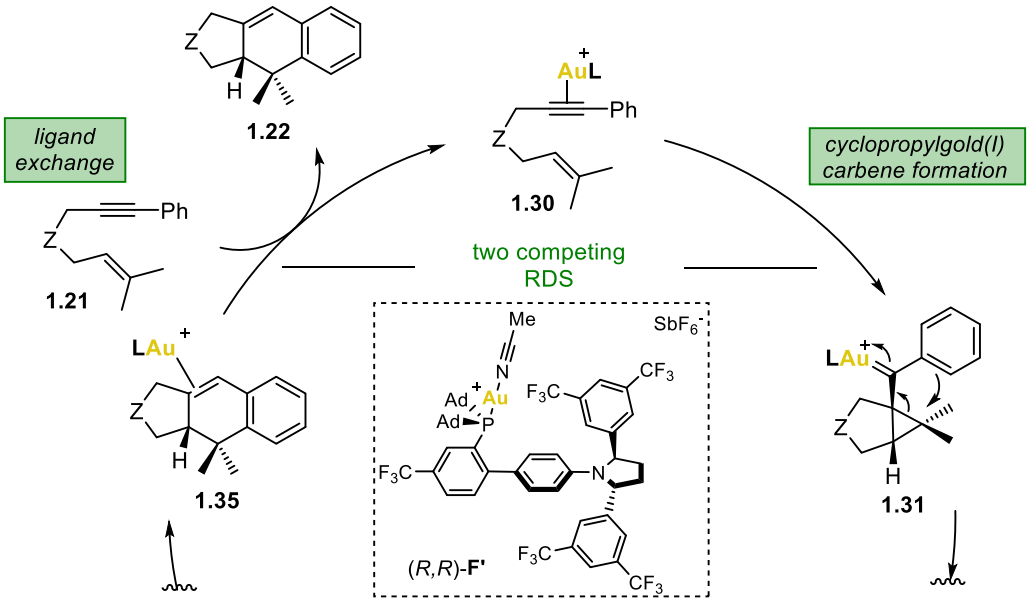

Scheme 1.18. Proposed rate-determining steps in the cyclization of **1.21** with (*R,R*)-**F'.**

1.5 Experimental Section

1.5.1 General information

Unless otherwise stated, all the reactions reported herein were performed under argon atmosphere. All reagents and solvents were purchased from commercial sources and used without further purification. The dry solvents used were passed through an activated alumina column on a PureSolvTM Solvent Purification System (SPS, Innovative Technologies, Inc., MA), or purchased from ACROS Organics as commercially available anhydrous solvents. The reaction monitoring was followed by NMR analysis, TLC (thin layer chromatography), UHPLC–MS (Agilent Technologies 1290 Infinity II, LC/MS with single–quad detector InfinityLab (APCI ionization source)) or by GC–MS. Thin layer chromatography was carried out using TLC aluminum sheets coated with 0.2 mm of silica gel (Merck Gf234), using UV light as the visualizing agent and an acidic solution of vanillin in ethanol or alternatively a basic solution of KMnO4 in water as stain, followed in both cases by heat. The chromatographic purifications were carried out using flash grade silica gel (SDS Chromatogel 60 ACC, 40–60 μm) as the stationary phase. Preparative thin layer chromatography was performed on TLC plates (Analtec Silica Gel GF UV254, 20×20 cm, 1000 μm or 2000 μm). NMR spectra were recorded at 298 K on Bruker Avance Ultrashield NMR spectrometers (300 MHz, 400 MHz, 500 MHz, and 500 MHz with CryoProbe). Chemical shifts (δ) are reported in parts per million (ppm) and referenced to residual solvent (For ^{1}H NMR: $CDCl_3$ at 7.26 ppm, CD_2Cl_2 at 5.31 ppm, C_6D_6 at 7.16 ppm, for $^{13}C\{^{1}H\}$ NMR: $CDCl_3$ at 77.16 ppm, CD_2Cl_2 at 54.00 ppm, C_6D_6 at 128.06 ppm). The following abbreviations were used to explain multiplicities: s = singlet, d = doublet, t = triplet, q = quartet, p = pentet, m = multiplet, br s = broad singlet. Coupling constants (*J*) are reported in Hertz (Hz). Mass spectra were recorded on a Waters LCT Premier Spectrometer (ESI and APCI) or on an Autoflex Broker Daltonics (MALDI and LDI). Specific optical rotation measurements were carried out on a Jasco P–1030 model polarimeter equipped with a PMT detector using the sodium line at 589 nm, and 1 mL (10 mm pathlength) or 2 mL (100 mm pathlength) cells. Melting points were determined using a Mettler Toledo MP70 melting point apparatus. Chiral HPLC analyses were performed on an Agilent Technologies 1200 series. SFC analyses were performed on an Agilent Technologies 1260 Infinity II, a Waters ACQUITY UPC2 System with diode array detector and by Chiral Technologies Europe analytical service. X-ray diffraction data were collected at 100 K on a Rigaku MicroMax-007HF, Mo Kα rotating anode, equipped with a Pilatus 200 K detector or on a Bruker APEX DUO, Mo Kα Microfocus source E025 IuS anode, equipped with an APEX DUO detector using omega scans.

1.5.2 Synthetic Procedures and Characterization Data

Synthesis of Complexes

Chiral Complex (*R*,*R*)-C

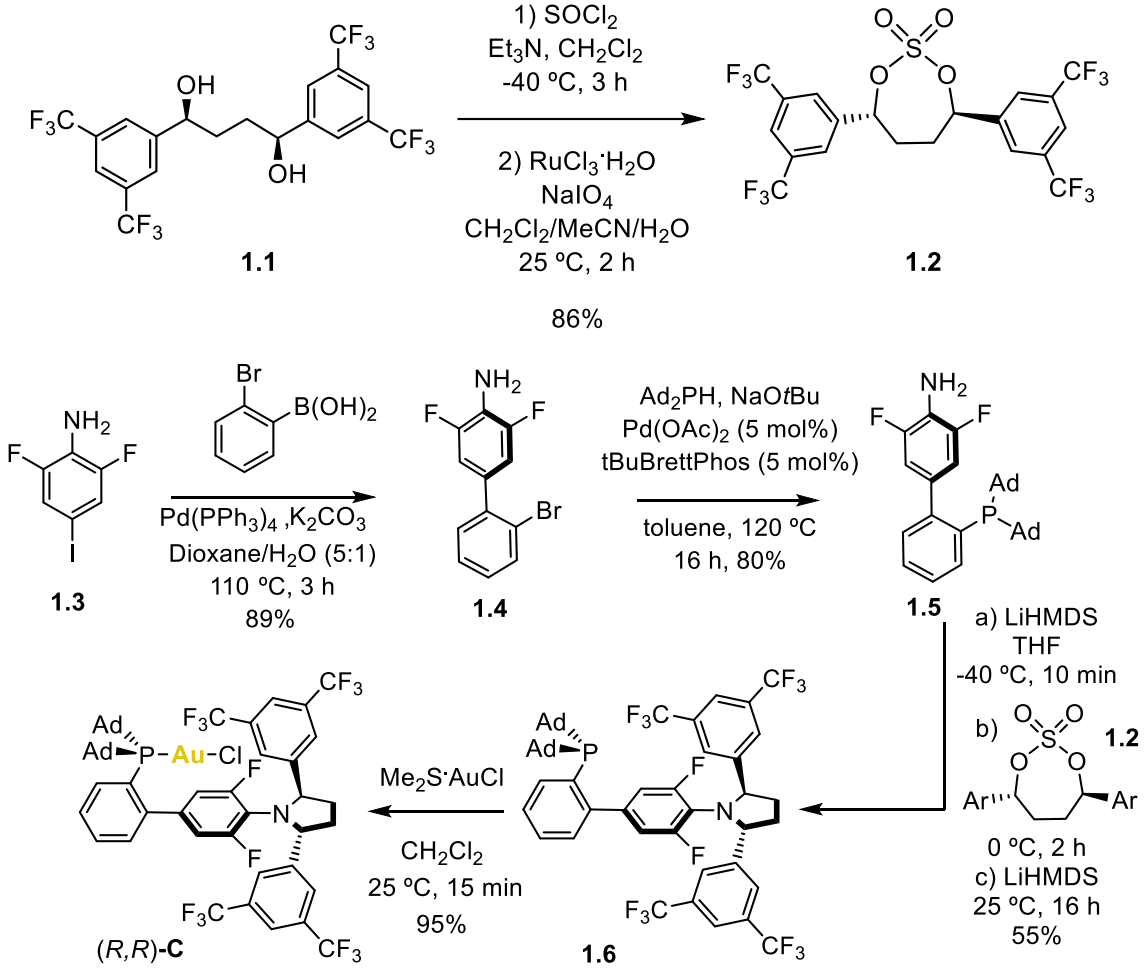

(4*R*,7*R*)-4,7-Bis(3,5-bis(trifluoromethyl)phenyl)-1,3,2-dioxathiepane 2,2-dioxide (1.2)

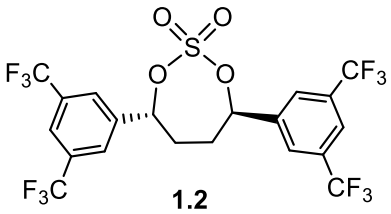

In a two-necked round bottom flask (1*S*,4*S*)-1,4-bis(3,5-bis(trifluoromethyl)phenyl)butane-1,4-diol **1.1** (0.70 g, 1.36 mmol, 1.0 equiv) was dissolved in CH_2Cl_2 (22.7 mL, 0.06 M) and triethylamine (828 mg, 1.14 mL, 8.18 mmol, 6 equiv) was added at –40 ºC. The reaction mixture was stirred at the same temperature for 30 min and then thionyl chloride (328 µL, 4.50 mmol, 3.3 equiv) was added. The reaction was stirred for additional 3 h at the same temperature. The reaction was quenched at -40 ºC by addition of water and CH_2Cl_2. The organic layer was separated and

the aqueous phase was extracted with CH_2Cl_2 (2x). The combined organic layers were dried over Na_2SO_4, filtered and concentrated. The crude product was used in the next step without purification. The crude sulfite was dissolved in CH_2Cl_2 (1.75 mL), MeCN (1.75 mL) and H_2O (2.5 mL) and ruthenium(III) chloride (2.83 mg, 13.6 μmol, 0.01 equiv) and sodium periodate (525 mg, 2.45 mmol, 1.8 equiv) were added sequentially. The reaction was stirred at 25 ºC for 2 h whereby the reaction progress was monitored by ^{1}H NMR. The reaction was diluted with CH_2Cl_2 and the organic layer was separated. The aqueous phase was extracted with CH_2Cl_2 (2x) and the combined organic layers were dried over Na_2SO_4, filtered and concentrated. Compound **1.2** (680 mg, 1.18 mmol, 86% yield) was obtained as a colourless solid and was used in the next step without purification.

^{1}H NMR (400 MHz, $CDCl_3$) δ 7.94 (s, 2H), 7.89 (s, 4H), 5.94 – 5.82 (m, 2H), 2.70 – 2.48 (m, 2H), 2.46 – 2.30 (m, 2H). **^{13}C{^{1}H} NMR** (126 MHz, CD_2Cl_2) δ 139.7, 132.9 (q, *J* = 33.9 Hz), 126.5 (d, *J* = 3.7 Hz), 123.6 (p, *J* = 3.8 Hz), 123.1 (q, *J* = 272.9 Hz), 83.1, 35.0. **^{19}F{^{1}H} NMR** (376 MHz, $CDCl_3$) δ –63.1. **HRMS** (ESI+) the exact mass calculated for $[C_{20}H_{12}F_{12}NaO_4S]^+$ is 599.0157 *m/z*; found $[M + Na]^+$ 599.0151 *m/z*. **M.p.** = >121 ºC (decomposition). **α_D^{589}**= –59.5 deg·cm^2·g^{-1} ($CHCl_3$, c 1.0, 298 K).

2'-Bromo-3,5-difluoro-[1,1'-biphenyl]-4-amine (1.4)

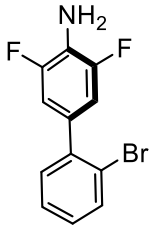

1.4

$Pd(PPh_3)_4$ (36.6 mg, 31.7 μmol, 4 mol%), (2-bromophenyl)boronic acid (175 mg, 871 μmol, 1.1 equiv), 2,6-difluoro-4-iodoaniline **1.3** (202 mg, 792 μmol, 1 equiv) and sodium carbonate (201 mg, 1.9 mmol, 2.4 equiv) were dissolved in water (800 μL) and 1,4-dioxane (3.1 mL) with a total concentration of 0.2 M. The reaction mixture was degassed for 5 min with argon and then stirred at 110 ºC in the MW for 3 h. The reaction mixture was allowed to cool to 24 ºC and EtOAc was added and filtered through celite. The layers were separated and the aqueous phase was extracted with EtOAc (2x). The combined organic layers were washed with brine, dried over Na_2SO_4 and concentrated. The crude was purified by SiO_2 flash column chromatography (cyclohexane/EtOAc 100:1) to yield title compound **1.4** (200 mg, 704 μmol, 89% yield) as an orange solid.

^{1}H NMR (500 MHz, $CDCl_3$) δ 7.67 (dd, *J* = 8.0, 1.3 Hz, 1H), 7.36 (td, *J* = 7.4, 1.3 Hz, 1H), 7.30 (dd, *J* = 7.7, 1.8 Hz, 1H), 7.21 (ddd, *J* = 8.0, 7.3, 1.9 Hz, 1H), 6.94 (dd, *J* = 7.3, 2.0 Hz, 2H), 3.83 (s, 2H). **^{13}C{^{1}H} NMR** (126 MHz, $CDCl_3$) δ 151.75 (dd, *J* = 240.4, 8.6 Hz), 141.07 (t, *J* = 2.3

Hz), 133.68, 131.61, 130.28 (t, *J* = 9.1 Hz), 129.26, 127.88, 123.81 (t, *J* = 16.3 Hz), 123.00, 112.88 – 112.31 (m). **$^{19}F\{^{1}H\}$ NMR** (471 MHz, $CDCl_3$) δ -132.88. **HRMS** (ESI+) the exact mass calculated for $[C_{12}H_9BrF_2N]^+$ is 283.9881 *m/z*; found $[M + H]^+$ 283.9879 *m/z*. **M.p.** = 67-70 °C.

2'-(Di((3S,5S,7S)-adamantan-1-yl)phosphaneyl)-3,5-difluoro-[1,1'-biphenyl]-4-amine (1.5)

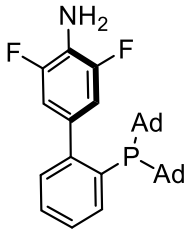

1.5

A 5 mL Schlenk flask was charged with 2'-bromo-3,5-difluoro-[1,1'-biphenyl]-4-amine **1.4** (90.0 mg, 317 µmol, 1 equiv), Pd(OAc)2 (2.64 mg, 12.7 µmol, 4 mol%), tBuBrettPhos (7.91 mg, 15.8 µmol, 5 mol%), NaO*t*Bu (60.9 mg, 634 µmol, 2.0 equiv) and toluene (1.5 mL, 0.2 M) and the resulting suspension was stirred for 15 min at 25 ºC. Di(1-adamantyl)phosphine (105 mg, 348 µmol, 1.1 equiv) was added and the reaction mixture was stirred at 110 ºC for 16 h. Then, the reaction was allowed to cool to 25 ºC and the crude was purified by SiO_2 flash column chromatography (cyclohexane/ EtOAc 100:1) to yield **1.5** (127 mg, 251 µmol, 79% yield) as a white solid.

^{1}H NMR (500 MHz, CDCl3) δ 7.86 (dt, J = 7.7, 1.6 Hz, 1H), 7.36 – 7.32 (m, 2H), 7.20 (ddd, J = 6.9, 4.0, 1.8 Hz, 1H), 6.70 (dd, J = 7.4, 1.8 Hz, 2H), 3.69 (s, 2H), 1.95 – 1.86 (m, 14H), 1.86 – 1.77 (m, 7H), 1.65 (d, J = 3.2 Hz, 11H). **$^{13}C\{^{1}H\}$ NMR** (126 MHz, CDCl3) δ 151.29 (d, J = 239.4 Hz), 136.80 (d, J = 2.9 Hz), 133.57, 130.83 (d, J = 5.9 Hz), 128.46, 125.78, 122.20, 113.42 (d, J = 17.9 Hz), 42.06 (d, J = 12.8 Hz), 37.06, 28.97 (d, J = 8.5 Hz). **$^{31}P\{^{1}H\}$ NMR** (202 MHz, CDCl3) δ 24.38. **$^{19}F\{^{1}H\}$ NMR** (471 MHz, CDCl3) δ -133.70. **HRMS** (ESI+) the exact mass calculated for $[C_{32}H_{39}F_2NP]^+$ is 506.2783 *m/z*; found $[M + H]^+$ 506.2777 *m/z*.

Ligand 1.6

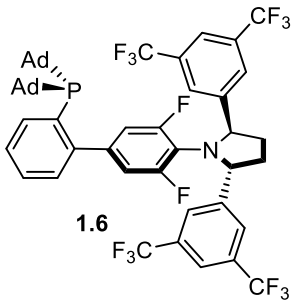

1.6

To a solution of 2'-(di((3S,5S,7S)-adamantan-1-yl)phosphaneyl)-3,5-difluoro-[1,1'-biphenyl]-4-amine **1.5** (120 mg, 237 µmol, 1 equiv) in dry THF (2.8 mL) at –40 °C were added a 1M solution of freshly prepared LiHMDS in THF (59.6 mg, 356 µL, 356 µmol, 1.5 equiv) under an atmosphere

of argon. The mixture was stirred for 10 min at the same temperature. Then a solution of (4R,7R)-4,7-bis(3,5-bis(trifluoromethyl)phenyl)-1,3,2-dioxathiepane 2,2-dioxide **1.2** (205 mg, 356 µmol, 1.5 equiv) in 4.2 mL of THF was added dropwise and the reaction mixture was slowly left to warm up to 0 ºC during 2h. Then more LiHMDS 1M solution in THF was added (59.6 mg, 356 µL, 356 µmol, 1.5 equiv) and the reaction mixture was left overnight at 25 ºC. The reaction was stopped and quenched by the addition of saturated aqueous NH_4Cl. The mixture was dissolved in EtOAc and water. The aqueous layer was extracted with EtOAc (2x). The combined organic solutions were washed with brine, dried over anhydrous Na_2SO_4 and concentrated in vacuo. The crude was purified by SiO_2 flash column chromatography (cyclohexane/EtOAc 15:1) to yield **1.6** (127 mg, 129 µmol, 55% yield) as a white solid.

^{1}H NMR (400 MHz, $CDCl_3$) δ 7.84 – 7.79 (m, 4H), 7.77 – 7.73 (m, 1H), 7.73 – 7.68 (m, 2H), 7.24 (dd, *J* = 5.8, 3.4 Hz, 2H), 7.02 (dt, *J* = 5.8, 3.7 Hz, 1H), 6.52 – 6.43 (m, 2H), 5.54 (t, *J* = 6.7 Hz, 2H), 2.76 – 2.59 (m, 2H), 2.13 – 1.99 (m, 2H), 1.78 – 1.49 (m, 30H). **^{13}C{^{1}H} NMR** (126 MHz, $CDCl_3$) δ 157.57 (dd, *J* = 245.5, 8.8 Hz), 149.02 (d, *J* = 33.1 Hz), 146.65, 140.09 (d, *J* = 7.4 Hz), 136.61 (d, *J* = 2.6 Hz), 133.55 (d, *J* = 30.7 Hz), 131.73 (q, *J* = 33.2 Hz), 129.82 (d, *J* = 5.9 Hz), 128.14, 127.15, 125.82, 123.45 (q, *J* =272.85 Hz), 121.62 – 120.82 (m), 118.43 (t, *J* = 14.6 Hz), 114.65 – 113.93 (m), 65.87 (t, *J* = 3.3 Hz), 41.75 (dd, *J* = 17.08, 13.3 Hz), 41.62 (d, *J* = 13.3 Hz), 37.15 (dd, *J* = 26.7, 9.0 Hz), 37.03-36.93 (m), 28.71 (dd, *J* = 8.4, 4.0 Hz), 26.93. **^{31}P{^{1}H} NMR** (162 MHz, $CDCl_3$) δ 24.05. **^{19}F{^{1}H} NMR** (376 MHz, $CDCl_3$) δ -62.92 (s, 12F), -121.14 (d, 2F, *J* = 10.5 Hz). **HRMS** (ESI+) the exact mass calculated for $[C_{52}H_{49}F_{14}NP]^+$ is 984.3374 m/z; found $[M + H]^+$ 984.3374 m/z. $\boldsymbol{\alpha_D^{589}}$ = +9.18 deg.cm^2.g^{-1} ($CHCl_3$, c 1.0, 300 K).

Complex (*R,R*)-C

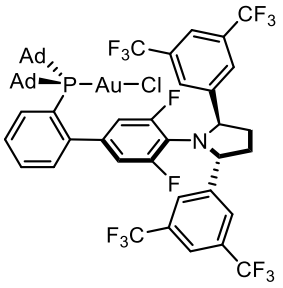

The title compound was synthesized adopting a modified procedure previously reported by our group. $Me_2S{\cdot}AuCl$ (10 mg, 36 µmol, 1 equiv) and ligand **1.6** (35mg, 36 µmol, 1 equiv) were dissolved in CH_2Cl_2 (0.6 mL, 60 mM) under an atmosphere of argon. The reaction mixture was stirred at 25 ºC for 30 min. The mixture was filtered through a syringe filter and concentrated. The crude was purified by SiO_2 flash column chromatography (cyclohexane/EtOAc 60:1 and then 30:1) to yield complex **(*R,R*)-C** (34 mg, 36 µmol, 79% yield) as a white solid.

^{1}H NMR (500 MHz, CD_2Cl_2) δ 7.86 (s, 4H), 7.79 (td, *J* = 7.4, 1.6 Hz, 1H), 7.72 (s, 2H), 7.48 – 7.38 (m, 2H), 6.86 (ddd, *J* = 7.5, 4.2, 1.8 Hz, 1H), 6.61 – 6.36 (m, 2H), 5.66 – 5.50 (m, 2H), 2.66 (qd, *J* = 5.1, 2.4 Hz, 2H), 2.12 – 2.09 (m, 2H), 2.09 – 1.87 (m, 18H), 1.63 (d, *J* = 13.5 Hz, 12H). **^{13}C{^{1}H} NMR** (126 MHz, CD_2Cl_2) δ 159.06 (dd, *J* = 148.1, 8.8 Hz), 148.15 (d, *J* = 11.5 Hz) 147.26, 139.42, 135.16, 133.27 (d, *J* = 7.4 Hz), 131.18 (q, *J* = 32.9 Hz), 130.37 (d, *J* = 2.3 Hz), 127.08, 126.90 (d, *J* = 6.0 Hz), 124.72, 123.00, 123,98 (q, *J* = 274.15 Hz), 121.27 (d, *J* = 4.4 Hz), 114.32 (d, *J* = 60.1, 21.1 Hz), 65.45, 42.87 (dd, *J* = 32.9, 23.8 Hz), 42.40 (dd, *J* = 40.5, 2.5 Hz), 36.17 (d, *J* = 5.6 Hz), 33.64, 28.68 (t, *J* = 9.7 Hz). **^{19}F{^{1}H} NMR** (471 MHz, CD_2Cl_2) δ -63.07 (s, 12H), -116.67 – -117.46 (m, 2H). **^{31}P{^{1}H} NMR** (202 MHz, CD_2Cl_2) δ 64.50. **HRMS** (ESI+) the exact mass calculated for $[C_{52}H_{49}AuClF_{14}NP]^+$ is 1216.2728 *m/z*; found $[M + H]^+$ 1216.2730 *m/z*. **M.p.** = >270°C (decomposition). $\boldsymbol{\alpha_D^{589}}$ = +21.4 deg.cm^2.g^{-1} (CH_2Cl_2, c 1.0, 304 K).

Chiral Complex (*R,R*)-D

3,5-Difluoro-4-iodoaniline (1.8)

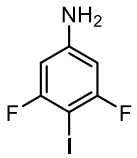

1.8

A round-bottomed flask was charged with 3,5-difluoroaniline **1.7** (1.94 g, 15.0 mmol, 1 equiv) and dissolved in 30 mL of acetonitrile. The mixture was cooled down to 0 ºC and N-Iodosuccinimide (3.38 g, 15.0 mmol, 1 equiv) was added. The cooling bath was removed, and the mixture was stirred for 30 min. The reaction mixture was poured into a solution of Na_2SO_3 in 200 mL H_2O to quench the leftover N-Iodosuccinimide. The mixture was extracted with Et_2O (2x). The combined organic phases were collected and washed with brine, dried over anhydrous Na_2SO_4 and concentrated in vacuo, rendering pink needles. Recrystallization from heptane yielded product **1.8** (3.4 g, 13 mmol, 89% yield) as a white solid.

^{1}H NMR (300 MHz, $CDCl_3$) δ 6.25 (dt, *J* = 7.9, 0.7 Hz, 2H), 3.95 (bs, 2H). **^{13}C{^{1}H} NMR** (101 MHz, $CDCl_3$) δ 164.44 (d, *J* = 8.7 Hz), 162.02 (d, *J* = 8.7 Hz), 149.26 (t, *J* = 13.0 Hz), 98.43 (dd, *J* = 28.1, 2.2 Hz). **^{19}F{^{1}H} NMR** (282 MHz, $CDCl_3$) δ -93.79. **HRMS** (APCI+) the exact mass calculated for $[C_6H_5F_2IN]^+$ is 255.9428 *m/z*; found $[M + H]^+$ 255.9429 *m/z.*

2'-Bromo-2,6-difluoro-[1,1'-biphenyl]-4-amine (1.9)

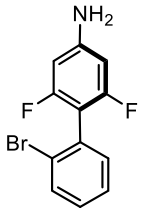

1.9

$Pd(PPh_3)_4$ (181 mg, 157 µmol, 4 mol%), (2-bromophenyl)boronic acid (1.58 g, 7.84 mmol, 2 equiv), 3,5-difluoro-4-iodoaniline **1.8** (1.00 g, 3.92 mmol, 1 equiv) and sodium carbonate (998 mg, 9.41 mmol, 2.5 equiv) were dissolved in water (3.9 mL) and 1,4-dioxane (15.7 mL) with a total concentration of 0.2 M. The reaction mixture was degassed for 5 min with argon and then stirred at 110 ºC in the MW for 3 h. The reaction mixture was allowed to cool to 24 ºC and EtOAc was added and filtered through celite. The layers were separated and the aqueous phase was extracted with EtOAc (2x). The combined organic layers were washed with brine, dried over Na_2SO_4 and concentrated. The crude was purified by SiO_2 flash column chromatography (cyclohexane/EtOAc 5:1) to yield title compound 2'-bromo-2,6-difluoro-[1,1'-biphenyl]-4-amine **1.9** (995 mg, 3.50 mmol, 89% yield) as an orange oil.

^{1}H NMR (500 MHz, $CDCl_3$) δ 7.69 (dd, *J* = 8.0, 1.3 Hz, 1H), 7.36 (td, *J* = 7.5, 1.3 Hz, 1H), 7.31 (dd, *J* = 7.7, 1.9 Hz, 1H), 7.27 – 7.22 (m, 1H), 6.32 – 6.25 (m, 2H), 3.95 (bs, 2H). **^{13}C{^{1}H} NMR** (126 MHz, $CDCl_3$) δ 161.85 (d, *J* = 10.2 Hz), 159.89 (d, *J* = 10.2 Hz), 148.41 (t, *J* = 13.7 Hz), 132.82, 131.57, 129.73, 127.20, 125.49, 107.90 (t, *J* = 21.1 Hz), 98.07 – 97.69 (m). **^{19}F{^{1}H} NMR** (376 MHz, $CDCl_3$) δ -112.46. **HRMS** (ESI+) the exact mass calculated for $[C_{12}H_9BrF_2N]^+$ is 283.9873 *m/z*; found $[M + H]^+$ 283.9881 *m/z.*

(2*R*,5*R*)-2,5-Bis(3,5-bis(trifluoromethyl)phenyl)-1-(2'-bromo-2,6-difluoro-[1,1'-biphenyl]-4-yl)pyrrolidine (1.10)

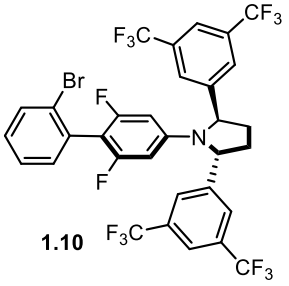

1.10

To a solution of 2'-bromo-2,6-difluoro-[1,1'-biphenyl]-4-amine **1.9** (15.5 mg, 54.5 µmol, 1 equiv) in dry THF (0.6 mL) at –78 °C were added a 1M solution of freshly prepared LiHMDS in THF (9.12 mg, 54.5 µL, 54.5 µmol, 1 equiv) under an atmosphere of argon. The mixture was stirred for 10 min at the same temperature. Then a solution of (4*R*,7*R*)-4,7-bis(3,5-bis(trifluoromethyl)phenyl)-1,3,2-dioxathiepane 2,2-dioxide **1.2** (31.4 mg, 54.5 µmol, 1 equiv) in

0.6 mL of THF was added dropwise and the reaction mixture was slowly left to warm up to 0 ºC during 2h. Then more LiHMDS 1M solution in THF was added THF (9.12 mg, 54.5 µL, 54.5 µmol, 1 equiv) and the reaction mixture was left overnight at 25 ºC. The reaction was stopped and quenched by the addition of saturated aqueous NH_4Cl. The mixture was dissolved in EtOAc and water. The aqueous layer was extracted with EtOAc (2x). The combined organic solutions were washed with brine, dried over anhydrous Na_2SO_4 and concentrated in vacuo. The crude was purified by SiO_2 flash column chromatography (cyclohexane/EtOAc 30:1) to obtain **1.10** (23 mg, 30 µmol, 55 % yield) as an orange solid.

^{1}H NMR (500 MHz, $CDCl_3$) δ 7.84 (s, 2H), 7.64 (s, 4H), 7.63 (dd, *J* = 8.1, 1.3 Hz, 1H), 7.31 (td, *J* = 7.5, 1.3 Hz, 1H), 7.24 (dd, *J* = 7.7, 1.8 Hz, 1H), 7.21 (ddd, *J* = 8.0, 7.2, 1.8 Hz, 1H), 5.97 – 5.86 (m, 2H), 5.38 (d, *J* = 7.2 Hz, 2H), 2.68 – 2.54 (m, 2H), 1.96 (d, *J* = 6.8 Hz, 2H). **^{13}C{^{1}H} NMR** (101 MHz, $CDCl_3$) δ 162.12, 159.62, 144.95, 132.82, 132.60, 132.6 (q, *J* = 33.7), 131.11, 129.84, 127.16, 126.20, 125.40, 124.64, 121.95 (d, *J* = 4.2 Hz), 107.70, 97.55 (t, *J* = 24.8 Hz), 63.00, 32.25. **^{19}F{^{1}H} NMR** (376 MHz, CDCl3) δ -62.93, -110.80 (dd, *J* = 77.3, 7.3 Hz). **HRMS** (APCI+) the exact mass calculated for $[C_{32}H_{19}BrF_{14}N]^+$ is 762.0455 *m/z*; found $[M + H]^+$ 762.0472 *m/z*.

1-(2'-Bromo-2,6-difluoro-[1,1'-biphenyl]-4-yl)pyrrolidine (1.14)

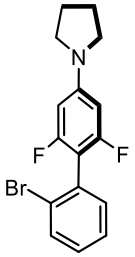

1.14

A literature reported synthetic procedure for similar substrates was followed.[54] 2'-bromo-2,6-difluoro-[1,1'-biphenyl]-4-amine (150 mg, 528 µmol, 1 equiv), 1,4-dibromobutane (228 mg, 126 µL, 1.06 mmol, 2 equiv) and potassium carbonate (80.3 mg, 581 µmol, 1.1 equiv) were placed in a MW vial and dissolved in 1 mL of distilled water. The reaction mixture was carried out in a MW at 120 ºC during 2 h. After completion of the reaction, the organic portion was extracted into ethyl acetate. Removal of the solvent under reduced pressure and purification by SiO_2 flash column chromatography (cyclohexane/EtOAc 20:1) to afford the crude product 1-(2'-bromo-2,6-difluoro-[1,1'-biphenyl]-4-yl)pyrrolidine **1.14** (80 mg, 0.19 mmol, 36 % yield) as a pale orange solid.

[54] Ju, Y.; Varma, R. S. Aqueous N-Heterocyclization of Primary Amines and Hydrazines with Dihalides: Microwave-Assisted Syntheses of *N* -Azacycloalkanes, Isoindole, Pyrazole, Pyrazolidine, and Phthalazine Derivatives, *J. Org. Chem.* **2006**, *71*, 135–141.

^{1}H NMR (400 MHz, $CDCl_3$) δ 7.67 (dd, *J* = 8.0, 1.3 Hz, 1H), 7.38 – 7.33 (m, 1H), 7.31 (dd, *J* = 7.5, 2.0 Hz, 1H), 7.22 (ddd, *J* = 8.1, 7.0, 2.1 Hz, 1H), 6.23 – 6.12 (m, 2H), 3.35 – 3.26 (m, 4H), 2.09 – 2.01 (m, 4H). **^{19}F{^{1}H} NMR** (376 MHz, $CDCl_3$) δ -112.81. **HRMS** (APCI+) the exact mass calculated for $[C_{16}H_{15}BrF_2N]^+$ is 338.0350 *m/z*; found $[M + H]^+$ 338.0349 *m/z*.

Chiral Complex (*R*,*R*)-E

2,3,5,6-Tetrafluoro-3'-methoxy-[1,1'-biphenyl]-4-amine (1.16)

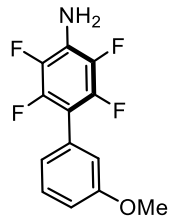

1.16

$Pd(PPh_3)_4$ (54.5 mg, 47.1 µmol, 5 mol%), (3-methoxyphenyl)boronic acid (122 mg, 1.46 mmol, 1.5 equiv), 4-bromo-2,3,5,6-tetrafluoroaniline (230 mg, 943 µmol, 1 equiv) and sodium carbonate (200 mg, 1.9 mmol, 2.0 equiv) were dissolved in water (600 µL) and 1,4-dioxane (3.0 mL) with a total concentration of 0.3 M. The reaction mixture was degassed for 5 min with argon and then stirred at 110 ºC in the MW for 3 h. The reaction mixture was allowed to cool to 24 ºC and EtOAc was added and filtered through celite. The layers were separated and the aqueous phase was extracted with EtOAc (2x). The combined organic layers were washed with brine, dried over Na_2SO_4 and concentrated. The crude was purified by SiO_2 flash column chromatography (cyclohexane/EtOAc 20:1) to yield title compound **1.16** (172 mg, 943 µmol, 67% yield) as a white solid.

^{1}H NMR (500 MHz, $CDCl_3$) δ 7.36 (td, *J* = 7.7, 0.9 Hz, 1H), 7.03 – 6.99 (m, 1H), 6.98 – 6.93 (m, 2H), 4.03 (bs, 2H), 3.84 (s, 3H). **^{13}C{^{1}H} NMR** (126 MHz, $CDCl_3$) δ 159.63, 144.25 (dddd, *J* = 243.7, 11.7, 7.3, 3.6 Hz), 136.92 (dddd, *J* = 238.5, 17.2, 6.0, 4.0 Hz), 129.52, 129.44 – 128.97 (m), 126.50 – 124.91 (m), 122.89 (t, *J* = 2.1 Hz), 116.12 (t, *J* = 2.0 Hz), 114.08, 108.23 (t, *J* = 17.3 Hz), 55.40. **^{19}F{^{1}H} NMR** (376 MHz, $CDCl_3$) δ -146.21 – -146.37 (m), -162.20 – -162.39 (m). **HRMS** (APCI+) the exact mass calculated for $[C_{13}H_{10}F_4NO]^+$ is 272.0693 *m/z*; found $[M + H]^+$ 272.0689 *m/z*.

(1*S*,4*S*)-1,4-Bis(3,5-bis(trifluoromethyl)phenyl)butane-1,4-diyl dimethanesulfonate (1.17)

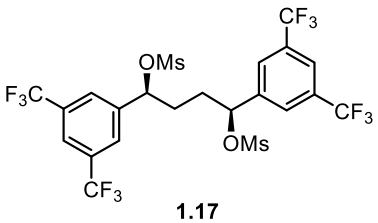

1.17

A solution of (1*S*,4*S*)-1,4-bis(3,5-bis(trifluoromethyl)phenyl)butane-1,4-diol **1.1** (550 mg, 1.07 mmol, 1 equiv) in 7 mL of dichloromethane was prepared in a two-necked flask under argon atmosphere and introduced in an -20 ºC acetone bath. Then, triethylamine (325 mg, 447 µL, 3 Eq, 3.21 mmol) and distilled methanesulfonyl chloride (306 mg, 208 µL, 2.67 mmol, 2.5 equiv) were added dropwise to the reaction mixture and left stirring. The course of the reaction was monitored by TLC (5:1 cy/EtOAc). Upon completion of reaction (3 h), the reaction mixture was extracted with EtOAc, washed with water, brine and dried over Na_2SO_4. The organic phase was evaporated to yield our compound **1.17** (600 mg, 895 µmol, 84% yield) as a white foam.

^{1}H NMR (400 MHz, $CDCl_3$) δ 7.90 (s, 6H), 6.03 – 5.91 (m, 2H), 2.94 (s, 6H), 2.15 (t, *J* = 4.3 Hz, 4H). **^{19}F{^{1}H} NMR** (376 MHz, $CDCl_3$) δ -63.07. **^{13}C{^{1}H} NMR** (101 MHz, $CDCl_3$) δ 141.33, 132.72 (q, *J* = 33.7 Hz), 126.43 (d, *J* = 4.0 Hz), 123.16 (p, *J* = 3.9 Hz), 123.00 (q, *J* = 273.2 Hz), 79.23, 38.93, 33.27. **HRMS** (ESI+) the exact mass calculated for $[C_{22}H_{18}F_{12}O_6S_2]^+$ is 693.0245 *m/z*; found $[M + H]^+$ 693.0257 *m/z*. α_D^{589} = -51.4 deg.cm^2.g^{-1} (CH_2Cl_2, c 1.0, 298 K).

(2*R*,5*R*)-2,5-Bis(3,5-bis(trifluoromethyl)phenyl)-1-(2,3,5,6-tetrafluoro-3'-methoxy-[1,1'-biphenyl]-4-yl)pyrrolidine (1.18)

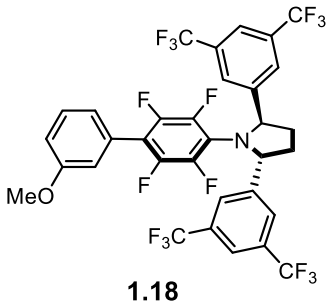

1.18

2,3,5,6-Tetrafluoro-3'-methoxy-[1,1'-biphenyl]-4-amine **1.16** (96 mg, 0.35 mmol, 1 equiv) and sodium hydride (280 mg, 60% Wt, 7.1 mmol, 20 equiv) were added as solids and performed cycles of vacuum/argon. Then, dry THF (4 mL) were added at 0 °C and left stirring for 10 minutes. A solution of (4*R*,7*R*)-4,7-bis(3,5-bis(trifluoromethyl)phenyl)-1,3,2-dioxathiepane 2,2-dioxide **1.2** (235 mg, 408 µmol, 1.2 equiv) in 4 mL of dry THF was added dropwise at 0ºC and the reaction mixture was slowly left to warm up to 25 ºC during 1 h. The reaction monitoring was done by UHPLC. The reaction was stopped, dilute with EtOAc and quenched by the careful addition of saturated aqueous NH_4Cl. The mixture was dissolved in EtOAc and water. The aqueous layer was

extracted with EtOAc (2x). The combined organic solutions were washed with brine, dried over anhydrous Na_2SO_4 and concentrated in vacuo. The crude was purified by SiO_2 flash column chromatography (cyclohexane/EtOAc 30:1) to yield product **1.18** (174 mg, 232 µmol, 66% yield) as a white solid.

^{1}H NMR (500 MHz, $CDCl_3$) δ 7.77 (s, 6H), 7.30 – 7.26 (m, 1H), 6.89 (ddd, *J* = 8.3, 2.6, 0.9 Hz, 1H), 6.84 (dt, *J* = 7.8, 1.3 Hz, 1H), 6.79 (dt, *J* = 2.7, 1.4 Hz, 1H), 5.60 (t, *J* = 6.6 Hz, 2H), 3.77 (s, 3H), 2.78 – 2.67 (m, 2H), 2.13 – 1.98 (m, 2H). **^{13}C{^{1}H} NMR** (126 MHz, $CDCl_3$) δ 159.59, 145.70, 144.21 (dd, *J* = 243.7, 11.7 Hz), 136.85 (dd, *J* = 238.5, 17.2 Hz), 132.35 (q, *J* = 33.5 Hz), 129.53, 128.53, 126.83 (d, *J* = 4.0 Hz), 124.35, 123.21 (m), 122.58, 122.05 (d, *J* = 3.8 Hz), 122.00, 120.01, 115.75, 114.68, 66.16 (t, *J* = 3.6 Hz), 55.44, 36.63. **^{19}F{^{1}H} NMR** (376 MHz, $CDCl_3$) δ -63.07, -144.41 (dd, *J* = 21.2, 9.1 Hz), -149.19 (dd, *J* = 21.2, 9.1 Hz). **HRMS** (APCI+) the exact mass calculated for $[C_{33}H_{20}F_{16}NO]^+$ is 750.1280 *m/z*; found $[M + H]^+$ 750.1284 *m/z*.

(2*R*,5*R*)-2,5-Bis(3,5-bis(trifluoromethyl)phenyl)-1-(2'-bromo-2,3,5,6-tetrafluoro-5'-methoxy-[1,1'-biphenyl]-4-yl)pyrrolidine (1.19)

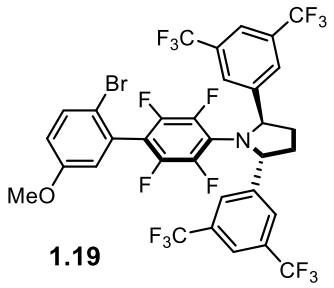

1.19

To a solution of (2*R*,5*R*)-2,5-bis(3,5-bis(trifluoromethyl)phenyl)-1-(2,3,5,6-tetrafluoro-3'-methoxy-[1,1'-biphenyl]-4-yl)pyrrolidine **1.18** (27 mg, 36 µmol, 1 equiv) in 2 mL of acetonitrile, 1-bromopyrrolidine-2,5-dione (5.8 mg, 32 µmol, 0.9 equiv) was added at -20 °C and the reaction mixture was slowly left to warm up to 25 ºC during 6 h. The solvents were evaporated and the crude was purified by SiO_2 flash column chromatography (cyclohexane/EtOAc 100:1 to 20:1) to yield product **1.19** (10 mg, 12 µmol, 34% yield) as a white solid.

^{1}H NMR (500 MHz, $CDCl_3$) δ 7.76 (s, 6H), 7.46 (d, *J* = 8.9 Hz, 1H), 6.79 (dd, *J* = 8.9, 3.1 Hz, 1H), 6.65 (d, *J* = 3.1 Hz, 1H), 5.58 (d, *J* = 7.4 Hz, 3H), 3.73 (s, 3H), 2.77 – 2.69 (m, 2H), 2.14 – 2.04 (m, 2H). **^{13}C{^{1}H} NMR** (126 MHz, $CDCl_3$) δ 158.78, 145.43, 144.25 (dd, *J* = 241.7, 11.2 Hz), 136.87 (dd, *J* = 237.5, 17.0 Hz), 133.59, 132.35 (q, *J* = 32.9), 129.41, 127.73 – 125.99 (m), 123.22 (q, *J* = 272.1 Hz), 121.99, 117.38, 116.83, 114.73, 66.38, 55.69, 36.97. **^{19}F{^{1}H} NMR** (471 MHz, $CDCl_3$) δ -62.95, -141.31 (ddd, *J* = 141.1, 21.8, 8.9 Hz), -149.27 (ddd, *J* = 509.6, 21.3, 9.3 Hz). **HRMS** (APCI+) the exact mass calculated for $[C_{33}H_{19}BrF_{16}NO]^+$ is 828.0410 *m/z*; found $[M + H]^+$ 828.0389 *m/z*.

Chiral Complex (*R,R*)-F'

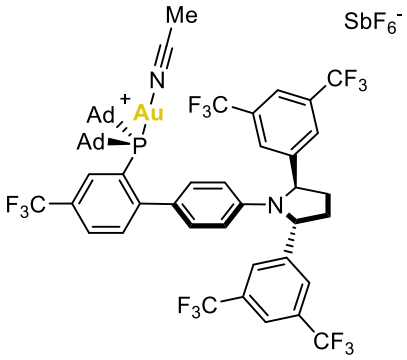

A two-necked flask is introduced in the glovebox and $AgSbF_6$ (33.0 mg, 96.1 µmol, 1.2 equiv) is dissolved in 2 mL of dry CH_2Cl_2. Then dry acetonitrile (32.9 mg, 42.0 µL, 801 µmol, 10 equiv) is added to the mixture. In a separate vial, Complex (*R,R*)-**F** (100 mg, 80.1 µmol, 1 equiv) is dissolved in 3 mL of dry CH_2Cl_2 and added dropwise under argon at 25 ºC to the reaction mixture. Immediately a white precipitate is formed. The reaction mixture was left stirring during 3 h, then filtered through a pad of Celite, and the solvent was evaporated under reduced pressure to give Complex (*R,R*)-**F'** (107 mg, 71.8 µmol, 90 % yield) as a white solid. Crystals were obtained by liquid diffusion technique in a mixture of benzene/pentane at 25 ºC.

^{1}H NMR (500 MHz, CD_2Cl_2) δ 8.05 (dd, *J* = 7.5, 1.8 Hz, 1H), 7.85 (s, 2H), 7.77 (s, 1H), 7.75 (d, *J* = 5.7 Hz, 4H), 7.38 (dd, *J* = 8.2, 4.1 Hz, 1H), 7.04 (dd, *J* = 8.4, 2.3 Hz, 1H), 6.81 (dd, *J* = 8.5, 2.3 Hz, 1H), 6.57 – 6.51 (m, 1H), 6.34 (dd, *J* = 8.5, 2.7 Hz, 1H), 5.43 (bs, 2H), 2.62 (s, 2H), 2.54 (s, 3H), 2.28 – 2.09 (m, 6H), 2.10 – 1.86 (m, 13H), 1.84 – 1.53 (m, 13H). **^{13}C{^{1}H} NMR** (126 MHz, CD_2Cl_2) δ 153.70, 145.93, 144.30, 135.13, 132.18 (q, *J* = 32.9 Hz), 130.96, 130.86, 130.19, 129.86, 127.98, 127.00, 124.92, 122.75, 121.72, 120.79, 115.13, 114.81, 63.41, 44.25 (d, *J* = 22.9 Hz), 43.22, 43.01, 42.16, 36.33, 36.25, 32.60, 29.20 (d, *J* = 10.0 Hz), 28.87 (d, *J* = 10.0 Hz), 2.84. **^{31}P{^{1}H} NMR** (202 MHz, CD_2Cl_2) δ 62.35. **^{19}F{^{1}H} NMR** (376 MHz, CD_2Cl_2) δ -63.07, -63.23. **HRMS** (ESI+) the exact mass calculated for $[C_{55}H_{52}AgF_{15}N_2P]^+$ is 1253.3289 *m/z*; found $[M + H]^+$ 1253.3253 *m/z*. α_D^{589} = 30.8 deg.cm^2.g^{-1} (CH_2Cl_2, c 1.0, 298 K).

Chiral Complex (*R,R*)-G

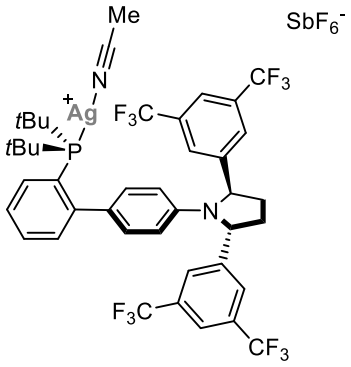

(5*R*)-2,5-Bis(3,5-bis(trifluoromethyl)phenyl)-1-(2'-(di-*tert*-butylphosphaneyl)-[1,1'-biphenyl]-4-yl)pyrrolidine (22 mg, 28 μmol, 1 equiv) dissolved in 0.20 mL of dry acetonitrile was added to a suspension of $AgSbF_6$ (4.7 mg, 14 μmol, 0.5 equiv) in 0.15 mL of dry acetonitrile under argon. The reaction mixture was stirred for 2 h in the dark at 25 ºC, then the solution was filtered through a Celite pad. Addition of Et_2O afforded the product as a white solid, which was filtered and washed with pentane to yield desired complex (*R,R*)-**G** (31 mg, 26 μmol, 95 % yield) as a white solid. Crystals were obtained by liquid diffusion of a mixture of toluene/pentane at 25 ºC.

^{1}H NMR (500 MHz, $CDCl_3$) δ 7.81-7.77 (m, 3H), 7.75 (s, 4H), 7.49 – 7.39 (m, 2H), 7.25 – 7.22 (m, 1H), 7.12 (dt, *J* = 8.5, 2.0 Hz, 1H), 6.85 (dd, *J* = 8.4, 2.2 Hz, 1H), 6.72 (dd, *J* = 8.4, 2.8 Hz, 1H), 6.29 (dd, *J* = 8.5, 2.7 Hz, 1H), 5.52 (bs, 2H), 2.61 (s, 2H), 2.21 (d, *J* = 0.7 Hz, 3H), 2.01 (d, *J* = 6.6 Hz, 2H), 1.40 (d, *J* = 15.9 Hz, 9H), 1.06 (d, *J* = 15.4 Hz, 9H). **^{13}C{^{1}H} NMR** (126 MHz, $CDCl_3$) δ 149.23 (d, *J* = 16.3 Hz), 145.55, 143.22, 138.05, 133.60 (d, *J* = 8.0 Hz), 132.48 (d, *J* = 6.0 Hz), 132.15 (q, *J* = 33.2 Hz), 131.06, 130.92, 129.71 (d, *J* = 9.1 Hz), 129.18, 127.22, 126.62, 124.52, 122.35, 121.50, 120.15, 114.66 (d, *J* = 25.2 Hz), 62.86, 35.32 (d, *J* = 11.1 Hz), 35.02 (dd, *J* = 10.8, 4.8 Hz), 32.31, 31.37 (dd, *J* = 10.1, 2.0 Hz), 30.09 (dd, *J* = 9.8, 2.2 Hz), 29.85, 21.59, 2.25. **^{31}P{^{1}H} NMR** (202 MHz, $CDCl_3$) δ 46.96 (d, $J_{^{31}P-^{109}Ag}$ = 762.3 Hz, $J_{^{31}P-^{107}Ag}$ = 660.8 Hz). **^{19}F{^{1}H} NMR** (471 MHz, $CDCl_3$) δ -62.63. **HRMS** (ESI+) the exact mass calculated for $[C_{40}H_{38}AgF_{12}NP]^+$ is 898.1596 *m/z*; found $[M + H]^+$ 898.1592 *m/z*. $\boldsymbol{\alpha_D^{589}}$ = 31.7 deg.cm^2.g^{-1} (CH_2Cl_2, c 1.0, 298 K).

Chiral Complex (*R,R*)-H

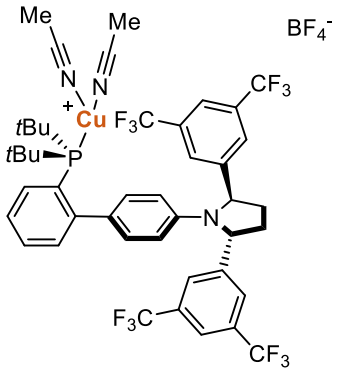

A Schlenk flask was charged with $[Cu(MeCN)_4]BF_4$ (9.1 mg, 29 µmol, 1 equiv) in 0.20 mL of dry CH_2Cl_2 and the mixture was stirred under argon at 25 ºC. Then (5*R*)-2,5-bis(3,5-bis(trifluoromethyl)phenyl)-1-(2'-(di-*tert*-butylphosphaneyl)-[1,1'-biphenyl]-4-yl)pyrrolidine (23 mg, 29 µmol, 1 equiv) was added, the mixture was stirred for 30 min, and then the solvent was evaporated to obtain Complex (*R,R*)-**H** (29 mg, 28 µmol, 97 % yield) as a white solid. Crystals were obtained by liquid diffusion of a mixture pentane/CH_2Cl_2.

^{1}H NMR (500 MHz, $CDCl_3$) δ 7.79 (d, *J* = 4.0 Hz, 6H), 7.78 – 7.72 (m, 1H), 7.43 (dtt, *J* = 30.7, 7.4, 1.3 Hz, 2H), 7.24 (ddd, *J* = 7.7, 4.8, 1.8 Hz, 1H), 7.06 (dt, *J* = 8.4, 2.5 Hz, 1H), 6.86 (dd, *J* = 8.4, 2.3 Hz, 1H), 6.78 (dd, *J* = 8.3, 2.8 Hz, 1H), 6.31 (dd, *J* = 8.4, 2.8 Hz, 1H), 5.64 (bs, 2H), 2.69 – 2.57 (m, 2H), 2.31 (s, 6H), 2.06 – 1.90 (m, 2H), 1.38 (d, *J* = 15.0 Hz, 9H), 1.06 (d, *J* = 14.6 Hz, 9H). **^{13}C{^{1}H} NMR** (126 MHz, $CDCl_3$) δ 149.25 (d, *J* = 19.1 Hz), 145.91, 143.27, 133.49, 132.05 (q, *J* = 33.3 Hz), 131.81 (d, *J* = 6.3 Hz), 130.97, 130.08, 129.31 (d, *J* = 9.4 Hz), 127.81, 127.55, 127.27 (d, *J* = 4.6 Hz), 126.72, 124.54, 122.38, 121.97, 121.35, 120.21, 119.16, 115.96, 115.21, 62.71, 34.93 (d, *J* = 3.7 Hz), 34.81 (d, *J* = 3.8 Hz), 32.35, 31.02 (d, *J* = 8.3 Hz), 29.74 (d, *J* = 8.2 Hz), 28.62, 2.46. **^{31}P{^{1}H} NMR** (202 MHz, $CDCl_3$) δ 32.09. **^{19}F{^{1}H} NMR** (471 MHz, $CDCl_3$) δ -62.60, -151.42. **HRMS** (ESI+) the exact mass calculated for $[C_{42}H_{41}CuF_{12}N_2P]^+$ is 895.2106 *m/z*; found $[M + H]^+$. 895.2104 *m/z*. α_D^{589} = 32.1 deg.cm^2.g^{-1} (CH_2Cl_2, c 1.0, 298 K).

Procedure for the formal [4+2] cycloaddition of 1,6-enyne 1.29

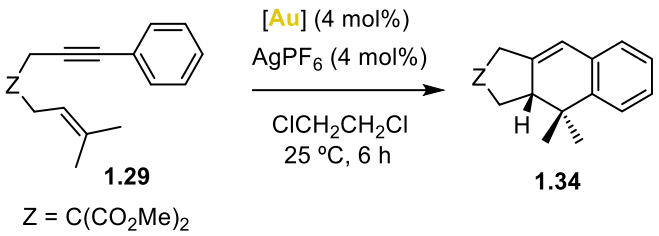

The procedure for this reaction was previously optimized in the group.[55] 1,6-Enyne **1.29** (1.0 equiv) and (*R,R*)-[Au] (4 mol%) were dissolved in dry 1,2-dichloroethane and a solution of $AgPF_6$ (4 mol%) in 1,2-dichloroethane (total concentration 0.05 M) was added dropwise. The reaction was stirred for the given time at 24 ºC in the dark, quenched by addition of 3 drops of NEt_3 and concentrated. Yield was determined by ^1H NMR using Ph_2CH_2 as internal standard.

Procedure for the synthesis of axially-chiral indol (1.23)

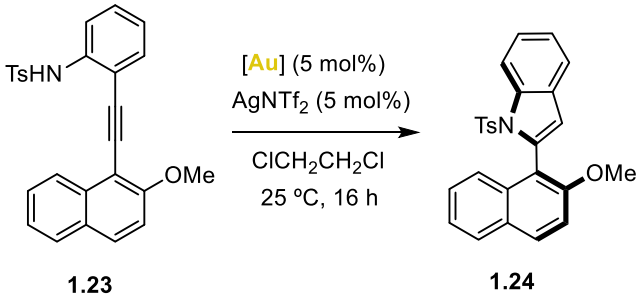

Ts-protected aniline **1.23** (1.0 equiv) and (*R,R*)-[Au] (5 mol%) were dissolved in 1,2-dichloroethane. A solution of $AgNTf_2$ (5 mol%) in 1,2-dichloroethane (total concentration 0.05 M) was added dropwise and the reaction was stirred at 25 ºC for 16 h. The reaction was quenched by addition of 3 drops of NEt_3 and concentrated. Yield was determined by ^1H NMR using Ph_2CH_2 as internal standard.

55 Nieto-Oberhuber, C.; López, S.; Muñoz, M. P.; Cárdenas, D. J.; Buñuel, E.; Nevado, C.; Echavarren, A. M. Divergent Mechanisms for the Skeletal Rearrangement and [2+2] Cycloaddition of Enynes Catalyzed by Gold, *Angew. Chem. Int. Ed Engl.* **2005**, *44*, 6146–6148.

1.5.3 Kinetic investigations

IR spectra

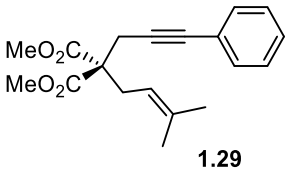

1.29

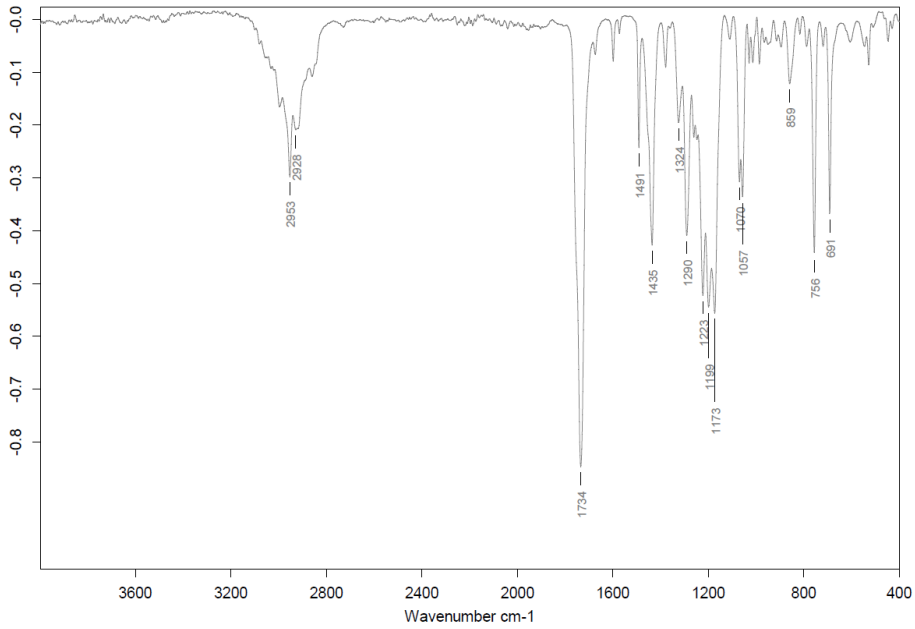

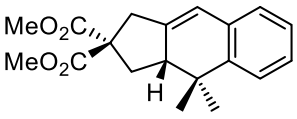

1.34

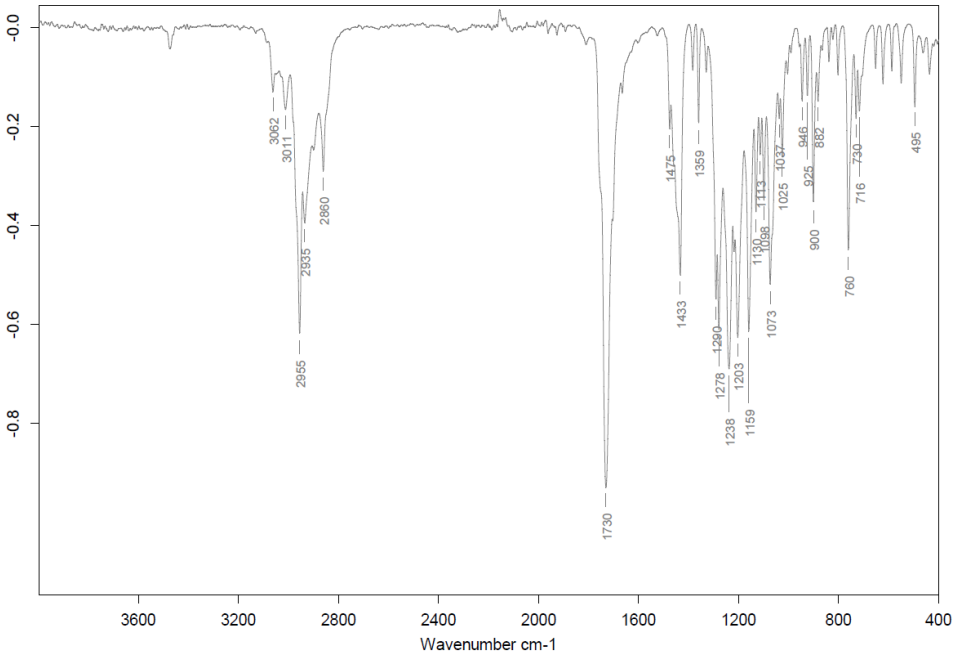

Variable Time Normalization Analysis (VTNA)

Order in substrate and catalyst

All operations were performed under inert atmosphere (glovebox and/or Schlenk line techniques and balloons) using anhydrous dichloromethane-d_2, dried over activated 3 Å MS for at least 24 h. Reaction conditions: [**1.21**] = 50/100/100/100/200 mM, [(*R,R*)-**F'**] = 7.5/5/7.5/10/7.5 mM Five oven-dried NMR tubes equipped with a rubber septum containing substrate **1.21**, 1,3,5-tribromobenzene as internal standard and gold complex (*R,R*)-**F'** in CD_2Cl_2 (500 µL) were prepared. Precisely, the following solutions were added in sequence into the different NMR tubes:

1) Substrate **1.21** and internal standard stock solution (100/200/200/200/400 µL), previously prepared by adding CD_2Cl_2 (1.4 mL) to the substrate (100.0 mg, 349.0 µmol) and 1,3,5-tribromobenzene (55.0 mg, 174.0 µmol).

2) CD_2Cl_2 (300.232.200.165.0 µL), obtaining a clear colorless solution.

To it, a solution of gold complex (*R,R*)-**F'** (100/68/100/135/100 µL) was added, bringing the total volume to 500 µL. The stock solution of complex (*R,R*)-**F'** was previously prepared by adding CD_2Cl_2 (700 µL) to complex (*R,R*)-**F'** (39.0 mg, 26.2 µmol). After the addition, the tube was shaken for few seconds, obtaining a clear colorless solution, and immediately inserted into a 500 MHz spectrometer equipped with cryoprobe. ^{1}H NMR spectra (8 scans each) were recorded at 3-minute intervals until full conversion. The first ^{1}H NMR was recorded 3 minutes after the addition of catalyst.

Data

Conversion data against the internal standard were extracted using Mestrenova (Fourier transform, automatic phase correction, baseline correction and integration of stacked spectra) and further manipulated with Excel. Data are reported in the tables below, rounded for clarity. The data was then elaborated following the variable time normalization analysis (VTNA) described by Burés. An order in substrate **1.21** of 0.6 caused the best overlap of the four curves in the graph below, as judged visually.

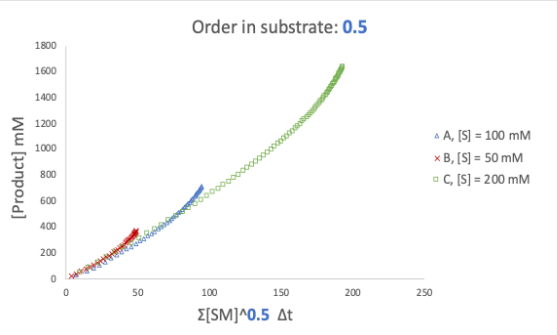

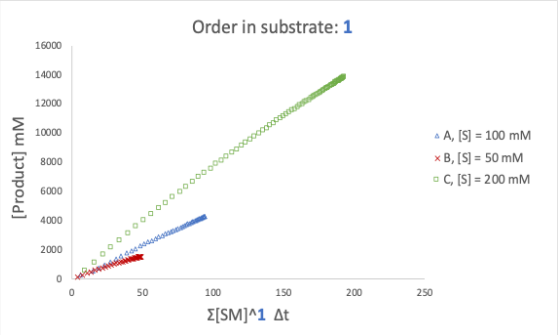

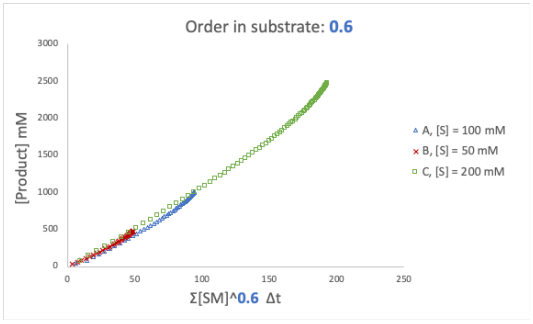

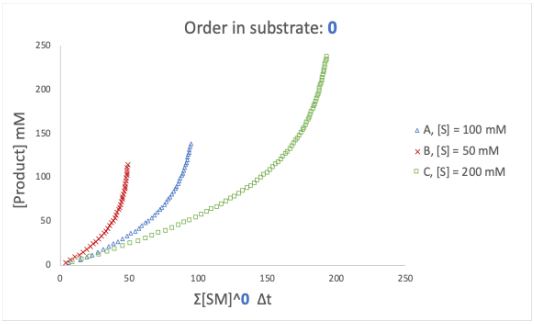

Data: 0.6 order in substrate **1.21** determined by VTNA analysis

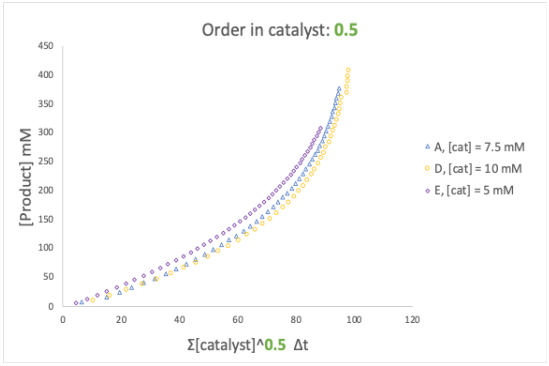

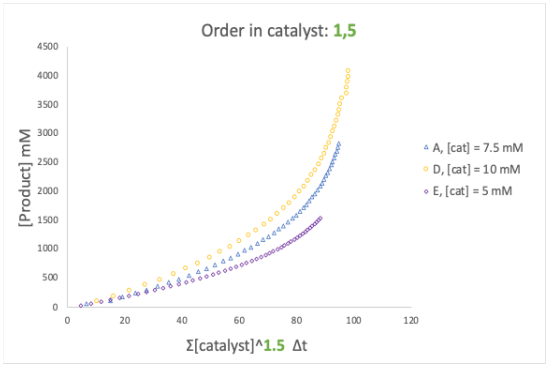

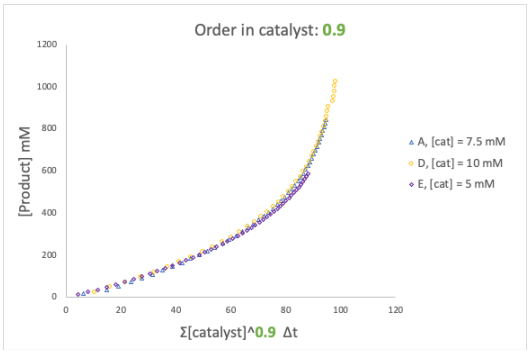

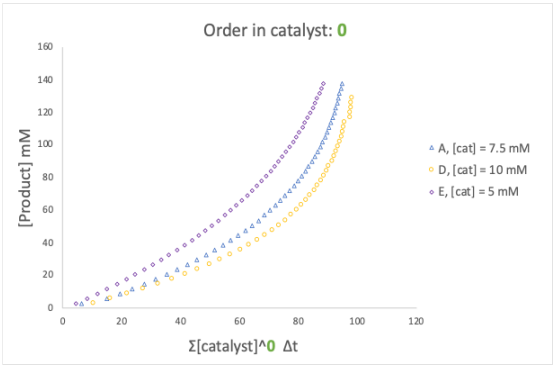

Data: 0.9 order in catalyst (*R,R*)-**F'** determined by VTNA analysis

A			**B**			**C**			**D**			**E**		
[S] = 100 mM **[cat]** = 7.5 mM			**[S]** = 50 mM **[cat]** = 7.5 mM			**[S]** = 200 mM **[cat]** = 7.5 mM			**[S]** = 100 mM **[cat]** = 10 mM			**[S]** = 100 mM **[cat]** = 5 mM		
t/ min	**[P]**/ mM	**[S]**/ mM	**t**/ min	**[P]**/ mM	**[S]**/ mM	**t**/ min	**[P]**/ mM	**[S]**/ mM	**t**/ min	**[P]**/ mM	**[S]**/ mM	**t**/ min	**[P]**/ mM	**[S]**/ mM
3	6.4	93.6	3	3.9	46.1	3	9,6	190	5	10.4	89.6	5	4.5	95.5
6	14.8	85.2	6	7.4	42.6	6	16,2	184	8	16.1	83.9	8	8.1	91.9
9	19.2	80.8	9	10.7	39.3	9	22,3	178	11	21.7	78.3	11	11.5	88.5
12	23.5	76.5	12	13.8	36.2	12	28,4	172	14	27.2	72.8	14	14.9	85.1
15	27.6	72.4	15	16.7	33.3	15	34,4	166	17	32.2	67.8	17	18.2	81.8
18	31.4	68.6	18	19.2	30.8	18	40,2	160	20	37.0	63.0	20	21.4	78.6
21	35.1	64.9	21	21.7	28.3	21	46,1	154	23	41.5	58.5	23	24.5	75.5
24	38.8	61.2	24	24.1	25.9	24	51,4	149	26	45.7	54.3	26	27.5	72.5
27	42.2	57.8	27	26.2	23.8	27	57,0	143	29	49.7	50.3	29	30.4	69.6
30	45.4	54.6	30	28.2	21.8	30	62,1	138	32	53.4	46.6	32	33.2	66.8
33	48.5	51.5	33	30.1	19.9	33	67,1	133	35	56.9	43.1	35	36.0	64.0
36	51.5	48.5	36	31.8	18.2	36	72,0	128	38	60.2	39.8	38	38.6	61.4
39	54.2	45.8	39	33.4	16.6	39	76,8	123	41	63.2	36.8	41	41.2	58.8
42	56.9	43.1	42	34.8	15.2	42	81,5	118	44	66.0	34.0	44	43.6	56.4
45	59.4	40.6	45	36.2	13.8	45	85,9	114	47	68.7	31.3	47	46.1	53.9
48	61.8	38.2	48	37.4	12.6	48	90,3	110	50	71.2	28.8	50	48.4	51.6
51	64.1	35.9	51	38.5	11.5	51	94,5	105	53	73.5	26.5	53	50.6	49.4
54	66.2	33.8	54	39.6	10.4	54	98,7	101	56	75.6	24.4	56	52.8	47.2
57	68.3	31.7	57	40.5	9.5	57	103	97,3	59	77.6	22.4	59	54.9	45.1
60	70.2	29.8	60	41.4	8.6	60	106	93,5	62	79.4	20.6	62	56.9	43.1
63	72.1	27.9	63	42.3	7.7	63	110	89,8	65	81.1	18.9	65	58.8	41.2
66	73.8	26.2	66	43.1	6.9	66	114	86,2	68	82.7	17.3	68	60.7	39.3
69	75.4	24.6	69	43.7	6.3	69	117	82,8	71	84.0	16.0	71	62.5	37.5
72	76.9	23.1	72	44.3	5.7	72	121	79,4	74	85.4	14.6	74	64.2	35.8
75	78.4	21.6	75	45.0	5.0	75	124	76,2	77	86.5	13.5	77	65.9	34.1
78	79.7	20.3	78	45.5	4.5	78	127	73,1	80	87.8	12.2	80	67.5	32.5
81	81.0	19.0	81	46.0	4.0	81	130	70,0	83	88.8	11.2	83	69.0	31.0
84	82.2	17.8	84	46.4	3.6	84	133	67,2	86	89.7	10.3	86	70.4	29.6
87	83.3	16.7	87	46.9	3.1	87	136	64,4	89	90.4	9.6	89	71.9	28.1
90	84.4	15.6	90	47.3	2.7	90	138	61,7	92	91.4	8.6	92	73.2	26.8
93	85.4	14.6	93	47.5	2.5	93	141	59,0	95	92.1	7.9	95	74.5	25.5

96	86.3	13.7	96	47.8	2.2	96	143	56,7	98	92.8	7.2	98	75.7	24.3
99	87.2	12.8	99	48.1	1.9	99	146	54,3	101	93.4	6.6	101	76.9	23.1
102	88.1	11.9	102	48.3	1.7	102	148	51,9	104	94.0	6.0	104	78.0	22.0
105	88.8	11.2	105	48.4	1.6	105	150	49,7	107	94.6	5.4	107	79.1	20.9
108	89.5	10.5	108	48.7	1.3	108	152	47,6	110	94.9	5.1	110	80.1	19.9
111	90.2	9.8	111	48.8	1.2	111	154	45,5	113	95.4	4.6	113	81.2	18.8
114	90.8	9.2	114	49.0	1.0	114	156	43,5	116	95.8	4.2	116	82.0	18.0
117	91.5	8.5	117	49.1	0.9	117	158	41,6	119	97.4	2.6	119	83.0	17.0
120	92.0	8.0				120	160	39,8	122	97.5	2.5	122	83.8	16.2
123	92.5	7.5				123	162	38,0	125	97.9	2.1	125	84.7	15.3
126	93.0	7.0				126	164	36,3	128	98.0	2.0	128	85.4	14.6
129	93.5	6.5				129	165	34,7	131	98.1	1.9	131	86.1	13.9
132	93.9	6.1				132	167	33,2				134	86.9	13.1
135	94.2	5.8				135	168	31,7				137	87.6	12.4
138	94.6	5.4				138	170	30,2				140	88.2	11.8
141	94.9	5.1				141	171	28,9				143	88.8	11.2
						144	172	27,7				146	89,4	10,6
						147	174	26,4				149	90,0	10,0
						150	175	25,1				152	90,4	9,6
						153	176	23,9				155	91,0	9,0
						156	177	22,9				158	91,4	8,6
						159	178	21,9				161	91,9	8,1
						162	179	21,0				164	92,3	7,7
						165	180	20,0				167	92,7	7,3
						168	181	19,1				170	93,2	6,8
						171	182	18,3				173	93,4	6,6
						174	183	17,5				176	93,8	6,2
						177	183	16,7				179	94,1	5,9
						180	184	15,8				182	94,5	5,5
						183	185	15,1				185	94,7	5,3
						186	185	14,6				188	95,0	5,0
						189	186	13,8				191	95,3	4,7
						192	187	13,1						
						195	187	12,6						
						198	188	12,0						

K_{obs} calculation

An excellent linear regression obtaining a value of $k_{obs} = 0.016\ mM^{-0.5}\ min^{-1}$.

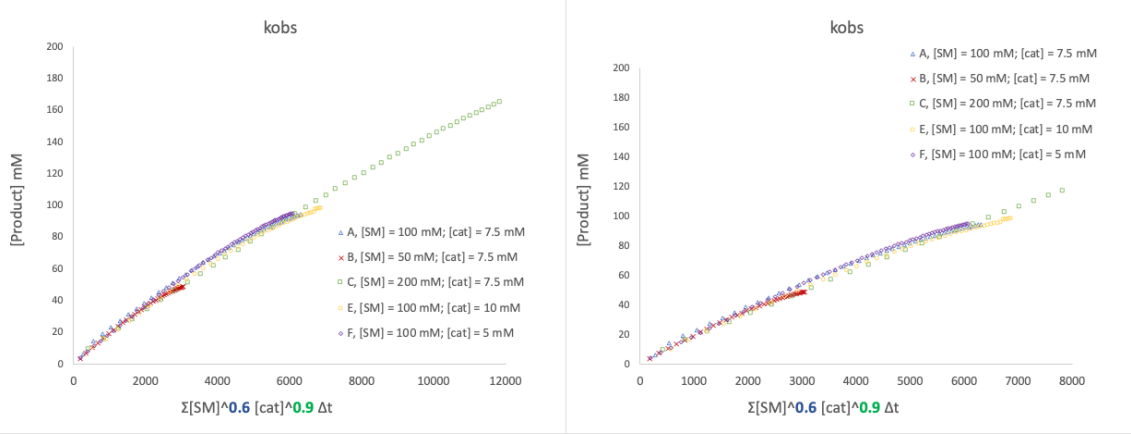

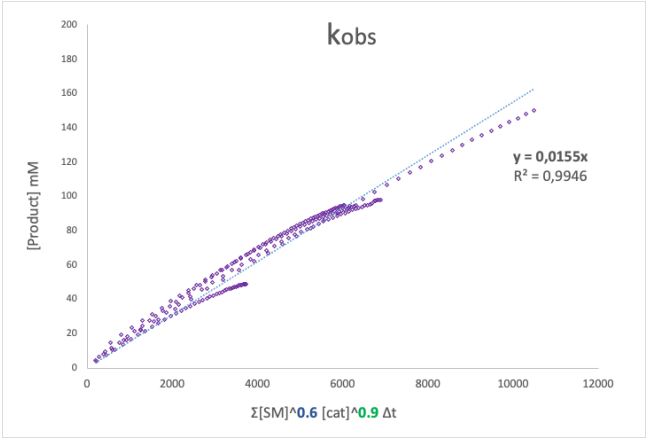

Product inhibition studies

All operations were performed under inert atmosphere (glovebox and/or Schlenk line techniques and balloons) using anhydrous dichloromethane-d_2, dried over activated 3 Å MS for at least 24 h. Reaction conditions: [**1.21**] = 100 mM, [(*R,R*)-**F'**] = 5 mM. Two oven-dried NMR tubes equipped with a rubber septum containing substrate **1.21**, 1,3,5-tribromobenzene as internal standard and gold complex (*R,R*)-**F'** in CD_2Cl_2 (500 µL) were prepared. Precisely, the following solutions were added in sequence into the different NMR tubes:

1) Substrate **1.21**, internal standard stock solution (200 µL), previously prepared by adding CD_2Cl_2 (560 µL) to the substrate (40.0 mg, 139.0 µmol) and 1,3,5-tribromobenzene (22.0 mg, 70.0 µmol).

2) Product **1.22** (0/50 µL), from stock solution prepared by dissolving product **1.22** (15.0 mg, 52.0 µmol) in 100 µL of CD_2Cl_2.

3) CD_2Cl_2 (200/150 µL), obtaining a clear colourless solution.

To it, a solution of gold complex (*R,R*)-**F'** (100 µL) was added, bringing the total volume to 500 µL. The stock solution of complex (*R,R*)-**F'** was previously prepared by adding CD_2Cl_2 (250 µL) to complex (*R,R*)-**F'** (9.0 mg, 6.3 µmol). After the addition, the tube was shaken for few seconds, obtaining a clear colourless solution, and immediately inserted into a 500 MHz spectrometer equipped with cryoprobe. ^{1}H NMR spectra (8 scans each) were recorded at 3-minute intervals until full conversion. The first ^{1}H NMR was recorded 3 minutes after the addition of catalyst.

Data

Conversion data against the internal standard were extracted using Mestrenova (Fourier transform, automatic phase correction, baseline correction and integration of stacked spectra) and further manipulated with Excel. Data are reported in the tables below, rounded for clarity. The data was then elaborated following the variable time normalization analysis (VTNA) described by Burés. An order in product **1.22** of -0.2 caused the best overlap of the four curves in the graph below, as judged visually.

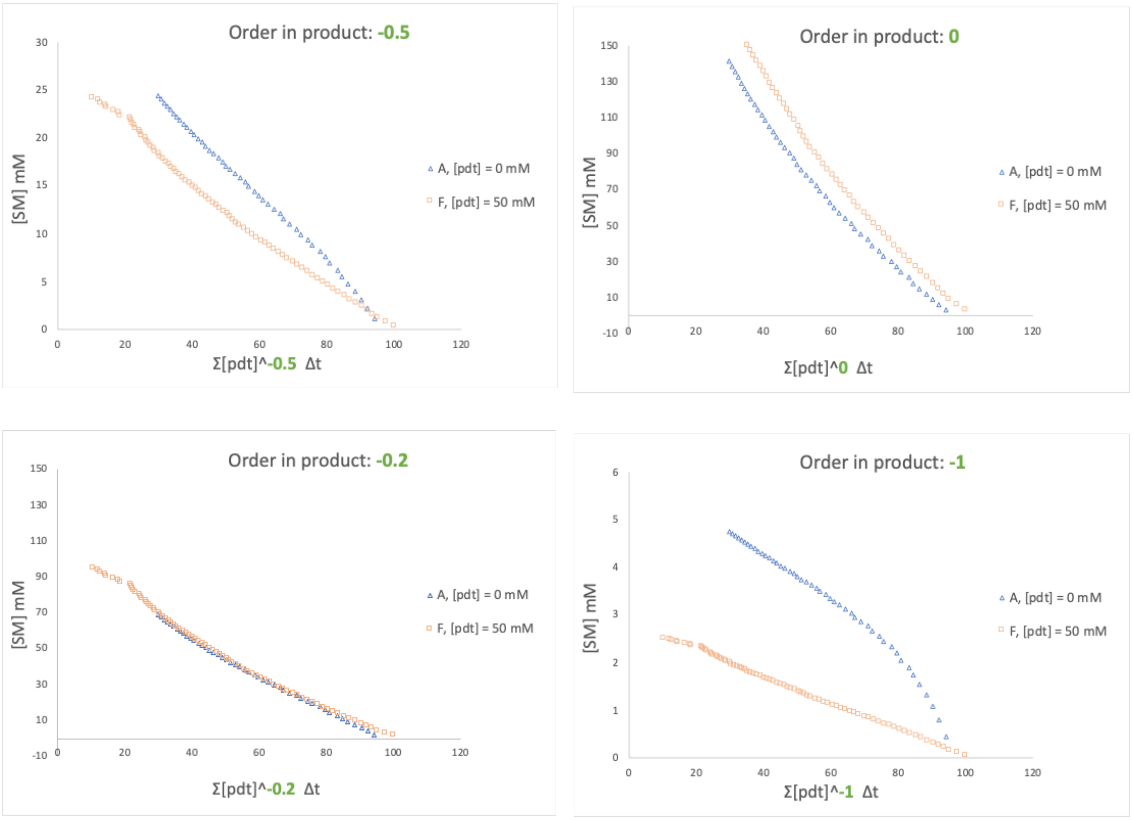

Data: -0.2 order in product **1.22** determined by VTNA analysis.

[S] = 100 mM **[cat]** = 5 mM **[P]** = 0 mM			**[S]** = 100 mM **[cat]** = 5 mM **[P]** = 50 mM		
t/ min	**[P]**/ mM	**[S]**/ mM	**t**/ min	**[P]**/ mM	**[S]**/ mM
3	5.6	94.4	4	52.2	97.8
6	7.6	92.4	7	54.7	95.3
9	9.5	90.5	10	56.2	93.8
12	11.5	88.5	13	57.7	92.3
15	13.5	86.5	16	59.4	90.6
18	15.2	84.8	19	61.1	88.9
21	16.6	83.4	22	62.8	87.2
24	19.0	81.0	25	64.5	85.5
27	20.1	79.9	28	66.4	83.6
30	21.9	78.1	31	67.7	82.3
33	24.2	75.8	34	69.4	80.6
36	25.4	74.6	37	70.9	79.1
39	27.6	72.4	40	72.3	77.7
42	28.7	71.3	43	74.0	76.0
45	30.8	69.2	46	75.4	74.6
48	32.6	67.4	49	76.8	73.2
51	33.6	66.4	52	78.6	71.4
54	35.4	64.6	55	79.6	70.4
57	37.2	62.8	58	81.4	68.6
60	38.7	61.3	61	82.7	67.3
63	40.1	59.9	64	83.9	66.1
66	41.2	58.8	67	85.4	64.6
69	43.1	56.9	70	86.7	63.3
72	44.1	55.9	73	88.1	61.9
75	45.7	54.3	76	89.2	60.8
78	47.0	53.0	79	90.6	59.4
81	48.5	51.5	82	91.8	58.2
84	49.8	50.2	85	93.2	56.8
87	50.9	49.1	88	94.3	55.7
90	52.1	47.9	91	95.8	54.2
93	53.5	46.5	94	96.8	53.2
96	54.7	45.3	97	97.9	52.1
99	55.9	44.1	100	98.0	51.3
102	57.0	43.0	103	99.2	50.8
105	57.9	42.1	106	100.5	49.5
108	59.2	40.8	109	101.6	48.4
111	60.3	39.7	112	102.6	47.4
114	61.4	38.6	115	103.6	46.4
117	62.3	37.7	118	104.7	45.3
120	63.4	36.6	121	105.7	44.3
123	64.4	35.6	124	106.7	43.3
126	65.4	34.6	127	107.7	42.3
129	66.3	33.7	130	108.7	41.3
132	67.3	32.7	133	109.7	40.3
135	68.2	31.8	136	110.7	39.3
138	69.0	31.0	139	111.6	38.4
141	70.0	30.0	142	112.6	37.4
144	70.8	29.2	145	113.5	36.5
			148	114.5	35.5
			151	115.3	34.7
			154	115.9	34.1
			157	116.7	33.3
			160	117.4	32.6
			163	118.4	31.6
			166	119.3	30.7
			169	119.8	30.2
			172	120.9	29.1
			175	121.1	28.9
			178	122.1	27.9
			181	122.8	27.2
			184	123.2	26.8
			187	123.6	26.4
			190	124.7	25.3
			193	125.3	24.7
			196	125.5	24.5
			199	126.6	23.4
			202	127.1	22.9
			205	127.6	22.4
			208	127.9	22.1

Eyring analysis (based on initial rates)

All operations were performed under inert atmosphere (glovebox and/or Schlenk line techniques and balloons) using anhydrous dichloromethane-d_2, dried over activated 3 Å MS for at least 24 h. Each tube was measured at a different temperature: 292, 295, 298, 301, 304 K.

Standard reaction conditions: [**1.21**] = 100 mM, [(*R,R*)**-F'**] = 5 mM

Five oven-dried NMR tubes equipped with a rubber septum containing substrate **1.21**,1,3,5-tribromobenzene as internal standard and gold complex (*R,R*)**-F'** in CD_2Cl_2 (500 μL) were prepared. Precisely, the following solutions were added in sequence into the NMR tubes:

1) Substrate **1.21** and internal standard stock solution (200 μL), previously prepared by adding CD_2Cl_2 (1400 μL) to the substrate (100.0 mg, 349.0 μmol) and 1,3,5-tribromobenzene (55.0 mg, 174.0 μmol).

2) CD_2Cl_2 (240 μL), obtaining a clear colourless solution.

To it, a white suspension of gold complex (*R,R*)**-F'** (60 μL) was added, bringing the total volume to 500 μL. The suspension of complex (*R,R*)**-F'** was previously prepared by adding CD_2Cl_2 (700 μL) to complex (*R,R*)**-F'** (26 mg, 17.5 umol). After the addition, the tube was shaken for few seconds, obtaining a clear colourless solution, and immediately inserted into a 500 MHz spectrometer equipped with cryoprobe. ^{1}H NMR spectra (8 scans each) were recorded at 60-second or 40-second intervals until 20% conversion of substrate. The first ^{1}H NMR was recorded 3 minutes after the addition of complex.

Data

Conversion data against the internal standard were extracted using Mestrenova (Fourier transform, automatic phase correction, baseline correction and integration of stacked spectra) and further manipulated with Excel. Linear correlations were observed for the concentration of product plotted against time at low conversions (up to 20%). For each data set, only the initial part of the slope possessing a linear correlation between product concentration and time was selected for interpolation. Rate constants (k_{obs}) were thus obtained from the slope of the linear regression, forcing the intecept at 0. The observed rate constant k_{obs} were divided by the concentration of catalyst (*R,R*)**-F'** (5.0 mM), since the reaction is first-order in catalyst, in order to obtain the rate constant k (s^{-1}). Data are reported in the table below, rounded for clarity.

T = 295K		**T = 297K**		**T = 299K**		**T = 301K**		**T = 303K**	
time/s	**[P]**/ mM	**time**/ s	**[P]**/ mM	**time**/ s	**[P]**/ mM	**time**/ s	**[P]**/ mM	**time**/ s	**[P]**/ mM
240	6.8	180	7.3	180	7.5	180	9.0	180	11.1
300	7.3	240	8.9	204	9.1	240	10.8	204	13.3
360	8.5	300	10.6	228	10.5	228	12.7	228	15.6
420	10.0	360	12.4	252	12.1	252	14.4	252	17.7
480	11.2	420	14.0	276	13.6	276	16.2	276	19.8
540	12.7	480	15.7	300	15.0	300	18.0	300	21.9
600	14.0	540	17.3	324	16.5	324	19.7		
660	15.3	600	18.9	348	17.9	348	21.4		
720	16.7	660	20.5	372	19.4	372	23.1		
780	17.9	720	22.1	396	20.7				
840	19.2			420	22.1				
900	20.5								
960	21.7								
y = **0.0231**x		y = **0.0321**x		y = **0.0505**x		y = **0.0584**x		y = **0.0697**x	
R^2 = 0.9992		R^2 = 0.997		R^2 = 0.9973		R^2 = 0.9933		R^2 = 0.975	

Data: Product formation at different temperatures at low conversions (up to 20%, first 20 minutes, based on the coloured bolded data in the table

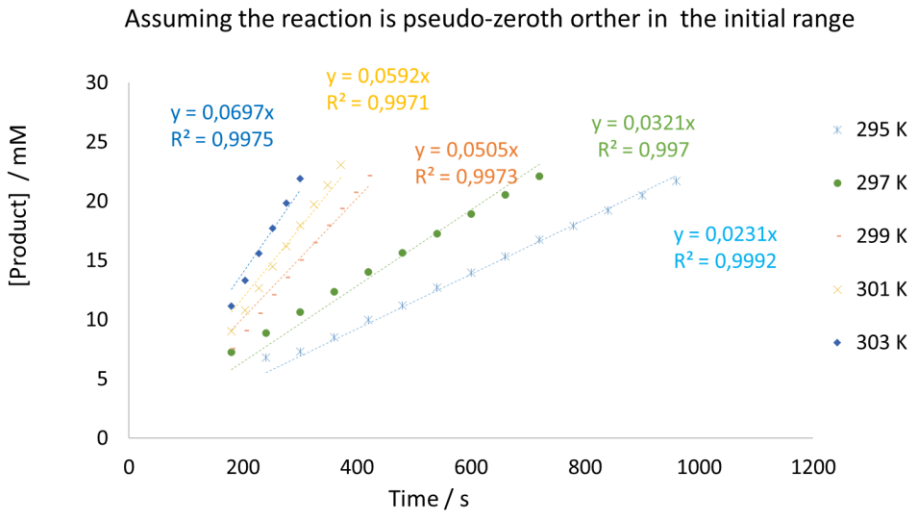

Calculation of thermodynamic activation parameters:

The errors associated to m and q values in the linear regression of the Eyring plot (y = mx + q) were calculated using the array function LINEST in Excel.

R (gas constant) = 0.0019872 kcal K^{-1} mol^{-1}

h (Planck's constant) = 6.6261×10^{-34} J s

k_B (Boltzmann constant) = 1.3806×10^{-23} J K^{-1}

κ (transmission coefficient) = assumed to be 1

Splitting the two parts of the Eyring plot, the parameters were calculated for each part.

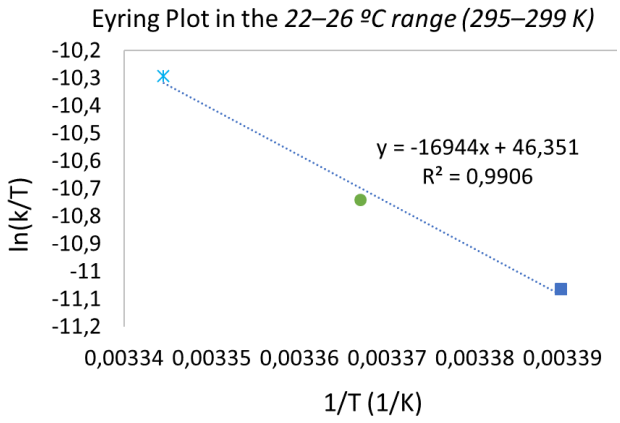

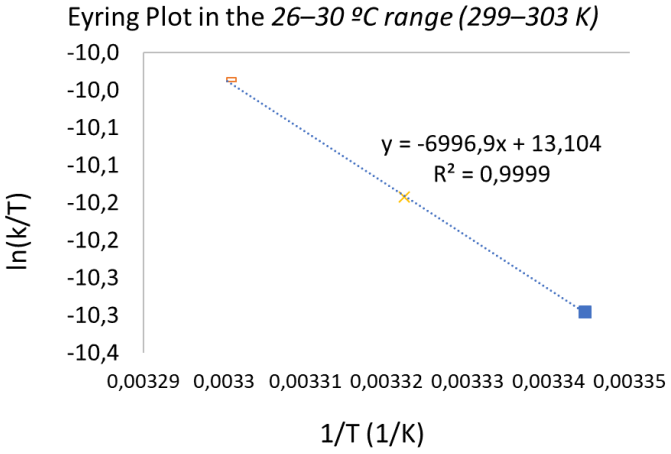

1.5.4 Crystallographic data

Complex (*R*,*R*)-C

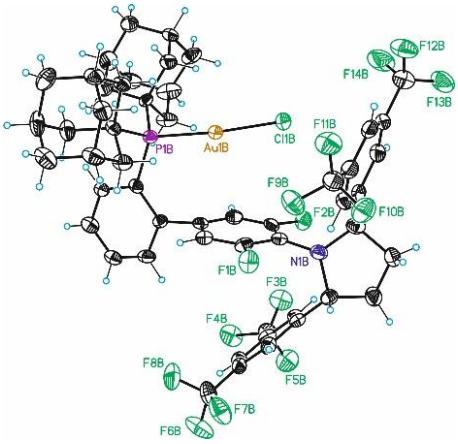

Identification code	IA-01-210
Empirical formula	$C_{116}\ H_{120}\ Au_2\ Cl_2\ F_{28}\ N_2\ P_2$
Formula weight	2600.91
Temperature	100(2)K
Wavelength	0.71073 Å
Unit cell dimensions	a = 17.6260(3)Å b = 92.8151(16)Å. c = 30.2671(6)Å g = 90°.
Volume	5328.86(16) $Å^3$
Z	2
Density (calculated)	1.621 Mg/m^3
Absorption coefficient	2.930 mm^{-1}
F(000)	2608
Crystal size	0.400 x 0.020 x 0.020 mm^3
Theta range for data collection	3.459 to 29.778°.
Index ranges	-13<=h<=13,-23<=k<=24,-41<=l<=41
Reflections collected	104074
Independent reflections	27464[R(int) = 0.0783]
Completeness to theta =29.778°	93.5%
Absorption correction	Multi-scan
Max. and min. transmission	1.00 and 0.76
Refinement method	Full-matrix least-squares on F^2
Data / restraints / parameters	27464/ 2164/ 1888
Goodness-of-fit on F^2	1.055
Final R indices [I>2sigma(I)]	R1 = 0.0486, wR2 = 0.0981
R indices (all data)	R1 = 0.0785, wR2 = 0.1072
Flack parameter	x =-0.025(4)
Largest diff. peak and hole	2.045 and -1.998 e.$Å^{-3}$

Complex (*R*,*R*)-F'

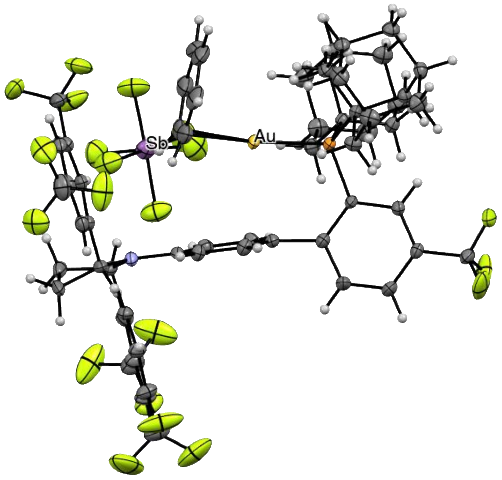

Identification code	IA0148lt	
Empirical formula	C_{82} H_{85} Au F_{21} N P Sb	
Formula weight	1833.19	
Temperature	100(2)K	
Wavelength	0.71073 Å	
Crystal system	orthorhombic	
Space group	P 21 21 21	
Unit cell dimensions	a = 14.6220(3)Å	a= 90°.
	b = 18.7537(3)Å	b = 90°.
	c = 28.2631(4)Å	g = 90°.
Volume	7750.2(2) $Å^3$	
Z	4	
Density (calculated)	1.571 Mg/m^3	
Absorption coefficient	2.355 mm^{-1}	
F(000)	3672	
Crystal size	0.400 x 0.300 x 0.200 mm^3	
Theta range for data collection	2.280 to 29.431°.	
Index ranges	-18<=h<=20,-25<=k<=25,-29<=l<=38	
Reflections collected	52895	
Independent reflections	19256[R(int) = 0.0257]	
Completeness to theta =29.431°	93.0%	
Absorption correction	Multi-scan	
Max. and min. transmission	1.00 and 0.67	
Refinement method	Full-matrix least-squares on F^2	
Data / restraints / parameters	19256/ 1138/ 1207	
Goodness-of-fit on F^2	1.021	
Final R indices [I>2sigma(I)]	R1 = 0.0272, wR2 = 0.0609	
R indices (all data)	R1 = 0.0316, wR2 = 0.0621	
Flack parameter	x =-0.0092(13)	
Largest diff. peak and hole	0.988 and -0.739 $e.Å^{-3}$	

Complex (*R*,*R*)-H

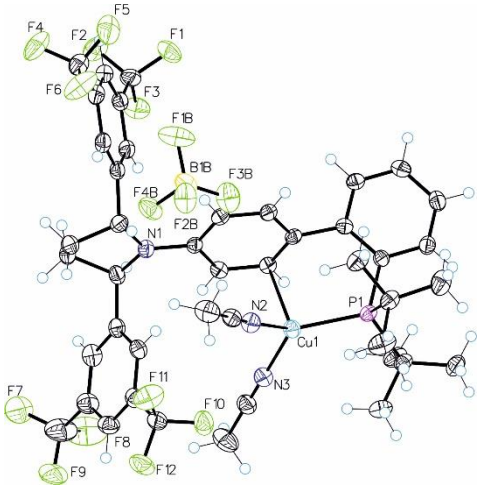

Identification code	IA-01-167
Empirical formula	$C_{45}H_{46}BCl_2CuF_{16}N_3P$
Formula weight	1109.11
Temperature/K	100(2)
Crystal system	orthorhombic
Space group	$P2_12_12_1$
a/Å	14.8198(2)
b/Å	15.8490(3)
c/Å	21.1780(4)
α/°	90
β/°	90
γ/°	90
Volume/Å^3	4974.27(15)
Z	4
ρ_{calc}g/cm^3	1.481
μ/mm^{-1}	0.674
F(000)	2256.0
Crystal size/mm^3	0.4 × 0.2 × 0.2
Radiation	Mo Kα (λ = 0.71073)
2Θ range for data collection/°	4.626 to 58.756
Index ranges	$-20 \leq h \leq 19$, $-21 \leq k \leq 21$, $-29 \leq l \leq 25$
Reflections collected	46228
Independent reflections	12375 [R_{int} = 0.0233, R_{sigma} = 0.0228]
Data/restraints/parameters	12375/535/798
Goodness-of-fit on F^2	1.051
Final R indexes [I>=2σ (I)]	R_1 = 0.0300, wR_2 = 0.0834
Final R indexes [all data]	R_1 = 0.0363, wR_2 = 0.0859
Largest diff. peak/hole / e Å^{-3}	0.25/-0.31

Complex (*R*,*R*)-G

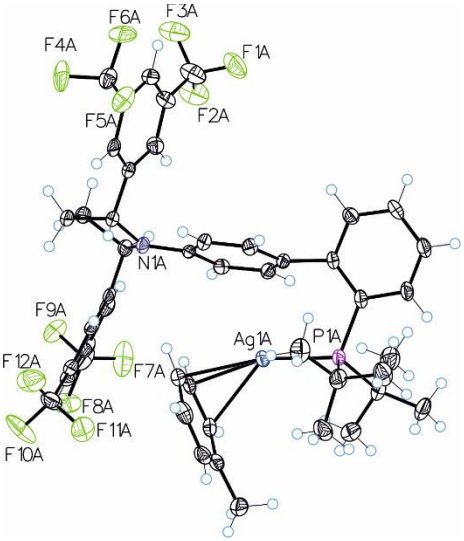

Identification code	IA-01-172_P1
Empirical formula	$C_{47}H_{46}NF_{18}PAgSb$
Formula weight	1227.44
Temperature/K	100.15
Crystal system	triclinic
Space group	P1
a/Å	9.5144(3)
b/Å	15.7263(4)
c/Å	18.0311(5)
α/°	106.026(2)
β/°	93.590(2)
γ/°	103.253(2)
Volume/Å^3	2501.05(12)
Z	2
ρ_{calc}g/cm^3	1.630
μ/mm^{-1}	1.064
F(000)	1220.0
Crystal size/mm^3	0.1 × 0.05 × 0.05
Radiation	MoKα (λ = 0.71073)
2Θ range for data collection/°	4.438 to 60.7
Index ranges	-13 ≤ h ≤ 13, -22 ≤ k ≤ 22, -25 ≤ l ≤ 24
Reflections collected	58394
Independent reflections	25065 [R_{int} = 0.0294, R_{sigma} = 0.0382]
Data/restraints/parameters	25065/584/1483
Goodness-of-fit on F^2	1.017
Final R indexes [I>=2σ (I)]	R_1 = 0.0320, wR_2 = 0.0824
Final R indexes [all data]	R_1 = 0.0362, wR_2 = 0.0843
Largest diff. peak/hole / e Å^{-3}	2.59/-0.50
Flack parameter	-0.015(7)

UNIVERSITAT ROVIRA I VIRGILI
MECHANISTIC STUDIES ON GOLD(I) AND GOLD(III) CATALYTIC TRANSFORMATIONS
Isabel Arranz De La Calle

UNIVERSITAT ROVIRA I VIRGILI
MECHANISTIC STUDIES ON GOLD(I) AND GOLD(III) CATALYTIC TRANSFORMATIONS
Isabel Arranz De La Calle

Chapter II

Study of Oxidative Addition Processes in Kochi Gold(I) Complexes

UNIVERSITAT ROVIRA I VIRGILI
MECHANISTIC STUDIES ON GOLD(I) AND GOLD(III) CATALYTIC TRANSFORMATIONS
Isabel Arranz De La Calle

2.1 Introduction

2.1.1. Gold(I)/Gold(III) oxidative addition

As mentioned in the general introduction, gold was considered for a long time as an inert material and consequently not synthetically useful. This idea was put in question by the successful development of gold catalysts for the electrophilic activation of C–C π-bonds,[1] and had to be discarded with the development in the past twenty years of catalytic cycles involving different Au(I)/Au(III) oxidation states.[2] Cross-coupling reactions are considered as one of the most crucial processes for the formation of C–C and C–X bonds, thus there has been a growing interest in examining the behavior of gold complexes in fundamental organometallic transformations, and their role in this type of catalytic cycles.[3] The scarcity of gold-catalyzed cross-coupling reactions is due to the reluctance of gold to alternate between its I and III oxidation states. Oxidative addition, typically the starting point for cross-coupling catalytic cycles, has been studied to be unfavorable for Au(I) complexes.[4] This is because the strong relativistic effects in gold[5] make the Au(I)/Au(III) pair to have an atypically high redox potential (E^0 = 1.41 V) in comparison to the Pd(0)/Pd(II) isoelectronic pair (E^0 = 0.92 V).[6]

Traditionally, several approaches that comprise using stoichiometric amounts of strong external oxidants have been employed to promote the access to Au(III) intermediates via 2-electron oxidation. In 2008, Tse and coworkers reported the first gold-catalyzed C–C coupling to produce biaryls, employing 2 mol% $HAuCl_4$ and hypervalent iodine $PhI(OAc)_2$ as the oxidant (Scheme

1 a) Hashmi, A. S. K. Gold-Catalyzed Organic Reactions, *Chem. Rev.* **2007**, *107*, 3180–3211. b) Dorel, R.; Echavarren, A. M. Gold(I)-Catalyzed Activation of Alkynes for the Construction of Molecular Complexity, *Chem. Rev.* **2015**, *115*, 9028–9072.

2 Joost, M.; Amgoune, A.; Bourissou, D. Reactivity of Gold Complexes towards Elementary Organometallic Reactions, *Angew. Chem. Int. Ed Engl.* **2015**, *54*, 15022–15045.

3 Rocchigiani, L.; Bochmann, M. Recent Advances in Gold(III) Chemistry: Structure, Bonding, Reactivity, and Role in Homogeneous Catalysis, *Chem. Rev.* **2021**, *121*, 8364–8451.

4 a) Livendahl, M.; Goehry, C.; Maseras, F.; Echavarren, A. M. Rationale for the Sluggish Oxidative Addition of Aryl Halides to Au(I), *Chem Commun* **2014**, *50*, 1533–1536. b) Livendahl, M.; Espinet, P.; Echavarren, A. M. Final Analysis: Is Gold a Catalyst in Cross-Coupling Reactions in the Absence of Palladium?, *Platin. Met. Rev.* **2011**, *55*, 212–214. c) Lauterbach, T.; Livendahl, M.; Rosellón, A.; Espinet, P.; Echavarren, A. M. Unlikeliness of Pd-Free Gold(I)-Catalyzed Sonogashira Coupling Reactions, *Org. Lett.* **2010**, *12*, 3006–3009.

5 a) P. Pyykko, J. P. Desclaux*, Acc. Chem. Res*. **1979**, *12*, 276–281; b) D.J. Gorin, F. D. Toste, *Nature,* **2007**, *446*, 395–403; c) P. Pyykkö*, Angew. Chem. Int. Ed*. **2004**, *43*, 4412–4456; *Angew. Chem*. **2004**, *116*, 4512-4557.

6 Bratsch, S. G. Standard Electrode Potentials and Temperature Coefficients in Water at 298.15 K, *J. Phys. Chem. Ref. Data* **1989**, *18*, 1–21.

2.1).[7] In the upcoming years, several contributions were made using sacrificial oxidants such as selectfluor[8] (F^+ donor) and other hypervalent iodine reagents.[9]

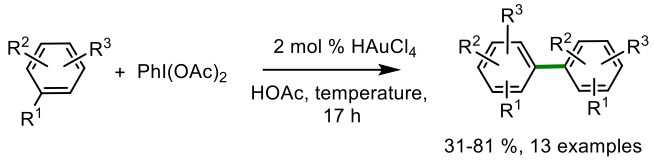

Scheme 2.1. Gold-catalyzed oxidative homocoupling of arenes.

Some years after, between 2010 and 2012, multiple research groups independently published numerous studies on gold-catalyzed oxy- and aminoarylation reactions of terminal alkenes. Russell and Lloyd-Jones used arylsilanes as coupling partners in the three-component oxyarylation of olefins[10] and Toste could expand the arylating fragments to arylboronic acids by using bimetallic gold(I) complex [dppm(AuBr)$_2$] (Scheme 2.2a).[7b,11] Concomitantly, Zhan and coworkers combined C–H functionalization and Au(I)/Au(III) catalysis to produce tricyclic indolines (Scheme 2.2b).[12]

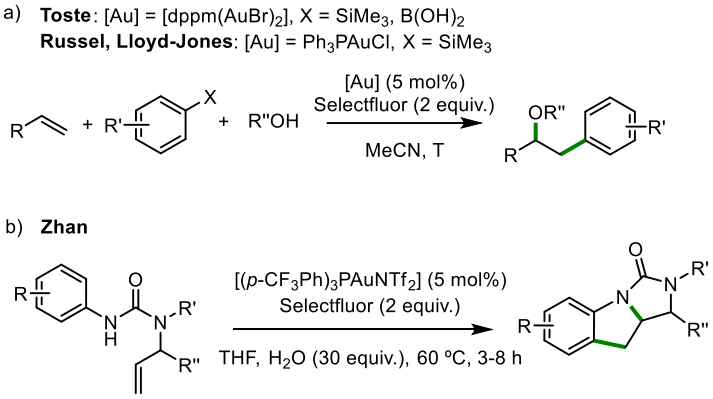

Scheme 2.2. Au(I)/Au(III)-catalyzed oxyarylations and aminoarylations of terminal olefins.

7 Kar, A.; Mangu, N.; Kaiser, H. M.; Beller, M.; Tse, M. K. A General Gold-Catalyzed Direct Oxidative Coupling of Non-Activated Arenes, *Chem. Commun.* **2008**, No. 3, 386–388.

8 a) Zhang, G.; Peng, Y.; Cui, L.; Zhang, L. Gold-Catalyzed Homogeneous Oxidative Cross-Coupling Reactions, *Angew. Chem. Int. Ed Engl.* **2009**, *48*, 3112–3115. b) Brenzovich, W. E. Jr.; Brazeau, J.-F.; Toste, F. D. Gold-Catalyzed Oxidative Coupling Reactions with Aryltrimethylsilanes, *Org. Lett.* **2010**, *12*, 4728–4731.

9 Ball, L. T.; Lloyd-Jones, G. C.; Russell, C. A. Gold-Catalysed Oxyarylation of Styrenes and Mono- and Gem-Disubstituted Olefins Facilitated by an Iodine(III) Oxidant, *Chem. – Eur. J.* **2012**, *18*, 2931–2937.

10 Ball, L. T.; Green, M.; Lloyd-Jones, G. C.; Russell, C. A. Arylsilanes: Application to Gold-Catalyzed Oxyarylation of Alkenes, *Org. Lett.* **2010**, *12*, 4724–4727.

11 Melhado, A. D.; Brenzovich, W. E.; Lackner, A. D.; Toste, F. D. Gold-Catalyzed Three-Component Coupling: Oxidative Oxyarylation of Alkenes, *J. Am. Chem. Soc.* **2010**, *132*, 8885–8887.

12 Zhang, G.; Luo, Y.; Wang, Y.; Zhang, L. Combining Gold(I)/Gold(III) Catalysis and C□H Functionalization: A Formal Intramolecular [3+2] Annulation towards Tricyclic Indolines and Mechanistic Studies, *Angew. Chem. Int. Ed.* **2011**, *50*, 4450–4454.

The use of strong oxidants is not the only path to Au(I) activation. In the early seventies Kochi[13] and Puddephatt[14] reported the oxidative addition of alkyl halides to simple alkyl phosphine gold(I) complexes. The reaction sequence occurs slowly at 25 ºC and starts with an oxidative addition of the C(sp^3)-I bond to gold; suggesting an S_N2-type mechanism. Some of the resulting Au(III) complexes were characterized by NMR techniques. A C(sp^3)-C(sp^3) reductive elimination was proposed to yield formally cross-coupled products (Scheme 2.3).

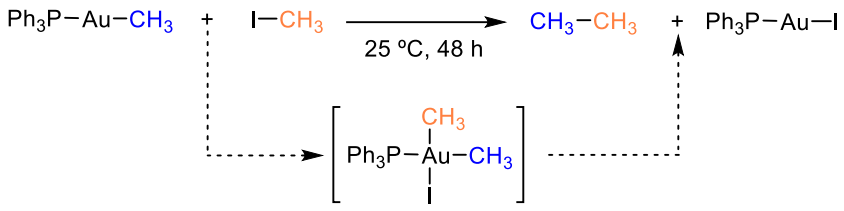

Scheme 2.3. Oxidative addition of methyl iodide to mononuclear gold(I) complexes and consequent reductive elimination of ethane.

Apart from these studies performed 50 years ago, research in the field of oxidative addition at gold(I) was not resumed until 2011, after which it experienced significant growth. Recent discoveries have demonstrated that the challenge of oxidative addition at gold(I) can be overcome by several strategies such as ligand design or strain release.

In 2015, Toste reported the access to stable Au(III) complexes through a mild oxidative addition of the strained C–C bond of phenylene to cationic IPrAu(I), formed upon halogen abstraction using silver salts.[15] The resulting Au(III) intermediates were trapped with DMF or *n*Bu_4NCl and their corresponding tetracoordinate complexes characterized by X-ray crystallography (Scheme 2.4). This work is notable as an example of how the oxidative addition is favored due to the energy release from a strained covalent bond and because the substrate, once coordinated, stabilizes the Au(III) center by providing it with an appropriate coordination geometry.

13 a) Tamaki, A.; Kochi, J. K. Oxidative Addition in the Coupling of Alkylgold(I) with Alkyl Halides. J. *Organomet. Chem*. **1974**, *64*, 411-425. b) Tamaki, A.; Magennis, S. A.; Kochi, J. K. Catalysis by Gold. Alkyl Isomerization, Cis-Trans Rearrangement, and Reductive Elimination of Alkylgold(III) Complexes, *J. Am. Chem. Soc.* **1974**, *96*, 6140–6148. c) Tamaki, A.; Magennis, S. A.; Kochi, J. K. Rearrangement and Decomposition of Trialkylgold(III) Complexes, *J. Am. Chem. Soc.* **1973**, *95*, 6487–6488.

14 a) Johnson, A.; Puddephatt, R. J. Oxidative Addition Reactions of Methylgold (I) Compounds, *Inorg. Nucl. Chem. Lett.* **1973**, *9*, 1175–1177. b) Johnson, A.; Puddephatt, R. J. Oxidative Addition Reactions of Methyl iodide with some methylgold(I) compounds. *J. Organomet. Chem*. **1975**, *85*, 115-121.

15 Wu, C.-Y.; Horibe, T.; Jacobsen, C. B.; Toste, F. D. Stable Gold(III) Catalysts by Oxidative Addition of a Carbon-Carbon Bond, *Nature* **2015**, *517*, 449–454.

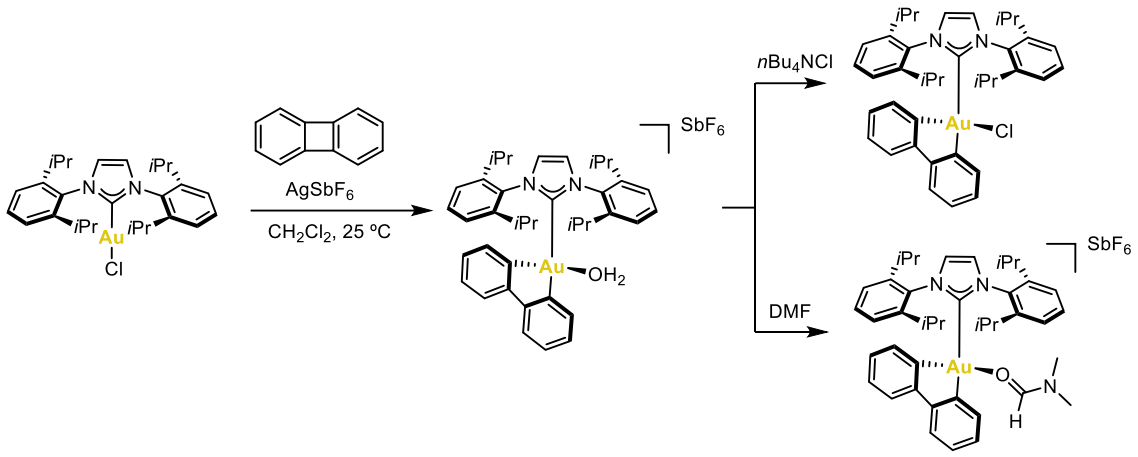

Scheme 2.4. Access to Au(III) complexes via oxidative addition of a strained C–C bond.

Within the ligand design approaches, the chelation-assisted method involves the generation of a Au(I) complex that is coordinated to a ligand with a functional group positioned near the metal center, making it susceptible to oxidative addition to the Au(I) atom. Following this principle, the oxidative addition of apolar σ-bonds (Si-Si and Sn-Sn) and polar C–X bonds to gold(I) has been achieved. Between 2011-2014, Bourissou, Amgoune and coworkers designed diphosphine ligands bearing Sn-Sn and Si-Si bonds (Scheme 2.5a),[16] being able to promote the oxidative addition reaction at -78 ºC and isolating the Au(III) square-planar complexes as stable solids. It resulted notable that in the case of σ-Si-Si bonds, its oxidative addition at Au(I) took place as well in the presence of $GaCl_3$ at -80 ºC, obtaining trigonal planar Au(III) complexes (Scheme 2.5b),[17] unstable above -60/-80 ºC temperatures. In parallel, Toste developed in 2014 a tethered substrate containing an allyl bromide from which oxidative addition was initiated at 40 ºC in acetonitrile (Scheme 2.5c).[18] Additionally in 2014, Bourissou's group contributed with the publication of an intramolecular oxidative addition of aryl halides. The first development of oxidative addition of C(sp^2)-X bonds (X = Br, I) to Au(I) was reported by the design of the 8-halonaphthyl phosphine ligand, which places the C(sp^2)-X bond nearby the Au(I) atom and stabilizes at the same time the (P,C)-cyclometalated Au(III) complexes formed remarkably at 25 ºC in 12 h (Scheme 2.5d).[19]

16 a) Gualco, P.; Ladeira, S.; Miqueu, K.; Amgoune, A.; Bourissou, D. Gold-Mediated Insertion of Oxygen into Silicon–Silicon Bond: An Original Au(I)/Au(III) Redox Sequence, *Organometallics* **2012**, *31*, 6001–6004. b) Lassauque, N.; Gualco, P.; Mallet-Ladeira, S.; Miqueu, K.; Amgoune, A.; Bourissou, D. Activation of a σ-SnSn Bond at Copper, Followed by Double Addition to an Alkyne, *J. Am. Chem. Soc.* **2013**, *135*, 13827–13834.

17 Joost, M.; Gualco, P.; Coppel, Y.; Miqueu, K.; Kefalidis, C. E.; Maron, L.; Amgoune, A.; Bourissou, D. Direct Evidence for Intermolecular Oxidative Addition of σ(Si□Si) Bonds to Gold, *Angew. Chem.* **2014**, *126*, 766–770.

18 Levin, M. D.; Toste, F. D. Gold-Catalyzed Allylation of Aryl Boronic Acids: Accessing Cross-Coupling Reactivity with Gold, *Angew. Chem. Int. Ed.* **2014**, *53*, 6211–6215.

19 Guenther, J.; Mallet-Ladeira, S.; Estevez, L.; Miqueu, K.; Amgoune, A.; Bourissou, D. Activation of Aryl Halides at Gold(I): Practical Synthesis of (P,C) Cyclometalated Gold(III) Complexes, *J. Am. Chem. Soc.* **2014**, *136*, 1778–1781.

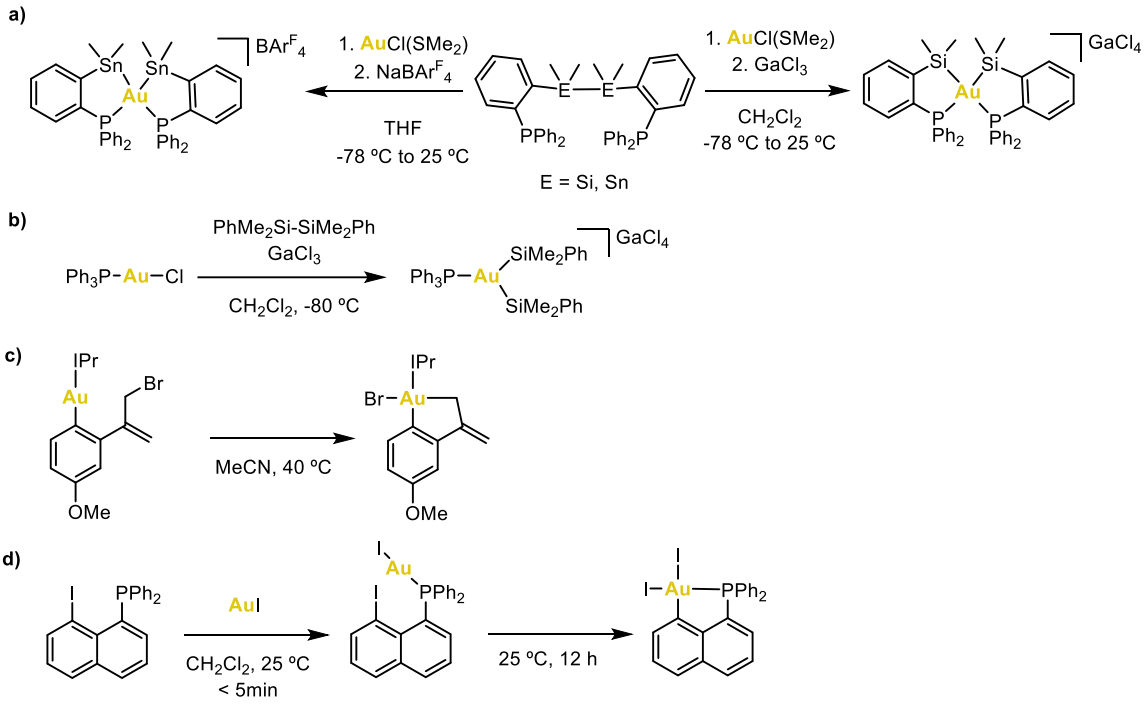

Scheme 2.5. Selected examples on the chelation-assisted oxidative addition at gold(I).

An alternative strategy consists of the design of bidentate ligands with small bite angles. The chelating ligands force the preorganization of the Au(I) center to a non-linear geometry, allowing the oxidative addition to take place more easily; given that the deformation energy needed to reach the square-planar geometry of Au(III) complexes is reduced. Using tricoordinate (DPCb) complexes with a labile triflimidate ligand (NTf_2^-), Amgoune, Bourissou, and their team demonstrated in 2014 that gold(I) can undergo oxidative addition of aryl iodides (Scheme 2.6a). The reaction occurs under mild conditions (from minutes to hours at -30 °C to 25 ºC). The resulting aryl gold(III) complexes were isolated and thoroughly characterized using NMR spectroscopy and X-ray diffraction.[20] Interestingly, the reactivity trend for *p*-substituted iodobenzenes is the opposite of what is typically observed with Pd(0) complexes,[21] as electron-rich substrates react faster than electron-poor ones with (DPCb) gold complexes (small P-Au-P bite angle around 90–100º). Furthermore, in the same group one year later, DPCb gold complexes were tested in the oxidative addition of strained C–C bonds (Scheme 2.6b). The resulting Au(III) complexes exhibited exceptional stability. A unique selectivity was observed in the activation of benzocyclobutenone, where the selectivity of oxidative addition could be achieved at either the

20 Joost, M.; Zeineddine, A.; Estévez, L.; Mallet−Ladeira, S.; Miqueu, K.; Amgoune, A.; Bourissou, D. Facile Oxidative Addition of Aryl Iodides to Gold(I) by Ligand Design: Bending Turns on Reactivity, *J. Am. Chem. Soc.* **2014**, *136*, 14654–14657.

21 Fauvarque, J.-F.; Pflüger, F.; Troupel, M. Kinetics of Oxidative Addition of Zerovalent Palladium to Aromatic Iodides, *J. Organomet. Chem.* **1981**, *208*, 419–427.

C(aryl)-C(O) or the C(alkyl)-C(O) bond, explained by kinetic and thermodynamic control.[22] Later on in 2018, Russell and coworkers developed a three-coordinated 2,2'-bipyridyl-chelated-gold(I) ethylene complex that reacted towards oxidative addition of C(sp^2)-I bonds,[23] as well as towards oxidative addition of alkenyl and alkynyl iodides in 2020 (Scheme 2.6c).[24]

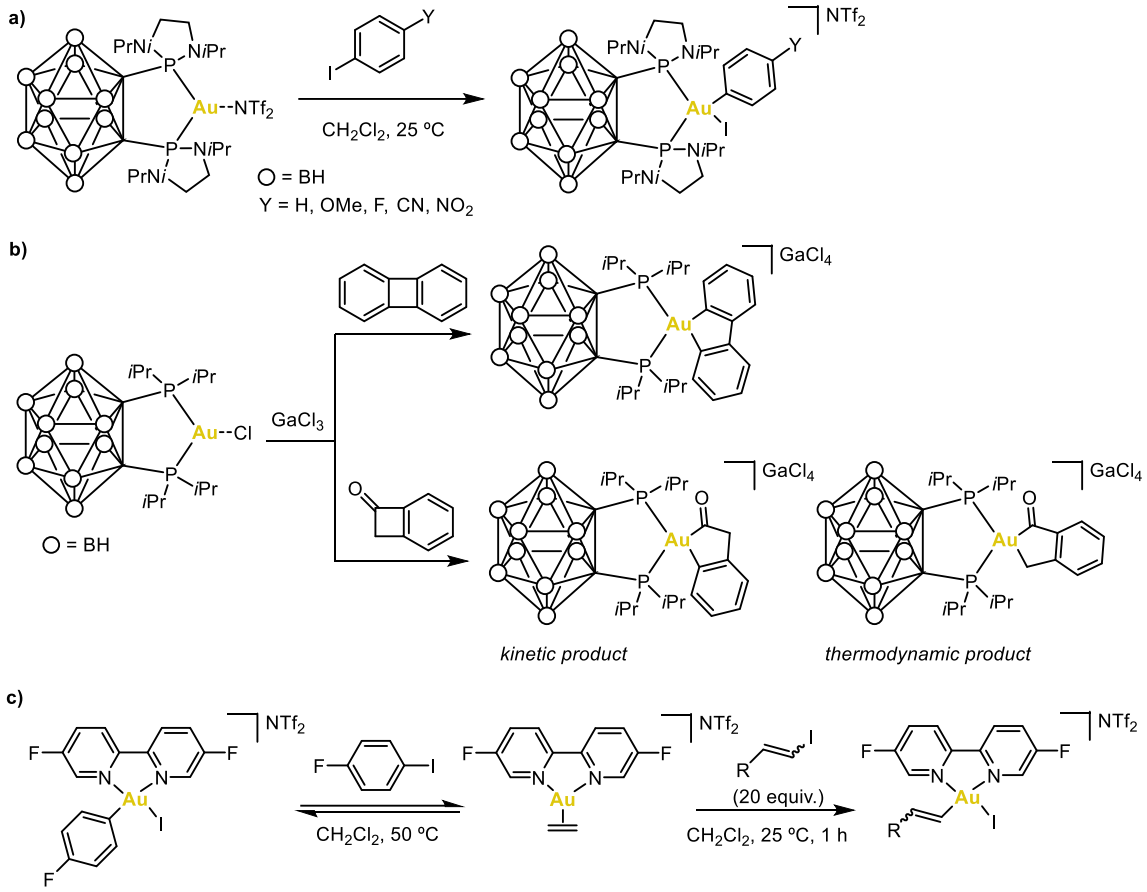

Scheme 2.6. Selected examples of bent, non-linear gold(I) complexes that undergo oxidative addition under mild conditions.

A different strategy applied to trigger oxidative addition to Au(I) is based on the use of hemilabile ligands. Bertrand and coworkers reported in 2016 a (CCAC)AuCl complex (CCAC = Cyclic Alkyl Amino Carbene) featuring a pendant imine moiety assisted in the oxidative addition of the strained C–C bond in biphenylene.[25] A year later, Bourissou's group used (MeDalPhos)AuCl,

22 Joost, M.; Estévez, L.; Miqueu, K.; Amgoune, A.; Bourissou, D. Oxidative Addition of Carbon-Carbon Bonds to Gold, *Angew. Chem. Int. Ed Engl.* **2015**, *54*, 5236–5240.

23 Harper, M. J.; Arthur, C. J.; Crosby, J.; Emmett, E. J.; Falconer, R. L.; Fensham-Smith, A. J.; Gates, P. J.; Leman, T.; McGrady, J. E.; Bower, J. F.; Russell, C. A. Oxidative Addition, Transmetalation, and Reductive Elimination at a 2,2′-Bipyridyl-Ligated Gold Center, *J. Am. Chem. Soc.* **2018**, *140*, 4440–4445.

24 Cadge, J. A.; Sparkes, H. A.; Bower, J. F.; Russell, C. A. Oxidative Addition of Alkenyl and Alkynyl Iodides to a AuI Complex, *Angew. Chem. Int. Ed.* **2020**, *59*, 6617–6621.

25 Chu, J.; Munz, D.; Jazzar, R.; Melaimi, M.; Bertrand, G. Synthesis of Hemilabile Cyclic (Alkyl)(Amino)Carbenes (CAACs) and Applications in Organometallic Chemistry, *J. Am. Chem. Soc.* **2016**, *138*, 7884–7887.

bearing a hemilabile tertiary amine in the oxidative addition of the strained substrate biphenylene as well as of the C–X bonds in different aryl, alkynyl and vinyl iodides (Scheme 2.7).[26] In line with these studies, Nevado introduced modifications to MeDalPhos ligand,[27] and Spokoyny prepared Au(III) complexes containing MeDalPhos that were effective arylating agents.[28]

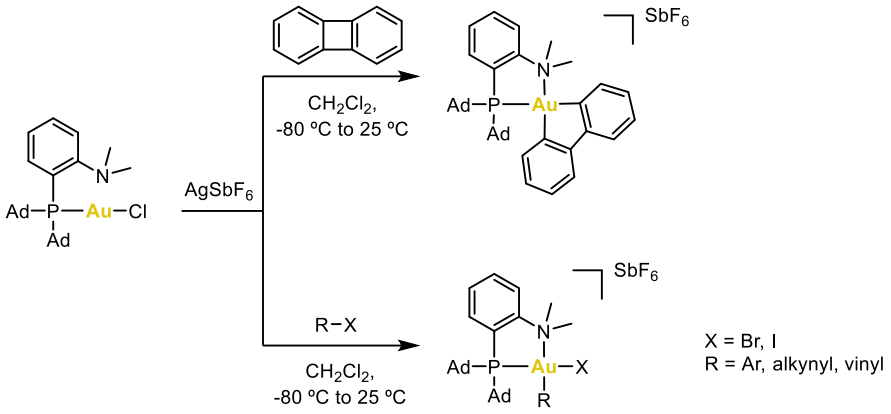

Scheme 2.7. Hemilabile ligand MeDalPhos stabilizes Au(III) complexes and promotes oxidative addition at gold(I).

In summary, the actual strategies to achieve oxidative addition to Au complexes via ligand design consist of the aforementioned chelation-assisted strategy, bidentate ligands with small bite angles, and hemilabile ligands. Combining oxidative addition with other essential organometallic transformations is crucial for developing synthetic methodologies that operate through oxidant-free Au(I)/Au(III) catalytic cycles.

The first catalytic system developed based on Kochi's seminal work[13] was reported by Levin and Toste in 2014. In this work the cross-coupling of allyl bromides and aryl boronic acids was achieved, catalyzed by a dinuclear gold(I) complex (Scheme 2.8). Simple (R_3P)AuCl complexes were tried but resulted to be significantly less active for the catalysis.[18] Stoichiometric reactions suggest a mechanism different from that typically observed with palladium. The process begins with transmetalation from boron to gold, followed by oxidative addition of allyl bromide to the resulting aryl-gold complex, and reductive elimination.

26 a) Zeineddine, A.; Estévez, L.; Mallet-Ladeira, S.; Miqueu, K.; Amgoune, A.; Bourissou, D. Rational Development of Catalytic Au(I)/Au(III) Arylation Involving Mild Oxidative Addition of Aryl Halides, *Nat. Commun.* **2017**, *8*, 565. b) Rodriguez, J.; Tabey, A.; Mallet-Ladeira, S.; Bourissou, D. Oxidative Additions of Alkynyl/Vinyl Iodides to Gold and Gold-Catalyzed Vinylation Reactions Triggered by the MeDalphos Ligand, *Chem. Sci.* **2021**, *12*, 7706–7712.

27 Genoux, A.; Biedrzycki, M.; Merino, E.; Rivera-Chao, E.; Linden, A.; Nevado, C. Synthesis and Characterization of Bidentate (P^N)Gold(III) Fluoride Complexes: Reactivity Platforms for Reductive Elimination Studies, *Angew. Chem. Int. Ed.* **2021**, *60*, 4164–4168.

28 Messina, M. S.; Stauber, J. M.; Waddington, M. A.; Rheingold, A. L.; Maynard, H. D.; Spokoyny, A. M. Organometallic Gold(III) Reagents for Cysteine Arylation, *J. Am. Chem. Soc.* **2018**, *140*, 7065–7069.

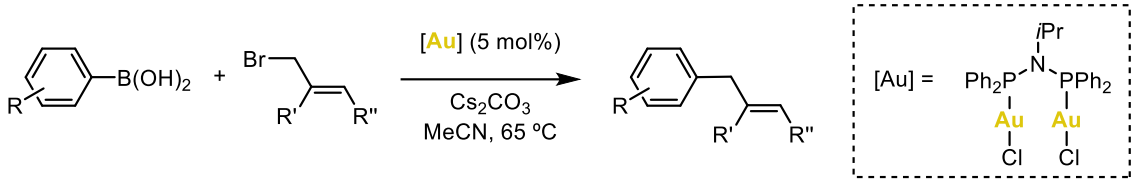

Scheme 2.8. Oxidant-free Au-catalyzed C(sp^3)-C(sp^2) cross-coupling reaction.

Ribas and coworkers designed a Au(I)/Au(III)-catalyzed cross-coupling transformation using a chelation-assisted strategy, by employing a cationic NHC-Au(I) complex and aryl halide triazamacrocyclic,[29] or 2-(2-halophenyl)pyridines[30] as substrates. The excellent performance of the MeDalPhos ligand (P-N ligand) in stabilizing Au(III) intermediates enabled the development of several Au(I)/Au(III) catalytic transformations, triggering an exponential growth in the field of cross-coupling reactions catalyzed by gold.[31] Apart from the gold-catalyzed reaction of aryl halides and electron-rich arenes in 2017 by Bourissou,[26a] in 2019 the same group reported the regioselective C3 arylation of indoles,[32] and in 2020 Patil and Bourissou independently continued with the C(sp^2)-N cross-coupling of aryl iodides and N-nucleophiles.[33] Additionally, P-N ligand assisted gold-catalyzed Heck reactions have been achieved, first in 2023 with aliphatic alkenes in the group of Patil, [34] and later on the same year with styrenes.[35]

29 Serra, J.; Whiteoak, C. J.; Acuña-Parés, F.; Font, M.; Luis, J. M.; Lloret-Fillol, J.; Ribas, X. Oxidant-Free Au(I)-Catalyzed Halide Exchange and Csp2–O Bond Forming Reactions, *J. Am. Chem. Soc.* **2015**, *137*, 13389–13397.

30 Serra, J.; Parella, T.; Ribas, X. Au(III)-Aryl Intermediates in Oxidant-Free C–N and C–O Cross-Coupling Catalysis, *Chem. Sci.* **2017**, *8*, 946–952.

31 McCallum, T. Heart of Gold: Enabling Ligands for Oxidative Addition of Haloorganics in Au(I)/Au(III) Catalysed Cross-Coupling Reactions, *Org. Biomol. Chem.* **2023**, *21*, 1629–1646.

32 Rodriguez, J.; Zeineddine, A.; Carrizo, E. D. S.; Miqueu, K.; Saffon-Merceron, N.; Amgoune, A.; Bourissou, D. Catalytic Au(I)/Au(III) Arylation with the Hemilabile MeDalphos Ligand: Unusual Selectivity for Electron-Rich Iodoarenes and Efficient Application to Indoles, *Chem. Sci.* **2019**, *10*, 7183–7192.

33 a) Rodriguez, J.; Adet, N.; Saffon-Merceron, N.; Bourissou, D. Au(I)/Au(III)-Catalyzed C–N Coupling, *Chem. Commun.* **2019**, *56*, 94–97. b) Akram, M. O.; Das, A.; Chakrabarty, I.; Patil, N. T. Ligand-Enabled Gold-Catalyzed C(Sp2)–N Cross-Coupling Reactions of Aryl Iodides with Amines, *Org. Lett.* **2019**, *21*, 8101–8105.

34 Bhoyare, V. W.; Sosa Carrizo, E. D.; Chintawar, C. C.; Gandon, V.; Patil, N. T. Gold-Catalyzed Heck Reaction, *J. Am. Chem. Soc.* **2023**, *145*, 8810–8816.

35 Wei, C.; Zhang, L.; Xia, Z. Hemilabile P,N-Ligand-Assisted Gold-Catalyzed Heck Reaction of Aryl and Styryl Iodides with Styrenes, *Org. Lett.* **2023**, *25*, 6808–6812.

2.2 Objectives

We wanted to further understand the mechanisms of the oxidative addition processes when simple ligand systems such as alkyl phosphines participate in Au(I)(Au(III) catalysis, and we wanted to apply this understanding to the development of more efficient catalytic systems involving mononuclear Au(I) catalysts. We will apply computational and experimental techniques to achieve these goals.

2.3 First set of computational studies

2.3.1 Computational details

Unless otherwise stated, all calculations were carried out using the Gaussian09 package.[36] All the reported energies are in kcal mol^{-1}. Free energies quoted were calculated at default temperature 298.15 K and include a +1.89 kcal mol^{-1} correction to reflect the 1M rather than ideal gas reference state.[37] Geometries were optimized to stationary points using the B3LYP[38] functional with Grimme's D3 dispersion correction[39] and the basis sets used were 6-31G(d,p)[40] for all elements except for Au, I, Br and Sn, where the SDD[41] basis set and ECP was employed. Single point calculations were performed with the cc-pVTZ[42] basis set for light atoms and cc-pVTZ-PP[43] basis set and ECP for Au, I, Br and Sn; using B3LYP-D3. Solvent effects were introduced with implicit model SMD[44] for toluene and iodomethane, using the same solvent in both optimization and single point calculations. All stationary points were confirmed through the absence of imaginary vibrations, and transition states were validated using IRC[45] calculations using LQA algorithm.

---

36 Gaussian 09, Revision B.1, Frisch, M. J., Trucks, G. W., Schlegel, H. B., Scuseria, G. E., Robb, M. A., Cheeseman, J. R., Scalmani, G., Barone, V., Mennucci, B., Petersson, G. A., Nakatsuji, H., Caricato, M., Li, X., Hratchian, H. P., Izmaylov, A. F., Bloino, J., Zheng, G., Sonnenberg, J. L., Hada, M., Ehara, M., Toyota, K., Fukuda, R., Hasegawa, J., Ishida, M., Nakajima, T., Honda, Y., Kitao, O., Nakai, H., Vreven, T., Montgomery, J. A., Peralta, Jr. J. E., Ogliaro, F., Bearpark, M., Heyd, J. J., Brothers, E., Kudin, K. N., Staroverov, V. N., Kobayashi, R., Normand, J., Raghavachari, K., Rendell, A., Burant, J. C., Iyengar, S. S., Tomasi, J., Cossi, M., Rega, N., Millam, J. M., Klene, M., Knox, J. E., Cross, J. B., Bakken, V., Adamo, C., Jaramillo, J., Gomperts, R., Stratmann, R. E., Yazyev, O., Austin, A. J., Cammi, R., Pomelli, C., Ochterski, J. W., Martin, R. L., Morokuma, K., Zakrzewski, V. G., Voth, G. A., Salvador, P., Dannenberg, J. J., Dapprich, S., Daniels, A. D., Farkas, Ö., Foresman, J. B., Ortiz, J. V., Cioslowski, J., Fox, D. J. Gaussian, Inc., Wallingford CT **2009.**

37 Luchini, G.; Alegre-Requena, J. V.; Funes-Ardoiz, I.; Paton, R. S. GoodVibes: Automated Thermochemistry for Heterogeneous Computational Chemistry Data, *F1000Research* **2020**, *9*, 291.

38 a) Becke, A. D. Density-Functional Exchange-Energy Approximation with Correct Asymptotic Behavior, *Phys. Rev. A* **1988**, *38*, 3098–3100. b) Density-functional Thermochemistry. III. The Role of Exact Exchange, *J. Chem. Phys.* **1993**, *98*, 5648–5652.

39 Grimme, S. Density Functional Theory with London Dispersion Corrections, *WIREs Comput. Mol. Sci.* **2011**, *1*, 211–228.

40 Hehre, W. J.; Ditchfield, R.; Pople, J. A. Self—Consistent Molecular Orbital Methods. XII. Further Extensions of Gaussian—Type Basis Sets for Use in Molecular Orbital Studies of Organic Molecules, *J. Chem. Phys.* **1972**, *56*, 2257–2261.

41 Andrae, D.; Häußermann, U.; Dolg, M.; Stoll, H.; Preuß, H. Energy-Adjustedab Initio Pseudopotentials for the Second and Third Row Transition Elements, *Theor. Chim. Acta* **1990**, *77*, 123–141.

42 Kendall, R. A.; Dunning, T. H., Jr.; Harrison, R. J. Electron Affinities of the First-row Atoms Revisited. Systematic Basis Sets and Wave Functions, *J. Chem. Phys.* **1992**, *96*, 6796–6806.

43 Peterson, K. A.; Figgen, D.; Dolg, M.; Stoll, H. Energy-Consistent Relativistic Pseudopotentials and Correlation Consistent Basis Sets for the 4d Elements Y–Pd, *J. Chem. Phys.* **2007**, *126*, 124101.

44 Marenich, A. V.; Cramer, C. J.; Truhlar, D. G. Universal Solvation Model Based on Solute Electron Density and on a Continuum Model of the Solvent Defined by the Bulk Dielectric Constant and Atomic Surface Tensions, *J. Phys. Chem. B* **2009**, *113*, 6378–6396.

45 Gonzalez, Carlos.; Schlegel, H. Bernhard. Reaction Path Following in Mass-Weighted Internal Coordinates, *J. Phys. Chem.* **1990**, *94*, 5523–5527.

2.3.2 Kochi's system[13a]

The oxidative addition of iodomethane to H_3C-Au$P(CH_3)_3$ **A1** was studied (Scheme 2.9) and after evaluating other mechanisms such as a concerted one, the most favorable was found to occur via an S_N2 reaction (**TSA2** = 20.6 kcal mol^{-1}). It is then a feasible barrier and supports the experimental results published back in the seventies. In this case, the alkylgold(I) complex **A1** would be behaving as a S_N2 nucleophile in the presence of an alkyl iodide as observed previously.[13,14]

In Kochi's publication, a reductive elimination was proposed from intermediate **A4** as only intermediate **A4** was detected by ^1H NMR. They propose an explanation for this fact, which is that the oxidative addition step is slower than the methyl/iodide exchange, so that **A3** does not attain concentrations high enough to be detected. Considering this, we observe that the hypothesis matches our results (intermediate **A4** more stable than **A3** after transmetalation with another molecule of starting material **A1**). However, the reductive elimination process from **A3** was calculated to be considerably lower in energy (**TSA3-5)** than from **A4** (**TSA4-6**).

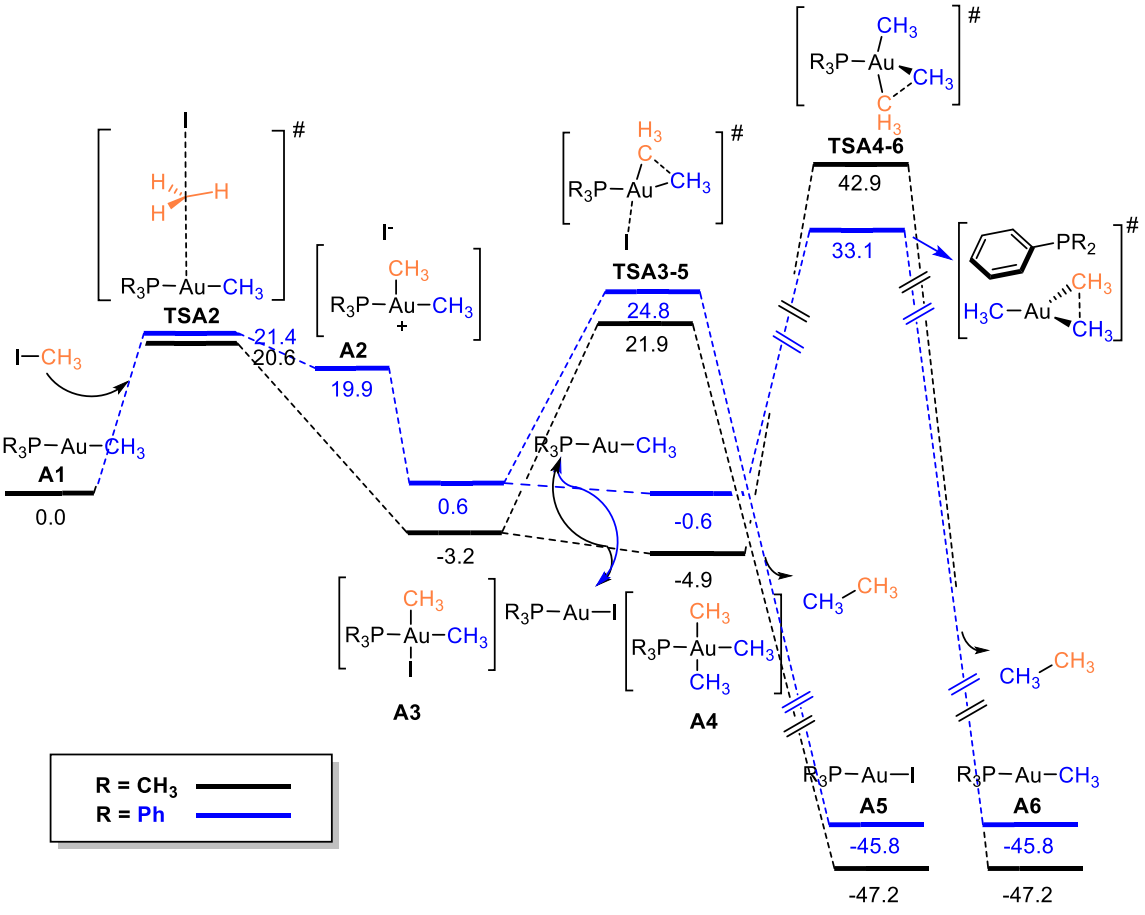

Scheme 2.9. Oxidative addition and reductive elimination in the coupling of alkylgold(I) **A1** with methyl iodide. SMD (iodomethane). Free energies in kcal mol^{-1}.

They also reported a slower outcome when performing the reaction using triphenylphosphine R = Ph (Scheme 2.9, blue) than when using trimethylphosphine R = Me (Scheme 2.9, black); which can be explained with the differences in energy barriers observed in the oxidative addition and reductive elimination.

2.3.3 Development of the catalytic system

With the aim of extending this reactivity to more synthetically interesting substrates, we wanted to expand the study to an allylic system (Scheme 2.10). We hypothesized the generation of intermediate R-Au-P(CH_3)$_3$ **2.3** via transmetalation with a tin reagent **2.2**, from which the oxidative addition of an alkyl halide **2.4** would occur, followed by a sequential reductive elimination of cross-coupled product **2.6**. The following catalytic cycle was proposed as an initial basis.

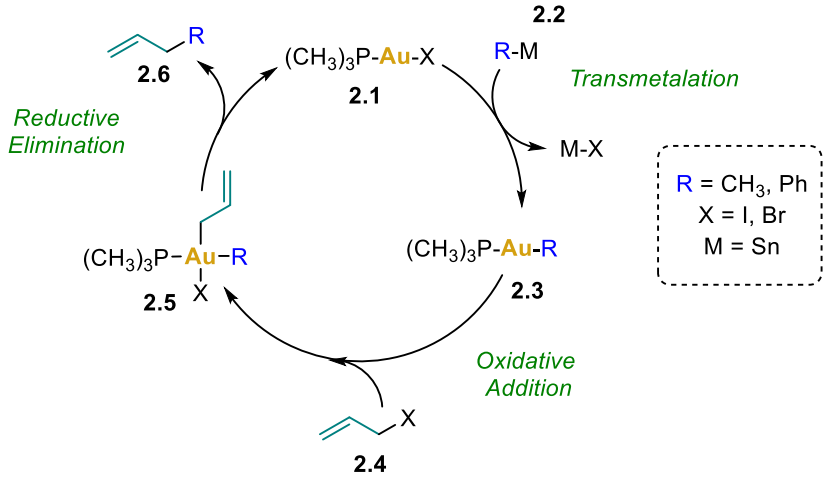

Scheme 2.10. Proposed catalytic cycle for the Au(I)/Au(III) catalyzed cross coupling reaction.

As a proof of concept, the first stannane chosen for evaluation was Sn(CH_3)$_4$. The calculated pathway is presented in parts below; first the transmetalation mechanism (Scheme 2.11) and finally the oxidative addition and reductive elimination steps (Scheme 2.12).

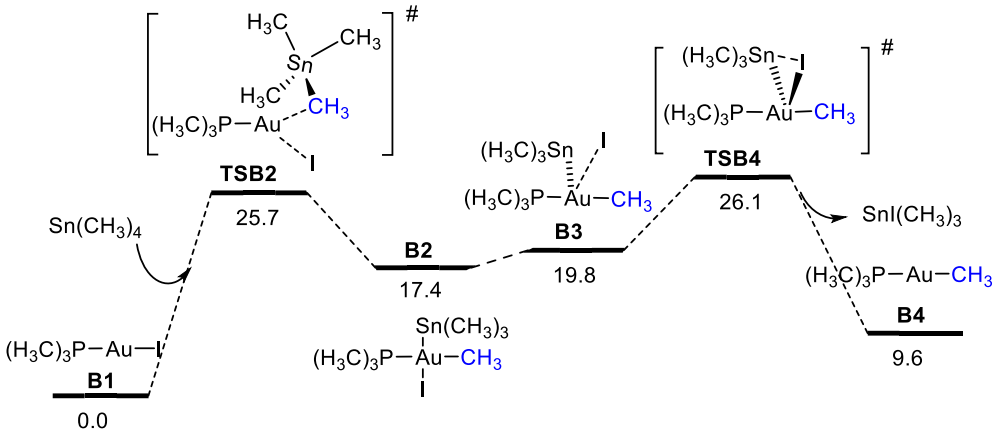

Scheme 2.11. Transmetalation pathway between IAuP(CH_3)$_3$ and Sn(CH_3)$_4$. Free energies in kcal mol^{-1}. SMD (iodomethane)

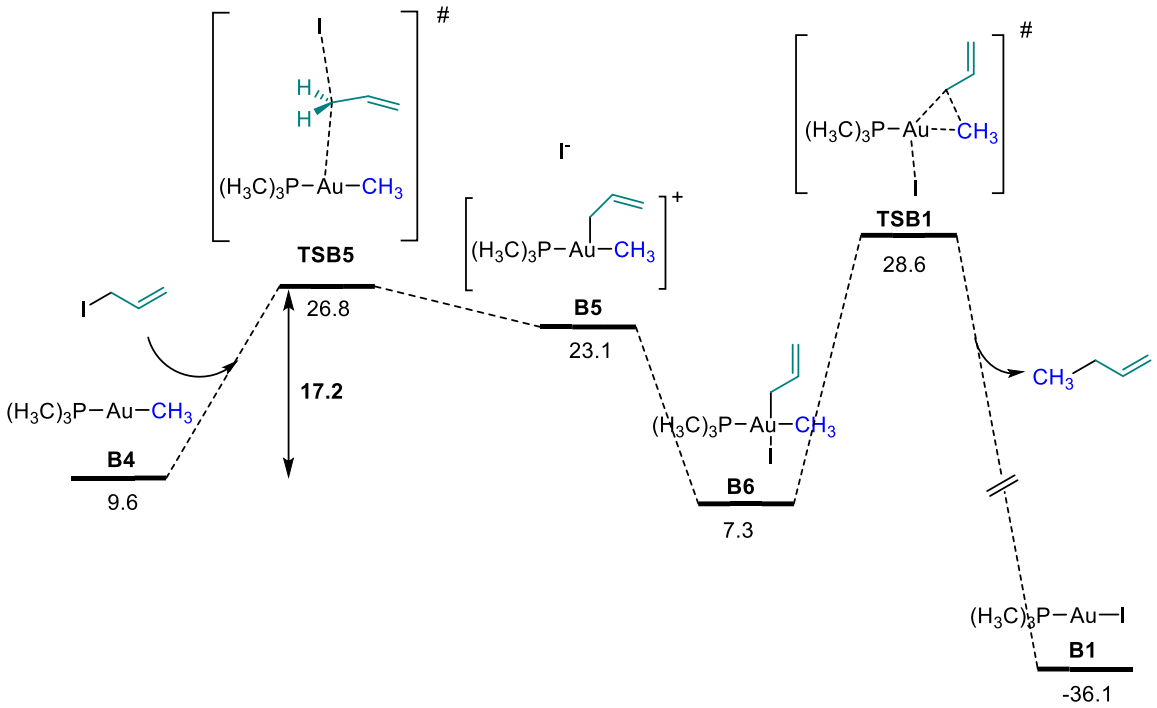

Scheme 2.12. Oxidative addition of allyl iodide to $CH_3AuP(CH_3)_3$ and subsequent reductive elimination of 1-butane. Free energies in kcal mol^{-1}. SMD (iodomethane)

Compared to Kochi's system, promising preliminary results were obtained, given that the oxidative addition of allyl iodide to the same H_3C-$AuP(CH_3)_3$ complex is lower in energy (Scheme 2.12, **TSB5** = 17.2) than the oxidative addition of methyl iodide (Scheme 2.9, **TSA2** = 20.6). However, with the aim of developing a catalytic system, the energy of the same transition state taking as reference **B1** is 26.8, which is a high value for R = CH_3. Therefore, other systems were considered, extending it to a variety of stannanes (R = methyl, vinyl, allyl, aryl). The results for different R groups are summarized in Table 2.1 for the proposed steps that take place in the catalytic cycle.

Table 2.1. Free energy barriers ($\Delta G^{\#}$, kcal mol^{-1}) for the gold catalyzed cross coupling reaction of allyl iodide. SMD (iodomethane).

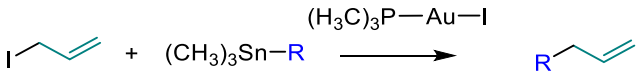

R group	Transmetalation	Oxidative addition	Reductive elimination
methyl	26.1	26.8	28.6
vinyl	22.0	23.7	22.7
allyl	25.0	26.1	23.5
aryl	21.9	24.8	23.8

It is worth mentioning that in the case of R = CH_3; the transmetalation pathway goes along an oxidative addition/reductive elimination sequence (Scheme 2.11).[46] However, when R is vinyl, allyl, phenyl, the mechanism first proceeds through coordination to the π system followed by direct concerted transmetalation (see the succeeding Schemes 2.13, 2.15 and 2.17).

To wrap up the results obtained on the assessment of the oxidative addition barriers for analogous systems using allyl iodide **2.4** as the reactant and varying the R ligand of the gold complex **2.3**, Table 2.2 is presented below. Variations where the methyl group is substituted with vinyl, allyl, and aryl groups are included. The corresponding free energy barriers for these systems remain similar: 17.2, 18.8, 17.5, and 19.0 kcal/mol, respectively. The more electron rich the metal center is in **2.3**, the easier the S_N2 reaction with allyl iodide.

Table 2.2. Model reactions used in the preliminary screening of activation barriers for oxidative addition. Free energies in kcal mol^{-1}, referenced to R-AuP$(CH_3)_3$. SMD (iodomethane).

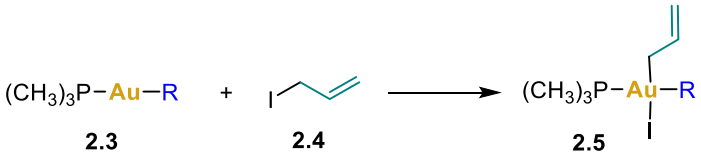

2.3 **2.4** **2.5**

R group	Methyl	Vinyl	Allyl	Aryl
Oxidative addition	17.2	18.8	17.5	19.0

As observed in Table 2.1, an energetically accessible pathway to complete the catalytic cycle was found. The barriers for R = vinyl, aryl are lower than 25 kcal/mol, which lies on the edge of room temperature allowed reactions. In the interest of accessibility and handling of the stannane, $PhSn(CH_3)_3$ was chosen as transmetalating agent to perform the experimental studies.

The schemes of the corresponding pathways are presented below.

46 Carrasco, D.; García-Melchor, M.; Casares, J. A.; Espinet, P. Dramatic Mechanistic Switch in Sn/AuI Group Exchanges: Transmetalation vs. Oxidative Addition, *Chem. Commun.* **2016**, *52*, 4305–4308.

R = vinyl

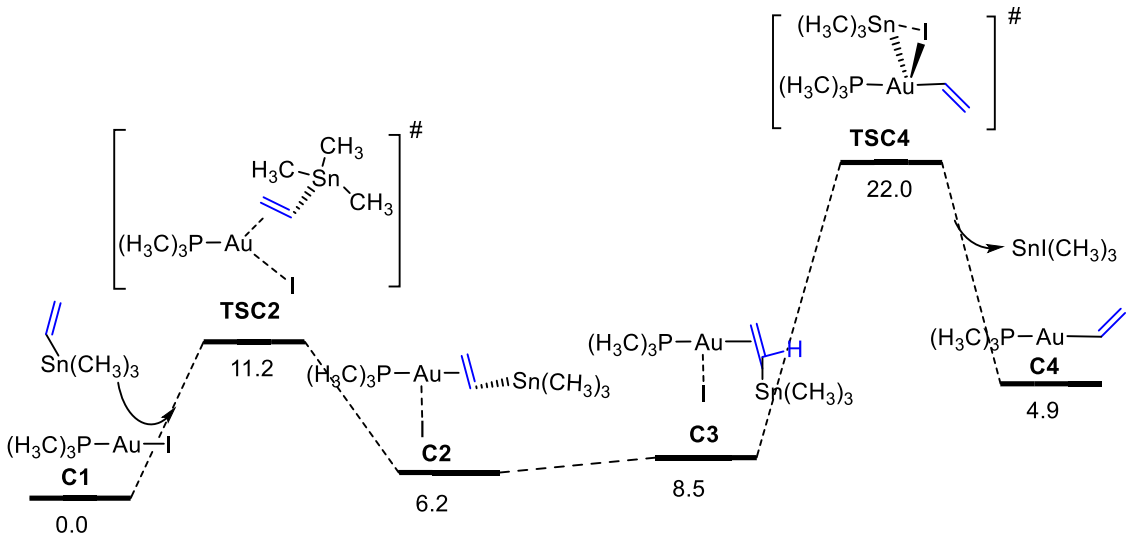

Scheme 2.13. Transmetalation pathway between $IAuP(CH_3)_3$ and vinyl-$Sn(CH_3)_3$. Free energies in kcal mol^{-1}. SMD (iodomethane).

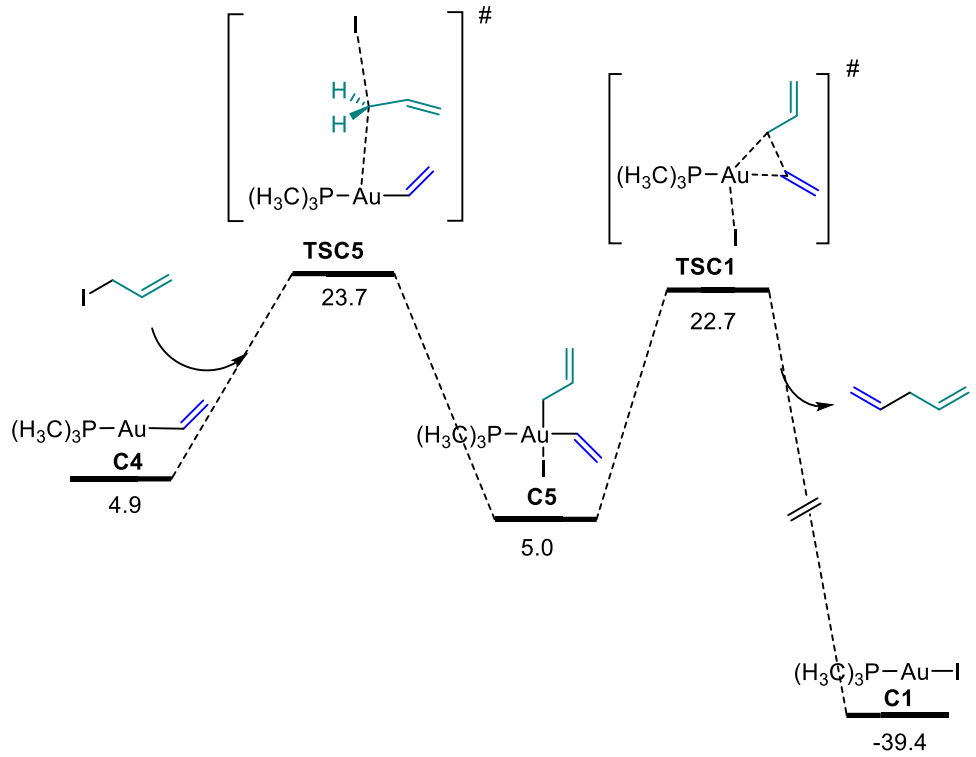

Scheme 2.14. Oxidative addition of allyl iodide to vinyl-$AuP(CH_3)_3$ and subsequent reductive elimination of 1,4-pentadiene. Free energies in kcal mol^{-1}. SMD (iodomethane).

R = allyl

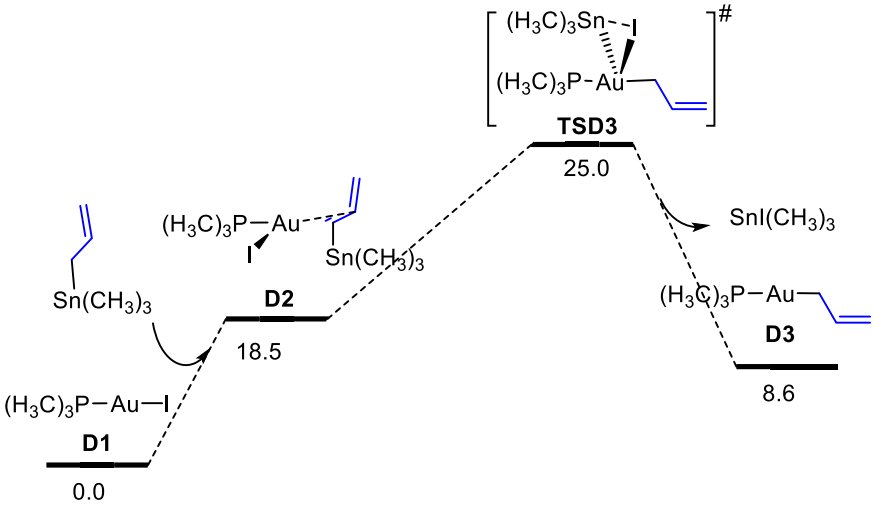

Scheme 2.15. Transmetalation pathway between $IAuP(CH_3)_3$ and allyl-$Sn(CH_3)_3$. Free energies in kcal mol^{-1}. SMD (iodomethane).

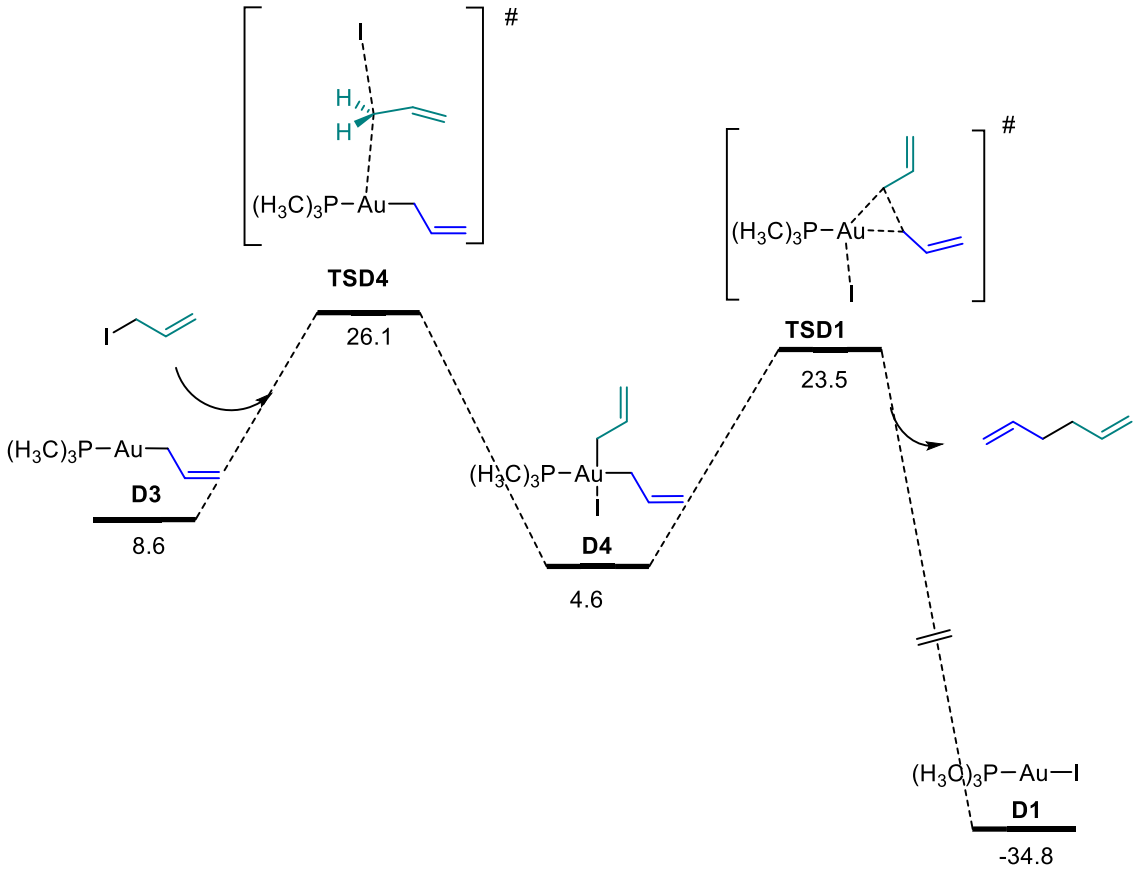

Scheme 2.16. Oxidative addition of allyl iodide to allyl-$AuP(CH_3)_3$ and subsequent reductive elimination of 1,5-hexadiene. Free energies in kcal mol^{-1}. SMD (iodomethane).

R = phenyl

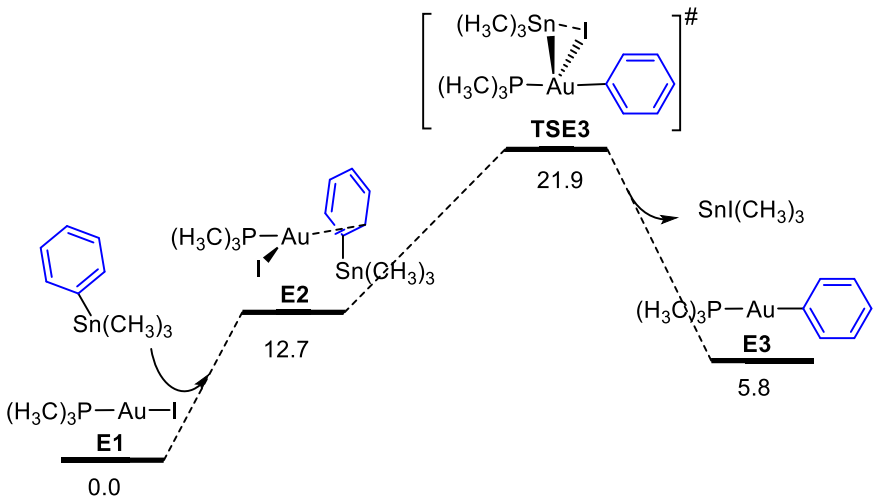

Scheme 2.17. Transmetalation pathway between $IAuP(CH_3)_3$ and phenyl-$Sn(CH_3)_3$. Free energies in kcal mol^{-1}. SMD (iodomethane).

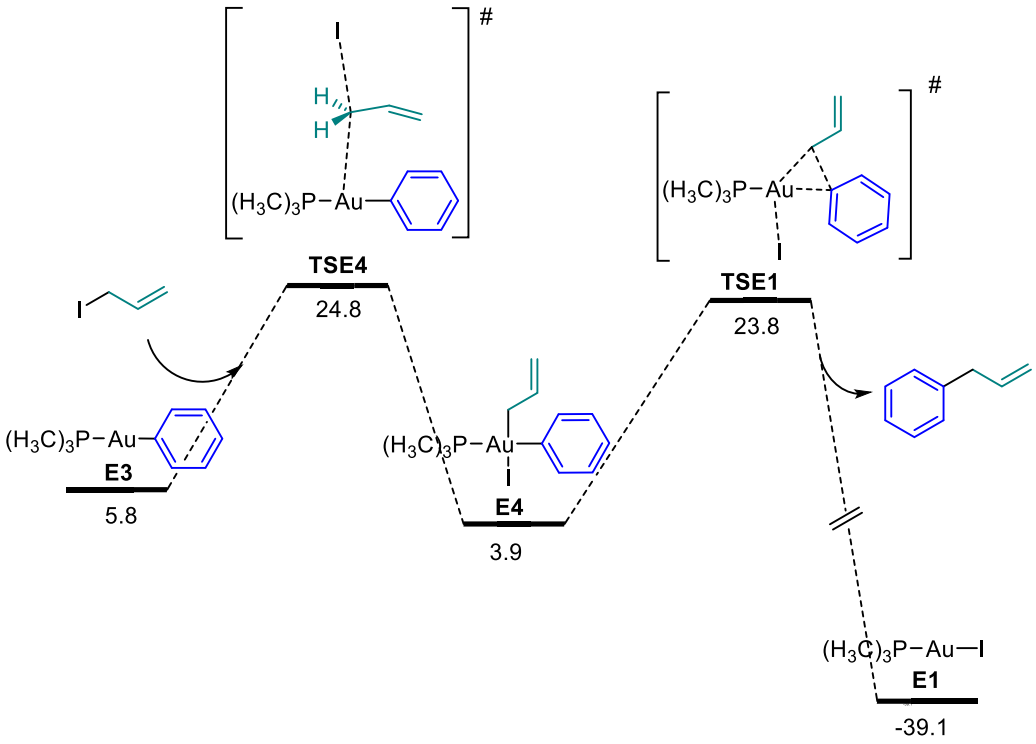

Scheme 2.18. Oxidative addition of allyl iodide to phenyl-$AuP(CH_3)_3$ and subsequent reductive elimination of allylbenzene. Free energies in kcal mol^{-1}. SMD (iodomethane).

2.4 Experimental results

2.4.1 Initial experimental study

Based on the computationally studied systems using $IAuP(CH_3)_3$ as catalyst, the first catalysis was attempted by submitting alkyl halide **2.4** and $PhSn(CH_3)_3$ **2.7** under catalytic conditions using trimethylphosphine gold(I) complexes. $IAuP(CH_3)_3$ was synthesized in 99% yield from $ClAuP(CH_3)_3$ following a reported procedure.[47]

Table 2.3. First catalytic experiments set up between allyl iodide and $PhSn(CH_3)_3$, using gold(I) complexes as catalysts.

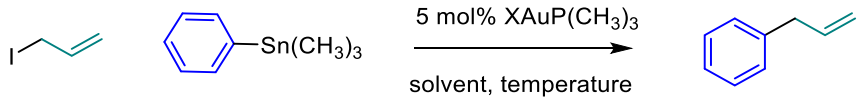

2.4 **2.7** **2.8**

Entry	Catalyst	Temperature ºC	Solvent	Ratio 2.4:2.8
1	$IAuP(CH_3)_3$	25-50	CD_2Cl_2	100:0
2	$IAuP(CH_3)_3$	90	toluene-d8	100:0
3	$ClAuP(CH_3)_3$	90	toluene-d8	90:10

Ratios determined by ^1H NMR spectroscopy after 64 h.

No reaction was observed at 25ºC nor at 50ºC performing the reaction in a sealed Young NMR tube (Table 2.3, entries 1 and 2) in CD_2Cl_2 nor in toluene. Both experiments resulted in a purple precipitate being formed after some time. Additionally, any apparent change in the ^1H or ^{31}P NMR spectra was observed, therefore highly likely to be gold nanoparticles coming from the decomposition of the catalyst. Parallelly, it was confirmed that when $IAuP(CH_3)_3$ is dissolved in CH_2Cl_2 in presence of allyl iodide **2.4**, it causes decomposition forming Au nanoparticles or nanoclusters (violet precipitate observed). The catalyst was then substituted by $ClAuP(CH_3)_3$ and after 64 h heating up at 90 ºC in toluene-d_8 in an NMR sealed tube, the desired coupled product **2.8** could be observed for the first time (Table 2.3, entry 3). Thus, the solvent chosen for the experiments was toluene in order to have a high boiling point solvent, and the alkyl halide reactant selected was a non-volatile substrate like cinnamyl bromide (boiling point 212 ºC). Toluene will be used from now on in all the calculations.

Taking into account the results collected in Table 2.3, a comparison between different complexes of the type $XAuP(CH_3)_3$ (X = Cl, Br, I) **E1** as catalysts was performed (Scheme 2.19). Even

47 Carrasco, D.; García-Melchor, M.; Casares, J. A.; Espinet, P. Dramatic Mechanistic Switch in Sn/AuI Group Exchanges: Transmetalation vs. Oxidative Addition, *Chem. Commun.* **2016**, *52*, 4305–4308.

though the transmetalation is more energetically demanding for X = Cl following the trend Cl > Br > I (**TSE3**, Table 2.4); the rest of steps in the catalytic cycle are more favourable due to $ClAuP(CH_3)_3$ is less stable compared to $IAuP(CH_3)_3$ (precisely 4.9 kcal mol^{-1}). Besides, this fact favours the total energy spam of the catalytic cycle.

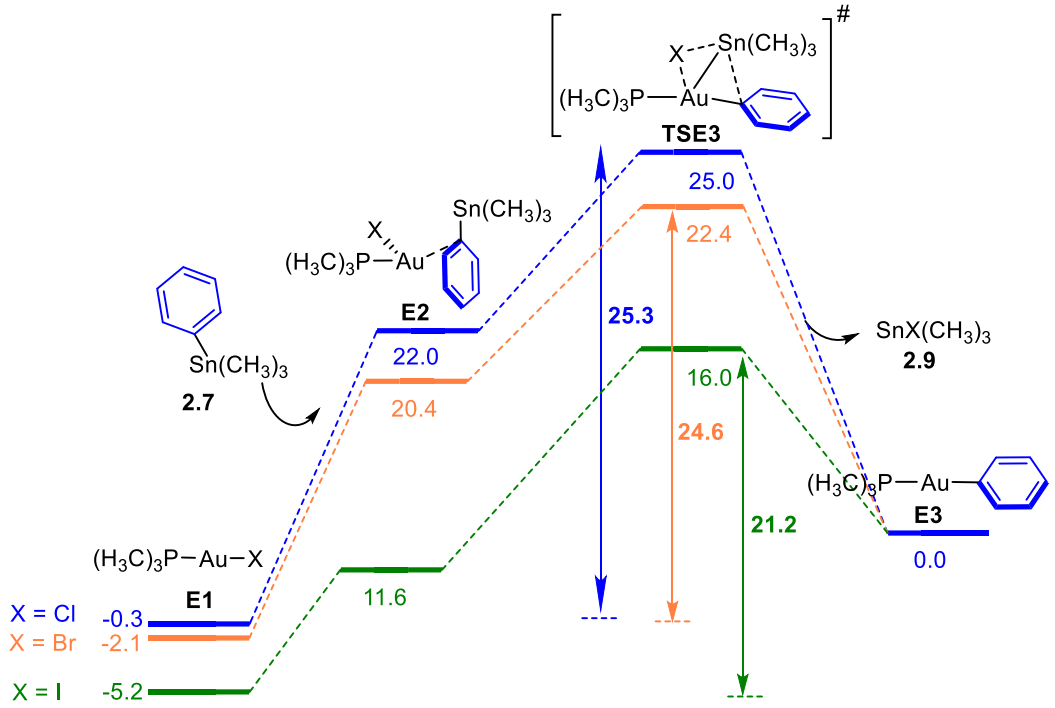

Scheme 2.19. Calculated free energy profile (kcal mol^{-1}) for the transmetalation pathway to yield common intermediate **E3** from which oxidative addition might occur. SMD (toluene).

Table 2.4. Summary of the free energy barriers in kcal mol^{-1} for the transmetalation step in the gold catalyzed cross-coupling reaction using different halide gold complexes.

$(CH_3)_3Sn{-}Ph$ + $X{-}Au{-}P(CH_3)_3$ ⟶ $Ph{-}Au{-}P(CH_3)_3$ + $(CH_3)_3Sn{-}X$

2.7 **E1** **E3** **2.9**

Solvent	$IAuP(CH_3)_3$	$BrAuP(CH_3)_3$	$ClAuP(CH_3)_3$
toluene	21.2	24.6	25.3

More experimental proof was gained when attempting the cross-coupling reaction of cinnamyl bromide **2.10** and $PhSn(CH_3)_3$ **2.7** in high boiling point solvents (Table 2.5). In this case, some conversion to product **2.11** was observed after 48h at 80ºC in DCE (entry 1). In order to be able to increase the temperature further, toluene was used as solvent and the reaction mixture was heated up to 110ºC, being able to reach higher conversions (entries 2 and 3). Interestingly, a similar result is obtained when $ClAuP(CH_3)_3$ and $IAuP(CH_3)_3$ are used, in contrast to the case in which allyl iodide **2.4** was the substrate.

Table 2.5. First catalytic reactions trials using cinnamyl bromide as substrate.

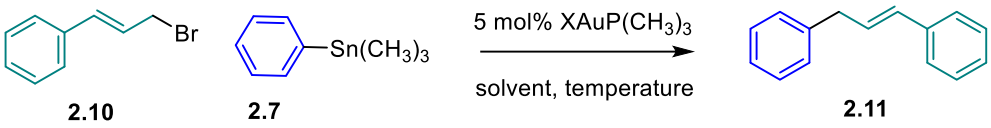

Entry	Catalyst	Temperature ºC	Solvent	Ratio 2.10/2.11
1	$ClAuP(CH_3)_3$	25-80	DCE	87:13
2	$ClAuP(CH_3)_3$	110	toluene	19:81
3	$IAuP(CH_3)_3$	110	toluene	39:61

Ratios calculated by ^1H NMR integration after 24 h.

The proposed catalytic cycle for this transformation that will be studied thoroughly is showcased in Scheme 2.20.

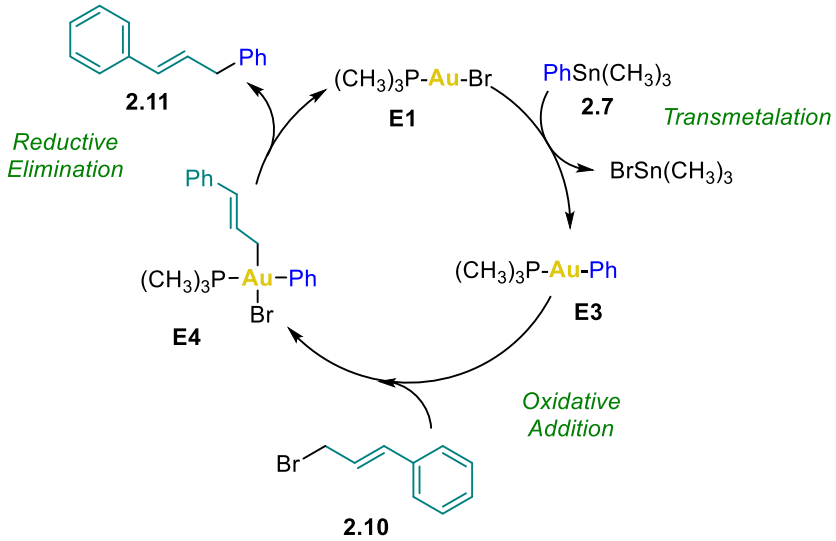

Scheme 2.20. Proposed catalytic scheme for the gold-catalyzed cross-coupling of cinnamyl bromide **2.10** and $PhSn(CH_3)_3$ **2.7**.

2.4.2 Catalyst screening

A screening of catalysts was performed using cinnamyl bromide **2.10** as substrate. The suitable conditions to be able to calculate the NMR yield properly were achieved when deuterated toluene was used in order to avoid evaporation of starting material, product or even internal standard.

Table 2.6. Catalyst screening in the cross-coupling gold catalyzed reaction.

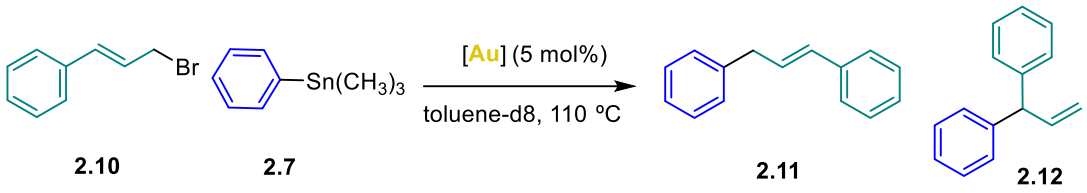

2.10 **2.7** **2.11** **2.12**

Entry	Catalyst	Yield 2.11 (% Conversion) 24 h	Yield 2.11 (% Conversion) 48 h	Yield 2.12 (%) 48 h
1	$ClAuP(CH_3)_3$	11 (22)	33 (59)	5
2	$IAuP(CH_3)_3$	11 (19)	17 (38)	5
3	ClAuJohnPhos	30 (50)	33 (76)	13
4	$ClAuPPh_3$	[a]	[a]	0
5	ClAu(CyJohnPhos)	[a]	[a]	0
6	$ClAuPEt_3$	**44** (66)	**48**[b]	2
7	$BrAuPEt_3$[c]	52 (78)	65 (95)	0

NMR yields and conversion determined by ^1H NMR using ethylbenzoate and 1,3,5-trimethoxybenzene as internal standards. [a] Full conversion to a variety of byproducts formed. [b] Isolated yield. [c] 10 mol%.

No formation of product **2.11** was observed when $ClAuPPh_3$ or ClAu(CyJohnPhos) (Table 2.6, entries 4 and 5) were used, a complex NMR was obtained with lots of byproducts being formed. $BrAuPMe_3$ was synthesized independently[48] and tested as catalyst (entry 7), giving the best performance even though the conditions are not comparable (10 mol% used). The best performance was obtained using gold complex $ClAuPEt_3$ (entry 6), achieving a 44% NMR yield after 24h and 48% isolated yield after 48h. Product **2.12** was detected in the reaction mixture and formed up to 13% yield when ClAuJonhPhos was used (entry 3) and down to 0% yield when $BrAuPEt_3$ was used (entry 7).

48 Adapted procedure of previous $IAu(CH_3)_3$ synthesis.

2.4.3 Control experiments

In order to gain a deeper understanding of the reaction, control experiments were performed. When $ZnCl_2$ was used instead of $ClAuP(CH_3)_3$ (entry 2), complete conversion was obtained, rendering two unidentified new compounds as an inseparable mixture. After ^1H NMR and GC-MS analysis, we can conclude that the mixture of compounds is composed of two isomers (high similarity in ^1H NMR; same m/z ratio and very similar retention time in GC-MS). From entry 3 it can be deduced that stannane **2.7** plays a role in the formation of cross-coupled product, as unreacted cinnamyl bromide was recovered.

Table 2.71. Control experiments

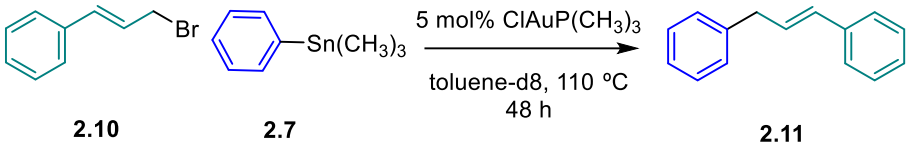

2.10 **2.7** **2.11**

Entry	Deviation standard conditions	Yield[a] (% Conversion)
1	-	33 (59)
2	Without catalyst, 5 mol% $ZnCl_2$	0[c]
3	No $PhSnMe_3$	0[d]
4[b]	Without catalyst, no internal standard	- (9)

[a] NMR yields determined by ^1H NMR using ethyl benzoate as internal standard. [b] Extremely cautious reaction setting to avoid possible cross-contamination with metals, therefore no internal standard was added. [c] Two new products were obtained. [d] Unreacted starting material.

Interestingly, in the absence of gold(I) complex (Table 2.7, entry 4) there is a slow background reaction running, that could be explained through a mechanism similar to the one depicted in Scheme 2.21, in which S_N2 attack of the phenyl in **2.7** to C1 of cinnamyl bromide **2.10** leads to the desired product **2.11**.

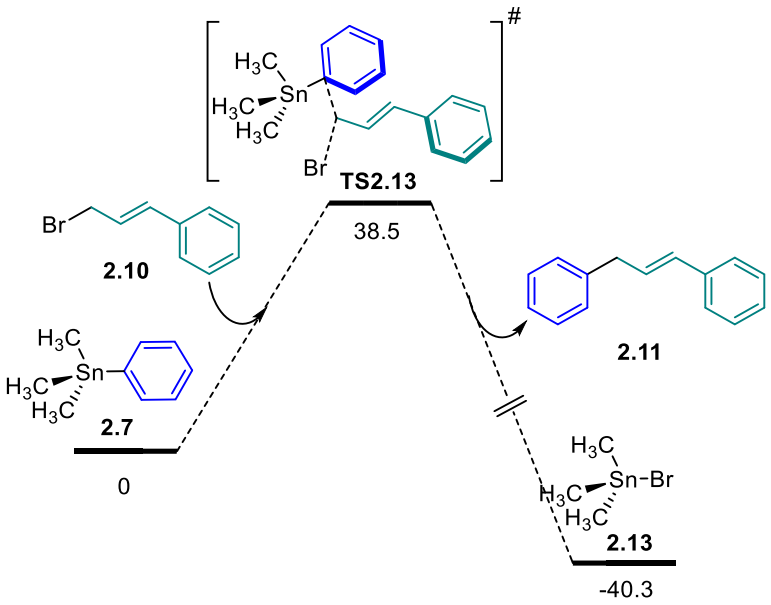

Scheme 2.21. Discarded pathway on the uncatalyzed formation of product **2.11**. SMD (toluene)

Therefore an experiment was designed in order to see the difference between the gold-catalyzed reaction and the uncatalyzed reaction. Two separate reactions were set under the same conditions and monitored by ^{1}H NMR; one adding 5 mol% of ClAuPEt$_3$ (Figure 2.1, blue dots) and a second one lacking the gold(I) complex (Figure 2.1, orange dots). As observed, when gold(I) is present, the formation of product is relatively fast, achieving 30% yield after 16 h, meanwhile a rather slow conversion to product **2.11** takes place reaching 8% after 3 days at 110 ºC. At this point after 48 h, 5 mol% of ClAuPEt$_3$ was added to the same reaction vessel and a clear increase in the rate formation of product **2.11** is seen, supporting the catalyst role of gold.

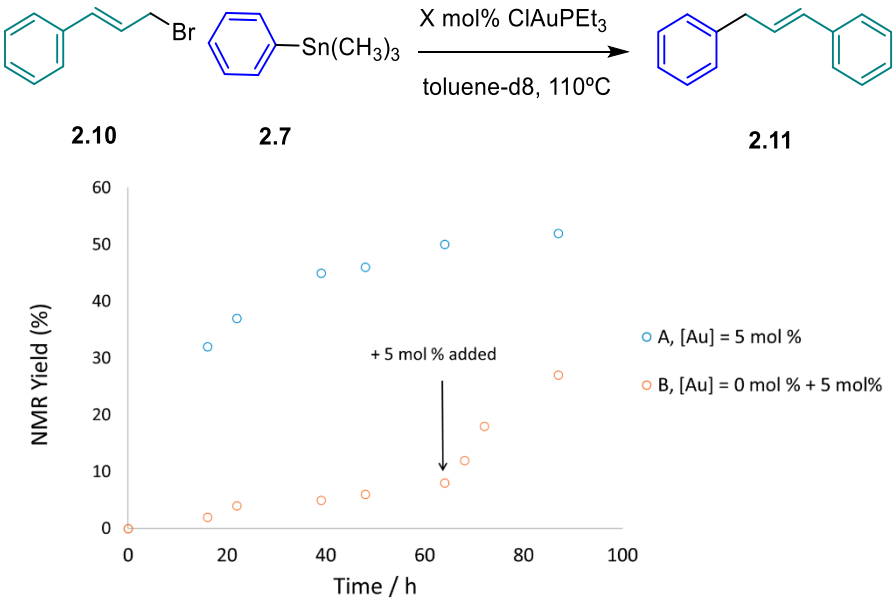

Figure 2.1. Plot representing the concentration of product **2.11** along reaction time. NMR yield calculated with respect to ethyl benzoate as internal standard.

Reaction Optimization

Table 2.6. Optimization of the gold(I) catalyzed reaction of cinnamyl bromide **2.10** and $PhSn(CH_3)_3$ **2.7**.

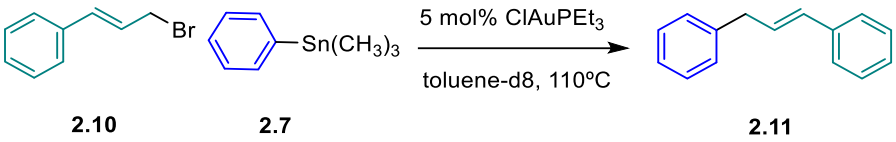

2.10 **2.7** **2.11**

Entry	Deviation standard conditions	Yield (% Conversion) 24 h	Yield (% Conversion) 87 h
1	-	44 (66)	48 (73)
2	4 equiv **2.10**	15 (60)	8 (79)
3	5 mol% + 5 mol%	40 (63)	50 (92)
4	LiCl (1 equiv.)	-	50 (87)

NMR yields and conversion calculated with respect to ethylbenzoate as internal standard.

It is noticeable that after the first 24 h the reaction does not evolve as fast (Table 2.6). Increasing the equivalents of starting material worsened the outcome of the reaction (entry 2); adding 5 mol% after 24h resulted in an insignificant increase on the conversion during the second 24 h (entry 3), hinting a possible catalyst decomposition. Finally, additive LiCl[49] did not increase the yield considerably (entry 4).

2.4.4 Substrate Scope

Different cinnamyl halides and cinnamyl carbonate were tested under the reaction conditions (Table 2.7) being able to find a surprising trend: only cinnamyl bromide reacts to yield the desired product. In the rest of cases mainly unreacted starting materials were recovered and no catalyst decomposition was observed (visually or by ^{31}P NMR).

49 delPozo, J.; Carrasco, D.; Pérez-Temprano, M. H.; García-Melchor, M.; Álvarez, R.; Casares, J. A.; Espinet, P. Stille Coupling Involving Bulky Groups Feasible with Gold Cocatalyst, *Angew. Chem. Int. Ed.* **2013**, *52*, 2189–2193.

Table 2.7. Substrate scope of the gold catalyzed cross-coupling reaction.

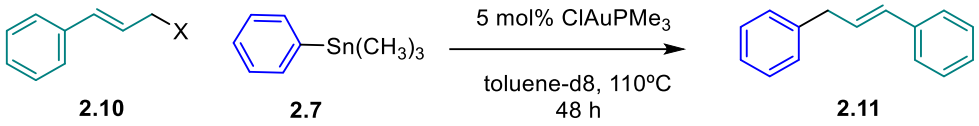

2.10 **2.7** **2.11**

Entry	Substrate	Yield (% Conversion)
1	Cinnamyl bromide	33(59)
2	Cinnamyl iodide	0 (0)
3	Cinnamyl chloride	0 (10)
4	Cinnamyl carbonate	0 (32)[a]

Yields determined by ^{1}H NMR integration using ethylbenzoate as internal standard. [a] Some evolution to cinnamyl alcohol and other byproducts.

2.4.5 Stoichiometric reactions

Stoichiometric reactions of the proposed catalytic cycle were performed in order to test the efficacy and support the proposed steps.

Transmetalation

For the transmetalation step between $ClAuP(CH_3)_3$ and $PhSn(CH_3)_3$ **2.7** at 110º C in toluene (entry 2, Table 2.8), intermediate **E3** was successfully observed in a 3:2 ratio **E1**/**E3** after 8 h. Nevertheless, when using $IAuP(CH_3)_3$, unreacted starting materials remained in the reaction mixture.

Table 2.8. Stoichiometric experiments in the transmetalation reaction between $PhSn(CH_3)_3$ and $XAuP(CH_3)_3$.

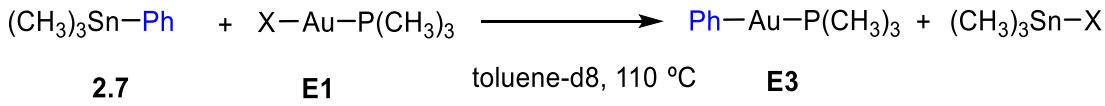

2.7 **E1** **E3**

Entry	Gold catalyst	Ratio[a] E1:E3
1	$IAuP(CH_3)_3$	100:0
2	$ClAuP(CH_3)_3$	3:2

[a] Ratios were determined by ^{1}H NMR spectroscopy after 8 h.

Oxidative Addition

In order to test the oxidative addition step in a stoichiometric manner, intermediate $PhAuP(CH_3)_3$ **E3** needed to be synthesized (Scheme 2.22). The first attempt to the synthesis was performed using PhLi, reported for a similar starting material,[50] being able to obtain intermediate **E3** as well as byproduct **2.14** in a 2:1 ratio (**E3/E1**).[51] Following another reported synthetic route,[52] which consists of the treatment with freshly prepared PhMgBr,[53] intermediate **E3** could be isolated in 96 % purity.

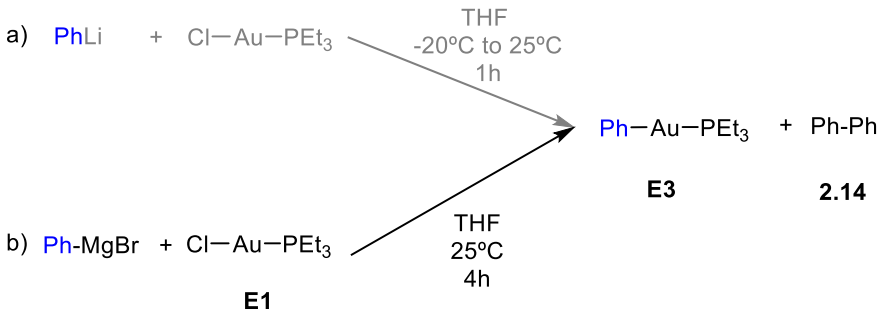

Scheme 2.22. Synthesis of intermediate **E3** by treatment with an organolithium reagent (a) and with freshly synthesized Grignard reagent (b).

Intermediate **E3** was then submitted to oxidative addition conditions by adding cinnamyl bromide **2.10** (Scheme 2.23). When the reaction was carried out in $CDCl_3$, a gold mirror deposited in the NMR tube walls was visible due to decomposition of the gold intermediate **E3** over time at 25ºC and consequent formation of by-product **2.14**. Taking this into account, the reaction was submitted in the absence of O_2 in an NMR young tube using toluene-d8, where the decomposition was proven not to occur at 25ºC.

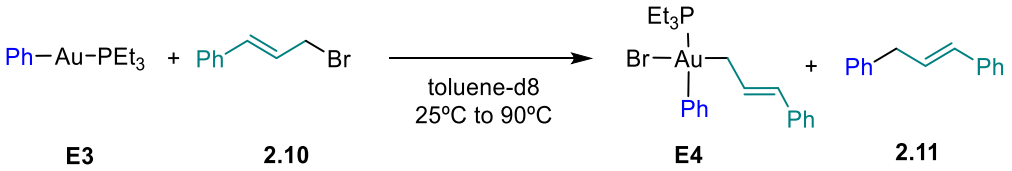

Scheme 2.23. Stoichiometric oxidative addition of cinnamyl bromide to $PhAuPEt_3$.

50 Peña-López, M.; Ayán-Varela, M.; Sarandeses, L. A.; Pérez Sestelo, J. Palladium-Catalyzed Cross-Coupling Reactions of Organogold(I) Reagents with Organic Electrophiles, *Chem. - Eur. J.* **2010**, *16*, 9905–9909.

51 Purification trials were unsuccessful as **E3** decomposes in silica and basic alumina. Recrystallization or pentane washing did not render a complete purification.

52 Carrasco, D.; García-Melchor, M.; Casares, J. A.; Espinet, P. Dramatic Mechanistic Switch in Sn/AuI Group Exchanges: Transmetalation vs. Oxidative Addition, *Chem. Commun.* **2016**, *52*, 4305–4308.

53 Piller, F. M.; Appukkuttan, P.; Gavryushin, A.; Helm, M.; Knochel, P. Convenient Preparation of Polyfunctional Aryl Magnesium Reagents by a Direct Magnesium Insertion in the Presence of LiCl, *Angew. Chem. Int. Ed.* **2008**, *47*, 6802–6806.

The oxidative addition complex **E4** was not observed, however, the cross-coupled product **2.11** was detected in low conversion by ^{1}H NMR (Scheme 2.24) when temperature was risen above 70 ºC (not formed after 3h at 70ºC). Other by-products were as well formed like **2.14** or cinammaldehyde.

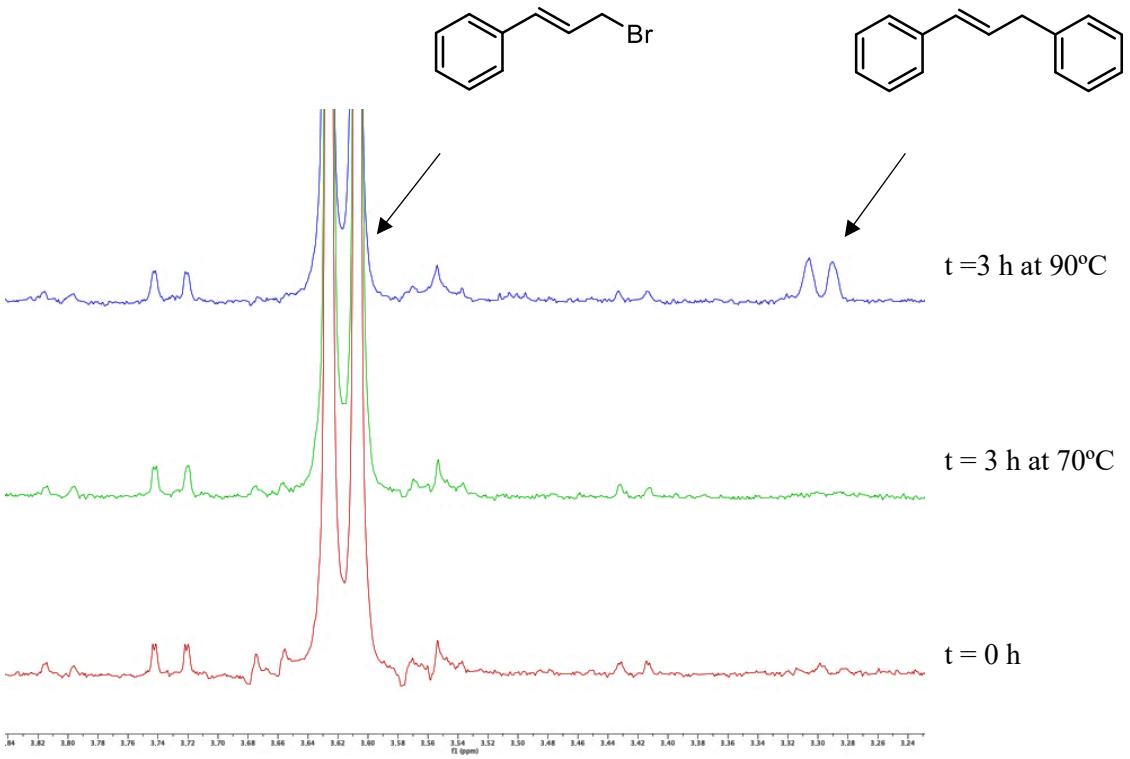

Scheme 2.24. ^{1}H NMR showing the appearance of cross-coupled product **2.11** after heating up at 90ºC.

2.4.6 Kinetic studies

In an attempt to gain insight into the reaction mechanism, the order in reactants was determined by applying VTNA method (Table 2.9).

Table 2.9. Conditions for the experiments where VTNA method was applied

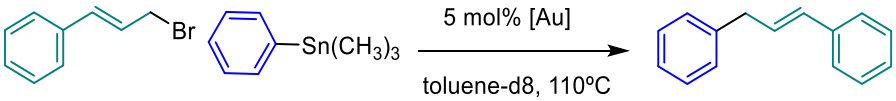

2.10 **2.7** **2.11**

Experiment	[Substrate] / mM	[$PhSn(CH_3)_3$] / mM	[Au] / mM
A	**100**	100	**10**
B	**200**	100	10
C	**50**	100	10
D	100	100	**5**
E	100	100	**10**
F	100	**100**	10
G	100	**200**	10
H	100	**50**	10

In experiments A-E, $BrAuPEt_3$ was used and F-H, $ClAuPEt_3$.

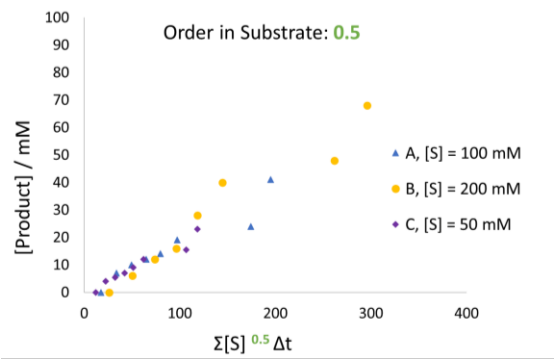

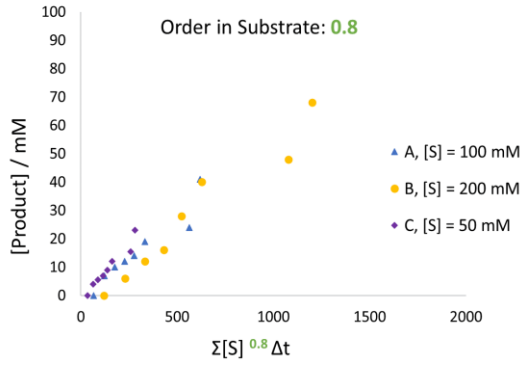

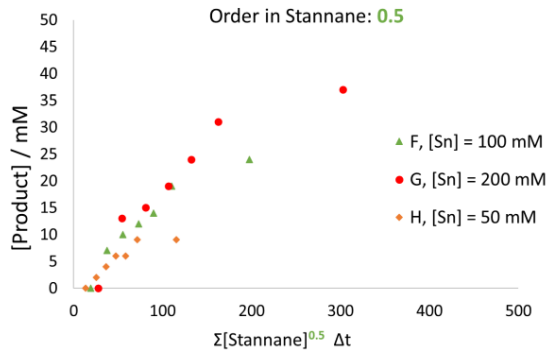

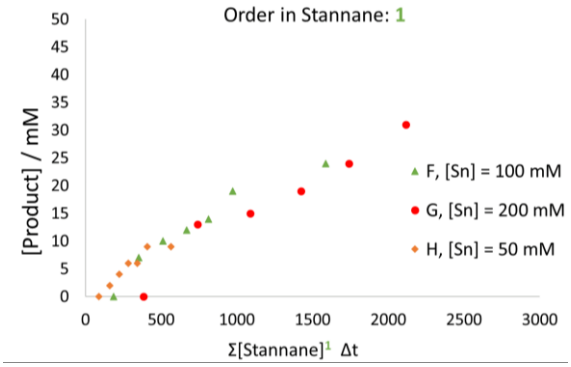

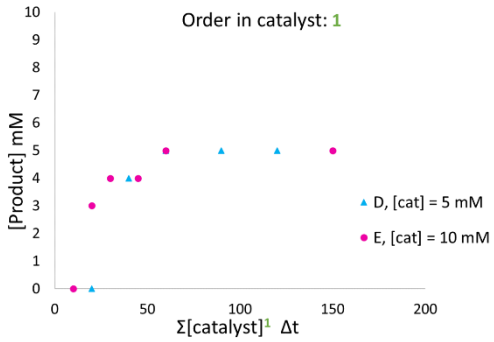

Figure 2.2. Best visual fits in the variable-time normalization analysis (VTNA) plots applied in the system for the determination of partial kinetic orders in substrate, stannane and catalyst.

The determination of partial kinetic orders of reaction of the reactants was done applying VTNA method.[54] The visual determination of the kinetic orders (Figure 2.2) led to the determination of a 0.5-0.8 kinetic order in cinnamyl bromide, 0.5-1 order in $PhSnMe_3$ and first order in $BrAuPEt_3$. These results could involve the presence of two rate determining steps.

Additionally, in the interest of assessing catalyst robustness under the reaction conditions, reaction progress kinetic analysis (RPKA) was applied. RPKA is a methodology developed to extract maximum information from a minimal number of experiments designed to be mathematically independent, via graphical manipulations of time course data. The RPKA methodology is known as the "same excess, [xs]" protocol, developed by Donna Blackmond.[55] In the following Table 2.10 are summarized the three reactions carried out.

Table 2.10. Reaction conditions of the designed experiments for the RPKA.

	[S] / mM	[Sn] / mM	[Pdt] / mM	[$ClAuPEt_3$] / mM	mol% Au
1	100	100	0	10	10
2	50	50	0	10	20
3	50	50	50	10	20

Note that the absolute concentration of the catalyst (not the mol%) is kept constant across the three experiments. The three reactions are conducted with the "same [xs]". This is significant because it means these conditions represent the same reaction initiated at different starting points: the initial substrate concentrations of [S] and [Sn] for the reaction in entry 1 will match those of

54 a) Burés, J. Variable Time Normalization Analysis: General Graphical Elucidation of Reaction Orders from Concentration Profiles, *Angew. Chem. Int. Ed.* **2016**, *55*, 16084–16087. b) What Is the Order of a Reaction?, *Top. Catal.* **2017**, *60*, 631–633. c) A Simple Graphical Method to Determine the Order in Catalyst, *Angew. Chem. Int. Ed.* **2016**, *55*, 2028–2031.

55 a) Blackmond, D. G. Reaction Progress Kinetic Analysis: A Powerful Methodology for Mechanistic Studies of Complex Catalytic Reactions, *Angew. Chem. Int. Ed.* **2005**, *44*, 4302–4320. b) Kinetic Profiling of Catalytic Organic Reactions as a Mechanistic Tool, *J. Am. Chem. Soc.* **2015**, *137*, 10852–10866.

the reaction in entry 2 when the former reaches 50% conversion. From this conversion point forward, the two reactions will have the same temporal substrate concentrations, resulting in identical kinetic profiles from this point onward. Thus, the kinetic profiles for the reactions in entry 1 and 2 provide a diagnostic for either product inhibition or catalyst deactivation. Entry 3 describes a reaction where $[S]_o$, $[Sn]_o$ and $[Pdt]_o$ are identical to those of the reaction in entry 1 at 50% conversion. If the kinetic profile of the reaction in entry 3 is identical to that of entry 1, product inhibition is implicated; if it is identical to that of entry 2, catalyst deactivation is implicated. As a means to compare the profiles of the three reactions, a "time-adjusted" profile is constructed simply by shifting the curves of entries 2 and 3 in time to the point where their concentrations are equal to that of the reaction of entry 1 (Figure 2.3).

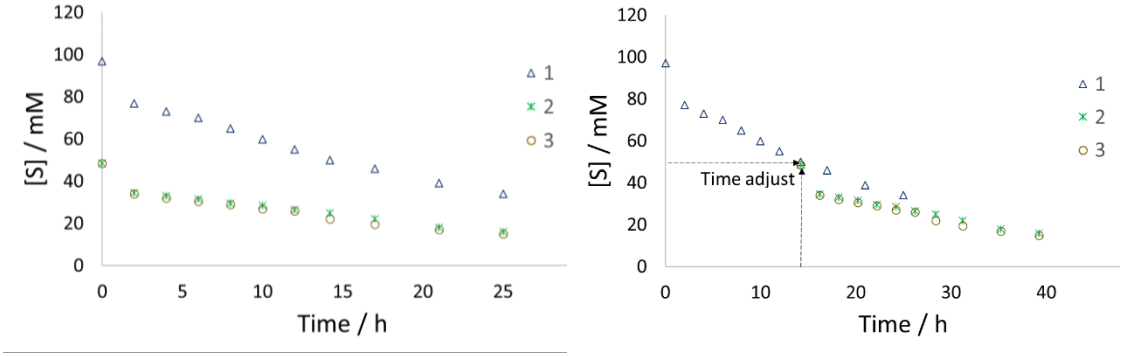

Figure 2.3. Reaction kinetic profiles (a) and modified time adjustments (b) for visualization. Kinetic profiles of the concentration of substrate vs time are shown.

As in this case the kinetic profile in entry 3 is identical to that in entry 2 (Figure 2.3), it means that catalyst deactivation is taking place in the reaction, as previously hinted. Additionally, it is deduced that product deactivation is not implicated in the process.

2.5 Further computational studies

2.5.1 Evaluation of mechanisms suggested by experiments

Other possible mechanisms that do not require oxidative addition were considered (Scheme 2.25), like the formation of π-allyl intermediate **E6**,[56] which is favourable through the rotation of C1-C2 bond of cinnamyl and the detaching of bromine from the gold coordination sphere (**TSE5** and **TSE6)**, arriving to a η^1-allyl bonding intermediate **E6**. However, the reductive elimination process from **E6** is slightly higher in energy (**TSE6-1**) than the reductive elimination from **E4** (**TSE4-1**).

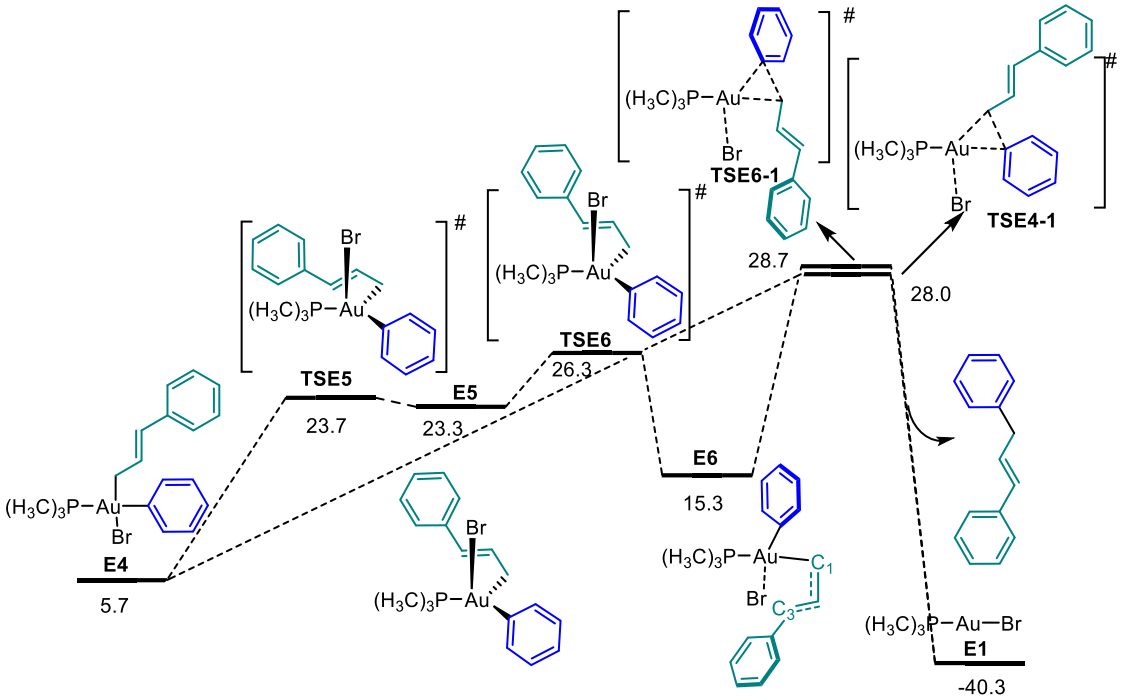

Scheme 2.25. Pathway on the formation of π-allyl intermediate and reductive elimination. Free energies in kcal mol^{-1}. SMD (toluene).

Additionally, other plausible pathways were studied (Scheme 2.26); like direct S_N1 reaction (**TSE7-1**). Nevertheless, the energy of dissociation of the C–Br bond in cinnamyl bromide **2.10** must be overcome to arrive to intermediate **E7**. It is highly likely that the required energy would be very high given the failed attempts to calculate it. Direct S_N2 attack of phenyl C_{ipso} to C1 of cinnamyl bromide (S_N2 oxidative addition on allyl) resulted in 35.2 kcal mol^{-1} (**TSE3-1**) as well as S_N2' pathway was calculated to have an inaccessible energy of 44.4 kcal mol^{-1} (**TSE'3-1**).

56 a) Rodriguez, J.; Szalóki, G.; Sosa Carrizo, E. D.; Saffon-Merceron, N.; Miqueu, K.; Bourissou, D. Gold(III) π-Allyl Complexes, *Angew. Chem. Int. Ed.* **2020**, *59*, 1511–1515. b) Vesseur, D.; Holmsen, M. S. M.; Bourissou, D. Au(III) π-Allyl Complexes: Synthesis, Structure, Reactivity, and Catalytic Applications, *ChemCatChem* **2023**, *15*, e202300851.

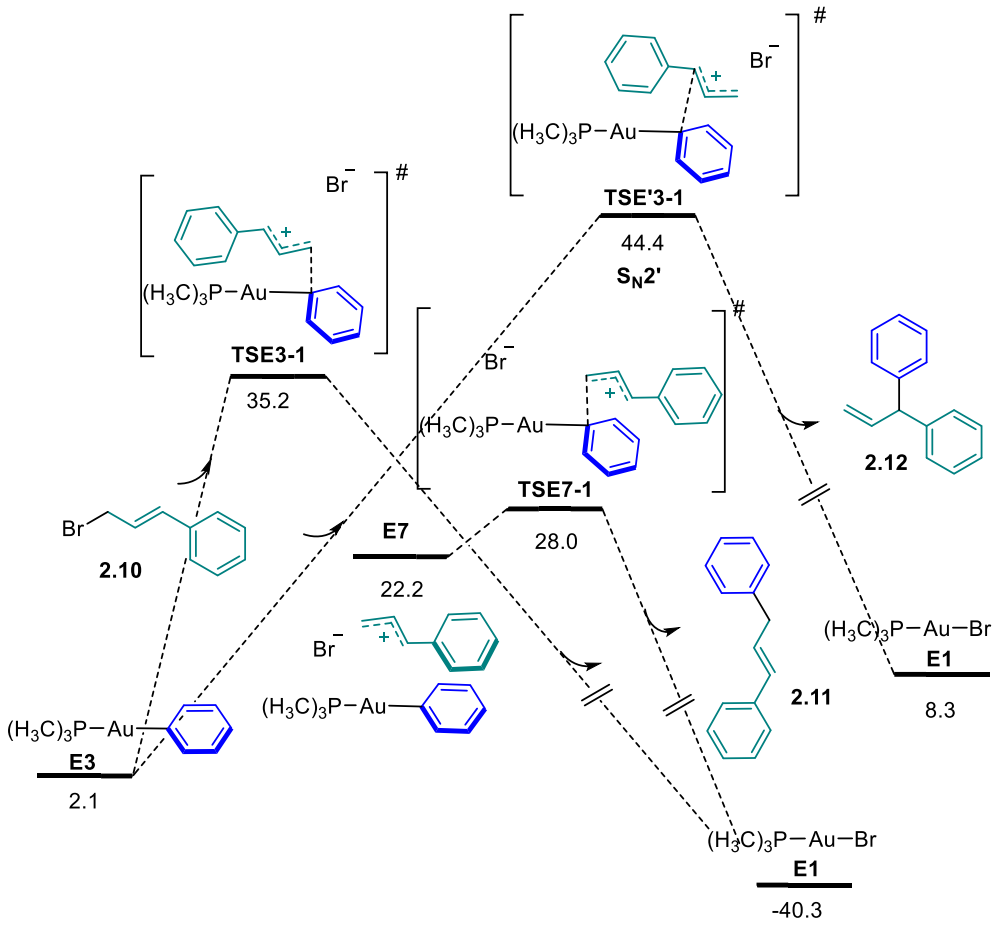

Scheme 2.26. Discarded alternative pathways to the oxidative addition/reductive elimination proposed mechanism. Free energies in kcal mol^{-1}. SMD (toluene).

With all the information gathered in hand, the refined system was calculated (Scheme 2.27) for cinnamyl bromide as substrate, and $BrAuP(CH_3)_3$ as catalyst. Transmetalation, oxidative addition and reductive elimination steps are indicated and have similar free energy barriers (**TSE3**, **TSE4** and **TSE1** respectively)

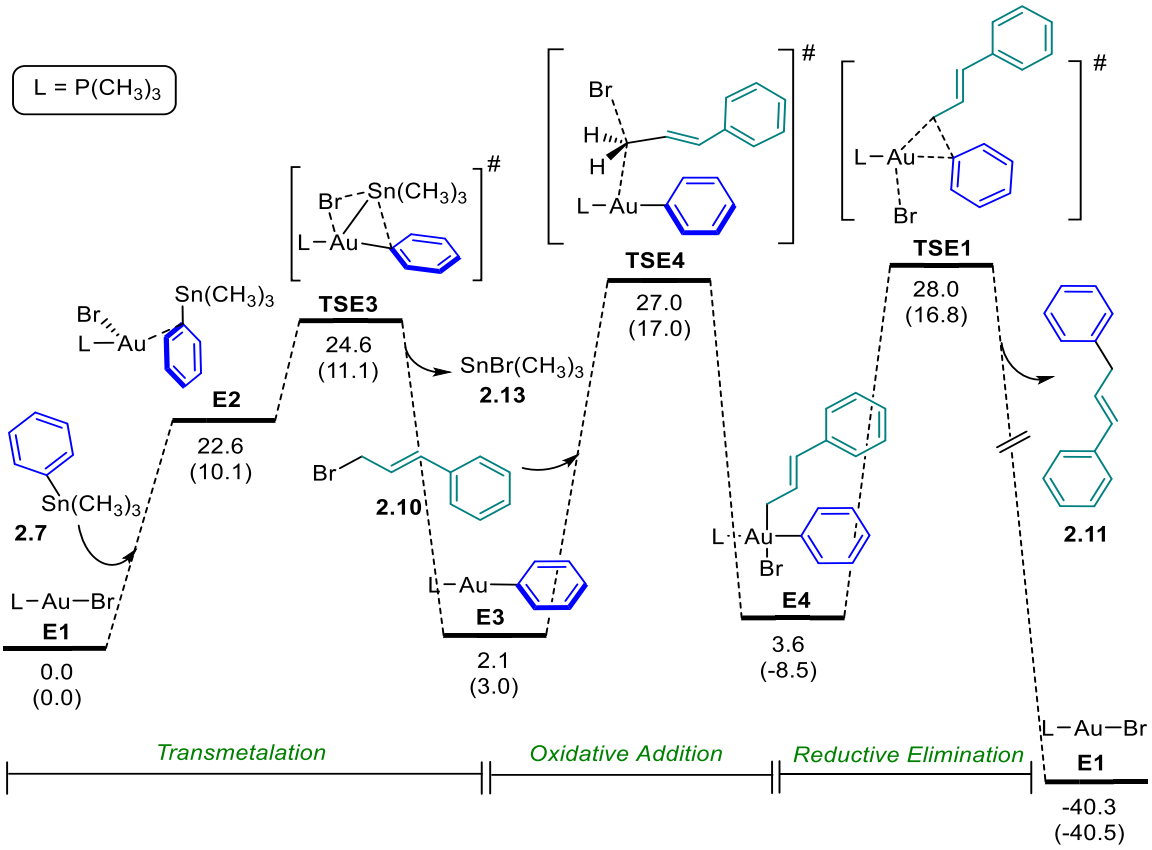

Scheme 2.27. Computed final proposed mechanism. Free energies and potential energies in parenthesis in kcal mol^{-1}. SMD (toluene).

2.5.2 DFT Benchmarking

In order to validate the method, a batch of single point calculations was performed on the structures in the free energy profile of the final system described before (Scheme 2.19). The initial benchmarking was performed with different functionals, including pure (BP86[57], M06-L[58]) and hybrid ones (BMK,[59] M06,[60] M06-HF[61], M062X, ωB97X-D[62]). The basis set used was is the same used for the single points: cc-pVTZ for light atoms and cc-pVTZ-PP for Au, Sn and I.

57 Becke, A. D. Density-Functional Exchange-Energy Approximation with Correct Asymptotic Behavior, *Phys. Rev. A* **1988**, *38*, 3098–3100.

58 Zhao, Y.; Truhlar, D. G. A New Local Density Functional for Main-Group Thermochemistry, Transition Metal Bonding, Thermochemical Kinetics, and Noncovalent Interactions, *J. Chem. Phys.* **2006**, *125*, 194101.

59 Boese, A. D.; Martin, J. M. L. Development of Density Functionals for Thermochemical Kinetics, *J. Chem. Phys.* **2004**, *121*, 3405–3416.

60 Zhao, Y.; Truhlar, D. G. The M06 Suite of Density Functionals for Main Group Thermochemistry, Thermochemical Kinetics, Noncovalent Interactions, Excited States, and Transition Elements: Two New Functionals and Systematic Testing of Four M06-Class Functionals and 12 Other Functionals, *Theor. Chem. Acc.* **2008**, *120*, 215–241.

61 Zhao, Y.; Truhlar, D. G. Density Functional for Spectroscopy: No Long-Range Self-Interaction Error, Good Performance for Rydberg and Charge-Transfer States, and Better Performance on Average than B3LYP for Ground States, *J. Phys. Chem. A* **2006**, *110*, 13126–13130.

62 Chai, J.-D.; Head-Gordon, M. Long-Range Corrected Hybrid Density Functionals with Damped Atom–Atom Dispersion Corrections, *Phys. Chem. Chem. Phys.* **2008**, *10*, 6615.

The initial benchmarking, based on potential energies, is outlined in Figure 2.4 and Table 2.11. A high diversity of the data was observed, up to a variation of 20.2 kcal mol^{-1} (for instance on the relative energy of **TSE4** with a maximum value of 30.4 when M062X-D3 was used and minimum 10.2 when BP86-D3 was used).

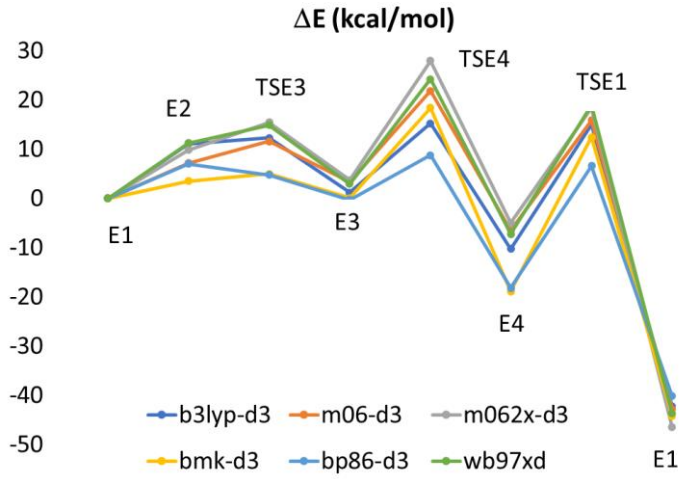

Figure 2.4. Graphical representation of potential energies in kcal mol^{-1} obtained on the benchmarking of the studied reaction. SMD (toluene).

Table 2.11. Benchmarking of DFT methods in relative potential energy (kcal mol^{-1}) for the cross-coupling gold catalyzed reaction mechanism proposed. SMD (toluene).

Method	E2	TSE3	E3	TSE4	E4	TSE1	E1
B3LYP-D3	10.1	11.1	3.0	17.0	-8.5	16.8	-40.5
M06-D3	9.0	12.9	5.3	23.9	-4.5	17.9	-40.7
M062X-D3	10.2	16.4	6.2	30.4	-2.5	20.8	-44.1
BMK-D3	2.0	4.7	1.7	20.1	-17.3	14.1	-42.5
BP86-D3	5.9	3.0	1.1	10.2	-16.8	8.0	-38.8
ωB97XD	11.2	15.3	4.7	26.0	-5.5	20.6	-41.9

In view of the diversity of DFT values, the calibration of the method was performed using linear-scaling coupled cluster theory (CCSD(T)),[63] in the understanding that this would be more accurate. The CCSD(T) method was used to benchmark 8 different density functionals with different Hartree Fock exchange fractions. Additional single-point energy calculations were

63 Goerigk, L.; Grimme, S. A Thorough Benchmark of Density Functional Methods for General Main Group Thermochemistry, Kinetics, and Noncovalent Interactions, *Phys. Chem. Chem. Phys.* **2011**, *13*, 6670.

performed in gas phase on the previously optimized geometries using ORCA 4.0 software[64] at the DPLNO-CCSD(T) level with a larger def2-TZVP basis set[65] (with ECP for internal electrons) for all atoms indistinctively. The second benchmarking where we included the wavefunction-based method DPLNO-CCSD(T) results is shown in Table 2.12. For this second benchmarking we moved from potential energies in solution to potential energies in vacuum in order to avoid possible distortions associated to the unbalanced consideration of entropic or solvation effects in the wavefunction-based method.[66]

Table 2.12. Second benchmarking in relative potential energy (kcal mol^{-1}) in gas phase including DPLNO-CCSD(T) for accuracy. Basis set used def2-TZVP.

Method	E2	TSE3	E3	TSE4	E4	TSE1	E1
B3LYP-D3	6.8	7.9	2.1	17.0	-9.2	15.7	-39.9
M06-L-D3	7.9	7.7	3.9	17.8	-8.9	14.9	-40.6
M06-D3	6.0	9.4	4.5	23.8	-5.6	16.8	-40.1
M062X-D3	6.7	13.1	5.5	31.3	-3.0	19.9	-43.5
M06-HF-D3	5.2	9.1	4.0	32.7	-9.4	17.5	-43.5
BMK-D3	-1.0	2.0	1.4	21.1	-16.9	13.3	-42.0
BP86-D3	2.6	-0.2	0.2	9.4	-17.6	6.7	-38.1
ωB97XD	8.0	12.1	4.0	26.9	-6.2	19.8	-41.3
DPLNO-CCSD(T)	8.2	11.5	2.1	32.9	-11.1	20.8	-38.0

The results obtained in the second benchmark in gas phase follow the same trend as the ones in the first benchmark including solvation. In order to quantify the differences in performance between the predicted potential energies of each functional and DPLNO-CCSD(T), the root mean-square deviation (RMSD) of all the intermediates and transitions states of the studied system were calculated and RMSD values are represented in Figure 2.5. In one hand, the best functionals

64 Neese, F. Software Update: The ORCA Program System, Version 4.0, *WIREs Comput. Mol. Sci.* **2018**, *8*.

65 Weigend, F.; Ahlrichs, R. Balanced Basis Sets of Split Valence, Triple Zeta Valence and Quadruple Zeta Valence Quality for H to Rn: Design and Assessment of Accuracy, *Phys. Chem. Chem. Phys.* **2005**, *7*, 3297.

66 Pérez-Soto, R.; Besora, M.; Maseras, F. The Challenge of Reproducing with Calculations Raw Experimental Kinetic Data for an Organic Reaction, *Org. Lett.* **2020**, *22*, 2873–2877.

according to the lowest RMSD values are ωB97XD and M06-HF-D3. On the other hand, the worst functioning methods are BP86-D3 and BMK-D3.

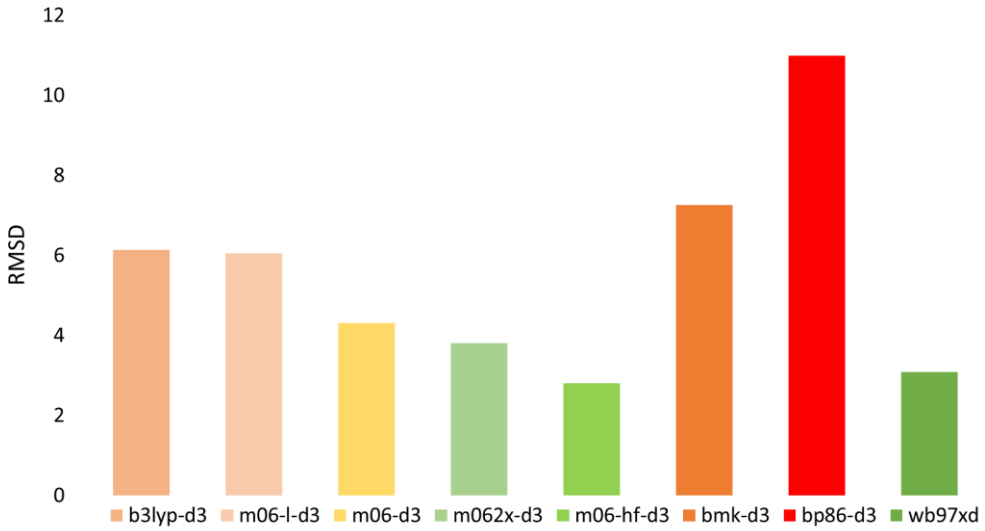

Figure 2.5. Root-mean-square deviation (RMSD) of the differences between the predicted potential energies with functional-D3/def2-TZVP and DLPNO-CCSD(T), in gas phase.

With the aim of solving the issue with the high dispersion of the data, relativistic effects were included in the ORCA 4.0 calculations using different all-electron basis sets, functionals and the zero order regular approximation (ZORA)[67] (Table 2.13).

Table 2.13. Potential energy in kcal mol^{-1} of the intermediates and transition states involved in the cross-coupling mechanism proposed.

Method (All electron)	**Functional**	**E2**	**TSE3**	E3	**TSE4**	**E4**	**TSE1**	**E1**
ZORA/def2-TZVP,SARC-ZORA(Sn, Au)	B3LYP-D3	-87.7						
ZORA/Jorge-TZP-DKH	B3LYP-D3	-30.4						
ZORA/ANO-dk3	B3LYP-D3	7.7	2.8	-0.8	23.7	-8.3	16.9	-24.8
ZORA/ANO-dk3	BP86-D3	-1.7	-8.7	-21.0		-3.3	3.2	-24.3
ZORA/ANO-dk3	ωB97XD	33.6	0.9	-12.3	21.1	3.8	21.7	-41.1

Analyzing the results, the basis sets Def2-TZVP, SARC-ZORA(Sn, Au) and Jorge-TZP-DKH resulted too small to describe the system and therefore ANO-dk3 was found to be optimal in this

67 Lenthe, E. van; Baerends, E. J.; Snijders, J. G. Relativistic Regular Two-component Hamiltonians, *J. Chem. Phys.* **1993**, *99*, 4597–4610.

regard. Then, having found the appropriate basis set, three functionals were tried (B3LYP-D3, BP86-D3 and ωB97XD). However, the results show that including all-electron basis sets have not helped us fix the discrepancy in energies in the functional benchmarking.

Reflecting on which is the origin of the high diversity of results, our proposal is that it lies on being something fundamental, related to the fact of having different oxidation states Au(I) and Au(III).[68] The first hint could be that if we observe closely the results in Figure 2.4, we see that with $ClAuP(CH_3)_3$ as reference, the dispersion of the Au(III) species, transition states as well as intermediates, is really high; meanwhile the dispersion of the relative energies of the Au(I) species is not, it converges to more or less the same value. Therefore and in the same way, the relative energies of a Pd-catalyzed oxidative addition transition state that goes from a Pd(0) to Pd(II) species was compared (Table 2.14).[69]

Table 2.14. Potential energies in gas phase (kcal mol^{-1}) on the oxidative addition of phenyl bromide to bistriphenylphosphine palladium (0). Basis set used was def2-TZVP.

	ΔE (kcal mol^{-1})								
	B3LYP-D3	M06-L-D3	M06-D3	M062X-D3	M06-HF-D3	BMK-D3	BP86-D3	ωB97XD	DPLNO - CCSD(T)
TS	2.8	-0.9	-0.2	7.0	2.8	-1.1	-7.8	5.3	**-1.6**

The dispersion of the data in the Pd system is considerably smaller than in the case of our Au(I)/Au(III) system, even though there is still variations on the potential energies when using the same variety of functionals.

Another DFT benchmark was performed in a working literature reported system by Bourissou in 2017 (Scheme 2.28).[70] In order to analyze and question if the dispersion of values is a typical feature in this kind of systems, the oxidative addition of iodobenzene to a cationic gold complex

68 a) Ducéré, J.-M.; Goursot, A.; Berthomieu, D. Comparative Density Functional Theory Study of the Binding of Ligands to Cu^{+} and Cu^{2+}: Influence of the Coordination and Oxidation State, *J. Phys. Chem. A* **2005**, *109*, 400–408. b) Quintal, M. M.; Karton, A.; Iron, M. A.; Boese, A. D.; Martin, J. M. L. Benchmark Study of DFT Functionals for Late-Transition-Metal Reactions, *J. Phys. Chem. A* **2006**, *110*, 709–716.

69 Besora, M.; Maseras, F. The Diverse Mechanisms for the Oxidative Addition of C–Br Bonds to $Pd(PR_3)$ and $Pd(PR_3)_2$ Complexes, *Dalton Trans.* **2019**, *48*, 16242–16248.

70 Zeineddine, A.; Estévez, L.; Mallet-Ladeira, S.; Miqueu, K.; Amgoune, A.; Bourissou, D. Rational Development of Catalytic Au(I)/Au(III) Arylation Involving Mild Oxidative Addition of Aryl Halides, *Nat. Commun.* **2017**, *8*, 565.

bearing an hemilabile P-N ligand (MeDalPhos) in the presence of the counterion SbF_6^- was explored (Table 2.15).

Table 2.15. Potential energies in gas phase in kcal mol^{-1}. Basis set used was def2-TZVP.

	ΔE (kcal mol^{-1})						
	B3LYP-D3	M06-D3	M062X-D3	BMK-D3	BP86-D3	ωB97XD	DPLNO - CCSD(T)
TSF2	-8.8	-12.6	-8.7	-15.1	-11.5	**-8.3**	**-4.7**
F2	-15.7	-18.3	**-12.5**	-21.8	-19.1	-15.0	**-12.3**
TSF3	-0.5	-2.3	**7.3**	-6.0	-9.1	2.0	**4.9**
F3	-17.6	-11.4	-5.8	-26.5	-27.0	-14.0	**-18.5**

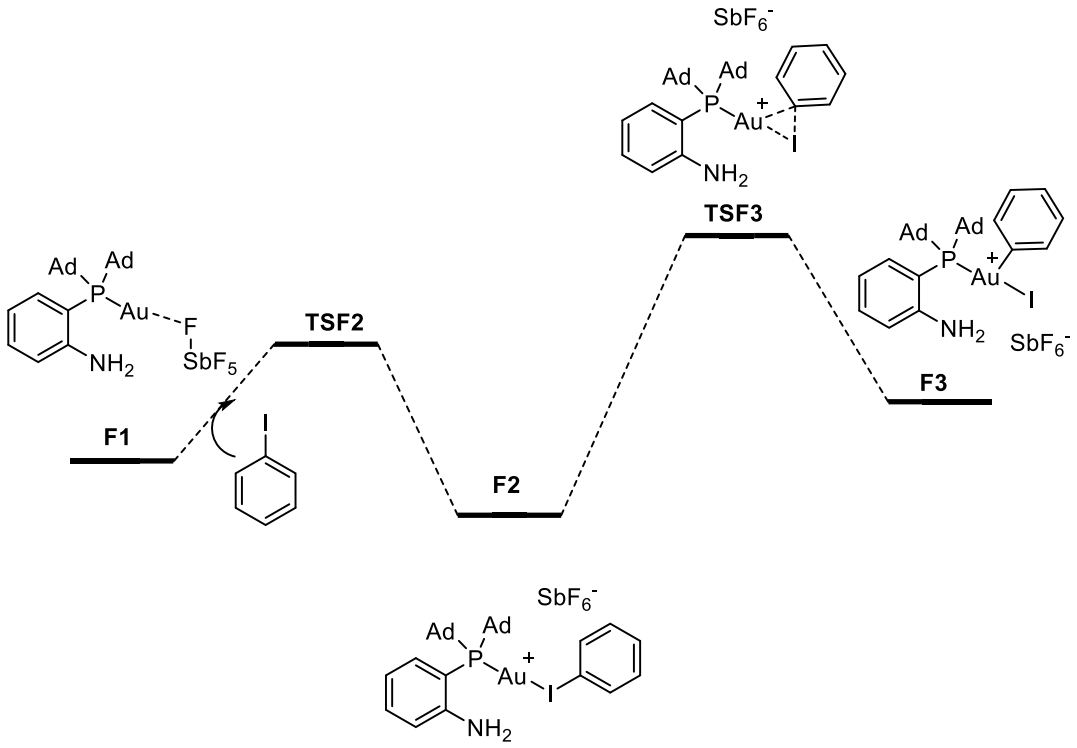

Scheme 2.28. Computed Bourissou's reported system for comparison on the functional benchmarking.

The trend in the benchmarking for the oxidative addition step replicates the one observed in our system, where the computed DLPNO-CCSD(T) reference data for the transition states as well as the intermediates results in a discordance of energies when varying the density functionals. The dispersion of the data for the potential energies in the oxidative addition step goes up to 16 kcal mol^{-1} in the reported system (comparable dispersion in regard to our system, with dispersion of data up to 23.1 kcal mol^{-1}).

Having analysed the unexpected effect on the potential energies the different systems, we wanted to take into consideration the relative Gibbs free energy ($\Delta G^{\#}$) of the oxidative addition transition states using CCSD(T), as represented in Table 2.16.

Table 2.16. Free energies in kcal mol^{-1} using CCSD(T) method in gas phase for the oxidative addition transition states of the studied systems.

	$\Delta G^{\#}$ (kcal mol^{-1})		
	Our system	Kochi	Bourissou
CCSD(T)	44.4	36.3	17.7

The free energy of the oxidative addition step in our Au(I)/Au(III) system is 44.0 kcal mol^{-1} in gas phase, which is a very high energy even for a reaction running at 110 ºC during 24 h; and 36.3 kcal mol^{-1} for Kochi's system, which is as well really high for a 25 ºC occurring reaction. However, regarding Bourissou's reported system mentioned before, the relative free energy associated to the oxidative addition barrier has a value of 17.7 kcal mol^{-1}, consistent with the experimental results obtained for a 25 ºC reaction.

Therefore, our benchmarking demonstrates that the processes involving Au(I)/Au(III) transitions are especially difficult to characterize computationally, and require comparison to CCSD(T) results for validation. In the specific systems we have studied it seems that the best results are provided by ωB97XD and some functionals of the M06 family, but not by others widely used such as B3LYP, and much less by BP86. We have also to admit that the best functionals yield free energy barriers that are incompatible with experimental observations, thus we have to consider that different mechanisms have to be considered, and that further research will be required in this concern.

2.6 Further experimental and computational work on stereochemistry[71]

With the objective of getting deeper insight into the reaction, we tested a substrate bearing stereodetermining elements **2.19** in the molecule that could guide us to determine whether the oxidative addition occurs through inversion or retention of configuration. Additionally, we wanted to examine as well if the possible formation of π-allyl could give access to the S_N2' product. The stereochemistry of the reaction was thought to be studied by submitting the *trans*-configurated allylic bromide **2.19** to the best catalytic reaction conditions developed for cinnamyl bromide.

71 Experimental part of this work was performed in collaboration with Dr. Anna Sadurní.

The synthesis of **2.19** was achieved following a reported route until **2.18**.[72] The last step to install the halogen was unsuccessfully attempted through a Corey-Kim bromination,[73] therefore an Appel reaction, following a reported procedure for a similar substrate,[74] was tried obtaining an inseparable mixture *anti:syn* = 85:15 (20% yield) (Scheme 2.29).

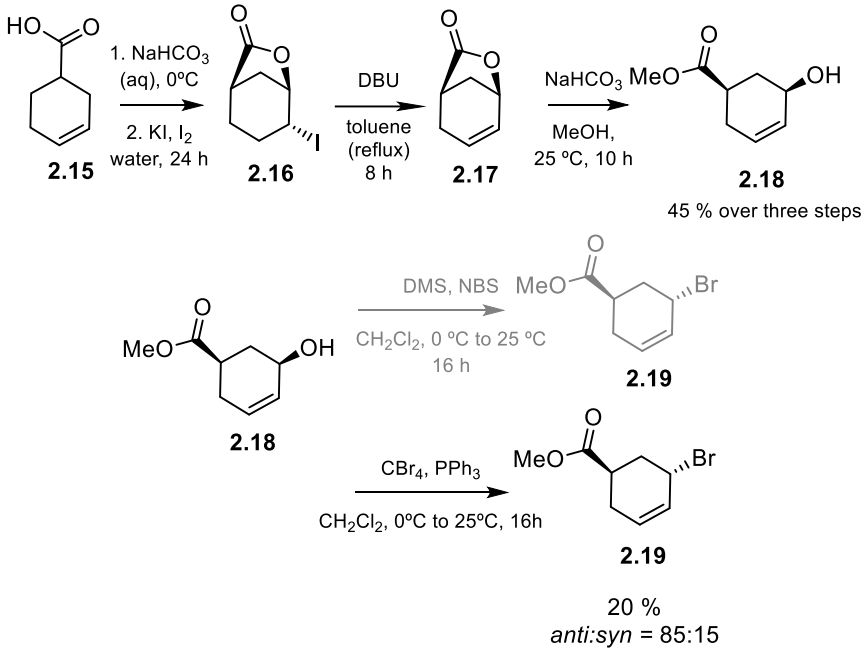

Scheme 2.29. Synthetic procedure for the synthesis of substrate **2.19**. Relative configurations shown.

In spite of not having the pure trans bromo allyl product **2.19**, the mixture of isomers was submitted to the gold(I) catalyzed reaction conditions (Scheme 2.30. The desired product **2.20** could be detected after 24 h by GC-MS and by ^{1}H NMR we could distinguish the formation of the *anti-p*roduct **2.20**,[75] in a 4:1 ratio **2.19**:**2.20**. The coupling of **2.19** with $PhSn(CH_3)_3$ **2.7** proceeded with overall retention of configuration.

72 Perez-Perez, M.-J.; Rozenski, J.; Busson, R.; Herdewijn, P. Application of the Mitsunobu-Type Condensation Reaction to the Synthesis of Phosphonate Derivatives of Cyclohexenyl and Cyclohexanyl Nucleosides, *J. Org. Chem.* **1995**, *60*, 1531–1537.

73 Corey, E. J.; Kim, C. U.; Takeda, M. A Method for Selective Conversion of Allylic and Benzylic Alcohols to Halides under Neutral Conditions, *Tetrahedron Lett.* **1972**, *13*, 4339–4342.

74 Dixon, B. R.; Bagi, C. M.; Brennan, C. R.; Brittelli, D. R.; Bullock, W. H.; Chen, J.; Collibee, W. L.; Dally, R.; Johnson, J. S.; Kluender, H. C. E.; Lathrop, W. F.; Liu, P.; Mase, C. A.; Redman, A. M.; Scott, W. J.; Urbahns, K.; Wolanin, J. J. Substituted 2-Arylimino Heterocycles and Compositions Containing Them, for Use as Progesterone Receptor Binding Agents, Substituted 2-Arylimino Heterocycles and Compositions Containing Them, for Use as Progesterone Receptor Binding Agents. WO2000042031A3, November 9, 2000.

75 NMR shifts of *anti* and *syn* products extracted from: Zhao, H.; Caldora, H. P.; Turner, O.; Douglas, J. J.; Leonori, D. A Desaturative Approach for Aromatic Aldehyde Synthesis via Synergistic Enamine, Photoredox and Cobalt Triple Catalysis, *Angew. Chem. Int. Ed.* **2022**, *61*, e202201870.

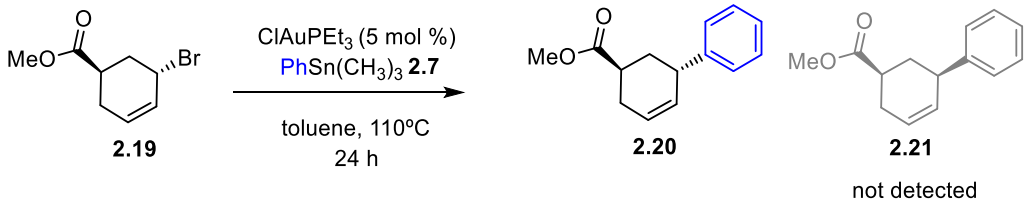

Scheme 2.30. Proposed experiment to understand the possible inversion or retention of configuration.

The catalysis was as well performed with any gold(I) catalyst and no conversion of any of the starting materials was observed.

The system was intended to be studied by DFT. First of all, we considered the possible conformations of our substituted cyclic allylic bromide **2.20**. The most stable chair conformation involves the methyl ester occupying the equatorial position and the bromine the axial position (Scheme 2.31).

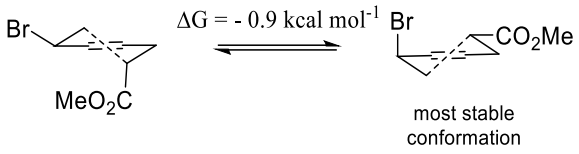

Scheme 2.31. Chair conformations of our substrate **2.19**. SMD (toluene).

The observed relative configuration of product **2.20** might be a consequence of an inversion of configuration of C1 (**TSG2**) (Scheme 2.32) rendering *cis*-configurated allyl bromide **2.19**, prior to the S_N2-like oxidative addition step where the configuration is inverted again (**TSG3**). In **TSG2**, a planar cationic allyl system is observed, at a distance of C1-Au: 3.2 Å; while the bromide moves above and under the planar system. The gold complex seems to be a spectator of the process. The other oxidative addition process, similar in energy but slightly favorable goes stepwise (**TSH2** and **TSH3**) until the formation of intermediate **H3**. It is worth mentioning that the barriers are accessible under the reaction conditions and cosely match the experimental results obtained (110 ºC and 24 h required to observe some conversion).

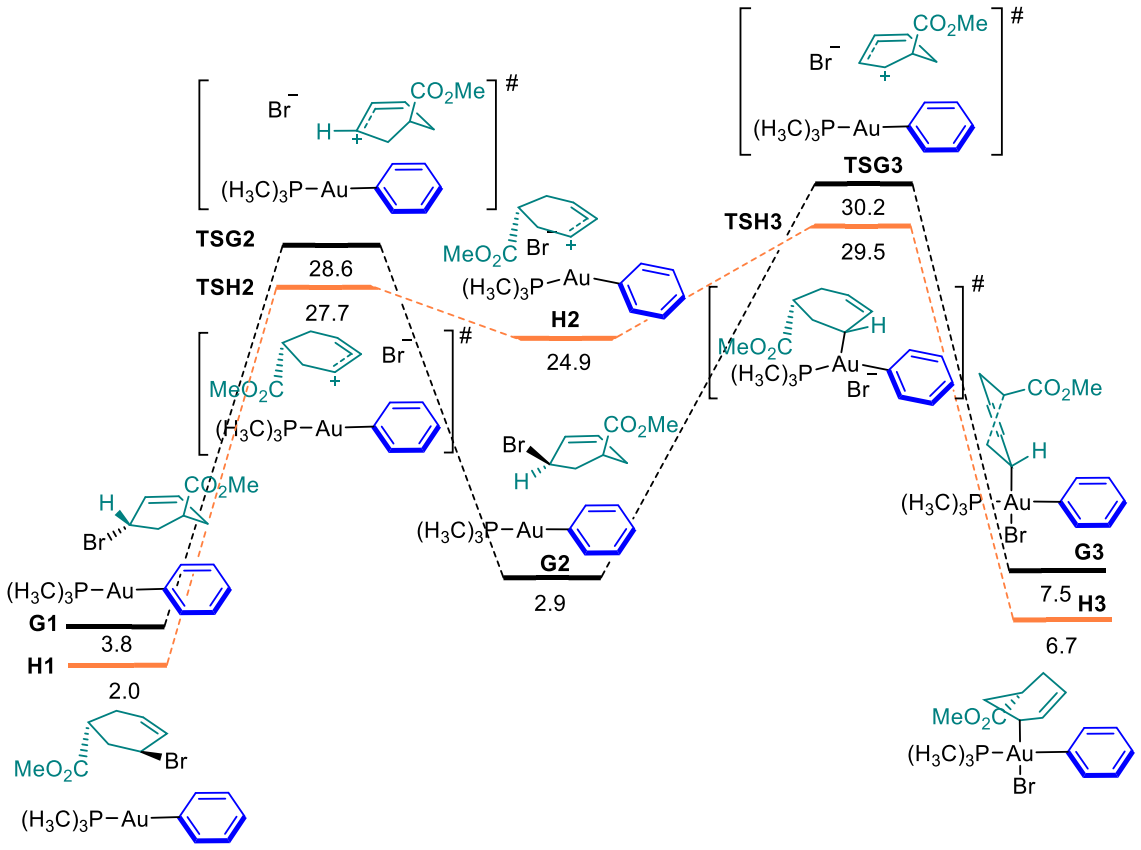

Scheme 2.32. Pathways in which oxidative addition is involved. Free energies in kcal mol^{-1}. SMD (toluene).

In this case, S_N2' pathway would yield the same trans coupled product **2.20**. The possible pathway was ruled out and not calculated due to the previously observed inaccessibility of S_N2' calculated pathway when cinnamyl bromide was the substrate, as analogy. The formation of π-allyl intermediate **H4** (Scheme 2.33) was discarded given the high energy required for its formation (**TSH4**).

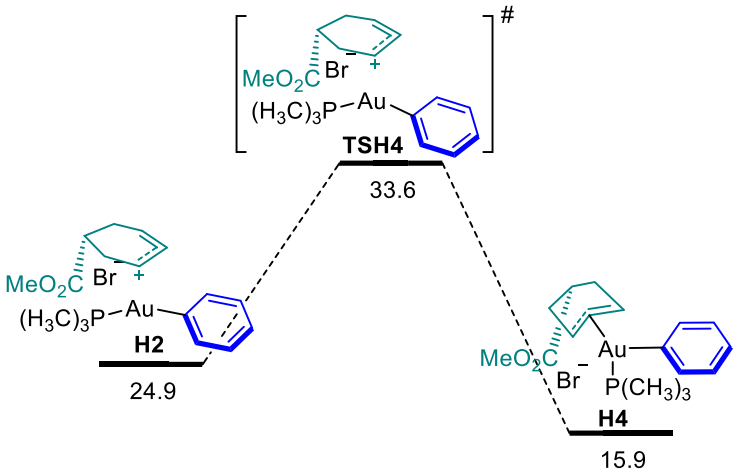

Scheme 2.33. π-allyl formation, discarded pathway. Free energies in kcal mol^{-1}. SMD (toluene).

Besides, S_N1 was evaluated (Scheme 2.34, **TSI2**), but the C–Br bond dissociation of the allyl bromide starting material was calculated to be 38 kcal mol^{-1}, implying a non-accessible pathway to **I1**.

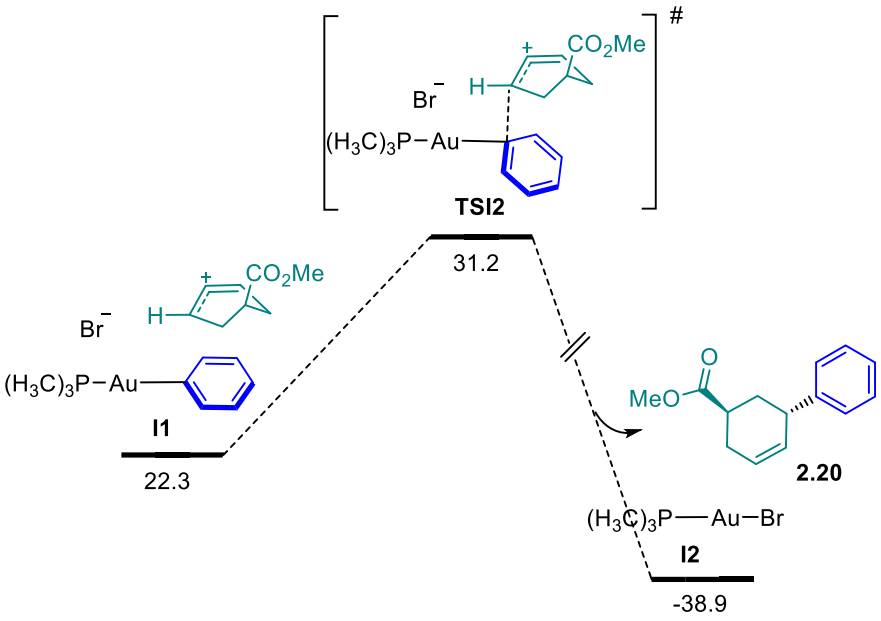

Scheme 2.34. Discarded S_N1 reaction due to **I1** is not accessible. Free energies in kcal mol^{-1}. SMD (toluene).

In order to obtain the *trans*-configurated coupled product **2.20** the reductive elimination must occur from one of the oxidative addition intermediates in which there is a trans relative position of gold(III) and the methyl ester, like **G4** (Scheme 2.35). However, both transition states to form *syn* (**TSH5**) and *anti* (**TSG5**) desired product **2.20** are equal in energy and surpass the limit of a 110 ºC running reaction.

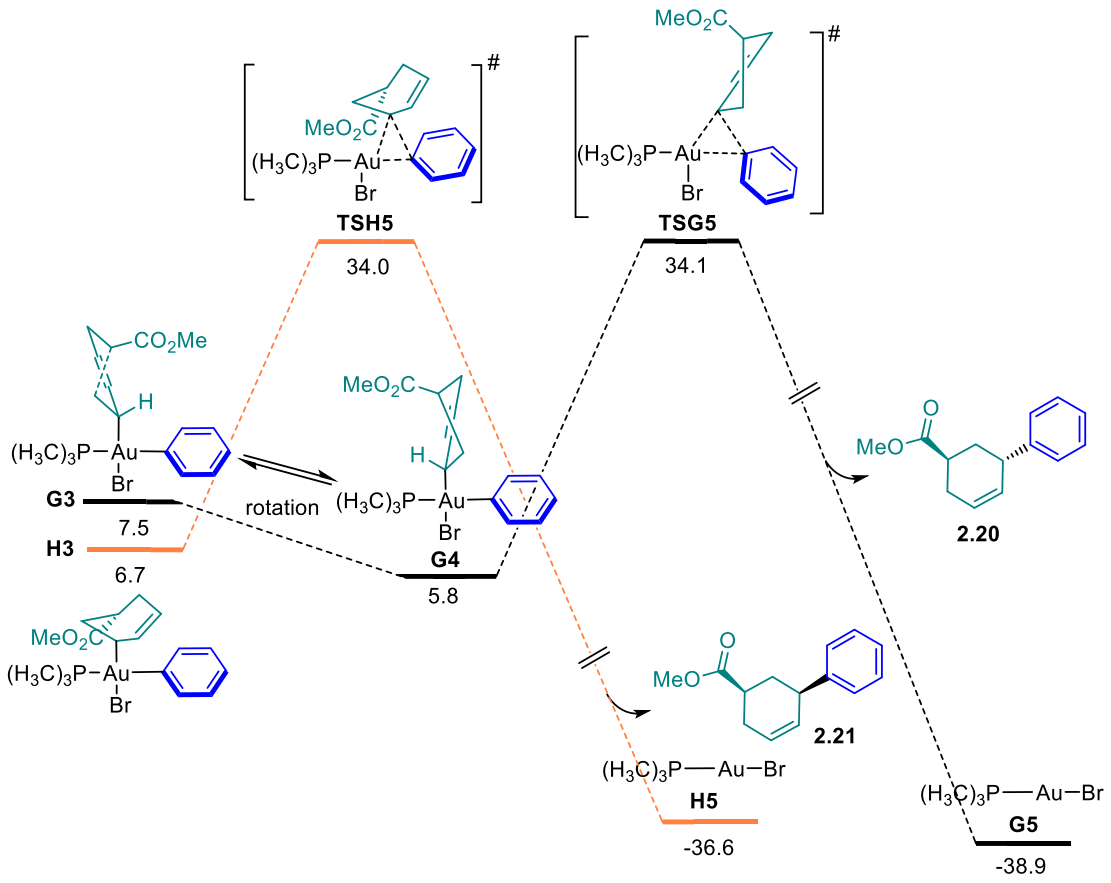

Scheme 2.35. Reductive elimination pathways from different oxidative addition complexes that give rise to *anti* and *syn* products. Free energies in kcal mol^{-1}. SMD (toluene).

After this evaluation of the system, we consider that there has to be an alternative pathway to access the *trans*-configurated observed product **2.20**, which we could not find. The system has several conformations and possible pathways to be explored, thus further exploration is needed.

2.7 Conclusions

We improved substantially our understanding of Au(I)/Au(III) catalytic systems involving simple ligands.

A catalytic system was developed employing mononuclear Au(I) complexes bearing simple alkyl phosphines as catalysts, in the cross-coupling reaction of allyl bromides and organostannane $PhSn(CH_3)_3$. The system was studied computationally, leading to the proposal of a plausible mechanism that involves an S_N2-type oxidative addition to gold(I). The envisioned catalytic steps consist of a concerted transmetalation of the phenyl group obtaining the intermediate PhAuL, from which oxidative addition of the allyl halide proceeds, ending with reductive elimination of cross-coupled product.

A deeper computational study of these systems demonstrated an unexpectedly complex behavior of this type of systems. A high dependence of the DFT energy on the identity of the functional was found, and the problem is associated to the description of the change of oxidation state at gold. BMK and BP86 functionals were found inappropriate for the description of Au(I)/Au(III) systems. The benchmarking was extended to other similar previously reported systems, detecting a comparable outcome in systems involving Au(I)/Au(III) species. On the other hand, a much lower dispersion of the data was observed when Pd(0)/Pd(II) oxidative addition process was evaluated. The difficulty in the computational characterization of the Au(I)/Au(III) catalytic processes makes complicated the use of calculations for this design, and opens the possibility that mechanisms not computed in this work may be operating. Further work will be necessary in this concern.

Moreover, the stereochemistry of the oxidative addition reaction was assessed, observing an overall retention of the reaction center. However, it is tentatively proposed that the reaction proceeds via stereoinvertive S_N2-type oxidative addition after a prior inversion of the configuration in the substrate, therefore a double inversion of configuration might be taking place. Further mechanistic studies are needed to support the proposed mechanism.

2.8 Experimental Section

2.8.1 General experimental methods

Most reagents and solvents were purchased from commercial sources and used without further purification. Cinnamyl bromide was purified until 97% purity as a white solid by distillation (Kügelrohr: 122 ºC, 2 mbar) from commercially available reagent, before using in reactions. The dry solvents used were passed through an activated alumina column on a PureSolv^{TM} Solvent Purification System (SPS, Innovative Technologies, Inc., MA), or purchased from ACROS Organics as commercially available anhydrous solvents. The reaction monitoring was followed by NMR analysis, TLC (thin layer chromatography), UHPLC–MS (Agilent Technologies 1290 Infinity II, LC/MS with single–quad detector InfinityLab (APCI ionization source)) or by GC–MS. Thin layer chromatography was carried out using TLC aluminum sheets coated with 0.2 mm of silica gel (Merck Gf234), using UV light as the visualizing agent and an acidic solution of vanillin in ethanol or alternatively a basic solution of $KMnO_4$ in water as stain, followed in both cases by heat. The chromatographic purifications were carried out using flash grade silica gel (SDS Chromatogel 60 ACC, 40–60 μm) as the stationary phase. Preparative thin layer chromatography was performed on TLC plates (Analtec Silica Gel GF UV254, 20×20 cm, 1000 μm or 2000 μm). NMR spectra were recorded at 298 K on Bruker Avance Ultrashield NMR spectrometers (300 MHz, 400 MHz, 500 MHz, and 500 MHz with CryoProbe). Chemical shifts (δ) are reported in parts per million (ppm) and referenced to residual solvent (For ^{1}H NMR: $CDCl_3$ at 7.26 ppm, CD_2Cl_2 at 5.31 ppm, C_6D_6 at 7.16 ppm, for $^{13}C\{^{1}H\}$ NMR: $CDCl_3$ at 77.16 ppm, CD_2Cl_2 at 54.00 ppm, C_6D_6 at 128.06 ppm). The following abbreviations were used to explain multiplicities: s = singlet, d = doublet, t = triplet, q = quartet, p = pentet, m = multiplet, br s = broad singlet. Coupling constants (*J*) are reported in Hertz (Hz). Mass spectra were recorded on a Waters LCT Premier Spectrometer (ESI and APCI) or on an Autoflex Broker Daltonics (MALDI and LDI). Specific optical rotation measurements were carried out on a Jasco P–1030 model polarimeter equipped with a PMT detector using the sodium line at 589 nm, and 1 mL (10 mm pathlength) or 2 mL (100 mm pathlength) cells. Melting points were determined using a Mettler Toledo MP70 melting point apparatus.

2.8.2 Synthetic procedures and characterization data

Bromo-triethylphosphinegold(I)

To a solution of chloro-triethylphosphinegold(I) (130.0 mg, 370.8 μmol, 1 equiv.) in 30 mL of acetone, it was added potassium bromide (882.5 mg, 7.4 mmol, 20 equiv.) and left stirring during 16 h. A white precipitate is formed after 1 h. The reaction was monitored by TLC and when reached full conversion, the reaction mixture, was filtered through celite and evaporated to yield $ (132.0 mg, 334 μmol, 90% yield) as a white solid.

^{1}H NMR (500 MHz, $CDCl_3$) δ 1.85 (dq, *J* = 10.2, 7.6 Hz, 2H), 1.26 – 1.17 (m, 3H). **^{13}C{^{1}H} NMR** (126 MHz, $CDCl_3$) δ 17.70, 9.01. **^{31}P NMR** (202 MHz, $CDCl_3$) δ 37.35. (from IA-03-171). **HRMS** (ESI+) calculated for $[C_6H_{15}AuP]^+$ = 315.0572 *m/z*; found $[M + H]^+$ 315.0558 *m/z*. **M.p.** = 86-89 ºC.

Methyl-5-bromocyclohex-3-ene-1-carboxylate (2.19)

To a solution of cyclohex-1-enylmethanol (100 mg, 0.64 mmol, 1 equiv) in CH_2Cl_2 (1 mL) at 0°C was added PPh_3 (185 mg, 0.7 mmol, 1.1 equiv) and CBr_4, (255 mg, 0.77 mmol, 1.2 equiv). The mixture was allowed to stir at 25 ºC overnight, then concentrated under reduced pressure. The residue was diluted with pentane and filtered. The filtrate was concentrated under reduced pressure and purified by silica gel flash column chromatography (20:1 to 10:1 cyclohexane/EtOAc) to give *trans*-configurated desired product $ as a transparent oil (20 % yield, 85% purity) as an inseparable mixture with the *cis*-configurated isomer.

^{1}H NMR (400 MHz, $CDCl_3$) δ 5.94 (dddt, *J* = 11.1, 4.6, 3.4, 1.6 Hz, 1H), 5.85 – 5.79 (m, 1H), 4.88 (ddq, *J* = 4.6, 3.0, 1.8 Hz, 1H), 3.72 (s, 3H), 3.13 – 3.01 (m, 1H), 2.58 – 2.51 (m, 1H), 2.51 – 2.46 (m, 1H), 2.41 (dq, *J* = 11.5, 2.5 Hz, 1H), 2.12 (ddd, *J* = 14.8, 12.5, 4.2 Hz, 1H). **^{13}C{^{1}H} NMR** (101 MHz, $CDCl_3$) δ 175.31, 128.98, 128.50, 52.06, 46.95, 35.16, 34.62, 27.57. **HRMS** (ESI+) calculated for $[C_8H_{11}O_2]^+$ = 139.0754 *m/z*; found $[M + H]^+$ 139.0750 *m/z*. **α_D^{589}** = -10.6 deg.cm^2.g^{-1} (CH_2Cl_2, c 1.0, 304 K).

General procedure for gold catalyzed allylation with cinnamyl bromide

In a MW vial equipped with a stirring bar, the corresponding gold(I) catalyst was weighted and added as a solid; $PhSn(CH_3)_3$ was added using a Hamilton syringe and 3 cycles of vacuum/Ar were performed. Then, the allyl halide was added as a solution in toluene-d_8 and heated up to 110 ºC for the given time. For the monitoring, the reaction mixture was allowed to cool down to 25 ºC, an aliquot was taken in an NMR tube, internal standard was added and submitted to ^{1}H and ^{31}P NMR spectroscopy.

2.8.3 Kinetic studies

Variable Time Normalization Analysis (VTNA)

All operations were set up with clean and new stirring bars and MW vials. Cinnamyl bromide was purified by distillation (122 ºC, 2 mbar) of the commercially available compound, obtaining a white solid/transparent oil in a 97 % purity.

Order in substrate

Reaction conditions: [SM] = 200/100/50 mM, [$PhSnMe_3$] = 100 mM, [$BrAuPEt_3$] = 10 mM. Three MW vials equipped with magnetic stirrer containing substrate (cinnamyl bromide), ethyl benzoate as internal standard, trimethyl(phenyl)stannane, and gold complex $BrAuPEt_3$ in deuterated toluene (3.8 mL) were prepared. Precisely, the following reagents were added in sequence into the different MW vials:

1) $BrAuPEt_3$ (15.0 mg, 38 mmol), added as solid.
2) Substrate and internal standard stock solution (1.52/3.04/0.76 mL) previously prepared by adding deuterated toluene (8.88 mL) to the substrate (437.6 mg, 2.22 mmol) and internal standard (333.5 mg, 2.22 mmol).
3) Deuterated toluene (2.28/0.76/3.04 mL).
4) Trimethyl(phenyl)stannane (69 mL), to obtain a clear solution.

After preparing the solution, the reaction vessel was sealed and heated up to 110 ºC. The aliquots for the kinetic monitoring were taken from the MW vials after releasing the pressure with a balloon and directly transferred to NMR tubes for measuring the corresponding ^1H NMR spectra (8 scans).

Data

Conversion data against the internal standard were extracted using Mestrenova (Fourier transform, automatic phase correction, baseline correction and integration of stacked spectra) and further manipulated with Excel. Data are reported in the tables below, rounded for clarity. The data was then elaborated following the variable time normalization analysis (VTNA) described by Burés. An order in stannane in between 0.5 and 1 caused the best overlap of the three curves in the graph below, as judged visually.

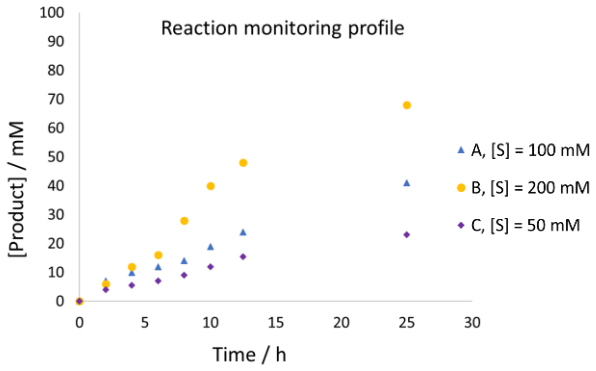

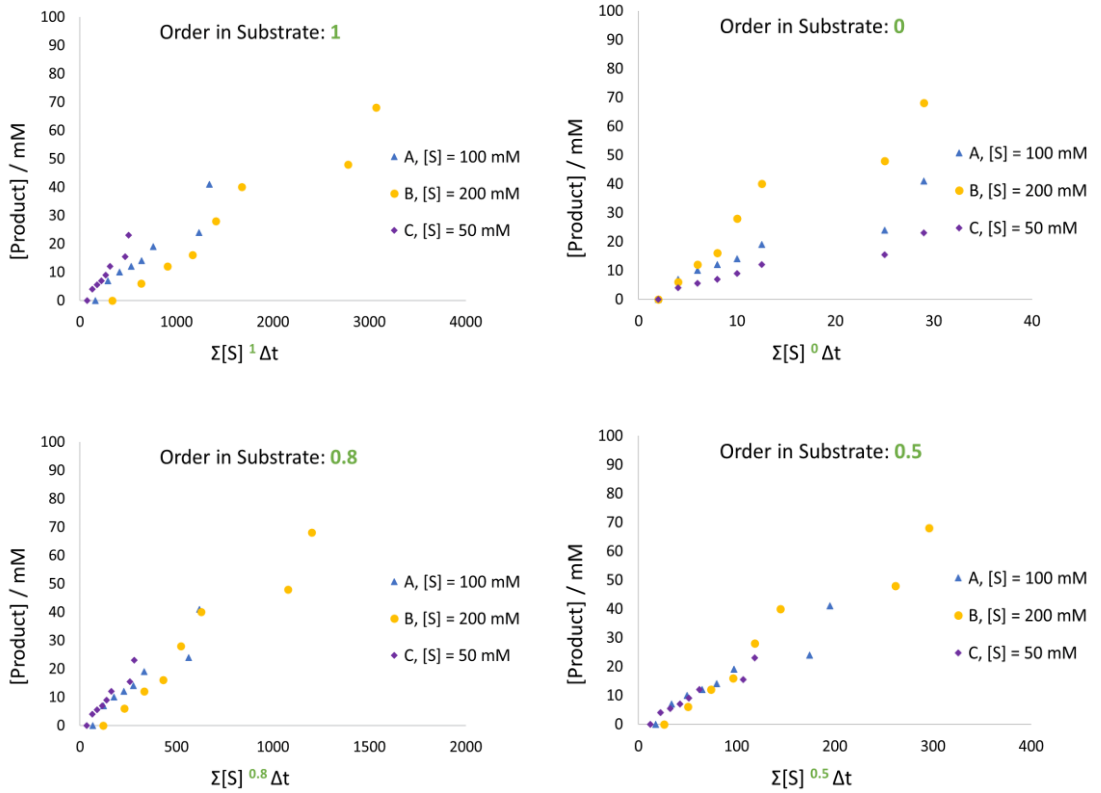

Figure 2.6. Reaction monitoring profile and VTNA, which enables the determination of the order in substrate (0.5-0.8 order).

Order in stannane

Reaction conditions: [SM] = 100 mM, [ClAuPEt$_3$] = 10 mM, [PhSnMe$_3$] = 50/100/200 mM. Three MW vials equipped with magnetic stirrer containing substrate (cinnamyl bromide), ethyl benzoate as internal standard, trimethyl(phenyl)stannane and gold complex ClAuPEt$_3$ in deuterated toluene (3.8 mL) were prepared. Precisely, the following reagents were added in sequence into the different MW vials:

1) Substrate and internal standard stock solution (1.52 mL) previously prepared by adding deuterated toluene (8.7 mL) to the substrate (428 mg, 2.17 mmol) and internal standard (326 mg, 2.17 mmol).

2) Trimethyl(phenyl)stannane stock solution (253/507/1013 mL) previously prepared by adding deuterated toluene (4.09 mL) to the stannane (739 mg, 3.07 mmol).

3) ClAuPEt$_3$ stock suspension (152 mL), previously prepared by adding the deuterated toluene (1,14 mL) to the gold complex (100 mg, 285 mmol).

4) Deuterated toluene (1.87/1.62/1.12 mL) obtaining a clear yellowish solution.

After preparing the solution, the reaction vessel was sealed and heated up to 110 ºC. The aliquotes for the kinetic monitoring were taken from the MW vials after releasing the pressure with a

balloon and directly transferred to NMR tubes for measuring the corresponding ^{1}H NMR spectra (8 scans).

Data

Conversion data against the internal standard were extracted using Mestrenova (Fourier transform, automatic phase correction, baseline correction and integration of stacked spectra) and further manipulated with Excel. Data are reported in the tables below, rounded for clarity. The data was then elaborated following the variable time normalization analysis (VTNA) described by Burés. An order in stannane in between 0.5 and 1 caused the best overlap of the three curves in the graph below, as judged visually.

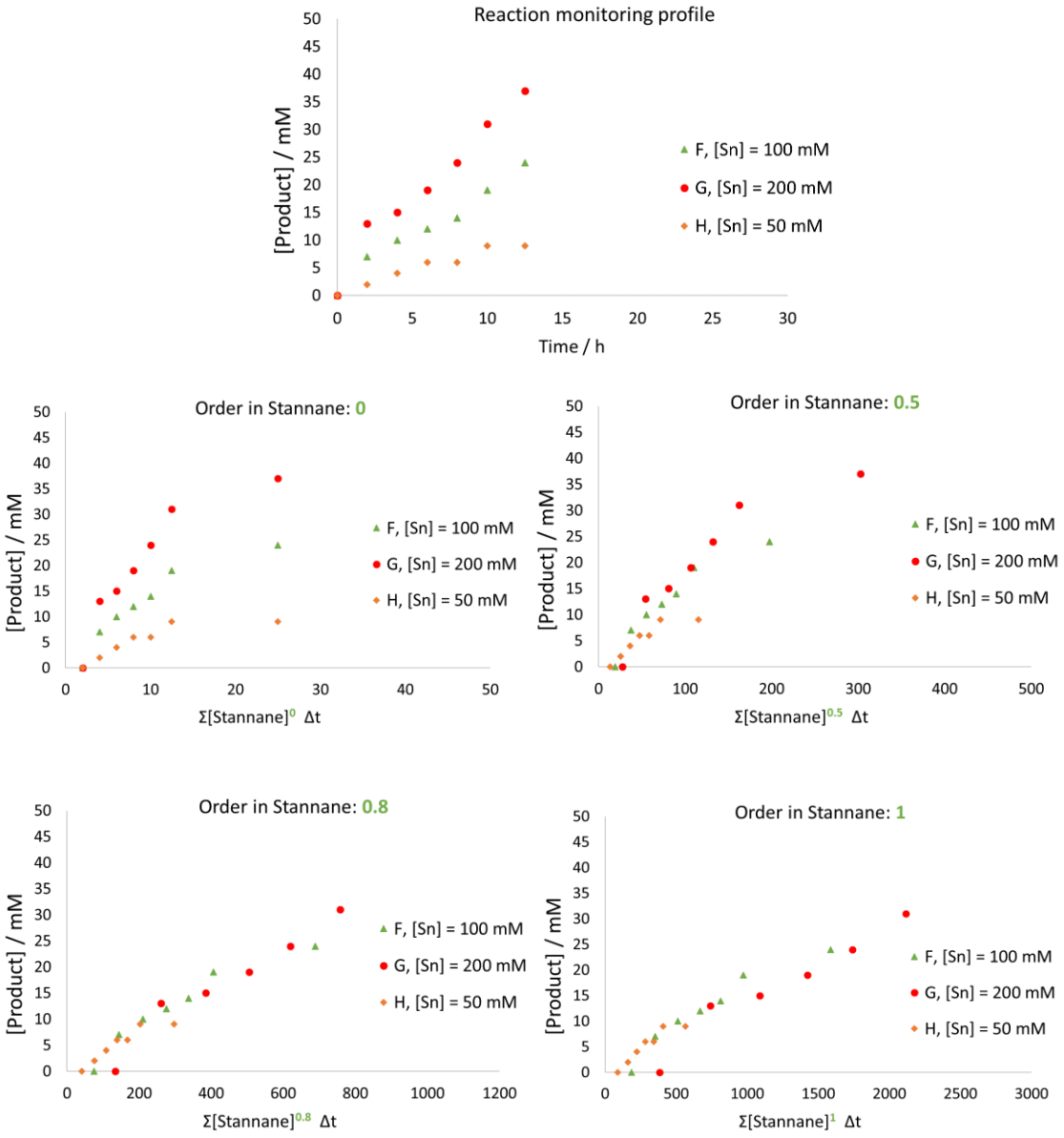

Figure 2.7. Reaction monitoring profile and VTNA, which enables the determination of the order in stannane (0.5-1 order)

Order in catalyst

Reaction conditions: [SM] = 100 mM, [$BrAuPEt_3$] = 5/10/20 mM, [$PhSnMe_3$] = 100 mM. Three MW vials equipped with magnetic stirrer containing substrate (cinnamyl bromide), ethyl benzoate as internal standard, trimethyl(phenyl)stannane and gold complex $BrAuPEt_3$ in deuterated toluene (3.8 mL) were prepared. Precisely, the following reagents were added in sequence into the different MW vials:

1) $BrAuPEt_3$ (7.5/15.0/30.0 mg), added as solid.
2) Substrate and internal standard stock solution (1.52 mL), previously prepared by adding deuterated toluene (8.88 mL) to the substrate (437.6 mg, 2.22 mmol) and internal standard (333.5 mg, 2.22 mmol).
3) Deuterated toluene (2.28 mL).
4) Trimethyl(phenyl)stannane (69 mL), to obtain a clear solution.

After preparing the solution, the reaction vessel was sealed and heated up to 110 ºC. The aliquotes for the kinetic monitoring were taken from the previously cooled to 25 ºC MW vials and directly transferred to NMR tubes for measuring the corresponding ^1H NMR spectra (8 scans).

Data

Conversion data against the internal standard were extracted using Mestrenova (Fourier transform, automatic phase correction, baseline correction and integration of stacked spectra) and further manipulated with Excel. Data are reported in the tables below, rounded for clarity. The data was then elaborated following the variable time normalization analysis (VTNA) described by Burés. An order in catalyst of 1 caused the best overlap of the three curves in the graph below, as judged visually.

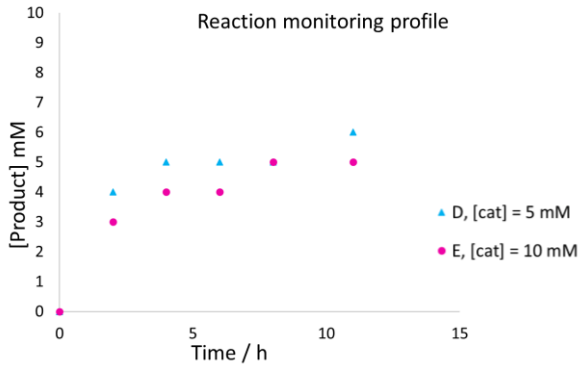

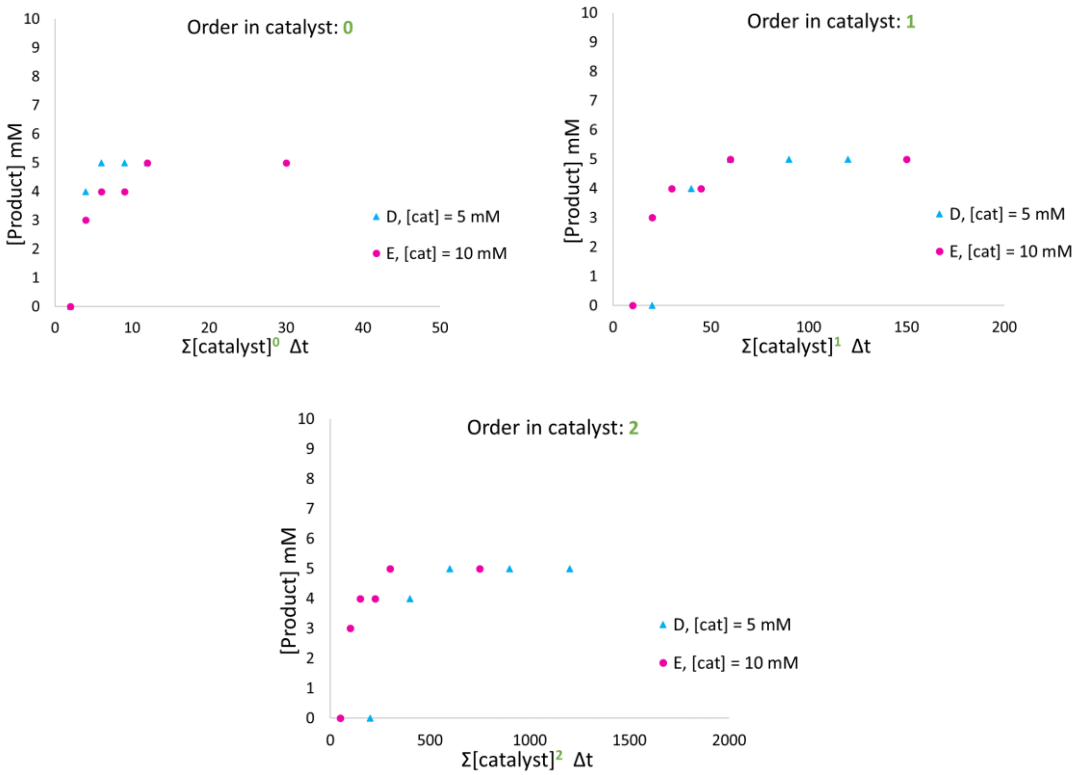

Figure 2.8. Reaction monitoring profile and VTNA, which enables the determination of the order in catalyst (first order).

Table 2.17. Partial concentrations of substrate [S] and product [P] during the monitoring of the VTNA experiments A-E.

A			**B**			**C**			**D**			**E**		
[S] = 100 mM **[Sn]** = 100 mM **[cat]** = 10 mM			**[S]** = 200 mM **[Sn]** = 100 mM **[cat]** = 10 mM			**[S]** = 50 mM **[Sn]** = 100 mM **[cat]** = 10 mM			**[S]** = 100 mM **[Sn]** = 100 mM **[cat]** = 5 mM			**[S]** = 100 mM **[Sn]** = 100 mM **[cat]** = 10 mM		
t/ min	**[S]**/ mM	**[P]**/ mM	**t**/ min	**[S]**/ mM	**[P]**/ mM	**t**/ min	**[S]**/ mM	**[P]**/ mM	**t**/ min	**[S]**/ mM	**[P]**/ mM	**t**/ min	**[S]**/ mM	**[P]**/ mM
0	91,0	0,0	0	182,0	0,0	0	45,5	0,0	0	87,0	0,0	0	87,0	0,0
2	67,0	7,0	2	154,0	6,0	2	27,5	4,0	2	72,0	3,0	2	72,0	4,0
4	63,0	10,0	4	144,0	12,0	4	26,0	5,5	4	69,0	4,0	4	65,0	5,0
6	61,0	12,0	6	130,0	16,0	6	24,5	7,0	6	66,0	4,0	6	60,0	5,0
8	56,0	14,0	8	128,0	28,0	8	22,5	9,0	8	62,0	5,0	8	53,0	5,0
10	52,0	19,0	10	114,0	40,0	10	19,5	12,0	11	57,0	5,0	11	46,0	6,0
12,5	47,0	24,0	12,5	102,0	48,0	12,5	16,5	15,5	14	52	7	14	38	6
25	29,0	41,0	25	74,0	68,0	25	9	23	32	31,0	9,0	32	15,0	8,0
29	25,0	45,0	29	72,0	72,0	29	8,5	24						

Table 2.18. Partial concentrations of substrate [S] and product [P] during the monitoring of the VTNA experiments F-H.

F			**G**			**H**		
[S] = 100 mM **[Sn]** = 100 mM **[cat]** = 10 mM			**[S]** = 100 mM **[Sn]** = 200 mM **[cat]** = 10 mM			**[S]** = 100 mM **[Sn]** = 50 mM **[cat]** = 10 mM		
t/ min	**[S]**/ mM	**[P]**/ mM	**t**/ min	**[S]**/ mM	**[P]**/ mM	**t**/ min	**[S]**/ mM	**[P]**/ mM
0	91,0	0,0	0	91,0	0,0	0	91,0	0,0
2	67,0	7,0	2	62,0	13,0	2	73,0	2,0
4	63,0	10,0	4	57,0	15,0	4	68,0	4,0
6	61,0	12,0	6	54,0	19,0	6	67,0	6,0
8	56,0	14,0	8	47,0	24,0	8	62,0	6,0
10	52,0	19,0	10	41,0	31,0	10	57,0	9,0
12,5	47,0	24,0	12,5	34,0	37,0	12,5	59,0	9,0
25	29,0	41,0	25	15,0	55,0	25	41,0	25,0

Reaction Progress Kinetic Analysis (RPKA): "Same excess"

Reaction conditions: [SM] = 100/50/50 mM, [$PhSnMe_3$] = 100/50/50, [$ClAuPEt_3$] = 10 mM, [Product] = 0/0/50 mM. Three MW vials equipped with magnetic stirrer containing substrate (cinnamyl bromide), ethyl benzoate as internal standard, trimethyl(phenyl)stannane, product and gold complex $ClAuPEt_3$ in deuterated toluene (4.8 mL) were prepared. Precisely, the following reagents were added in sequence into the different MW vials:

1) Substrate and internal standard stock solution (1.92/0.96/0.96 mL) previously prepared by adding deuterated toluene (4.2 mL) to the substrate (206.7 mg, 1.05 mmol) and internal standard (157.5 mg, 1.05 mmol).

2) Trimethyl(phenyl)stannane stock solution (640/320/320 mL) previously prepared by adding deuterated toluene (1.70 mL) to the stannane (306.1 mg, 1.27 mmol).

3) $ClAuPEt_3$ (16.7 mg, 48 mmol), added as solid.

4) Deuterated toluene (2.24/3.52/2.56 mL) obtaining a clear yellowish solution.

After preparing the solution, the reaction vessel was sealed and heated up to 110 ºC. The aliquotes for the kinetic monitoring were taken from the MW vials after releasing the pressure with a balloon and directly transferred to NMR tubes for measuring the corresponding ^1H NMR spectra (8 scans).

Catalyzed vs uncatalyzed reaction

Reaction conditions: [SM] = 100 mM, [$ClAuPEt_3$] = 0/0/5 mM. Three MW vials equipped with magnetic stirrer containing substrate (cinnamyl bromide), ethyl benzoate as internal standard, trimethyl(phenyl)stannane and gold complex $ClAuPEt_3$ in deuterated toluene (3.6 mL) were prepared. Precisely, the following reagents were added in sequence into the different MW vials:

1) Substrate, internal standard and trimethyl(phenyl)stannane stock solution (3.6 mL), previously prepared by adding deuterated toluene (13.8 mL) to the substrate (272.4 mg, 1.38 mmol), organostannane (275 mL, 1.52 mmol) and internal standard (207.6 mg, 1.38 mmol).

2) $ClAuPEt_3$ (0/0/6.3 mg), obtaining a clear yellowish solution.

After preparing the solution, the reaction vessel was sealed and heated up to 110 ºC. The aliquotes for the kinetic monitoring were taken from the previously cooled to 25 ºC MW vials (leaving one of the non-containing gold vials untouched during 64 h) and directly transferred to NMR tubes for measuring the corresponding ^1H NMR spectra (8 scans). After 64 h of reaction, in the untouched vial without gold, 6.3 mg of $ClAuP(CH_3)_3$ were added and the reaction was monitored until no more evolution to products.

2.8.4 Computed structures and energies

Table 2.19. Oxidative addition and reductive elimination in the coupling of $(R_3P)AuCH_3$ with methyl iodide reported by Kochi. B3LYP-D3/6- 31G(d,p)+SDD(Au, Br, Sn); SMD (iodomethane). HLT: B3LYP-D3/cc-pVTZ+cc-pVTZ-PP (Au, Br, Sn); SMD (iodomethane)

	R	E / Hartree	G / Hartree	E_{HLT} / Hartree
CH_3I		-51.3348	-51.3208	-335.7390
CH_3CH_3		-79.8408	-79.7861	-79.8680
A1	CH_3	-636.8716	-636.7554	-636.9601
TSA2		-688.1953	-688.0504	-972.6811
A3		-688.2324	-688.0842	-972.7223
A4		-716.6553	-716.4710	-716.7741
TSA3-5		-688.1933	-688.0482	-972.6791
A5		-608.4478	-608.3686	-892.9100
TSA4-6		-716.5790	-716.3975	-716.6952
A1	Ph	-1,212.1138	-1,211.8530	-1,212.3884
TSA2		-1,263.4388	-1,263.1476	-1,548.1097
A2		-1,263.4414	-1,263.1505	-1,548.1119
A3		-1,263.4722	-1,263.1768	-1,548.1470
A4		-1,291.8974	-1,291.5646	-1,292.2017
TSA3-5		-1,263.4343	-1,263.1421	-1,548.1053
A5		-1,183.6891	-1,183.4641	-1,468.3372
TAS4-6		-1,291.8397	-1,291.5118	-1,292.1431

Table 2.20. Oxidative addition, reductive elimination and transmetalation steps in the coupling of $(R_3P)AuI$ with allyl iodide in the presence of $Sn(CH_3)_4$. B3LYP-D3/6-31G(d,p)+SDD(Au, Br, Sn); SMD (iodomethane). HLT: B3LYP-D3/cc-pVTZ+cc-pVTZ-PP (Au, Br, Sn); SMD (iodomethane)

	E / Hartree	G / Hartree	E_{HLT} / Hartree
$Sn(CH_3)_4$	-163.0528	-162.9417	-374.1033
B1	-608.4478	-608.3688	-892.9101
TSB2	-771.4837	-771.2757	-1266.9903
B2	-771.4975	-771.2869	-1267.0062
B3	-771.4935	-771.2854	-1266.9998

TSB4	-771.4841	-771.2737	-1266.9921
SnI(CH_3)$_3$	-134.6115	-134.5376	-630.0380
B4	-636.8716	-636.7554	-636.9601
Allyl iodide	-128.7371	-128.6936	-413.1678
TSB5	-765.6047	-765.4305	-1050.1149
B5	-765.6109	-765.4358	-1050.1217
B6	-765.6364	-765.4557	-1050.1526
TSB1	-765.5993	-765.4262	-1050.1110
1-butane	-157.2390	-157.1549	-157.2940

Table 2.21. Oxidative addition, reductive elimination and transmetalation steps in the coupling of (R_3P)AuI with allyl iodide in the presence of vinyl-Sn(CH_3)$_3$. B3LYP-D3/6-31G(d,p)+SDD(Au, Br, Sn); SMD (iodomethane). HLT: B3LYP-D3/cc-pVTZ+cc-pVTZ-PP (Au, Br, Sn); SMD (iodomethane)

	E / Hartree	**G / Hartree**	**E_{HLT} / Hartree**
C1	-608.4478	-608.3688	-892.9101
(vinyl)Sn(CH_3)$_3$	-201.1277	-201.0123	-412.1928
TSC2	-809.5840	-809.3705	-1305.1040
C2	-809.5911	-809.3807	-1305.1091
C3	-809.5907	-809.3773	-1305.1084
TSC4	-809.5660	-809.3513	-1305.0882
SnI(CH_3)$_3$	-134.6115	-134.5376	-630.0380
C4	-674.9525	-674.8341	-675.0550
Allyl iodide	-128.7371	-128.6936	-413.1678
TSC5	-803.6851	-803.5067	-1088.2092
C5	-803.7146	-803.5303	-1088.2450
TSC1	-803.6864	-803.5077	-1088.2112
1,4-pentadiene	-195.3173	-195.2300	-195.3878

Table 2.22. Oxidative addition, reductive elimination and transmetalation steps in the coupling of (R_3P)AuI with allyl iodide in the presence of allyl-$Sn(CH_3)_3$. B3LYP-D3/6-31G(d,p)+SDD(Au, Br, Sn); SMD (iodomethane). HLT: B3LYP-D3/cc-pVTZ+cc-pVTZ-PP (Au, Br, Sn); SMD (iodomethane)

	E / Hartree	G / Hartree	E_{HLT} / Hartree
D1	-608.4477	-608.3688	-892.9100
(allyl)$Sn(CH_3)_3$	-240.4527	-240.3124	-451.5313
TSD3	-848.8875	-848.6463	-1344.423
$SnI(CH_3)_3$	-134.6115	-134.5376	-630.0379
D3	-714.2733	-714.1281	-714.3895
Allyl iodide	-128.7371	-128.6936	-413.1677
TSD4	-843.0104	-842.8052	-1127.545
D4	-843.0421	-842.8322	-1127.585
TSD1	-843.0137	-842.8088	-1127.549
1,5-hexadiene	-234.6371	-234.5241	-234.7197

Table 2.23. Oxidative addition, reductive elimination and transmetalation steps in the coupling of (R_3P)AuI with allyl iodide in the presence of Ph-$Sn(CH_3)_3$. B3LYP-D3/6-31G(d,p)+SDD(Au, Br, Sn); SMD (iodomethane). HLT: B3LYP-D3/cc-pVTZ+cc-pVTZ-PP (Au, Br, Sn); SMD (iodomethane)

	E / Hartree	G / Hartree	E_{HLT} / Hartree
E1	-608.4478	-608.3688	-892.9101
$PhSn(CH_3)_3$	-354.7987	-354.6391	-565.9127
E2	-963.2550	-962.9991	-1458.8198
TSE3	-963.2393	-962.9785	-1458.8100
E3	-828.6236	-828.4592	-828.7753
Allyl iodide	-128.7371	-128.6936	-413.1678
$SnI(CH_3)_3$	-134.6115	-134.5376	-630.0380
TSE4	-957.3559	-957.1318	-1241.9289
E4	-957.3871	-957.1590	-1241.9662
TSE1	-957.3582	-957.1333	-1241.9314
allylbenzene	-348.9881	-348.8572	-349.1066

Table 2.24. Comparative in the transmetalation pathway for the formation of E3 when using different halides X (Cl, Br, I). B3LYP-D3/6- 31G(d,p)+SDD(Au, Br, Sn); SMD (toluene). HLT: B3LYP-D3/cc-pVTZ+cc-pVTZ-PP (Au, Br, Sn); SMD (toluene)

	X	E / Hartree	G / Hartree	E_{HLT} / Hartree
E1	Cl	-1057.2123	-1057.1302	-1057.3302
E2		-1412.0005	-1411.7405	-1623.2239
TSE3		-1411.9954	-1411.7323	-1623.2221
$SnCl(CH_3)_3$		-583.3875	-583.3113	-794.4690
E1	Br	-610.4051	-610.3247	-1014.0210
E2		-965.2002	-964.9397	-1579.9165
TSE3		-965.1933	-964.9312	-1579.9149
$SnBr(CH_3)_3$		-136.5766	-136.5019	-751.1570
E1	I	-608.4416	-608.3624	-892.9046
E2		-963.2430	-962.9849	-1458.8078
TSE3		-963.2314	-962.9718	-1458.8025
$SnI(CH_3)_3$		-134.6084	-134.5340	-630.0364
2.7		-354.7975	-354.6373	-565.9114
E3		-828.6188	-828.4542	-828.7708

Table 2.25. Discarded mechanism for the formation of cross-coupled product. B3LYP-D3/6- 31G(d,p)+SDD(Au, Br, Sn); SMD (toluene). HLT: B3LYP-D3/cc-pVTZ+cc-pVTZ-PP (Au, Br, Sn); SMD (toluene)

	E / Hartree	G / Hartree	E_{HLT} / Hartree
2.7	-354.7975	-354.6373	-565.9115
2.13	-136.5766	-136.5019	-751.1570
2.10	-361.7805	-361.6614	-765.4384
2.11	-580.0647	-579.8597	-580.2576
TS2.13	-716.5479	-716.2525	-1331.3044

Table 2.26. Formation of π-allyl intermediate and reductive elimination. B3LYP-D3/6-31G(d,p)+SDD(Au, Br, Sn); SMD (toluene). HLT: B3LYP-D3/cc-pVTZ+cc-pVTZ-PP (Au, Br, Sn); SMD (toluene)

	E / Hartree	**G / Hartree**	**E_{HLT} / Hartree**
E4	-1190.4205	-1190.1163	-1594.2275
TSE5	-1190.3970	-1190.0933	-1594.1949
E5	-1190.3970	-1190.0944	-1594.1945
TSE6	-1190.3961	-1190.0923	-1594.1942
E6	-1190.4119	-1190.1068	-1594.2131
TSE4-1	-1190.3865	-1190.0837	-1594.1872
TSE6-1	-1190.3885	-1190.0856	-1594.1861
E1	-610.4051	-610.3247	-1014.0210

Table 2.27. Alternative discarded pathways to the oxidative addition/reductive elimination mechanism proposed. B3LYP-D3/6- 31G(d,p)+SDD(Au, Br, Sn); SMD (toluene). HLT: B3LYP-D3/cc-pVTZ+cc-pVTZ-PP (Au, Br, Sn); SMD (toluene)

	E / Hartree	**G / Hartree**	**E_{HLT} / Hartree**
E3	-828.6189	-828.4543	-828.7708
E1	-610.4051	-610.3247	-1014.0210
2.10	-361.7805	-361.6614	-765.4384
2.11	-580.0647	-579.8597	-580.2576
E7	-1190.3955	-1190.0948	-1594.1935
TSE7-1	-1190.3878	-1190.0876	-1594.1843
TSE3-1	-1190.3784	-1190.0791	-1594.1719
2.12	-580,0522	-579,8462	-580,2450
TS'E3-1	-1190.3679	-1190.0665	-1594.1594

Table 2.28. Oxidative addition, reductive elimination and transmetalation processes, including intermediates and transition states. B3LYP-D3/6- 31G(d,p)+SDD(Au, Br, Sn); SMD (toluene). HLT: B3LYP-D3/cc-pVTZ+cc-pVTZ-PP (Au, Br, Sn); SMD (toluene)

	E / Hartree	**G / Hartree**	**E_{HLT} / Hartree**
2.7	-354.7975	-354.6373	-565.9115
E1	-610.4051	-610.3247	-1014.0210
E2	-965.2002	-964.9397	-1579.9165
TSE3	-965.1933	-964.9312	-1579.9149
2.13	-136.5766	-136.5019	-751.1570
E3	-828.6189	-828.4543	-828.7708
2.1	-361.7805	-361.6616	-765.4384
TSE4	-1190.3905	-1190.0898	-1594.1868
E4	-1190.4205	-1190.1165	-1594.2275
TSE1	-1190.3865	-1190.0839	-1594.1872
2.11	-580.0647	-579.8598	-580.2576

Table 2.29. Benchmark of geometries. Functional-D3/cc-pVTZ+cc-pVTZ-PP(Au, Br, Sn); SMD (toluene). Potential energies in Hartrees.

	2.7	**E1**	**E2**	**TSE3**	**2.15**	**2.10**
B3LYP	-565.9115	-1014.0210	-1579.9165	-1579.9149	-751.1570	-765.4384
M06	-565.6029	-1013.8585	-1579.4470	-1579.4408	-751.0723	-765.1547
M062X	-565.5859	-1013.8461	-1579.4157	-1579.4058	-751.0508	-765.3718
BMK	-564.7384	-1011.7452	-1576.4804	-1576.4762	-748.7555	-763.7669
BP86	-565.9383	-1014.2298	-1580.1588	-1580.1633	-751.2946	-765.5277
ωB97XD	-565.7634	-1013.9683	-1579.7138	-1579.7072	-751.1031	-765.2924

	E3	**TSE4**	**E4**	**TSE1**	**2.11**
B3LYP	-828.7708	-1594.1868	-1594.2275	-1594.1872	-580.2576
M06	-828.3806	-1593.5057	-1593.5509	-1593.5152	-579.7502
M062X	-828.3713	-1593.7045	-1593.7570	-1593.7199	-579.9771
BMK	-827.7254	-1591.4631	-1591.5226	-1591.4725	-579.8176
BP86	-828.8718	-1594.3850	-1594.4280	-1594.3884	-580.2332
ωB97XD	-828.6210	-1593.8795	-1593.9297	-1593.8881	-580.0195

Table 2.30. Second benchmark of geometries. Functional-D3/def2-TZVP; gas phase. Potential energies in Hartrees.

	2.7	**E1**	**E2**	**TSE3**
B3LYP	-565.9089	-3171.2769	-3737.1749	-3737.1732
M06	-565.9169	-3171.1292	-3737.0335	-3737.0338
M06	-565.6058	-3170.9725	-3736.5687	-3736.5634
M062X	-565.5783	-3170.9966	-3736.5642	-3736.5540
M06-HF	-565.5130	-3171.1208	-3736.6255	-3736.6193
BMK	-564.7399	-3169.0753	-3733.8168	-3733.8120
BP86	-565.9368	-3171.6312	-3737.5639	-3737.5683
ωB97XD	-565.7616	-3171.2552	-3737.0041	-3736.9976
DPLNO-CCSD(T)	-564.3500	-3168.4125	-3732.7494	-3732.7441

	2.15	**2.10**	**E3**
B3LYP	-2908.4136	-2922.6921	-828.7688
M06	-2908.3433	-2922.4941	-828.6965
M06	-2908.1859	-2922.2674	-828.3853
M062X	-2908.2044	-2922.5219	-828.3617
M06-HF	-2908.2715	-2922.7871	-828.3559
BMK	-2906.0872	-2921.0968	-827.7257
BP86	-2908.6951	-2922.9255	-828.8725
ωB97XD	-2908.3898	-2922.5766	-828.6207
DPLNO-CCSD(T)	-2905.9115	-2920.3815	-826.8476

	TSE4	E4	TSE1	2.11
B3LYP	-3751.4372	-3751.4789	-3751.4393	-580.2510
M06	-3751.1684	-3751.2111	-3751.1731	-580.1323
M06	-3750.6219	-3750.6688	-3750.6330	-579.7512
M062X	-3750.8426	-3750.8972	-3750.8607	-579.9651
M06-HF	-3751.0973	-3751.1644	-3751.1216	-580.0979
BMK	-3748.7911	-3748.8516	-3748.8035	-579.8163
BP86	-3751.7834	-3751.8264	-3751.7876	-580.2279
ωB97XD	-3751.1608	-3751.2136	-3751.1721	-580.0143
DPLNO-CCSD(T)	-3747.1801	-3747.2501	-3747.1993	-578.8805

Table 2.31. Mechanisms explored on stereochemistry. B3LYP-D3/6- 31G(d,p)+SDD(Au, Br, Sn); SMD (toluene). HLT: B3LYP-D3/cc-pVTZ+cc-pVTZ-PP (Au, Br, Sn); SMD (toluene)

	E / Hartree	G / Hartree	E_{HLT} / Hartree
G1	-1303.9794	-1303.6532	-1707.8320
TSG2	-1303.9508	-1303.6249	-1707.7921
G2	-1303.9787	-1303.6532	-1707.8305
TSG3	-1303.9457	-1303.6218	-1707.7877
G3	-1303.9793	-1303.6492	-1707.8300
G4	-1303.9806	-1303.6513	-1707.8319
TSG5	-1303.9409	-1303.6124	-1707.7859
H1	-1303.9873	-1303.6590	-1707.8370
TSH2	-1303.9564	-1303.6281	-1707.7961
H2	-1303.9614	-1303.6324	-1707.8011
TSH3	-1303.9565	-1303.6229	-1707.7984
H3	-1303.9833	-1303.6529	-1707.8315
TSH4	-1303.9454	-1303.6185	-1707.7853

H4	-1303.9719	-1303.6440	-1707.8144
TSH5	-1303.9485	-1303.6170	-1707.7892
I1	-1303.9547	-1303.6318	-1707.7992
TSI2	-1303.9485	-1303.6207	-1707.7899
I2	-610.4051	-610.3247	-1014.0210
2.20	-693.6243	-693.3930	-693.8644
2.21	-693.6257	-693.3926	-693.8626

UNIVERSITAT ROVIRA I VIRGILI
MECHANISTIC STUDIES ON GOLD(I) AND GOLD(III) CATALYTIC TRANSFORMATIONS
Isabel Arranz De La Calle

Chapter III

Generation of Gold(I) Carbenes via Transmetalation of Zinc Reagents

UNIVERSITAT ROVIRA I VIRGILI
MECHANISTIC STUDIES ON GOLD(I) AND GOLD(III) CATALYTIC TRANSFORMATIONS
Isabel Arranz De La Calle

3.1 Introduction

3.1.1 Gold(I) carbenes

Carbenes have been often proposed as key intermediates in many gold(I)-catalyzed transformations.[1] Within these transformations, the cycloisomerization of 1,*n*-enynes has gained significant interest due to its ability to produce complex structures in an atom-economical manner (Scheme 3.1a).[2] Other notable examples include the nucleophilic addition of *N*-oxides or sulfoxides to electrophilic (η^2-alkyne)gold(I) complexes (Scheme 3.1b),[3] and the cycloaddition of dialkyl compounds, which yields gold vinylidene intermediates (Scheme 3.1c).[4] Besides reactions involving alkynes, processes such as the gold(I)-catalyzed decomposition of diazo compounds (Scheme 3.1d),[5] and the opening of cyclopropenes (Scheme 3.1e)[6] have also been proposed to

1 See reviews on this topic: a) Wang, Y.; Muratore, M. E.; Echavarren, A. M. Gold Carbene or Carbenoid: Is There a Difference?, *Chem. – Eur. J.* **2015**, *21*, 7332–7339. b) Harris, R. J.; Widenhoefer, R. A. Gold Carbenes, Gold-Stabilized Carbocations, and Cationic Intermediates Relevant to Gold-Catalysed Enyne Cycloaddition, *Chem. Soc. Rev.* **2016**, *45*, 4533–4551. c) Navarro, M.; Bourissou, D. Chapter Two - π-Alkene/Alkyne and Carbene Complexes of Gold(I) Stabilized by Chelating Ligands. *Adv. Organomet. Chem.*, **2021**, *76*, 101–144.

2 a) López, S.; Herrero-Gómez, E.; Pérez-Galán, P.; Nieto-Oberhuber, C.; Echavarren, A. M. Gold(I)-Catalyzed Intermolecular Cyclopropanation of Enynes with Alkenes: Trapping of Two Different Gold Carbenes, *Angew. Chem. Int. Ed.* **2006**, *45*, 6029–6032. b) Taduri, B. P.; Sohel, S. M. A.; Cheng, H.-M.; Lin, G.-Y.; Liu, R.-S. Pt- and Au-Catalyzed Oxidative Cyclization of 2-Ethenyl-1-(Prop-2′-Yn-1′-Ol)Benzenes to Naphthyl Aldehydes and Ketones: Catalytic Oxidation of Metal-Alkylidene Intermediates Using H_2O and H_2O_2, *Chem. Commun.* **2007**, No. 24, 2530–2532. c) Escribano-Cuesta, A.; López-Carrillo, V.; Janssen, D.; Echavarren, A. M. Gold-Catalyzed Reactions of 1,5- and 1,6-Enynes with Carbonyl Compounds: Cycloaddition vs. Metathesis, *Chem. – Eur. J.* **2009**, *15*, 5646–5650. d) Pérez-Galán, P.; Martin, N. J. A.; Campaña, A. G.; Cárdenas, D. J.; Echavarren, A. M. Carbocations or Cyclopropyl Gold Carbenes in Cyclizations of Enynes, *Chem. – Asian J.* **2011**, *6*, 482–486.

3 a) Shapiro, N. D.; Toste, F. D. Rearrangement of Alkynyl Sulfoxides Catalyzed by Gold(I) Complexes, *J. Am. Chem. Soc.* **2007**, *129*, 4160–4161. b) Ye, L.; Cui, L.; Zhang, G.; Zhang, L. Alkynes as Equivalents of α-Diazo Ketones in Generating α-Oxo Metal Carbenes: A Gold-Catalyzed Expedient Synthesis of Dihydrofuran-3-Ones, *J. Am. Chem. Soc.* **2010**, *132*, 3258–3259. c) Schulz, J.; Jašíková, L.; Škríba, A.; Roithová, J. Role of Gold(I) α-Oxo Carbenes in the Oxidation Reactions of Alkynes Catalyzed by Gold(I) Complexes, *J. Am. Chem. Soc.* **2014**, *136*, 11513–11523.

4 a) Ye, L.; Wang, Y.; Aue, D. H.; Zhang, L. Experimental and Computational Evidence for Gold Vinylidenes: Generation from Terminal Alkynes via a Bifurcation Pathway and Facile C–H Insertions, *J. Am. Chem. Soc.* **2012**, *134*, 31–34. b) Hashmi, A. S. K.; Braun, I.; Nösel, P.; Schädlich, J.; Wieteck, M.; Rudolph, M.; Rominger, F. Simple Gold-Catalyzed Synthesis of Benzofulvenes—*Gem*-Diaurated Species as "Instant Dual-Activation" Precatalysts, *Angew. Chem. Int. Ed.* **2012**, *18*, 4456–4460.

5 a) Fructos, M. R.; Belderrain, T. R.; de Frémont, P.; Scott, N. M.; Nolan, S. P.; Díaz-Requejo, M. M.; Pérez, P. J. A Gold Catalyst for Carbene-Transfer Reactions from Ethyl Diazoacetate, *Angew. Chem.* **2005**, *117*, 5418–5422. b) Prieto, A.; Fructos, M. R.; Mar Díaz-Requejo, M.; Pérez, P. J.; Pérez-Galán, P.; Delpont, N.; Echavarren, A. M. Gold-Catalyzed Olefin Cyclopropanation, *Tetrahedron* **2009**, *65*, 1790–1793.

6 a) Li, C.; Zeng, Y.; Wang, J. Au-Catalyzed Isomerization of Cyclopropenes: A Novel Approach to Indene Derivatives, *Tetrahedron Lett.* **2009**, *50*, 2956–2959. b) Hadfield, M. S.; Bauer, J. T.; Glen, P. E.; Lee, A.-L. Gold(I)-Catalysed Alcohol Additions to Cyclopropenes, *Org. Biomol. Chem.* **2010**, *8*, 4090–4095.

generate these highly electrophilic species. More recently, metallocarbene species have been identified as crucial in the retro-Buchner reaction of cycloheptatrienes (Scheme 3.1f).[7]

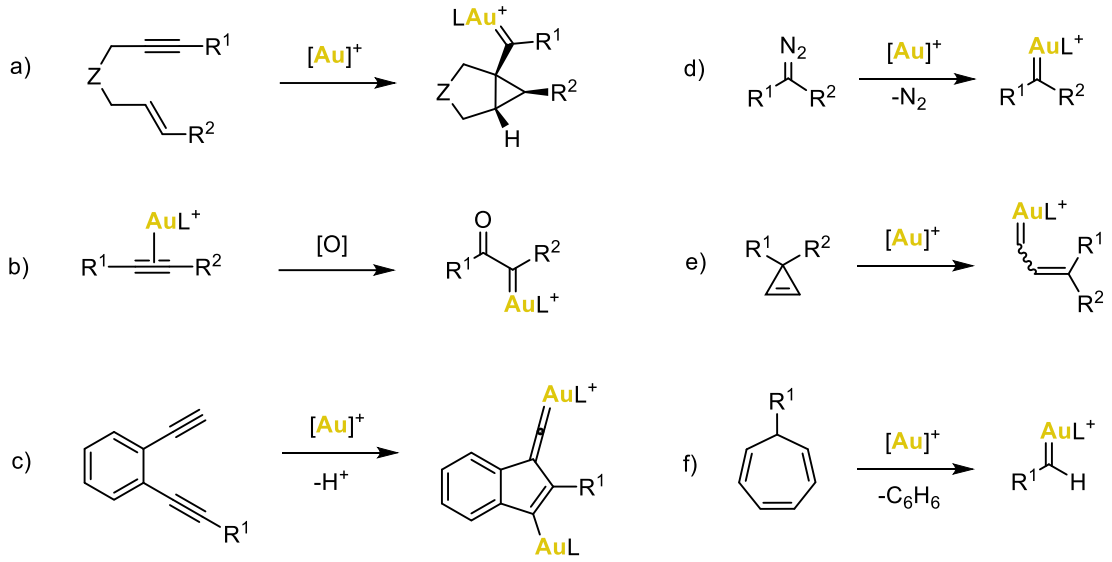

Scheme 3.1. Generic reactions involving gold(I) carbenes as main intermediates.

Although the nature of gold(I) carbenes was questioned in the past, in recent decades numerous theoretical and experimental studies have suggested that the reactivity of these species can be explained by a continuum ranging from a metal-coordinated carbocation to a metal-stabilized singlet carbene (Scheme 3.2).[1a]

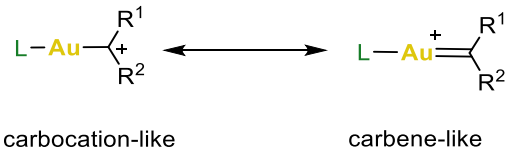

Scheme 3.2. Resonance forms used to represent gold(I) carbenes.

In 2009, Toste and Goddard presented a bonding model for gold (I) carbenes. They proposed that both the ligand (L) and the carbene can donate their electron pairs to gold, forming a three-center four-electron σ-hyperbond (Figure 3.1, left). Furthermore, the gold center contributes with π-backdonation from its filled 5*d* orbitals to both the ancillary ligand and the carbene moiety (Figure 3.1, right).[8]

7 a) Solorio-Alvarado, C. R.; Wang, Y.; Echavarren, A. M. Cyclopropanation with Gold(I) Carbenes by Retro-Buchner Reaction from Cycloheptatrienes, *J. Am. Chem. Soc.* **2011**, *133*, 11952–11955. b) Yin, X.; Mato, M.; Echavarren, A. M. Gold(I)-Catalyzed Synthesis of Indenes and Cyclopentadienes: Access to (±)-Laurokamurene B and the Skeletons of the Cycloaurenones and Dysiherbols, *Angew. Chem.* **2017**, *129*, 14783–14787.

8 Benitez, D.; Shapiro, N. D.; Tkatchouk, E.; Wang, Y.; Goddard, W. A.; Toste, F. D. A Bonding Model for Gold(I) Carbene Complexes, *Nat. Chem.* **2009**, *1*, 482–486.

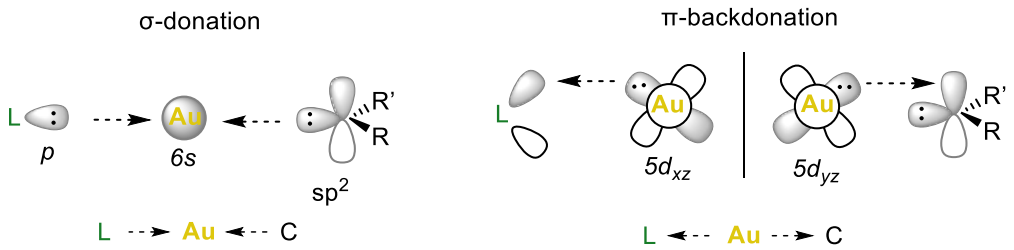

Figure 3.1. Bonding diagram of the most important interactions in gold(I) carbenes.

Taking into account the competition of the ligand and the carbene for the gold(I) π-backdonation, the bonding position degree on the spectrum is primarily influenced by the electronic properties of both fragments (Figure 3.2). A decrease in carbon-gold σ-bonding and an increase in gold-carbon π-bonding will result in structures with more carbene-like characteristics. Additionally, ancillary ligands that are strong σ-donors and weak π-acids will further enhance the carbene-like character by promoting π-backdonation from gold to carbon.

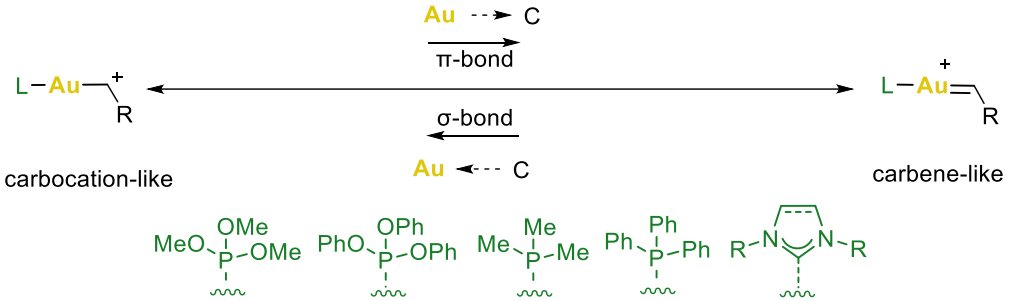

Figure 3.2. Ancillary ligand influence on the carbocation/carbene character of gold(I) carbenes.

Gold(I) carbenes can be considered as an extreme form of Fischer carbenes, which have a π-donating group attached to the carbenic center. This group stabilizes the empty π orbital on the carbene carbon through π-donation from one of the substituent lone electron pairs (Figure 3.3, left). Consequently, the metal-to-carbon π-backdonation is weak, making the carbon atom positively charged and the carbene showed an electrophilic character. Since gold is the most electronegative of all transition metals, its π-backdonation is minimal, resulting in highly electrophilic carbenes (Figure 3.3, right).

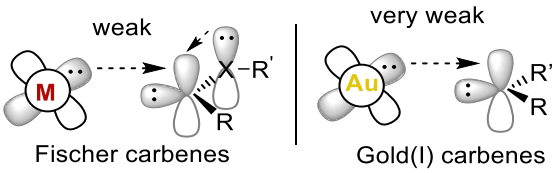

Figure 3.3. Bonding structure of Fischer carbenes and gold(I) carbenes.

3.1.2 Gold(I) carbenoids

Given the weak π-backdonation from gold(I), some authors suggested using the term gold(I) carbenoid instead of gold(I) carbene.[9] Although both species exhibit similar reactivity, carbenoids are organometallic species with reactivity related to carbenes, where an sp^3 carbon is bonded to a metal (M) and a leaving group (X). The removal of the leaving group X will generate the metallocarbene species (Figure 3.4).[10] Several studies have been conducted on the synthesis and analysis of gold(I) carbenoids.

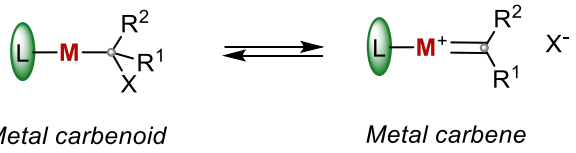

Figure 3.4. Interconversion between metal carbenoids and carbenes.

The first well-characterized example of a gold(I) carbenoid was reported in 1977. In this pioneering work, the synthesis of the chloromethylgold(I) complex **3.1** utilized toxic and potentially explosive diazomethane (Scheme 3.3).[11] In 1999, gold(I) carbenoid **3.1** was synthesized using an alternative method involving the in situ formation of [$Mg(CH_2Cl)Cl$] at low temperature (Scheme 3.3).[12] Remarkably, the iodomethylgold(I) carbenoid **3.2** rapidly decomposes at room temperature producing ethylene.

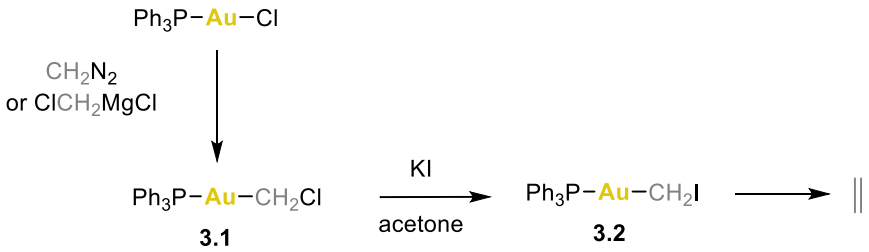

Scheme 3.3. Synthetic procedure of gold carbenoids **3.1** and **3.2**.

Other methods to synthesize gold(I) carbenoids with various substituents at the Csp^3 center bound to gold consist of treating the complex $(Ph_3PAu)_3OBF_4$ with a base in the presence of $CHCl_3$ and

9 Seidel, G.; Fürstner, A. Structure of a Reactive Gold Carbenoid, *Angew. Chem. Int. Ed.* **2014**, *53*, 4807–4811.

10 a) Bernardi, F.; Bottoni, A.; Miscione, G. P. Metal Carbene or Carbenoid Complexes? A Theoretical Study of the Active Form of Transition Metal Catalysts in Cyclopropanation and Olefin Metathesis Reactions, *Organometallics* **2000**, *19*, 5529–5532. b) Closs, G. L.; Moss, R. A. Carbenoid Formation of Arylcyclopropanes from Olefins, Benzal Bromides, and Organolithium Compounds and from Photolysis of Aryldiazomethanes. *J. Am. Chem. Soc.* **1964**, *86*, 4042-4053.

11 Nesmeyanov, A. N.; Perevalova, É. G.; Smyslova, E. I.; Dyadchenko, V. P.; Grandberg, K. I. Reaction of Gold Compounds and Diazomethane, *Bull. Acad. Sci. USSR Div. Chem. Sci.* **1977**, *26*, 2417–2419.

12 Steinborn, D.; Becke, S.; Herzog, R.; Günther, M.; Kircheisen, R.; Stoeckli-Evans, H.; Bruhn, C. Heteroatomfunktionalisierte Methylgold-Komplexe: Synthese und Struktur von Chlormethyl(triphenylphosphin)- und Phenylthiomethyl(trimethylphosphin)gold, *Z. Für Anorg. Allg. Chem.* **1998**, *624*, 1303–1307.

$CHCl_2CN$, which yields $Ph_3PAuCCl_3$ **3c**,[13] and $Ph_3PAuCCl_2CN$ **3d**, [14] respectively. Additionally, the reaction of $(CH_3)_3PAuCl$ with $LiCH_2SPh$ resulted in the stable phenylthiomethylgold(I) complex **3e** (Figure 3.5).[12]

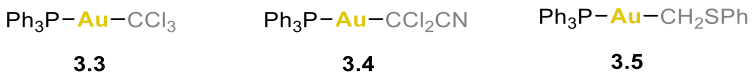

Figure 3.5. Gold(I) carbenoids bearing different substituents.

As mentioned before, metal carbenoids exhibit comparable reactivity to their carbene counterparts,[10b,15] and provide a promising alternative to otherwise non-isolable species. Until 2017, there was limited knowledge regarding gold(I) carbenoids and their reactivity.[11-14] At that time, our group presented the synthesis of readily accessible gold(I) carbenoids with bulky ligands, serving as gold carbene equivalents in solution.[16] The method consists on the methanol-promoted decomposition of trimethylsilyldiazomethane at 25 ºC (Scheme 3.4), thus avoiding the use of potentially explosive diazomethane or low temperature in situ procedures. Treating phosphine, phosphite, and NHC gold chloride complexes with trimethylsilyldiazomethane in benzene solution in the presence of methanol yielded gold carbenoids **3.1a–d** in a few minutes.

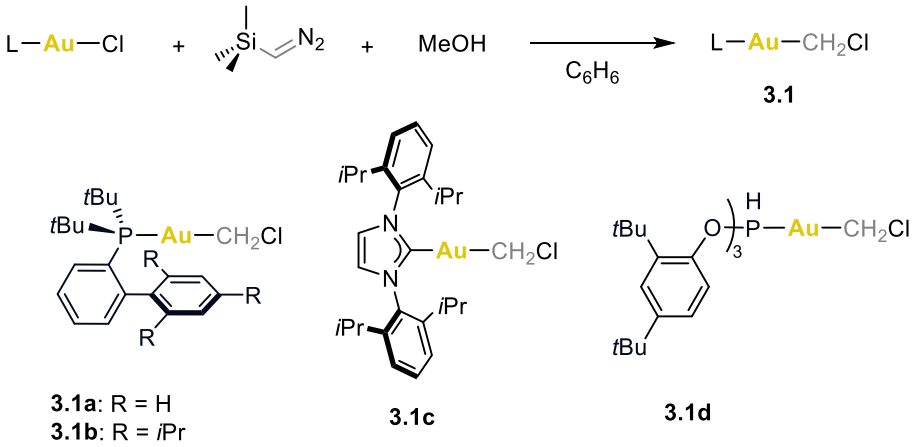

Scheme 3.4. Synthesis of chloromethylgold(I) complexes **3.1**.

These carbenoids, upon activation with a chloride scavenger, show the expected reactivity of gold(I) carbenes in solution: homocoupling, olefin cyclopropanation and Buchner reaction.

13 Perevalova, E. G.; Smyslova, E. I.; Grandberg, K. I. Auration of Chloroform, *Bull. Acad. Sci. USSR Div. Chem. Sci.* **1982**, *31*, 2506–2506.

14 Perevalova, É. G.; Struchkov, Yu. T.; Dyadchenko, V. P.; Smyslova, E. I.; Slovokhotov, Yu. L.; Grandberg, K. I. Cyanomethyl Derivatives of Gold, *Bull. Acad. Sci. USSR Div. Chem. Sci.* **1983**, *32*, 2529–2536.

15 H. Gessner, V. Stability and Reactivity Control of Carbenoids: Recent Advances and Perspectives, *Chem. Commun.* **2016**, *52*, 12011–12023.

16 Sarria Toro, J. M.; García-Morales, C.; Raducan, M.; Smirnova, E. S.; Echavarren, A. M. Gold(I) Carbenoids: On-Demand Access to Gold(I) Carbenes in Solution, *Angew. Chem. Int. Ed.* **2017**, *56*, 1859–1863.

3.1.3 Characterization of gold(I) carbenes

To characterize gold(I) carbenes, the presence of heteroatoms or highly conjugated systems at the carbene center is essential, in order to compensate the lack of the stabilization that a stronger π-donating metal would provide. However, if these substituents become too effective, the typical reactivity of an electrophilic carbene is internally "quenched," causing the resulting complex to lose the expected reactivity for gold catalysis.[17]

Aumann generated in 1982 the first Fischer-type gold(I) carbene, using a transmetalation protocol from a tungsten carbene (Scheme 3.5).[18] Employing dimethylamine and phenyl as substituents directly attached to the carbene carbon, gold(I) carbene **3.6** was sufficiently stabilized and isolated in solid form.

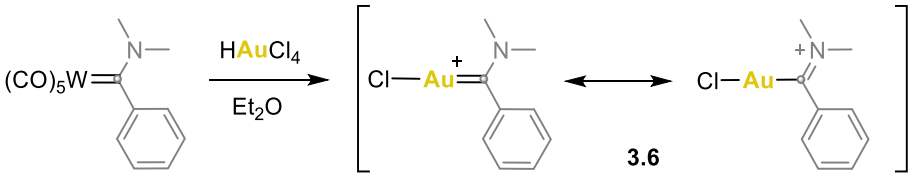

Scheme 3.5. First synthesis towards isolable gold(I) carbene **3.6** and main resonance forms.

A well-known approach for obtaining carbene complexes of late transition metals involves carbene transfer between the two metal centers.[19] Gold(I) carbenes bearing common ancillary ligands in gold(I) catalysis like NHC or phosphine **3.7**, were synthesized by formal transmetalation of chromium carbenes (Scheme 3.6).[20]

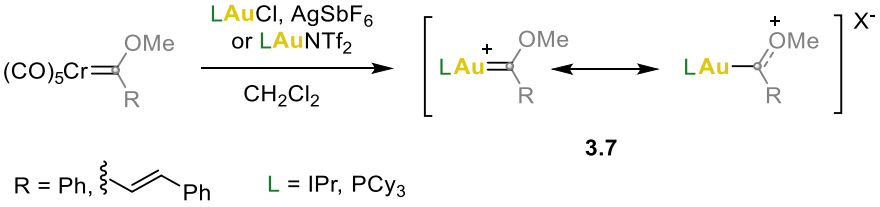

Scheme 3.6. Synthesis of gold(I) carbenes stabilized by heteroatoms via transmetalation.

17 Fürstner, A.; Davies, P. W. Catalytic Carbophilic Activation: Catalysis by Platinum and Gold Pi Acids, *Angew. Chem. Int. Ed Engl.* **2007**, *46*, 3410–3449.

18 Schubert U.; Ackermann, K.; Aumann, R. Chloro (dimethylamino(phenyl) carbene) gold(I), $ClAuC(C_6H_5)N(CH_3)_2$, *Cryst. Struct. Commun*, **1982**., *11*, 591-594.

19 Gómez-Gallego, M.; Mancheño, M. J.; Sierra, M. A. Catalytic Transmetalation from Group 6 Fischer Carbene Complexes: An Emerging Powerful Tool in Organic Synthesis, *Acc. Chem. Res.* **2005**, *38*, 44–53.

20 a) Seidel, G.; Gabor, B.; Goddard, R.; Heggen, B.; Thiel, W.; Fürstner, A. Gold Carbenoids: Lessons Learnt from a Transmetalation Approach, *Angew. Chem.* **2014**, *126*, 898–901. b) Fañanás-Mastral, M.; Aznar, F. Carbene Transfer Reactions from Chromium(0) to Gold(I): Synthesis and Reactivity of New Fischer-Type Gold(I) Alkenyl Carbene Complexes, *Organometallics* **2009**, *28*, 666–668.

Following the same synthetic route, Brooner and Widenhoefer published the access to cyclopropyl methoxy gold(I) carbenes **3.8** (Scheme 3.7).[21] Their X-Ray structures provided, for the first time, experimental proof of gold's π-back donation to the carbene, based on the observed bond length perturbations in the cyclopropyl ring.

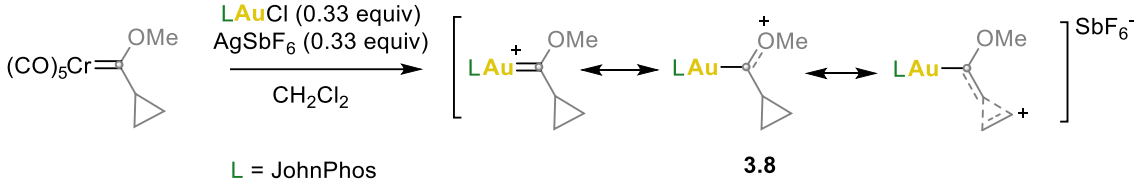

Scheme 3.7. Fisher-type gold(I) carbene synthesis and main resonance forms.

In all cases (**3.7** and **3.8**), a methoxy group is bonded to C1, resulting in air-stable compounds, though absence of carbene-like reactivity was observed. Apart from having heteroatoms attached to the carbene, the optimal balance has been achieved by conjugating the carbene with suitably substituted arenes,[22] through extensive steric shielding that prevents any reaction partner from accessing the highly electrophilic site,[23] or by delocalizing the charge density within an aromatic ring system.[24]

The first example of a gold(I) carbene without π-conjugated heteroatoms as substituents was reported by Fürstner's team in 2014.[22] Diaryl gold(I) carbene **3.9** possesses electron-rich substituents in the para position of the aryl groups to stabilize the carbene (Scheme 3.8). The procedure in this case proceeds at -50 ºC, obtaining gold(I) carbene complex **3.9**, which exhibited carbene reactivity, leading to cyclopropanation reactions when treated with electron-rich alkenes.

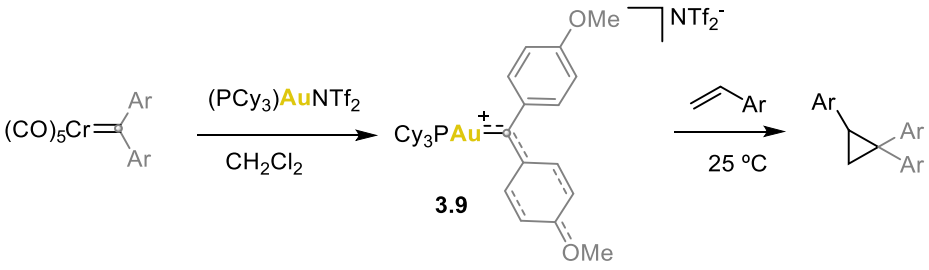

Scheme 3.8. Synthesis of diaryl gold(I) carbene **3.9** and gold(I)-promoted cyclopropanation.

Following an alternative strategy different from the abovementioned carbene transfer, in 2014 Widenhoefer and coworkers were able to generate complex **3.10**, bearing JohnPhos as ancillary

21 Brooner, R. E. M.; Widenhoefer, R. A. Experimental Evaluation of the Electron Donor Ability of a Gold Phosphine Fragment in a Gold Carbene Complex, *Chem. Commun.* **2014**, *50*, 2420–2423.
22 Seidel, G.; Fürstner, A. Structure of a Reactive Gold Carbenoid, *Angew. Chem. Int. Ed.* **2014**, *53*, 4807–4811.
23 Hussong, M. W.; Rominger, F.; Krämer, P.; Straub, B. F. Isolation of a Non-Heteroatom-Stabilized Gold–Carbene Complex, *Angew. Chem. Int. Ed.* **2014**, *53*, 9372–9375.
24 Harris, R. J.; Widenhoefer, R. A. Synthesis, Structure, and Reactivity of a Gold Carbenoid Complex That Lacks Heteroatom Stabilization, *Angew. Chem. Int. Ed.* **2014**, *53*, 9369–9371.

ligand, via hydride abstraction (Scheme 3.9).[24] The stability of cycloheptatrienylidene **3.10** is given by the delocalization of the charge over the aromatic fragment.

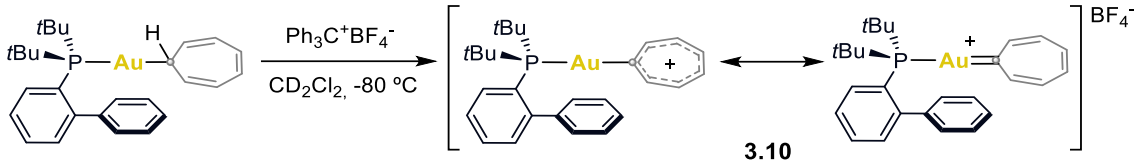

Scheme 3.9. Hydride abstraction synthetic strategy for the generation of gold(I) carbene **3.10**.

In parallel, in the same year, Straub and coworkers reported the isolation of gold(I) carbene **3.12** by treatment of gold(I) complex **3.11** with (dimesityl)diazomethane (Scheme 3.10).[23] Through the synthesis and characterization of **3.12** it was possible to support the model proposed by Toste,[8] where it was hypothesized that σ-donating ligands in gold(I) would enhance the π-backdonation required for the carbene stability. Furthermore, **3.12** resulted to be highly stable due to the NHC ancillary ligand that provided steric shielding of the carbene center. However, no typical carbene reactivity was observed.

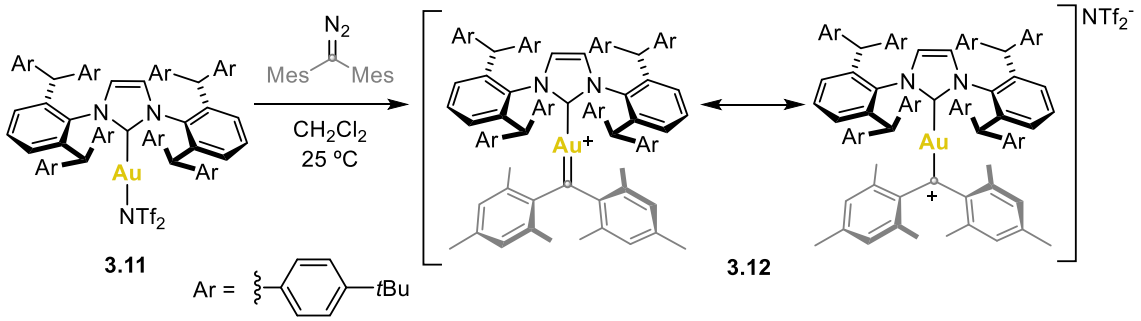

Scheme 3.10. Gold(I) carbene **3.12** synthesis and main resonance forms.

3.2 Objectives

Seeking for an alternative synthesis of gold(I) carbenoids and moving away from the use of diazo compounds,[16,25] we proposed to develop a new method based on the transmetalation of organozinc reagents $XZnCH_2I$ (X = Cl, Br)[26] **3.13** with gold(I) complexes LAuCl (Scheme 3.11).[12]

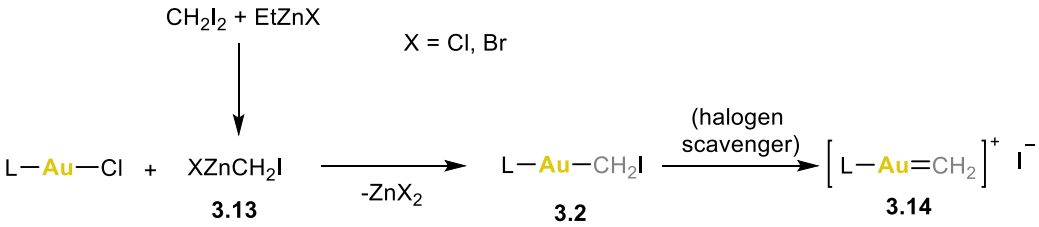

Scheme 3.11. Generation of gold(I) carbenoids **3.2** by transmetalation with organozinc reagents.

We wanted to investigate as well the formation of the corresponding unsubstituted gold(I) carbenes 3.14, that could occur spontaneously in situ from 3.2 carbenoids,[16] or could be induced by halogen scavengers (Scheme 3.11).

The development of a catalytic system based on the generation of carbenes **3.14** was considered, as well as the use of reagents such as $IZnCHI_2$,[27] $TfOZnCHCl_2$,[26] or X_2BCHI_2[28] to generate $LAuCHI_2$ carbenoids **3.16**, so far unknown species (Scheme 3.12).

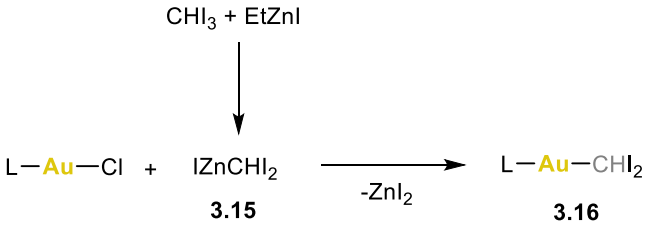

Scheme 3.12. Generation of diiodomethyl gold(I) carbenoids **3.16**.

Additionally, halomethylboronate reagents ICH_2BX_3K could also be used in the transmetalation,[29] instead of organozinc reagents.

---

25 García-Morales, C.; Pei, X.-L.; Sarria Toro, J. M.; Echavarren, A. M. Direct Observation of Aryl Gold(I) Carbenes That Undergo Cyclopropanation, C–H Insertion, and Dimerization Reactions, *Angew. Chem. Int. Ed.* **2019**, *58*, 3957–3961.

26 Taillemaud, S.; Charette, A. B. Spectroscopic Characterization of Heterohalogenic Dihalomethylzinc Carbenoids: Application to a More Efficient Chlorocyclopropanation Reaction. *Organometallics*, **2022**, *41*, 83-92.

27 Allouche, E. M. D.; Taillemaud, S.; Charette, A. B. Spectroscopic Characterization of (Diiodomethyl)Zinc Iodide: Application to the Stereoselective Synthesis and Functionalization of Iodocyclopropanes, *Chem. Commun.* **2017**, *53*, 9606–9609.

28 Sayes, M.; Benoit, G.; Charette, A. B. Borocyclopropanation of Styrenes Mediated by UV-Light Under Continuous Flow Conditions, *Angew. Chem. Int. Ed.* **2018**, *57*, 13514–13518.

29 a) Molander, G. A.; Ham, J. Synthesis of Functionalized Organotrifluoroborates via Halomethyltrifluoroborates, *Org. Lett.* **2006**, *8*, 2031–2034. b) Hartog, T. den; Toro, J. M. S.; Chen, P. A Palladium-Catalyzed Methylenation of Olefins Using Halomethylboronate Reagents, *Org. Lett.* **2014**, *16*, 1100–1103.

3.3 Results and discussion[30]

3.3.1 Synthesis of gold(I) carbenoids

As mentioned in the introduction of this chapter, chloromethyl gold (I) complexes have been synthesized using potentially hazardous diazocompounds or low temperatures. Our research group previously described the synthesis of different chloromethyl gold carbenoids, [$LAuCH_2Cl$], by the reaction of trimethylsilildiazomethane with the corresponding gold(I) chloride precursors in the presence of methanol. Considering these results, we decided to develop an alternative route for the synthesis of iodomethyl gold (I) complexes based on the transmetalation of organozinc reagents $XZnCH_2I$ or $XZnCHI_2$ (X = Cl, Br) with gold(I) chloride precursors LAuX.

Therefore, firstly zinc carbenoids **3.13**[26] and **3.15**[27] were synthesized according to the reported literature and were characterized by NMR in 90 and 80% NMR yields, respectively (Scheme 3.13). The stability of compounds **3.13** and **3.15** differs significantly when monitored by ^{1}H NMR. Zinc carbenoid **3.13** begins to decompose after 2-3 hours at 25 ºC and under argon atmosphere, whereas compound **3.15** remains stable for up to 2 days under identical conditions.

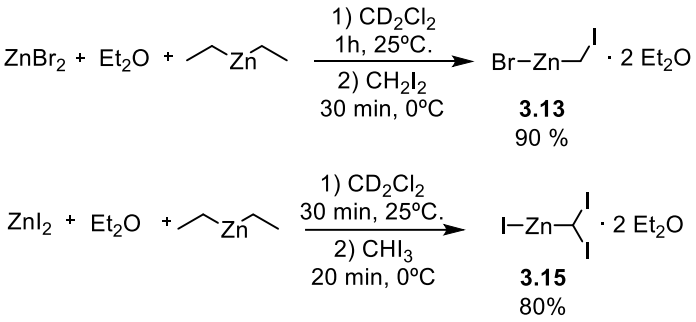

Scheme 3.13. Synthetic procedure for the obtention of zinc carbenoids **3.13** and **3.15**. Yields were determined by ^{1}H NMR using triphenylmethane as internal standard.

With the freshly prepared solutions of both zinc carbenoids in hand, they were added dropwise to a JohnPhosAuCl **3.17a** solution in dry CD_2Cl_2 at 25 ºC. We were able to detect spectroscopically gold(I) carbenoid **3.16a**; however, **3.2a** was not formed when zinc carbenoid **3.13** was used under the same conditions (Scheme 3.14).

30 Experimental work performed in collaboration with Dr. Elena Borrego.

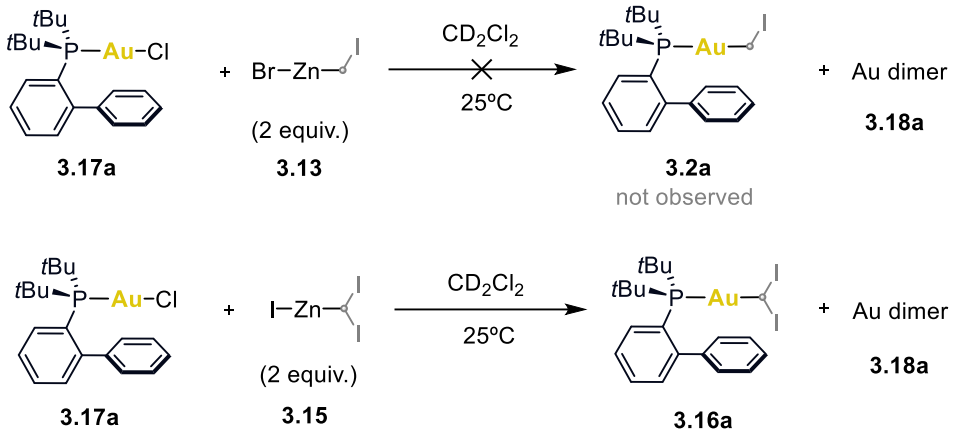

Scheme 3.14. Attempts towards the formation of gold(I) carbenoids **3.2** and **3.16a**.

The major compound observed when using zinc carbenoid **3.15** and the only compound formed when using **3.13** was proposed to be a halogen-bridged gold dimer **3.18a** in agreement with NMR experiments, TLC and UHPLC-MS analysis.

Gold carbenoid **3.16a** was characterized in the crude of the reaction by mono and bidimensional NMR. In ^{1}H NMR, a broad doublet at 3.97 ppm ($J_{H\text{-}P}$ = 2.6 Hz) by coupling with phosphorous present in JohnPhos ligand attached to gold(I) (Figure 3.6).

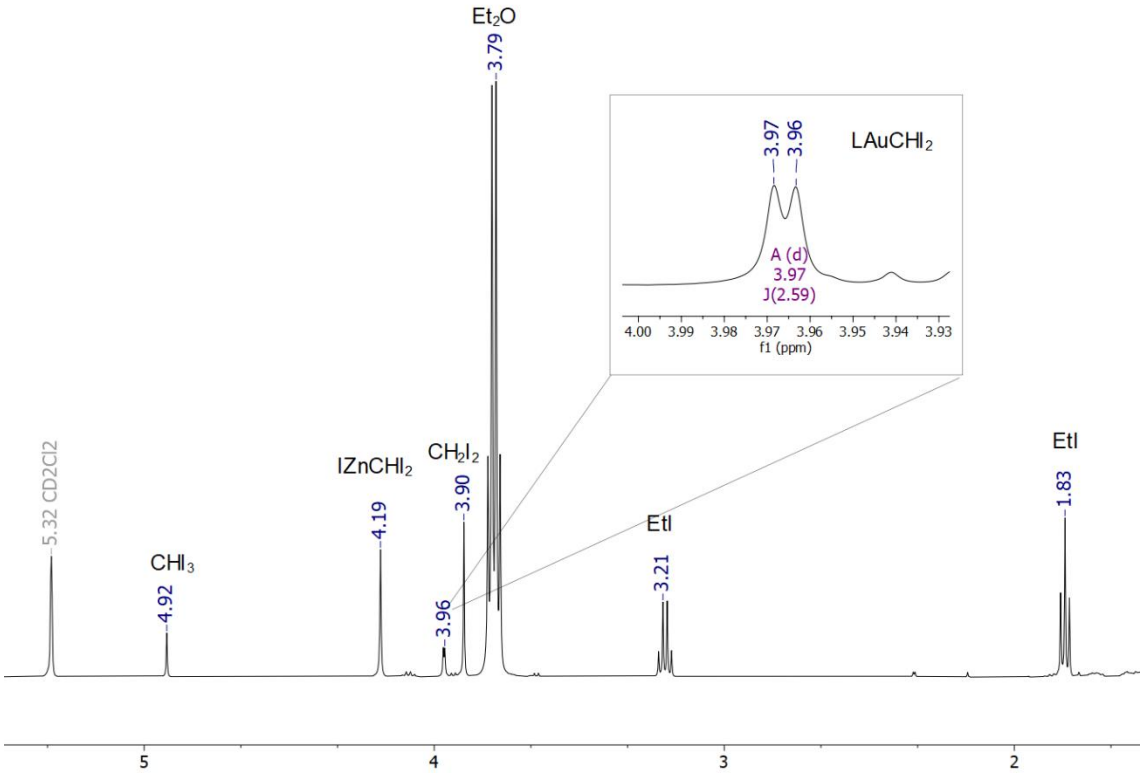

Figure 3.6. Section of ^{1}H NMR in CD_2Cl_2 of the crude reaction in the formation of gold(I) carbenoid **3.16a**.

The $^{31}P\{^{1}H\}$ NMR spectrum shows the signals of both the gold dimer **3.18a** and gold(I) carbenoid **3.16a** at 69.51 and 61.57 ppm respectively (Figure 3.7).

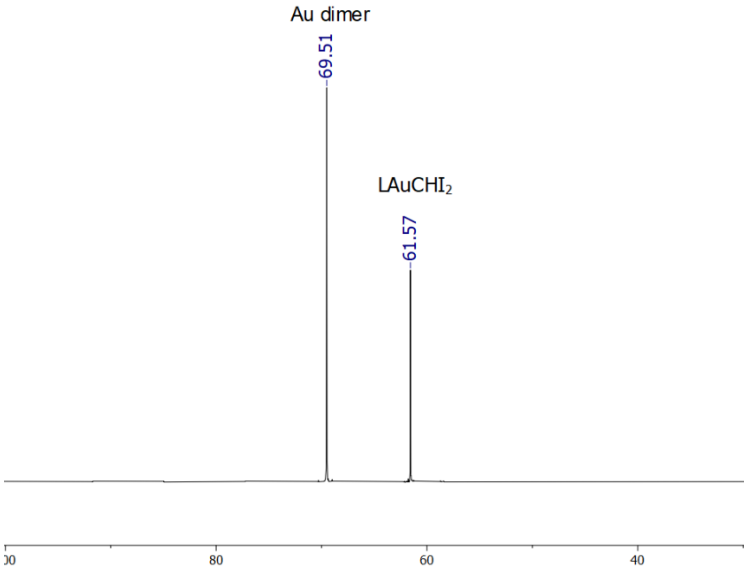

Figure 3.7. $^{31}P\{^{1}H\}$ NMR in CD_2Cl_2 of the crude reaction in the formation of gold(I) carbenoid **3.16a**.

Additionally, both $^{13}C\{^{1}H\}$ NMR and ^{1}H-^{13}C HSQC corroborate the correlation between the broad doublet at 3.97 ppm in ^{1}H NMR and another doublet in $^{13}C\{^{1}H\}$ NMR at -9.02 ppm with $J^{13C\text{-}31P}$ = 132.80 Hz (Figures 3.8 and 3.9).

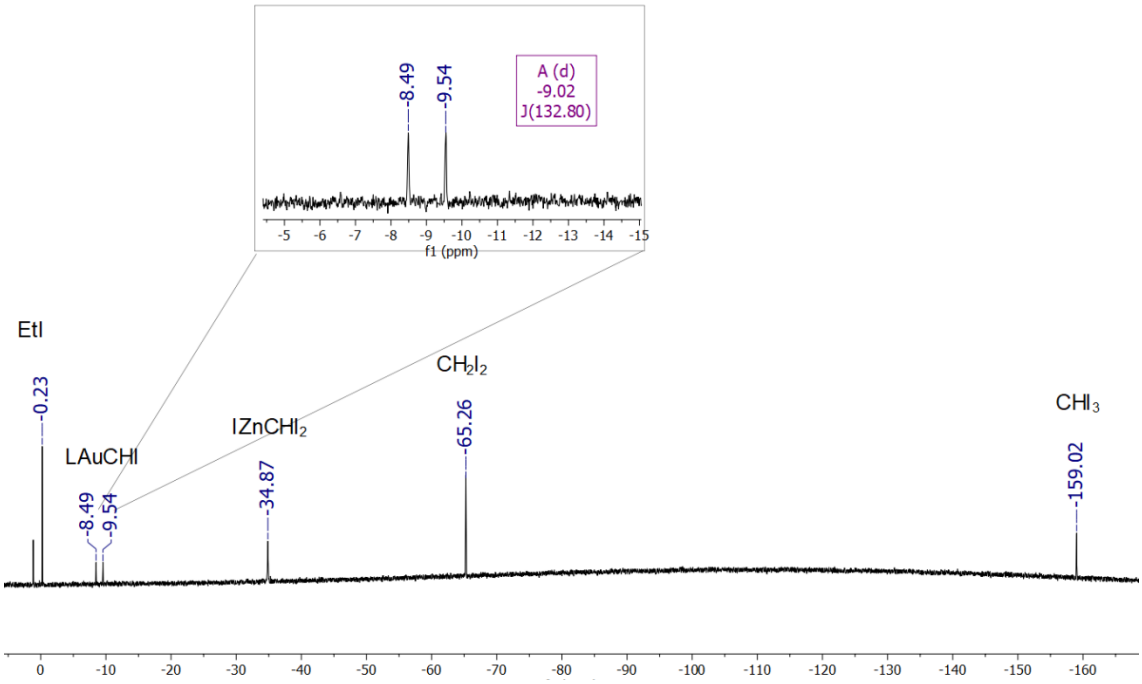

Figure 3.8. Section of $^{13}C\{^{1}H\}$ NMR in CD_2Cl_2 of the crude reaction in the formation of **3.16a.**

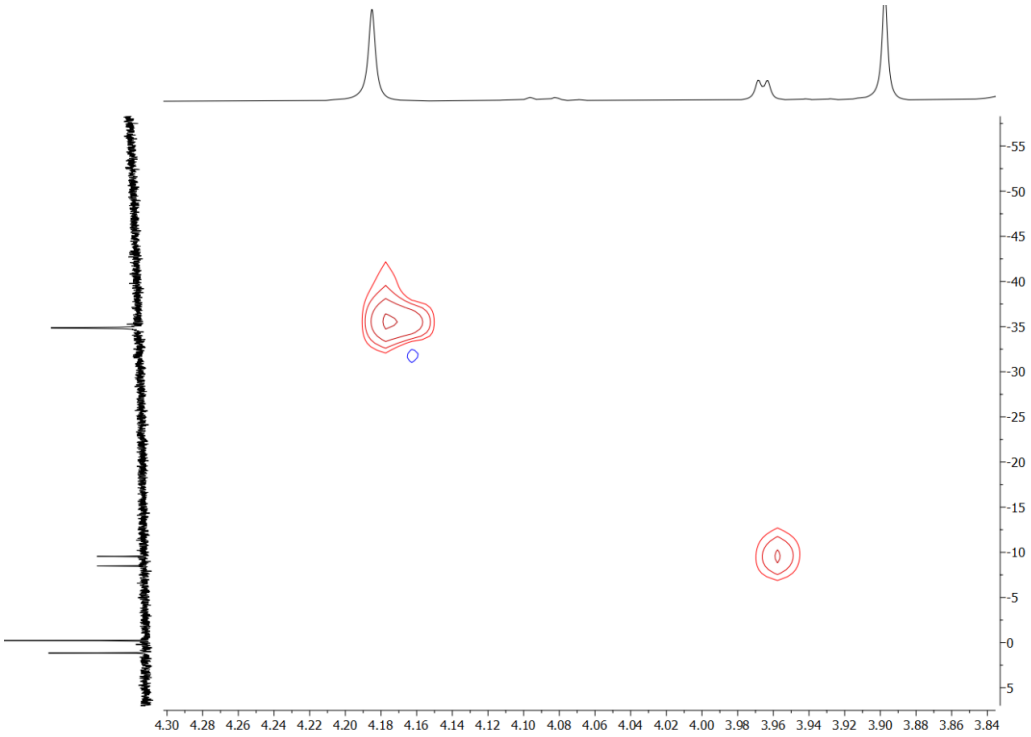

Figure 3.9. Section of ^{1}H-^{13}C HSQC in CD_2Cl_2 of the crude reaction in the formation of gold(I) carbenoid **3.16a**

Another bidimensional NMR correlation was observed through ^{1}H-^{31}P HMBC, confirming the $^{31}P\{^{1}H\}$ and ^{1}H NMR carbenoid signals and highlighting their proximity (Figure 3.10).

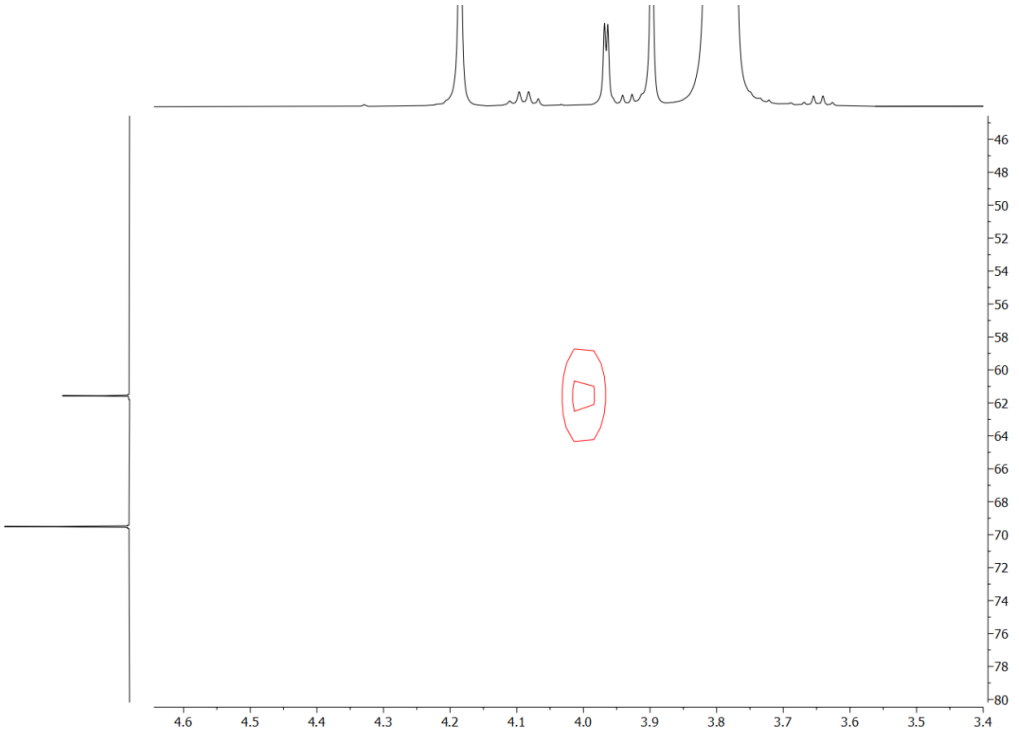

Figure 3.10. Section of ^{1}H-$^{31}P\{^{1}H\}$ HMBC in CD_2Cl_2 of the crude reaction in the formation of gold(I) carbenoid **3.16a**

3.3.2 Scope

The synthesis of several diiodidemethylgold(I) carbenoids **3.16a-d** bearing different phosphine ligands was attempted by the reaction between zinc carbenoid **3.15** and the corresponding gold (I) chloride complex **3.17a-d** in dry CD_2Cl_2 at 25 ºC (Table 3.1). Gold(I) carbenoids **3.16a-c** were obtained with yields between 25-75% and characterized by ^{1}H, $^{13}C\{^{1}H\}$, $^{31}P\{^{1}H\}$, HSQC and HMBC NMR experiments. In all cases, except when **3c** was used as precursor, the major compound observed in the reaction mixture was gold dimer **3.18a-b**. The compounds **3a-c** decompose under argon in the Young NMR tube after 1-5 hours, obtaining as degradation product **3.18a-c** in all cases. When triphenylphosphine was used as ligand, no formation of the corresponding gold(I) carbenoid **3.16d** was detected.

Table 3.1. Generation of gold(I) carbenoids **3.16a-d** via transmetalation with organozinc **3.15**. NMR yields and characteristic carbene shifts of final desired products.

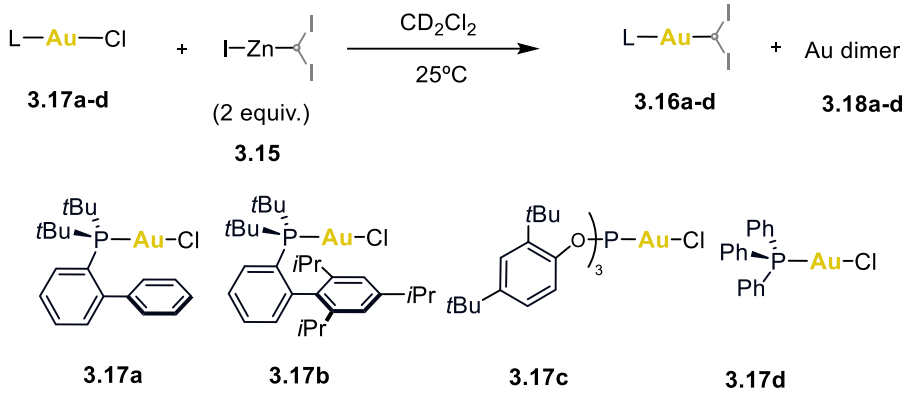

Au carbenoid	^{1}H NMR (ppm)	$^{13}C\{^{1}H\}$ NMR (ppm)	$^{31}P\{^{1}H\}$ NMR (ppm)	Ratio 3.16:3.18	NMR Yield (%)[a]
3.16a	3.97 (d, J_{H-P}= 2.59 Hz)	-9.02 (d, J_{C-P}= 132.80 Hz)	61.57	1:1.7	25
3.16b	3.85 (d, J_{H-P}= 2.01 Hz)	-8.68 (d, J_{C-P}= 133.81 Hz)	59.45	1:2	30
3.16c	4.76 (d, J_{H-P}= 3.65 Hz)	-24.97 (d, J_{C-P}= 213.06 Hz)	118.58	4.6:1 1:1.6[b]	75
3.16d	-	-	-	-	-

[a] NMR yields were determined using triphenylmethane as internal standard in CD_2Cl_2 as soon as the reaction was set. [b] Ratio after 1 h at 25 ºC.

3.3.3 Low temperature experiments

To avoid the formation of gold dimer **3.18**, the stability of gold carbenoids **3.16a** and **3.2a** was studied by carrying out low temperature ^{1}H and $^{31}P\{^{1}H\}$ NMR spectra. The thermal stability of gold carbenoid **3.16a** was studied by ^{1}H and $^{31}P\{^{1}H\}$ NMR experiments at low temperatures ranging from -90 ºC to -40 ºC. The reaction temperature was increased by 10 ºC every hour. Only the spectra that are different at the same temperature are shown.

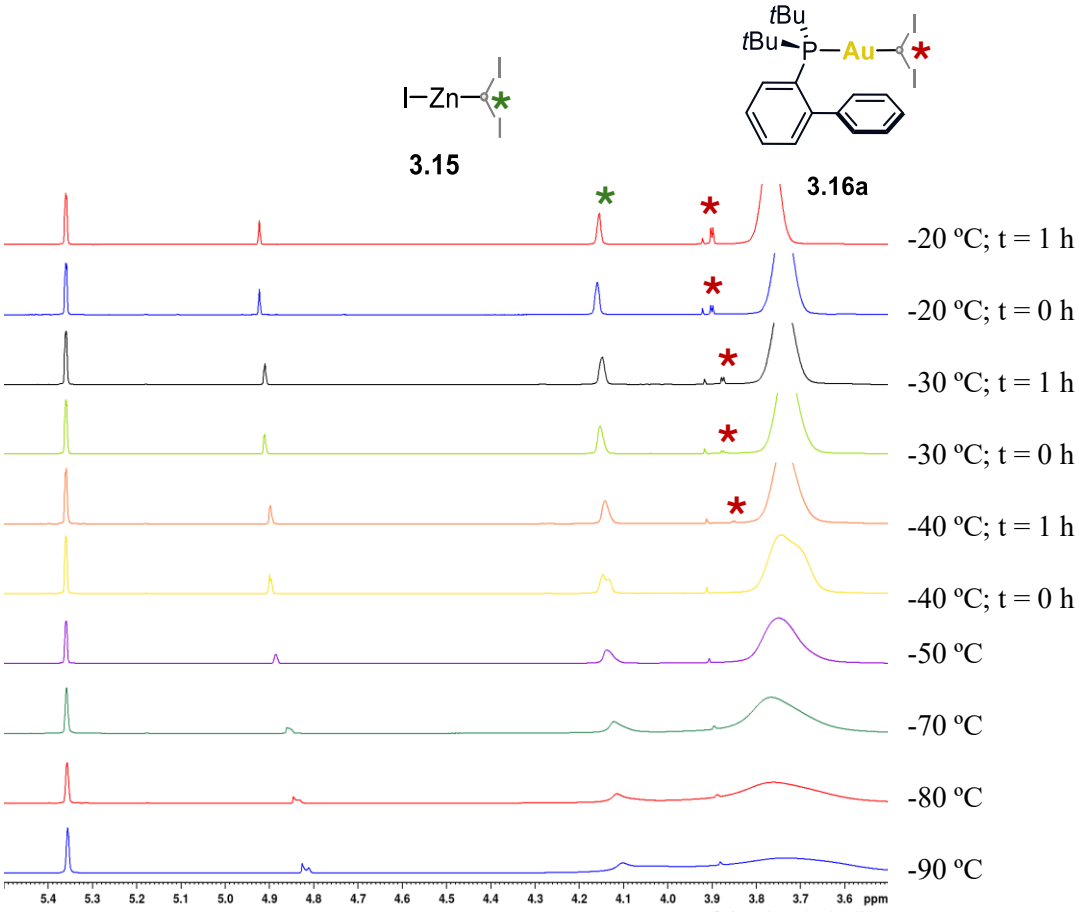

Figure 3.11. Low temperature (-90 to -20 ºC) ^{1}H NMR stability experiments in CD_2Cl_2 of **3.16a** formation.

The desired product **3.16a** began to be observed at -40 ºC with no formation of Au dimer **3.18a** (Figures 3.11 and 3.12).

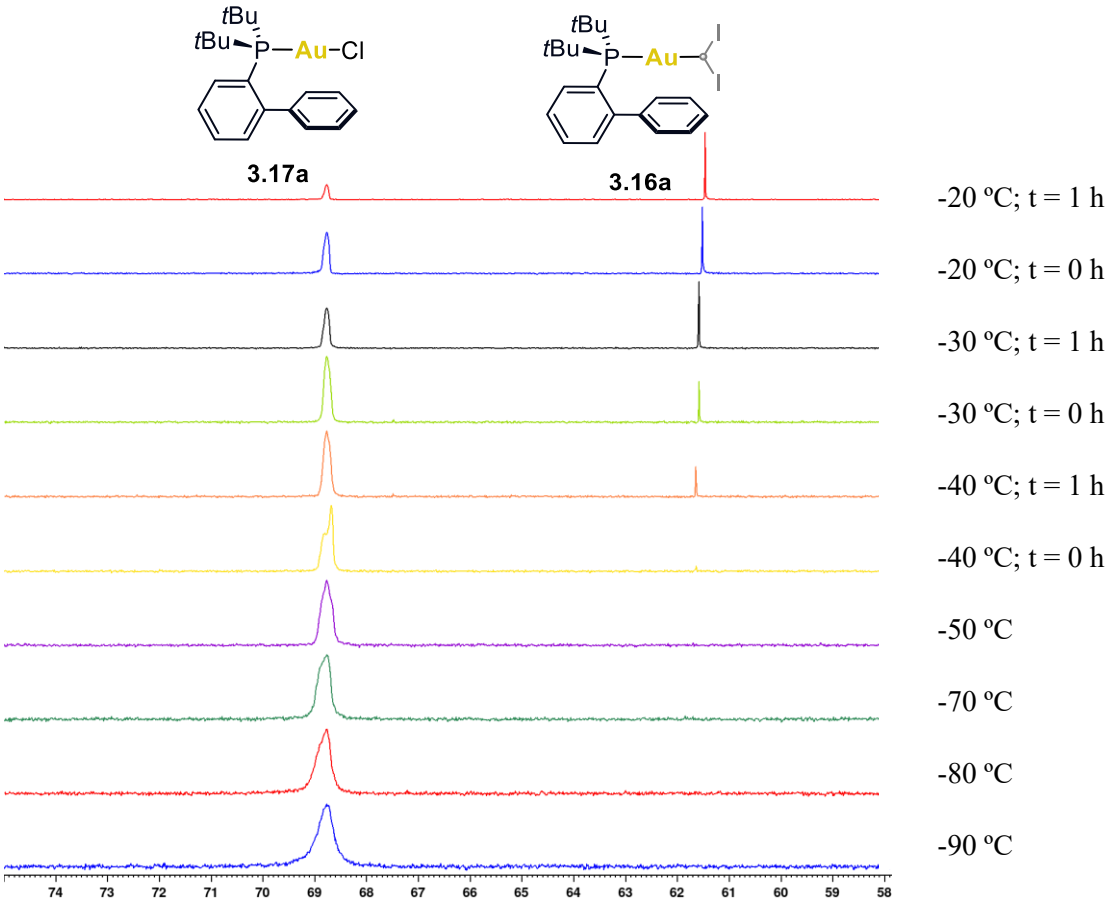

Figure 3.12. Low temperature (-90 to -20 ºC) $^{31}P\{^{1}H\}$ NMR stability experiments in CD_2Cl_2 of **3.16a** formation.

Additionally, we studied the range in which the gold carbenoid complex **3.16a** was stable. The study was carried out by taking ^{1}H and $^{31}P\{^{1}H\}$ NMR spectra at low temperatures from -10 ºC to 0 ºC. The reaction temperature was increased from -10 ºC to 0 ºC after 90 minutes. At -10 ºC we could observe a mixture of both the starting material JohnPhosAuCl **3.17a** and gold(I) carbenoid **3.16a**. Nevertheless, at 0 ºC the signal of **3.16a** started to disappear, **3.17a** completely reacted and formation of Au dimer **3.18a** was spotted (Figure 3.13). Therefore, we could conclude that the formation of **3.18a** occurs at higher temperatures than -10 ºC by decomposition of our desired gold(I) carbenoid **3.16a**. These results showed that the isolation and crystallization of **3.16a** might be possible at -30º C or -20 ºC.

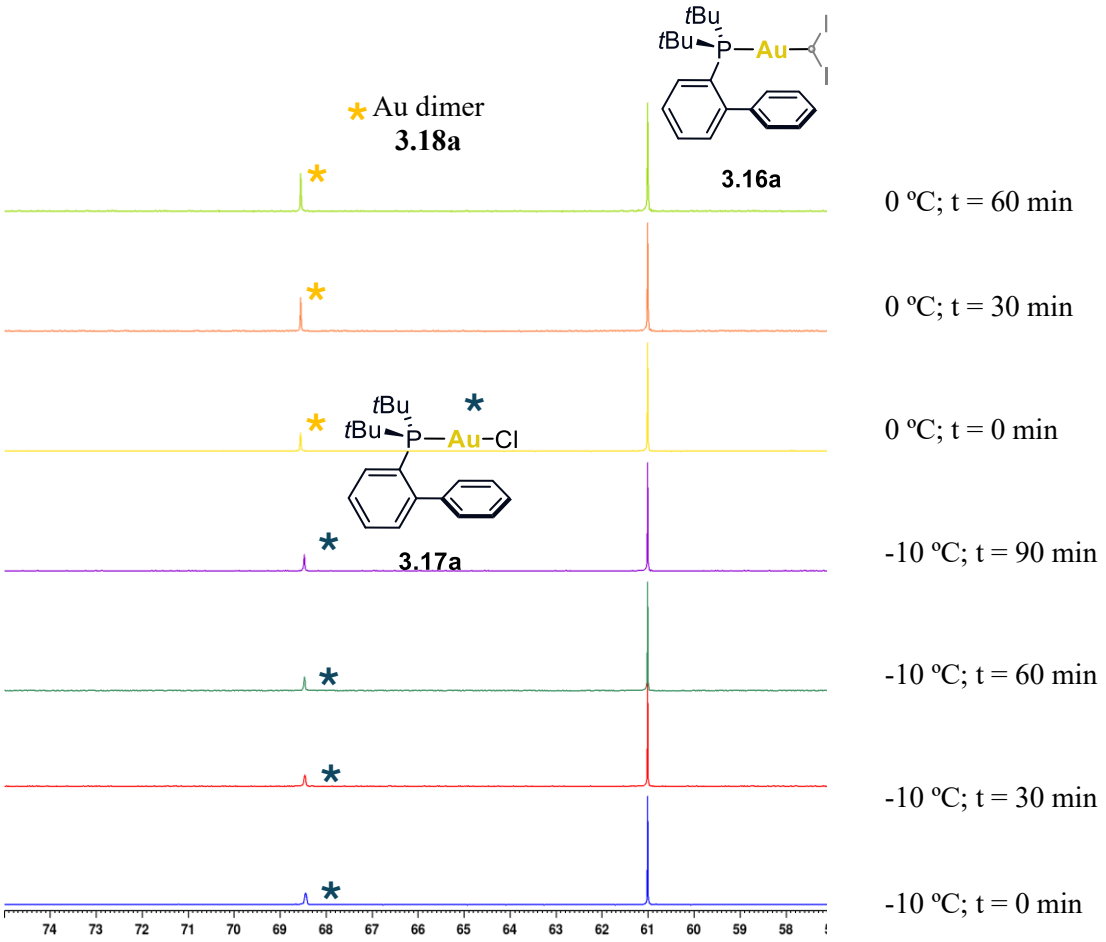

Figure 3.13. Low temperature (-10 to 0 ºC) ^{1}H NMR stability experiments in CD_2Cl_2 of **3.16a** formation.

The isolation of gold carbenoid **3.16a** was unsuccessfully attempted by various methods. A quick flash column chromatography under nitrogen using silica or aluminum oxide ended in complete decomposition, only recovering dimer **3.18a** as a white solid. As we were able to avoid the formation of gold dimer **3.18a**, the generation of gold(I) carbenoid **3.16a** via transmetalation was pursued at -10 ºC, and to minimize the amount of zinc carbenoid **3.15** in the reaction mixture, only 1 equivalent was added to the reaction obtaining full conversion after 1 h (Scheme 3.15). Thus, crystallization trials were carried out under these conditions. However, even crystallization under inert atmosphere at low temperatures (down to -50 ºC) by liquid diffusion, in combinations of dry solvents like CH_2Cl_2/pentane, CH_2Cl_2/toluene or CH_2Cl_2/benzene, resulted challenging.

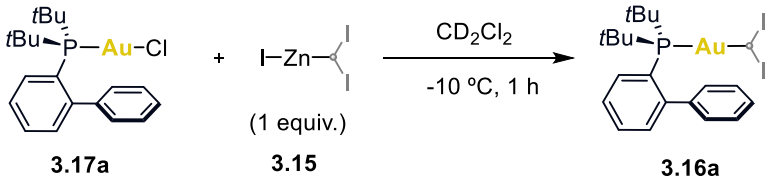

Scheme 3.15. Optimized reaction for the obtention of **3.16a**.

Parallelly, as **3.2a** was not observed at 25 ºC, we thought about exploring its formation at lower temperatures. In a similar manner as previously shown for **3.16a**, ^{1}H, $^{13}C\{^{1}H\}$ and $^{31}P\{^{1}H\}$ NMR experiments were measured at low temperatures ranging from -90 ºC to -40 ºC. The reaction temperature was increased by 10 ºC every hour. Along the experiments, we were able to detect that the desired product **3.2a** began to be observed at -90 ºC. Gold carbenoid **3.2a** was stable until -70 ºC, temperature at which the signal of **3.2a** started to disappear and Au dimer **3.18a** was observed.

Gold carbenoid JohnPhosAuCH$_2$I **3.2a** was characterized at -50 ºC in the crude of the reaction by mono and bidimensional NMR. In ^{1}H NMR, a broad doublet at 1.78 ppm ($J_{H\text{-}P}$ = 2.2 Hz) by coupling with phosphorous present in JohnPhos ligand attached to gold(I) (Figure 3.14). As a comparison, previously reported in the group JohnPhosAuCH$_2$Cl carbenoid ^{1}H NMR shift of the carbene appeared more deshielded, at 2.96 ppm as a doublet $J_{H\text{-}P}$ = 3.6 Hz.[16]

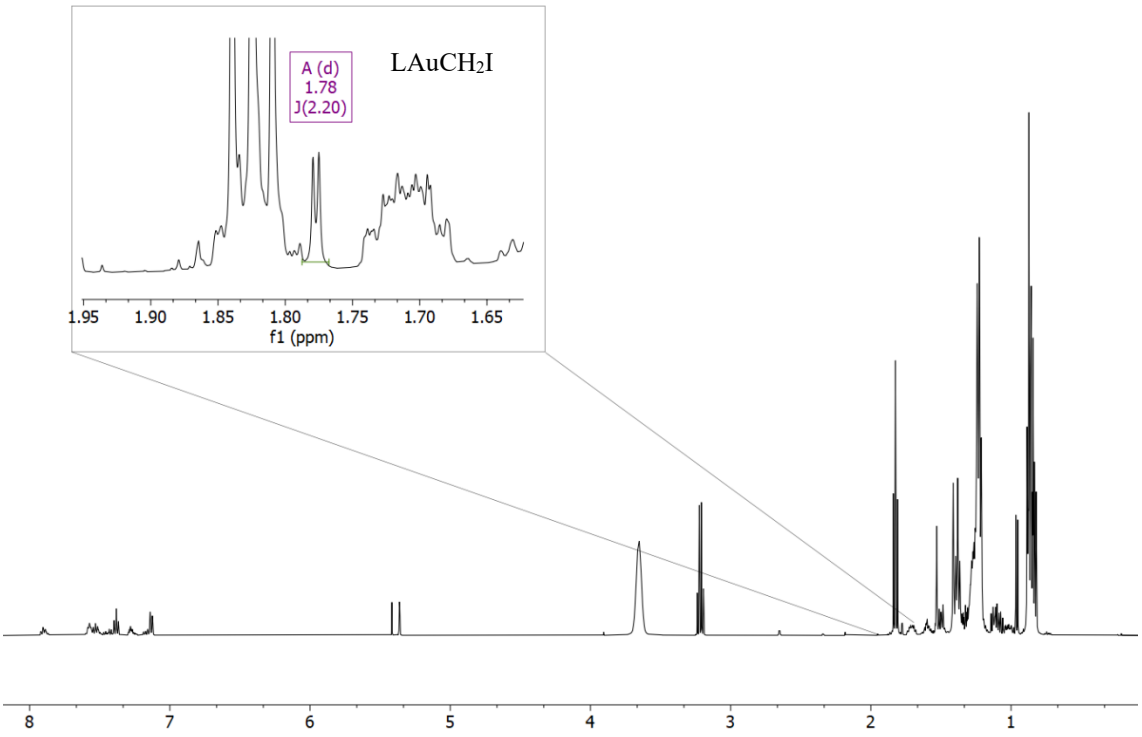

Figure 3.14. ^{1}H NMR spectra in CD_2Cl_2 at -50 ºC of the crude reaction in the formation of gold(I) carbenoid **3.2a**.

The $^{31}P\{^{1}H\}$ NMR spectrum shows the peaks of the JohnPhosAuCl, the gold dimer **3.18a** and gold(I) carbenoid **3.2a**, which was tentatively assigned to 66.34 ppm peak (Figure 3.15).

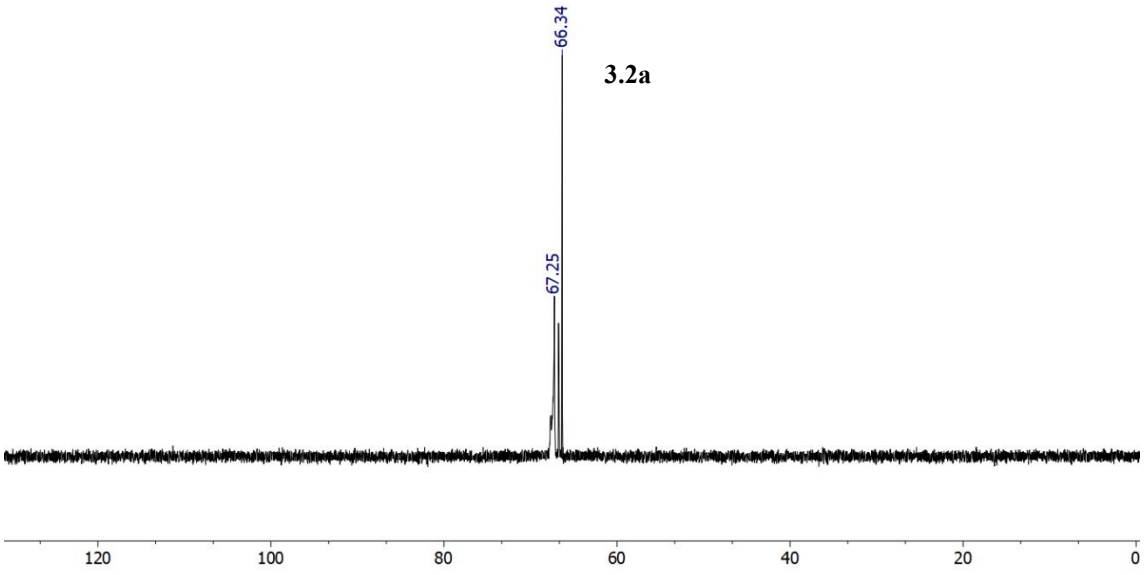

Figure 3.15. $^{31}P\{^{1}H\}$ NMR in CD_2Cl_2 at -50 ºC of the crude reaction in the formation of gold(I) carbenoid **3.2a**.

Moreover, $^{13}C\{^{1}H\}$ NMR and ^{1}H-^{13}C HSQC corroborate the correlation between the broad doublet at 1.78 ppm in ^{1}H NMR and the doublet observed in $^{13}C\{^{1}H\}$ NMR at 10.09 ppm with $J^{13C\text{-}31P}$ = 112.79 Hz (Figures 3.16 and 3.17). By comparison with JohnPhosAuCH$_2$Cl, its $^{13}C\{^{1}H\}$ NMR signal of the carbene appeared at significantly different chemical shift: 53.58 ppm as a doublet with $J_{C\text{-}P}$ = 112.6 Hz.[16]

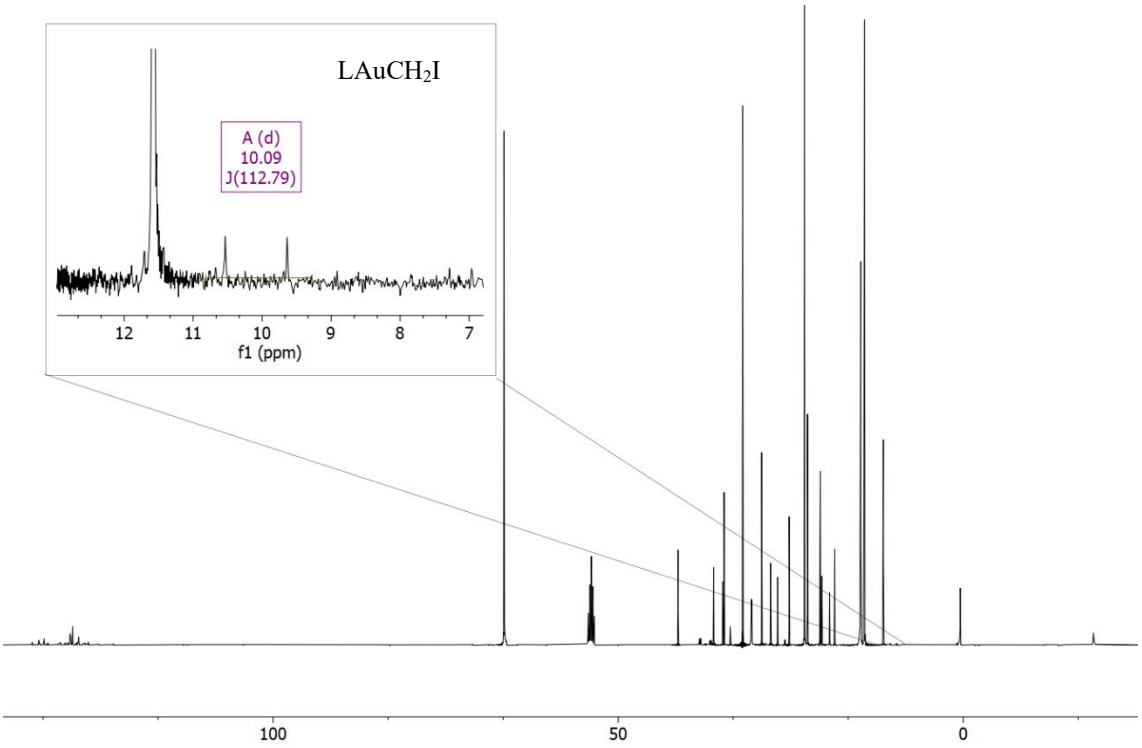

Figure 3.16. $^{13}C\{^{1}H\}$ NMR at -50 ºC in CD_2Cl_2 of the crude reaction in the formation of **3.2a**

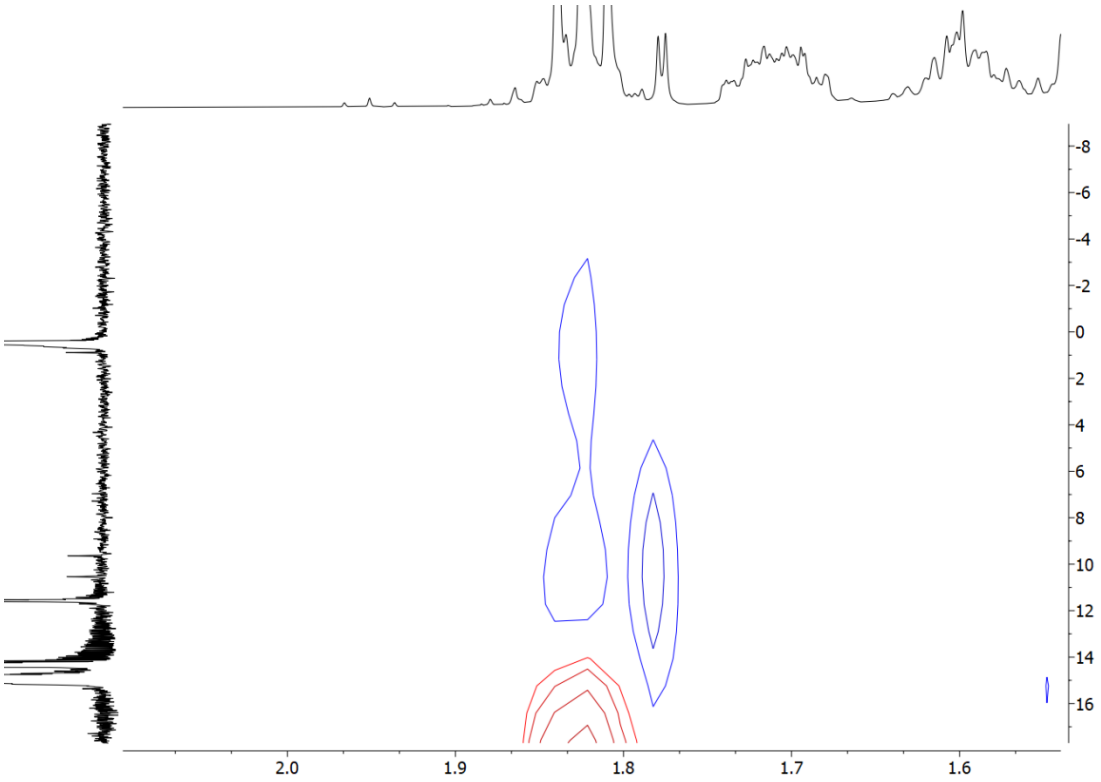

Figure 3.17. Section of ^{1}H-^{13}C HSQC in CD_2Cl_2 at -50 ºC of the crude reaction in the formation of gold(I) carbenoid **3.2a**

3.3.4 Iodomethylation by formal C(sp^2)–H bond functionalization of benzene

The reactivity of gold carbenoid **3.16a** upon activation with several halogen scavengers was tested by reaction with benzene. The expected reactivity for **3.16a** was the involvement of the complex in the so-called Buchner reaction, as reported by our group for chloromethylgold carbenoid **3.1a**.[16] Nonetheless, tropylium iodide **3.21** was not observed in the crude of the reaction; the product derived from formal insertion of a carbene CR^1R^2 group into a C(sp^2)–H bond, benzyl iodide **3.20**, was detected instead (Scheme 3.16). The preference of NHC gold(I) carbenes formed by extrusion of dinitrogen from ethyl diazoacetate (N_2=$CHCO_2Et$) for the obtention of products derived from direct C(sp^2)–H bond modification over the products derived from the Buchner reaction had been reported previously by our group,[31] showcasing a coinage-metal effect. Both possible processes had been reported to be accomplished with the help of diazo compounds and metal-based catalysts as the carbene source.[32]

To corroborate the formation of **3.20**, it was synthesized using a reported procedure,[33] and its formation was confirmed by GC-MS. The ^{1}H-NMR analysis of the crude reaction did not provide enough information about the formation of **3.20** due to overlapping of signals. Therefore, the product formation was quantified by GC-FID using a calibration plot.

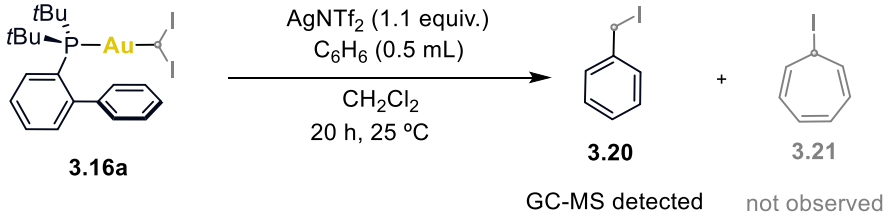

Scheme 3.16. C–H functionalization of benzene, observed reactivity derived from carbenes.

To rule out the involvement of zinc carbenoid **3.15** or the halide scavenger in the reaction, control experiments were carried out in the absence of gold carbenoid **3.16a** (Table 3.2, entries 1-4). The in situ generation of gold(I) carbene was discarded as well (Table 3.2, entry 5). Benzyl iodide **3.20** was observed when solutions of carbenoid were treated with different halide scavengers for 20 h at 25 ºC (Table 3.2, entries 6,7,8). The desired product was obtained in a 76% yield when

31 Fructos, M. R.; Besora, M.; Braga, A. A. C.; Díaz-Requejo, M. M.; Maseras, F.; Pérez, P. J. Mechanistic Studies on Gold-Catalyzed Direct Arene C–H Bond Functionalization by Carbene Insertion: The Coinage-Metal Effect, *Organometallics* **2017**, *36*, 172–179.

32 For some examples, see: a) Caballero, A.; Díaz-Requejo, M. M.; Fructos, M. R.; Olmos, A.; Urbano, J.; Pérez, P. J. Catalytic Functionalization of Low Reactive C(Sp3)–H and C(Sp2)–H Bonds of Alkanes and Arenes by Carbene Transfer from Diazo Compounds, *Dalton Trans.* **2015**, *44*, 20295–20307. b) Davies, H. M. L.; Manning, J. R. Catalytic C–H Functionalization by Metal Carbenoid and Nitrenoid Insertion, *Nature* **2008**, *451*, 417–424.

33 Das, D.; H Anal, J. M.; Rokhum, S. L. A Mild and Highly Chemoselective Iodination of Alcohol Using Polymer Supported DMAP, *J. Chem. Sci.* **2016**, *128*, 1695–1701.

the reaction took place in presence of $AgNTf_2$, meanwhile when $AgBF_4$ was used as halide scavenger, no formation of **3.20** was observed (Table 3.2, entry 9).

Table 3.2. Control experiments and halide scavenger screening in the C–H functionalization of benzene by diiodomethylgold(I) carbenoid **3.16a**

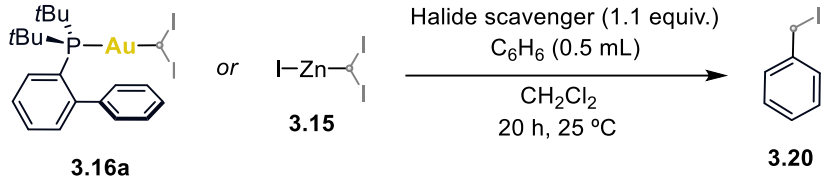

Entry	Metal	Halide Scavenger	Yield (%)[a]
1	-	-	-
2	**3.15**	-	-
3	**3.15**	$AgNTf_2$	-
4	-	$AgNTf_2$	-
5	**3.16a**	-	1
6	**3.16a**	$AgNTf_2$	76
7	**3.16a**	$TMSNTf_2$	4
8	**3.16a**	$NaBAr_4^F$	16
9	**3.16a**	$AgBF_4$	-

[a] Yields were determined by GC-FID using calibration plot.

As carbene-like reactivity was observed, the detection of the gold(I) carbene **3.19a** complex was unsuccessfully attempted by ^1H NMR at -90 ºC in CD_2Cl_2 (Scheme 3.17). Future trials will be pursued using alternative halide scavengers.

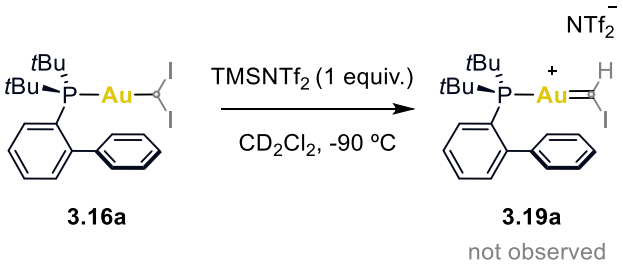

Scheme 3.17. Designed experiment for the detection of proposed intermediate **3.19a** gold(I) carbene.

3.3.5. Computational analysis

As the C–H bond functionalization was found in this system and with the aim of getting a deeper insight into the reaction mechanism, DFT calculations were performed. We used a B3LYP-D3 functional, with a 6-311+G(d,p) basis set for light atoms and SDD for I and Au, with implicit SMD solvation for benzene.

The results are summarized in Scheme 3.18. We started from the gold(I) carbene **A1** bearing trimethylphosphine as ancillary ligand. In the presence of a benzene molecule **3.22**, intermediate **A2** is formed. From intermediate **A2**, two different paths are possible. The lowest energy path goes through transition state **TSA3** and involves the highly electrophilic carbene reaction in an electrophilic aromatic substitution with benzene, to reach Wheland intermediate **A3**.[31] This path would ultimately lead to the obtention of 7-iodo-1,3,5-cycloheptatriene **A6**, not observed in the crude reaction, was found via cyclopropanation (**TSA5**) from the **A3** intermediate leading to norcaradiene **A5** and final electrocyclic ring opening via **TSA6**, recovering the aromaticity when barrierless tropylium iodide would form. The higher energy path from **A3** would lead directly through **TSA4** to the experimentally observed benzyl iodide species **A4**.

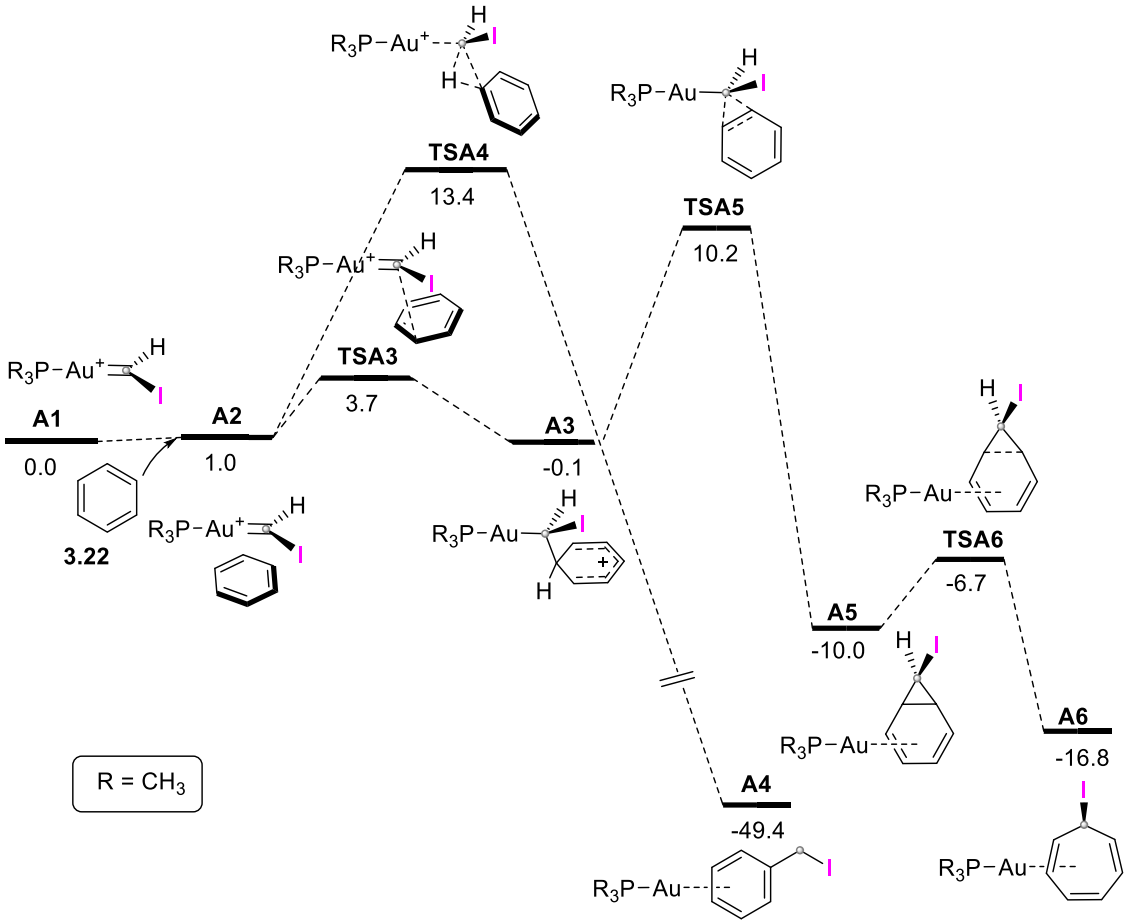

Scheme 3.18. Free energies in kcal mol^{-1}. B3LYP-D3/6-311+G(d,p) for light atoms and SDD for I and Au/SMD(benzene).

The free energy profile in Scheme 3.18 does not reproduce the experimental observation, but we notice that the difference in barriers between the two path is quite small (13.4 kcal mol^{-1} for **TSA4** vs 10.2 kcal mol^{-1} for **TSA5**). We think that there must be a lower in energy reaction pathway to access benzyl iodide. A promising option would be the participation of a base (NTf_2^- in our case, counteranion of the halide scavenger) taking the hydrogen in the aromatic ring in Wheland intermediate **A3**, recovering aromaticity (**A7**) and final protodeauration to yield **A4** (Scheme 3.19). Due to time limitations, these possibilities could not be fully explored and further examination in this regard will be needed.

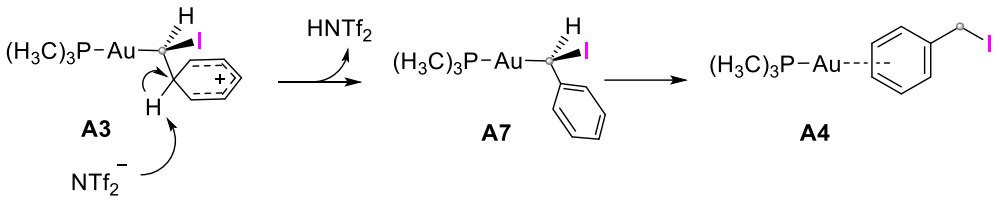

Scheme 3.19. Proposed missing steps in the elucidation of the mechanism for the formation of benzyl iodide.

3.4 Conclusions

We have developed a new method to access iodomethyl and diiodomethylgold(I) carbenoids via transmetalation with zinc carbenoids (Scheme 3.20). Several ancillary ligands to gold were tested in the reaction at 25 ºC and we were able to detect the products **3.16a-c** by ^{1}H, $^{13}C\{^{1}H\}$ and $^{31}P\{^{1}H\}$ NMR. Similarly, carbenoid **3.2a** was only detected in the range of -90 to -50 ºC.

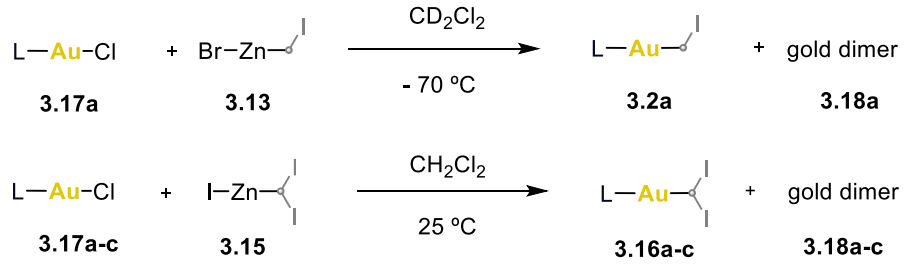

Scheme 3.20. Unfolded strategy for the synthesis of iodomethyl and diiodomethylgold(I) carbenoids.

The stability of gold(I) carbenoid **3.16a** under argon atmosphere is limited at 25 ºC and its behavior was studied at low temperatures down to -90 ºC by ^{1}H and $^{31}P\{^{1}H\}$ NMR. The formation of gold dimer **3.18a** was avoided by performing the reaction at lower temperatures (-10 ºC).

The newly synthesized diiodomethylgold(I) carbenoids were tested in the reaction with benzene in the presence of a halogen scavenger (Scheme 3.21). Their reactivity is contrary to that observed for chloromethylgold(I) carbenes.[16] Our compounds yielded the product of iodomethylation by formal C–H insertion of benzene **3.20** instead of the Buchner reaction product **3.21**.

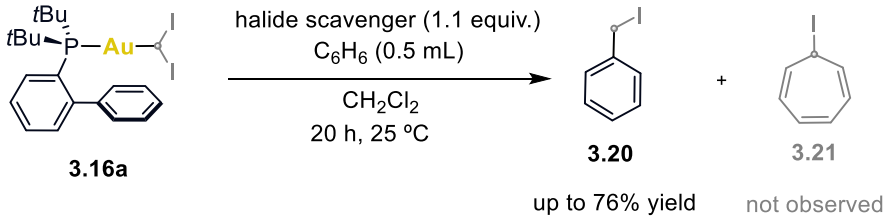

Scheme 3.21. Observed carbene-like reactivity of synthesized diiodomethylgold(I) carbenoids.

The attempted detection of gold(I) carbene derived from **3.16a** was unsuccessful, as well as the crystallization of gold(I) carbenoid **3.16** bearing different ligands.

DFT calculations were performed in the C–H functionalization reaction observed, proposing the formation of Wheland intermediate **A3** (Scheme 3.22), from which rearomatization and final protodeauration would yield the desired benzyl iodide product **3.20**. Further calculations are needed to confirm this mechanism.

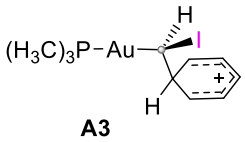

A3

Scheme 3.22. Suggested Wheland intermediate in the C(sp^2)-H functionalization of benzene.

3.5 Experimental section

3.5.1 General experimental methods

Unless otherwise stated, all the reactions reported herein were performed under argon atmosphere using standard Schlenk techniques. All reagents and solvents were purchased from commercial sources and used without further purification. The dry solvents used were passed through an activated alumina column on a PureSolvTM Solvent Purification System (SPS, Innovative Technologies, Inc., MA), or purchased from ACROS Organics as commercially available anhydrous solvents. CD_2Cl_2 was dried over activated 4 Å molecular sieves and stored under argon before use. The reaction monitoring was followed by NMR analysis, UHPLC–MS (Agilent Technologies 1290 Infinity II, LC/MS with single–quad detector InfinityLab (APCI ionization source)) or by GC–MS. NMR spectra were recorded at 298 K on Bruker Avance Ultrashield NMR spectrometers (300 MHz, 400 MHz, 500 MHz, and 500 MHz with CryoProbe). Chemical shifts (δ) are reported in parts per million (ppm) and referenced to residual solvent (For ^{1}H NMR: $CDCl_3$ at 7.26 ppm, CD_2Cl_2 at 5.31 ppm, C_6D_6 at 7.16 ppm, for $^{13}C\{^1H\}$ NMR: $CDCl_3$ at 77.16 ppm, CD_2Cl_2 at 54.00 ppm, C_6D_6 at 128.06 ppm). The following abbreviations were used to explain multiplicities: s = singlet, d = doublet, t = triplet, q = quartet, p = pentet, m = multiplet, br s = broad singlet. Coupling constants (*J*) are reported in Hertz (Hz).

3.5.2 Synthetic procedures and characterization data

General procedure for the preparation of gold(I) carbenoids.

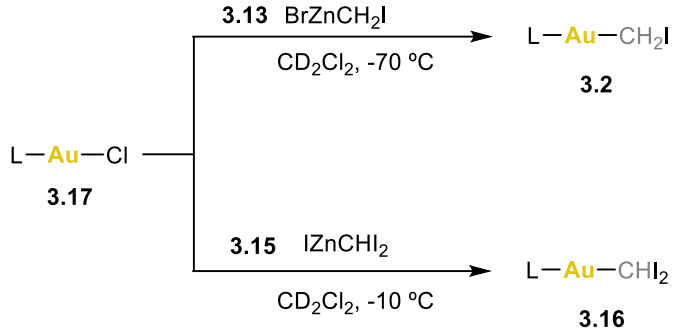

Scheme 3.23. Formation of gold(I) carbenoids **3.2** and **3.16** via transmetalation avoiding the dimer as by-product.

Having freshly prepared the corresponding 0.4 M solution of **3.13** or **3.15** in dry CD_2Cl_2 or CH_2Cl_2 following the reported procedures in the literature,[26,27] gold(I) chloride complex **3.17** is weighted in a Schlenk tube under argon and dissolved in dry CD_2Cl_2 or CH_2Cl_2 to obtain a 0.1 M solution. Then, zinc carbenoid (1 equiv.) previously filtered under argon is added dropwise at -10 ºC for obtaining **3.16** and at -70 ºC for **3.2**. and left stirring at the same temperature for 1 h. By carrying out the reactions at these low temperatures, the formation of gold dimer is avoided.

Iodomethylgold(I) carbenoid (**3.2a**)

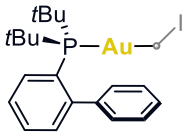

3.2a

Distinctive signals at -50 ºC: **^{1}H NMR** (500 MHz, CD_2Cl_2) δ 1.78 ppm (bd, $J_{H\text{-}P}$= 2.2 Hz). **^{13}C{^{1}H} NMR** (126 MHz, CD_2Cl_2) δ 10.09 ppm (d, $J_{C\text{-}P}$= 112.79 Hz). **^{31}P{^{1}H} NMR** (202 MHz, CD_2Cl_2) δ 66.34 ppm. **^{1}H-^{13}C HSQC** (CD_2Cl_2, -50 ºC), correlation between H at 1.78 ppm and C at 10.09 ppm.

Diiodomethylgold(I) carbenoid (3.16a)

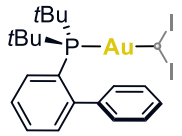

3.16a

Distinctive signals: ^{1}**H NMR** (500 MHz, CD_2Cl_2) δ 3.97 ppm (bd, J_{H-P}= 2.59 Hz). ^{13}**C{^{1}H} NMR** (126 MHz, CD_2Cl_2) δ -9.02 ppm (d, J_{C-P}= 132.80 Hz). ^{31}**P{^{1}H} NMR** (202 MHz, CD_2Cl_2) δ 61.57 ppm. ^{1}**H-**^{13}**C HSQC** (CD_2Cl_2, 25 ºC), correlation between H at 3.97 ppm and C at -9.02 ppm. ^{1}**H-**^{31}**P HMBC** (CD_2Cl_2, 25 ºC), correlation between H at 3.97 ppm and P at 61.57 ppm.

Diiodomethylgold(I) carbenoid (3.16b)

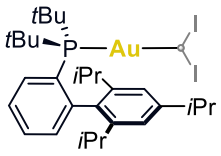

3.16b

Distinctive signals: ^{1}**H NMR** (500 MHz, CD_2Cl_2) δ 3.87 ppm (bd, J_{H-P}= 2.01 Hz). ^{13}**C{^{1}H} NMR** (126 MHz, CD_2Cl_2) δ -8.68 ppm (d, J_{C-P}= 133.81 Hz). ^{31}**P{^{1}H} NMR** (202 MHz, CD_2Cl_2) δ 59.45 ppm. ^{1}**H-**^{13}**C HSQC** (CD_2Cl_2, 25 ºC), correlation between H at 3.87 ppm and C at -8.68 ppm.

Diiodomethylgold(I) carbenoid (3.16c)

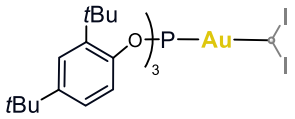

3.16c

Distinctive signals: ^{1}**H NMR** (500 MHz, CD_2Cl_2) δ 4.76 ppm (bd, J_{H-P}= 3.65 Hz). ^{13}**C{^{1}H} NMR** (126 MHz, CD_2Cl_2) δ -24.97 ppm (d, J_{C-P}= 213.06 Hz). ^{31}**P{^{1}H} NMR** (202 MHz, CD_2Cl_2) δ 118.58 ppm. ^{1}**H-**^{13}**C HSQC** (CD_2Cl_2, 25 ºC), correlation between H at 4.76 ppm and C at -24.97 ppm.

General procedure for the C–H functionalization of benzene

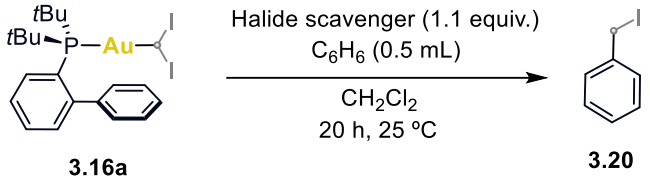

Scheme 3.24. Generic procedure for the synthesis of benzyl iodide **3.20**.

To a suspension of freshly formed gold(I) carbenoid **3.16a** in CH_2Cl_2 (25 µmol, 0.1 M) synthesized following the previously mentioned procedure, dry CH_2Cl_2 (250 µL) were added under argon and subsequently a solution of halide scavenger (27.5 µmol, 1.1 equiv) dissolved in dry benzene (0.5 mL) was added at 25 ºC. If the halide scavenger is not soluble in benzene, it was added as solid. The reaction was left stirring at the same temperature during 20 h, after which the reaction mixture was diluted to 5 mL of CH_2Cl_2 in a volumetric flask for the quantification. Yields were determined by GC-FID using a calibration plot.

3.5.3 Computational details

Unless otherwise stated, all calculations were carried out using the Gaussian09 package.[34] All the reported energies are in kcal mol^{-1}. Free energies quoted were calculated at default temperature 298.15 K and include a +1.89 kcal mol^{-1} correction to reflect the 1M rather than ideal gas reference state.[35] Geometries were optimized to stationary points using the B3LYP[36] functional with Grimme's D3 dispersion correction[37] and the basis sets used were 6-31G(d,p)[38] for all elements except for Au and I, where the SDD[39] basis set and ECP was employed. Single point calculations were performed with the 6-311+G(d,p) basis set for light atoms and SDD basis set and ECP for Au and I, using B3LYP-D3. Solvent effects were introduced with implicit model SMD[40] for benzene. All stationary points were confirmed through the absence of imaginary vibrations, and transition states were validated using IRC[41] calculations using LQA algorithm.

34 Gaussian 09, Revision B.1, Frisch, M. J., Trucks, G. W., Schlegel, H. B., Scuseria, G. E., Robb, M. A., Cheeseman, J. R., Scalmani, G., Barone, V., Mennucci, B., Petersson, G. A., Nakatsuji, H., Caricato, M., Li, X., Hratchian, H. P., Izmaylov, A. F., Bloino, J., Zheng, G., Sonnenberg, J. L., Hada, M., Ehara, M., Toyota, K., Fukuda, R., Hasegawa, J., Ishida, M., Nakajima, T., Honda, Y., Kitao, O., Nakai, H., Vreven, T., Montgomery, J. A., Peralta, Jr. J. E., Ogliaro, F., Bearpark, M., Heyd, J. J., Brothers, E., Kudin, K. N., Staroverov, V. N., Kobayashi, R., Normand, J., Raghavachari, K., Rendell, A., Burant, J. C., Iyengar, S. S., Tomasi, J., Cossi, M., Rega, N., Millam, J. M., Klene, M., Knox, J. E., Cross, J. B., Bakken, V., Adamo, C., Jaramillo, J., Gomperts, R., Stratmann, R. E., Yazyev, O., Austin, A. J., Cammi, R., Pomelli, C., Ochterski, J. W., Martin, R. L., Morokuma, K., Zakrzewski, V. G., Voth, G. A., Salvador, P., Dannenberg, J. J., Dapprich, S., Daniels, A. D., Farkas, Ö., Foresman, J. B., Ortiz, J. V., Cioslowski, J., Fox, D. J. Gaussian, Inc., Wallingford CT **2009.**

35 Luchini, G.; Alegre-Requena, J. V.; Funes-Ardoiz, I.; Paton, R. S. GoodVibes: Automated Thermochemistry for Heterogeneous Computational Chemistry Data, *F1000Research* **2020**, *9*, 291.

36 a) Becke, A. D. Density-Functional Exchange-Energy Approximation with Correct Asymptotic Behavior, *Phys. Rev. A* **1988**, *38*, 3098–3100. b) Density-functional Thermochemistry. III. The Role of Exact Exchange, *J. Chem. Phys.* **1993**, *98*, 5648–5652.

37 Grimme, S. Density Functional Theory with London Dispersion Corrections, *WIREs Comput. Mol. Sci.* **2011**, *1*, 211–228.

38 Hehre, W. J.; Ditchfield, R.; Pople, J. A. Self—Consistent Molecular Orbital Methods. XII. Further Extensions of Gaussian—Type Basis Sets for Use in Molecular Orbital Studies of Organic Molecules, *J. Chem. Phys.* **1972**, *56*, 2257–2261.

39 Andrae, D.; Häußermann, U.; Dolg, M.; Stoll, H.; Preuß, H. Energy-Adjustedab Initio Pseudopotentials for the Second and Third Row Transition Elements, *Theor. Chim. Acta* **1990**, *77*, 123–141.

40 Marenich, A. V.; Cramer, C. J.; Truhlar, D. G. Universal Solvation Model Based on Solute Electron Density and on a Continuum Model of the Solvent Defined by the Bulk Dielectric Constant and Atomic Surface Tensions, *J. Phys. Chem. B* **2009**, *113*, 6378–6396.

41 Gonzalez, Carlos.; Schlegel, H. Bernhard. Reaction Path Following in Mass-Weighted Internal Coordinates, *J. Phys. Chem.* **1990**, *94*, 5523–5527.

3.5.4 Computed structures and energies

Table 3.3. Formation of benzyl iodide and 7-iodo-1,3,5-cycloheptatriene.

B3LYP-D3/6- 31G(d,p)+SDD(Au, I); SMD (benzene). HLT: B3LYP-D3/6- 311+G(d,p) +SDD(Au, I); SMD (benzene)

	E / Hartree	**G / Hartree**	**E_{HLT} / Hartree**
3.22	-232.2661	-232.1899	-232.3245
A1	-646.8343	-646.7425	-646.8960
A2	-879.1198	-878.9354	-879.2354
TSA3	-879.1188	-878.9330	-879.2322
A3	-879.1278	-878.9411	-879.2393
TSA4	-879.1010	-878.9168	-879.2154
A4	-879.2067	-879.0194	-879.3186
TSA5	-879.1125	-878.9240	-879.2249
A5	-879.1462	-878.9568	-879.2577
TSA6	-879.1408	-878.9507	-879.2531

UNIVERSITAT ROVIRA I VIRGILI
MECHANISTIC STUDIES ON GOLD(I) AND GOLD(III) CATALYTIC TRANSFORMATIONS
Isabel Arranz De La Calle

UNIVERSITAT ROVIRA I VIRGILI
MECHANISTIC STUDIES ON GOLD(I) AND GOLD(III) CATALYTIC TRANSFORMATIONS
Isabel Arranz De La Calle

Summary and General Conclusions

UNIVERSITAT ROVIRA I VIRGILI
MECHANISTIC STUDIES ON GOLD(I) AND GOLD(III) CATALYTIC TRANSFORMATIONS
Isabel Arranz De La Calle

Summary and General Conclusions

The research conducted in this Doctoral Thesis is summarized in the following results:

A complete mechanistic picture was obtained for the role of the mode of action of the ligands in the family of biaryl-pyrrolidinyl phosphine gold(I) complexes. The family of chiral gold(I) complexes was expanded by including electron withdrawing substituents in its structure. Additionally, gold(I) was replaced in the chiral complex with silver(I) and copper(I); this led to the observation of a trend in enantioinduction and reactivities in asymmetric catalysis Au>Ag>Cu, that could be correlated with some studied structural properties of the complexes. Additionally, kinetic studies were carried out in the formal [4+2] cycloaddition reaction of 1,6-enyne catalyzed by an isolated cationic chiral gold(I) complex. Two competing rate-determining steps are proposed for the reaction: the formation of the cyclopropyl gold(I) carbene and the ligand exchange.

The oxidative addition of allyl halides to gold(I) complexes was better understood through a series of experiments and calculations. A catalytic system was developed employing mononuclear Au(I) complexes bearing simple alkyl phosphines as catalysts, in the cross-coupling reaction of allyl bromides and $PhSn(CH_3)_3$. A deeper computational study of these systems demonstrated an unexpectedly complex behavior of this type of systems. A high dependence of the DFT energy on the identity of the functional was found, and the problem is associated to the description of the change of oxidation state at gold. Moreover, the stereochemistry of the oxidative addition reaction was assessed, observing an overall retention of the reaction center, proposed to occur via two consecutive stereoinversions.

Finally, the development of a new method to access iodomethyl and diiodomethylgold(I) carbenoids via transmetalation with zinc carbenoids was achieved for several ancillary ligands to gold. The stability of the carbenoids was studied as well as their carbene-like reactivity in the reaction with benzene, yielding the product of formal C-H insertion in the presence of a halogen scavenger. DFT calculations were performed in the C-H functionalization reaction observed, proposing the formation of a Wheland intermediate, from which rearomatization and final protodeauration gives the observed benzyl iodide.

UNIVERSITAT ROVIRA I VIRGILI
MECHANISTIC STUDIES ON GOLD(I) AND GOLD(III) CATALYTIC TRANSFORMATIONS
Isabel Arranz De La Calle

UNIVERSITAT ROVIRA I VIRGILI
MECHANISTIC STUDIES ON GOLD(I) AND GOLD(III) CATALYTIC TRANSFORMATIONS
Isabel Arranz De La Calle

UNIVERSITAT ROVIRA I VIRGILI
MECHANISTIC STUDIES ON GOLD(I) AND GOLD(III) CATALYTIC TRANSFORMATIONS
Isabel Arranz De La Calle

UNIVERSITAT
ROVIRA i VIRGILI